

**Cobalt and Chromium Amino-bis(phenolate) Complexes for Epoxide
Homopolymerization and Copolymerization with Carbon Dioxide**

By

Kenson Ambrose

A thesis submitted to the School of Graduate Studies

in partial fulfillment of the requirements for the degree of

Doctor of Philosophy

Department of Chemistry

Memorial University of Newfoundland

January 2019

St. John's

Newfoundland

Abstract

Chemical transformations of CO₂ into useful materials have received significant attention in the past as it is a potential C1 feedstock of very high abundance. This attention originates from the increased abundance of CO₂ in the earth's atmosphere due to anthropogenic processes such as fossil fuel combustion. The use of CO₂ as a C1 feedstock will not lead to a decrease in atmospheric CO₂ concentrations but rather as an alternative starting material to petroleum derived small molecules. Metal-catalyzed reactions of CO₂ with epoxides into either polycarbonate via copolymerization or cyclic carbonates via cycloaddition are potentially lucrative methods for CO₂ use. In this work, Co(II)/(III) complexes bearing tripodal amino-bis(phenolate) ligands were synthesized and characterized by NMR, MALDI-TOF mass spectrometry, elemental analysis and X-ray diffraction, then investigated for catalytic activity toward CO₂ and epoxide coupling in the presence of the following co-catalysts: TBAB (tetrabutylammonium bromide), PPNCI (bis(triphenylphosphine)iminium chloride) or DMAP (4-dimethylaminopyridine). Co(III) complexes also contained ancillary ligands such as [2,4-DNP]⁻ (2,4-dinitrophenolate), OAc⁻ (acetate) and ⁻O₂CCF₃ (trifluoroacetate) and showed selectivity toward cyclic carbonate production. A Co(II) complex, however, contained coordinated KOAc (observed via X-ray diffraction and elemental analyses) and was selective toward polycarbonate production where OAc⁻ served as a minor initiator during the copolymerization process, as determined by end-group analysis using MALDI-TOF mass spectrometry. The coordinated KOAc is believed to play an important role in overall

catalyst activity as other reported catalysts with similar structure, but not containing KOAc, showed little to no copolymerization.

Cr(III) complexes bearing slightly different amino-bis(phenolate) ligands were also synthesized and investigated as catalyst for reactions of CO₂ with epoxides. A Cr(III) complex with a ligand containing *tert*-butyl groups in the *ortho* and *para* positions of the phenolate O-donors, was highly active toward CHO (cyclohexene oxide) ring-opening homopolymerization to produce high molecular weight PCHO (poly(cyclohexene oxide)) without the use of a co-catalyst and even in the presence of CO₂. Modification of this complex by introducing methyls into the *ortho* and *para* positions of the phenolate donors switched activity to CHO/CO₂ copolymerization, with high selectivity and CO₂ incorporation. This complex showed the fastest rate of CO₂/epoxide copolymerization with PPNN₃ as a co-catalyst, when monitored using in situ FTIR spectroscopy. Kinetics studies of the CHO/CO₂ copolymerization process showed a first order dependence on catalyst concentration.

Acknowledgements

I would first like to sincerely thank my supervisor, Dr. Christopher Kozak for accepting me into his research group and giving me such a life-changing opportunity to work in such an exciting area of chemistry. I am truly grateful for all his guidance and advice over the years which have helped and motivated me to become a better scientist and have further taught me how to accept and overcome many challenges and responsibilities. His patience in one-on-one group meetings, teaching me how to write scientifically, helping with coursework and demonstrating techniques in the lab, all the while having a great sense of humor has truly made graduate school an amazing experience. Whether it may be changing a glove box catalyst or demonstration of nitrogen triiodide detonation, I will always remember that the number one emphasis in the lab was safety which he always made sure of. I would also like to thank Dr. Francesca Kerton for all her valued criticism and advice over the years in group meetings which have contributed significantly to my research and studies. I am truly grateful and always had a sense of motivation from her natural drive and determination for chemistry research.

Secondly, I would like to thank Dr. Yuming Zhao for giving me suggestions during committee meetings, Dr. Celine M. Schneider for training and help with NMR, Julie Collins, Jennifer N. Murphy and Dr. Katherine N. Robertson for solving my crystal structures, Linda Winsor for training and lots of help with MALDI-TOF and ESI MS, Adam G. Beaton for training on TGA and DSC and Nick Ryan for helping with IR data collection.

I would also like to thank NSERC (Dr. Kozak's research grant), Department of Chemistry, School of Graduate Studies (SGS), Graduate Students' Union (GSU) and Memorial University for funding, which was a huge contribution to the successful completion of my PhD studies.

A further thank-you goes out to past and present members of the Green Chemistry and Catalysis group, especially Kaijie Ni, Hart Plommer, Katalin Devaine-Pressing, Ali Elkurtehi and Dalal Alhashmialameer for their friendly help and advice in the lab. Thank-you Tim Anderson, Kori Andrea, Erika Butler, George Margoutidis, Julian Vidal and Yi Liu for your friendship and making this a wonderful journey, whether it may be at conferences, social gatherings or even scientific discussions in the lab. I also want to thank Margo Frost who helped me edit my thesis.

Last but not least, I would like to thank my family members, my parents (Marie and Franklyn Ambrose), my brothers (Kervin and Kerishlyn), for their love and support from thousands of miles away. I would like to express my deepest gratitude to my loving girlfriend, Jennifer Nicole Murphy. I am truly grateful for her love, patience, understanding, advice and words of encouragement throughout my program, both in and out of the lab. You have truly made this an amazing journey.

Table of Contents

Abstract.....	ii
Acknowledgements	iv
List of Tables	xii
List of Schemes	xiv
List of Figures.....	xvi
List of Abbreviations and Units.....	xxiv
List of Appendices.....	xxix
Chapter 1: Introduction	1
1.1 Green chemistry	1
1.1.1 Brief introduction to green chemistry principles.....	1
1.1.2 Carbon dioxide utilization as a renewable feedstock.....	3
1.1.3 Overview on polycarbonate synthesis	6
1.1.4 Catalytic coupling of CO₂ with epoxides	9
1.2 Brief history of metal-catalyzed coupling of CO₂ with epoxides	15
1.2.1 Cobalt complexes as catalysts for coupling of CO₂ with epoxides.....	17
1.2.1.1 Binary catalysts	18
1.2.1.2 Bifunctional catalysts.....	30
1.3 Chromium complexes for coupling of CO₂ with epoxides	44

1.3.1 Salan, salen and related catalyst systems	44
1.3.2 Other catalyst systems bearing tetradentate ligands	55
1.3.3 Other types of catalyst systems	64
1.4 Ring-opening polymerization of epoxides	65
1.4.1 Types of ROP mechanisms	65
1.4.2 Selected catalysts for ROP of epoxides	67
1.5 Objectives of this thesis	72
1.6 References	75
 Chapter 2: Synthesis and Characterization of Co(III) Amino-bis(phenolate)	
Complexes as Catalysts for Cyclic Carbonate Production from CO₂ and Epoxides	84
2.1 Introduction	84
2.2 Results and discussion	88
2.2.1 Synthesis of Co(III) amino-bis(phenolate) complexes	88
2.2.1.1 Co(2,4-DNP) amino-bis(phenolate) complexes	88
2.2.1.2 Co(OAc) amino-bis(phenolate) complexes	95
2.2.1.3 Co(O₂CCF₃) amino-bis(phenolate) complexes	97
2.2.1.4 Other attempted syntheses of Co(III) amino-bis(phenolate) complexes	98
2.2.2 Coupling of epoxides with CO₂ using Co(III) amino-bis(phenolate) complexes	101

2.3 Conclusions	105
2.4 Experimental	106
2.4.1 General experimental procedures and instrumentation	106
2.4.2 Synthesis of cobalt complexes	107
2.4.2.1 Synthesis of complex 2.6a	107
2.4.2.2 Synthesis of 2.6b	109
2.4.2.3 Synthesis of 2.6c	110
2.4.2.4 Attempted synthesis of 2.6d	110
2.4.2.5 Attempted synthesis of [CoClL_n] complexes (2.6e and 2.8e).....	111
2.4.2.6 Attempted synthesis of 2.6f	111
2.4.3 Representative CO₂/epoxide coupling procedure	112
2.4.4 X-ray crystallography procedure	112
2.5 References	113
 Chapter 3: Synthesis and Characterization of Co(II) Amino-bis(phenolate)	
complexes as Catalysts for Copolymerization of CO₂ and Cyclohexene Oxide	118
3.1 Introduction.....	118
3.2 Results and discussion	121
3.2.1 Synthesis of Co(II) complex	121
3.2.2 Copolymerization of CO₂ and CHO.....	125

3.2.3 Polycarbonate end group analysis	132
3.3 Conclusions	135
3.4 Experimental	136
3.4.1 General experimental considerations	136
3.4.2 Synthesis of 3.1	137
3.4.3 Representative procedure for CO₂/epoxide copolymerization	138
3.4.4 X-ray crystallography procedure	138
3.5 References	140
 Chapter 4: Chromium Amino-bis(phenolate) Complexes as Catalysts for Ring-	
Opening Polymerization (ROP) of Cyclohexene Oxide.....	147
4.1 Introduction	147
4.2 Results and discussion	150
4.2.1 Synthesis and characterization of Cr(III) complexes	150
4.2.2 ROP of cyclohexene oxide using 4.1 – 4.4	158
4.2.3 Kinetic studies	164
4.3 Conclusions	169
4.4 Experimental	170
4.4.1 General experimental considerations	170
4.4.2 Synthesis of 4.1	171

4.4.3 Synthesis of 4.2	172
4.4.4 Synthesis of 4.3	173
4.4.5 Synthesis of 4.4	173
4.4.6 Representative ring-opening polymerization of cyclohexene oxide	174
4.4.7 X-ray diffraction analysis procedure for 4.1	174
4.4 References	176
 Chapter 5: Synthesis and Characterization of a Cr(III) Amino-bis(phenolate)	
Complex as a Catalyst for Copolymerization of Cyclohexene Oxide and CO₂:	
Modification of Compound 4.1.	181
5.1 Introduction	181
5.2 Results and discussion	185
5.2.1 Cr(III) complex modification and characterization	185
5.2.2 Copolymerization of CHO and CO₂ using 5.1.....	192
5.2.3 Polycarbonate end-group analysis.....	199
5.3 Conclusions	205
5.4 Experimental	205
5.4.1 General experimental considerations.....	205
5.4.2 Synthesis of 5.1	207
5.4.3 Representative procedure for CHO/CO₂ copolymerization	208

5.4.4 X-ray diffraction analysis procedure for 5.1a	209
5.4.5 X-ray diffraction analysis procedure for 5.1b	209
5.5 References	210
Chapter 6: Attempted Experiments, Future Directions and Conclusions.....	214
6.1 Introduction.....	214
6.2 Discussion.....	216
6.2.1 Ring-opening polymerization of cyclohexene carbonate using 3.1.....	216
6.2.2 CO₂/epoxide coupling and attempted copolymerization, and UV/vis studies using 4.1	217
6.2.3 Terpolymerization of epoxides using 5.1	220
6.3 Experimental	222
6.3.1 Attempted ring-opening polymerization of CHC	222
6.4 Ideas for future directions.....	223
6.5 Conclusions.....	224
6.6 References	229

List of Tables

Table 1.1: CHO/PA/CO ₂ terpolymerization catalyzed by 1.24a /PPNCl. ⁷³	52
Table 2.1: Cycloaddition of various epoxides and CO ₂ using compounds Co(III)X amino-bis(phenolate) complexes (where X is [2,4-DNP] ⁻ , OAc, or ⁻ O ₂ CCF ₃). ^a	104
Table 3.1: Copolymerization of CO ₂ and CHO using 2.1 , 2.2 and 3.1 . ^a	131
Table 4.1: Results from ROP reactions of CHO using complexes 4.1 – 4.4 . ^a	163
Table 5.1: Copolymerization of CO ₂ and CHO using 5.1 . ^a	199
Table 6.1: Cycloaddition of propylene oxide and CO ₂ using 4.1 . ^a	218
Table 6.2: Terpolymerization of CO ₂ /CHO/epoxides using 5.1 . ^a	222
Table C - 1: Crystal data and structure refinement of Compound 2.9a .	276
Table C - 2: Bond lengths from structural data of 2.9a .	277
Table C - 3: Bond angles from structural data of 2.9a .	277
Table C - 4: Selected bond lengths for 3.1 .	277
Table C - 5: Selected bond angles for 3.1 .	278
Table C - 6: Crystal data and structure refinement of Cr(III) amino-bis(phenolate) complexes.	281
Table C - 7: Bond lengths from structural data of 4.1'' .	282
Table C - 8: Bond angles from structural data of 4.1'' .	283
Table C - 9: Bond lengths from structural data of 5.1a .	284
Table C - 10: Bond angles from structural data of 5.1a .	285
Table C - 11: Bond lengths from structural data of 5.1b .	286
Table C - 12: Bond angles from structural data of 5.1b .	287

Table C - 13: Crystal data and structure refinement data for 5.2	290
Table C - 14: Bond lengths from structural dat of 5.2	291
Table C - 15: Bond angles from structural data of 5.2	292

List of Schemes

Scheme 1.1: Synthesis of polycarbonate using phosgene and BPA.....	7
Scheme 1.2: Asahi-Kasei's phosgene free process for BPA-PC production.	10
Scheme 1.3: Metal-catalyzed coupling of epoxides with CO ₂ for polycarbonate or cyclic carbonate formation.	12
Scheme 1.4: General reaction mechanism for coupling epoxides (propylene oxide) with CO ₂ to yield either polycarbonate or cyclic carbonate. ¹⁹	14
Scheme 1.5: Attempted synthesis of PGAC via oxidation of poly(1,2-glycerol carbonate) (A) and successful synthesis via BG/CO ₂ copolymerization followed by Pd/C-catalyzed deprotection (B). ⁵⁸	41
Scheme 1.6: Salen-Co(III)I complex activated by phosphorane to generate a bifunctional catalyst system (top). The proposed reaction mechanism (bottom). ⁶⁰	43
Scheme 1.7: Post-functionalization of poly-3,4-cyclohexadiene carbonate using thioglycolic acid via a thiol-ene click reactions.....	50
Scheme 1.8: Recycling of BEP from polycarbonate using heat.....	51
Scheme 1.9: Bis(hydroxyquinoline)Cr(III)-OAc ^F complexes used by Müller, Sundermeyer and co-workers for reactions involving CO ₂ and CHO. ⁸¹	59
Scheme 1.10: Inner-sphere mechanism proposed by Müller and co-workers for CO ₂ /CHO coupling reactions using a bis(hydroxyquinoline)Cr(III)-OAc ^F . ⁸¹	60
Scheme 1.11: Anionic ROP mechanism initiated by alkali metal alkoxides.	66
Scheme 1.12: Illustration of metal-mediated ROP of epoxides using aluminum-based species.	67

Scheme 2.1: General synthetic route for Co(II)/(III) complexes used in this work.	88
Scheme 2.2: Synthetic route for complex 2.6a	90
Scheme 2.3: Unsuccessful synthetic route for complex 2.9a	95
Scheme 2.4: Synthetic route to compound 2.6b	96
Scheme 3.1: Synthesis of Co(II) amino-bis(phenolate) complexes 2.1 , 2.2 and 3.1	122
Scheme 3.2: Coupling of CO ₂ and CHO producing PCHC and CHC.	126
Scheme 4.1: Synthetic route to Cr(III) amino-bis(phenolate) complexes 4.1 – 4.4	150
Scheme 4.2: ROP of CHO producing PCHO.	158
Scheme 5.1: Synthetic route for preparation of Cr(III) amino-bis(phenolate) complex 5.1 . 5.1a formation discussed in text.	185
Scheme 5.2: Copolymerization of CO ₂ and CHO producing PCHC.	193
Scheme 6.1: Synthetic route to new Co(III) amino-bis(phenolate) complex.	223
Scheme 6.2: General synthetic route to polyesters and polyethers using epoxides and cyclic anhydrides.	224

List of Figures

Figure 1.1: Trends in CO ₂ atmospheric concentration. Dashed line represents mid-month mean values whereas continuous line represents the same but with correction applied.....	4
Figure 1.2: Some chemical processes involving CO ₂ utilization for synthesis of potentially useful organic molecules. \$ = industrialized processes. Reprinted by permission from RightsLink [®] : Springer Nature, Nature Communications, Q. Liu, L. Wu, R. Jackstell and M. Beller, <i>Nat. Commun.</i> , 2015, 6 , 5933-5947, Copyright 2015.	6
Figure 1.3: Phosgene process for production of polycarbonate (PC).	8
Figure 1.4: Commonly used co-catalysts for CO ₂ / epoxide coupling reactions.	12
Figure 1.5: Different initiation pathways for CO ₂ /epoxide coupling reactions. (A) Dinuclear intramolecular mechanism. (B) Intermolecular dinuclear mechanism. (C) Metal catalyst/co-catalyst mononuclear mechanism. (D) Mononuclear intramolecular mechanism.	15
Figure 1.6: Trend in the number of publications on CO ₂ and epoxide coupling. Analysis from SciFinder [®] ; search terms “carbon dioxide and epoxide coupling”, April 2018.....	17
Figure 1.7: First reported cobalt catalyst for CO ₂ /epoxide copolymerization reactions...	18
Figure 1.8: Bimetallic Co(III)-salen complex for copolymerization of CO ₂ with PO.....	19
Figure 1.9: Co-TAML metal complex reported by Berry and co-workers as a catalyst for cyclic carbonate synthesis from CO ₂ and epoxides.	20
Figure 1.10: Immobilized (<i>R,R</i>)-Co(II)-salen complex used as a catalyst for propylene carbonate synthesis from CO ₂ and <i>rac</i> -PO.	21

Figure 1.11: Co(II)/(III) amino-bis(phenolate) complex for cycloaddition of CO ₂ and PO.	22
Figure 1.12: Di-cobalt(III) catalyst for copolymerization of CHO and CO ₂ .	23
Figure 1.13: Cobaltoporphyrin complexes used as catalysts for coupling of PO and CO ₂ .	24
Figure 1.14: Cobaloxime complexes for cycloaddition of epoxides and CO ₂ .	26
Figure 1.15: Copolymerization reaction of CO ₂ and BGE using a variety of Co(III)X-salen complexes.	27
Figure 1.16: Racemic dinuclear Co(III)X-salen complex for copolymerization of CO ₂ and <i>meso</i> -epoxides.	29
Figure 1.17: Mono and bifunctional Co(III)-salen catalysts.	31
Figure 1.18: Co(III) complex of salen-type ligand tethered by four quaternary ammonium salts for terpolymerization of CO ₂ , PO and other epoxides.	33
Figure 1.19: Multichiral Co(III)-salen asymmetric catalyst used for copolymerization of PO and CO ₂ .	34
Figure 1.20: 2,4-DNP-Co(III)-salen complex bearing Lewis basic substituents for PO/CO ₂ copolymerization and CHO/PO/CO ₂ terpolymerization.	35
Figure 1.21: Co-TTMAPP-I ₄ bifunctional complexes used as catalysts for PO/CO ₂ coupling to produce cyclic carbonate.	36
Figure 1.22: Bifunctional Co(III)-salen complexes with appended <i>n</i> -propyl-NEt ₃ Me ⁺ and <i>n</i> -propyl-NCy ₂ Me ⁺ quaternary ammonium salts.	38
Figure 1.23: Proposed epoxide activation pathways by a nucleophilic co-catalyst for binary (A) and bifunctional (B) catalyst systems.	39

Figure 1.24: <i>Rac</i> -salen-Co(III)-NO ₃ complex used as a catalyst for terpolymerization of 4-vinylcyclohexene oxide (VCHO)/PO/CO ₂ .	42
Figure 1.25: Chromium-salan complexes for coupling of epoxides and CO ₂ .	45
Figure 1.26: [ONSO]-Cr(III) complexes for copolymerization of CO ₂ and CHO.	46
Figure 1.27: Original salen-Cr(III)/DMAP binary catalyst system.	46
Figure 1.28: Reaction profile for production of PC from CO ₂ and propylene oxide.	48
Figure 1.29: Epoxides compared by Darensbourg and co-workers for reactivity in copolymerization reactions with CO ₂ .	48
Figure 1.30: Bifunctional (1.22b) salen-Cr(III) and binary (1.23b) salen-Cr(III) complexes used as catalyst for coupling reactions of isobutene oxide, 2,3-epoxy-2-methylbutane and <i>cis</i> and <i>trans</i> 2-butene oxide and CO ₂ .	49
Figure 1.31: Mono- and dinuclear salen-Cr(III)-X catalyst used for synthesis of polycarbonates from CHO/CO ₂ copolymerization and CHO/CO ₂ /PA terpolymerization.	52
Figure 1.32: (Salophen)Cr(III)X analogs reported by North and co-workers.	54
Figure 1.33: Cr(III) N ₄ -pyridine-carboxamide complexes for coupling of CO ₂ with CHO or PO.	55
Figure 1.34: Cr(III) hexacoordinate complexes reported by Bulto and co-workers for coupling CO ₂ and CHO. Ar = 2,4-di- <i>tert</i> -butyl phenol.	57
Figure 1.35: Most active Cr(III)-iminopyrrole and Cr(III)-acac-aminopyrrole complexes reported by Duchateau and co-workers for CHO/CO ₂ coupling reactions.	58
Figure 1.36: Porphyrin-Cr(III) complexes used as catalyst in CO ₂ /epoxide coupling reactions.	60

Figure 1.37: Various Cr(III) amino-bis(phenolate) complexes used for copolymerization of CO ₂ and CHO.	62
Figure 1.38: [OSSO]Cr(III)X complexes used for copolymerization of 4-vinylcyclohexene oxide and CO ₂	64
Figure 1.39: Bimetallic salen-Co(III)Cl complexes and co-catalysts used for ROP of propylene oxide.....	68
Figure 1.40: Aluminium-based metal complexes used as catalyst for ROP of epoxides.	69
Figure 1.41: Alcohol/Phosphazene active species for ROP of styrene oxide.....	71
Figure 2.1: Examples of epoxides used in CO ₂ /epoxide cycloaddition reactions for cyclic carbonate synthesis and their commonly used abbreviations.	84
Figure 2.2: ¹ H NMR spectrum of complex 2.6a with expanded aromatic region (insert).	91
Figure 2.3: Partially labelled molecular structure of compound 2.9a . Thermal ellipsoids are drawn at 50% probability with hydrogens and co-crystallized dichloromethane molecule omitted for clarity.....	94
Figure 2.4: Chloride-bridged dimer of 2.8e observed during MALDI-TOF MS analysis (<i>m/z</i> 1123.7).	100
Figure 3.1: Partially labelled asymmetric unit of the molecular structure of compound 3.1 (left), and a line drawing showing connectivity (right). Dashed lines in drawing show where the asymmetric unit connects to the adjacent unit to form a hexacobalt complex. Thermal ellipsoids are drawn at 10% probability with hydrogens omitted for clarity..	125

Figure 3.2: In situ FTIR reaction profile of polycarbonate (green) and cyclic carbonate (red) formation resulting from bands at 1751 and 1804 cm^{-1} , respectively. Inset: three-dimensional stack plot collected every 60 s for Table 3.1 entry 7.....	127
Figure 3.3: Magnified section (m/z 3120 – 3570) of the MALDI-TOF mass spectrum of PCHC obtained in Table 3.1, entry 1.....	133
Figure 3.4: Magnified MALDI-TOF mass spectrum (low mass region, m/z 1860 – 2160) of PCHC obtained from Table 3.1, entry 9. Calculated mass fragments (below observed spectrum) and proposed polymer structures shown.....	134
Figure 3.5: Magnified MALDI-TOF mass spectrum (higher mass region, m/z 3310 – 4010) of PCHC obtained from Table 3.1, entry 9. Calculated mass fragments (below observed spectrum) and proposed polymer structures shown.	135
Figure 4.1: MALDI-TOF mass spectrum of 4.1 in positive reflectron mode showing a comparison between experimental and calculated isotopic patterns.	151
Figure 4.2: Proposed equilibrium for 4.1 . (a) orange-brown color shown in toluene which is most likely the ionic complex and (b) a green color shown in THF for the neutral complex.....	153
Figure 4.3: Observed fragments of 4.1 and DMAP using MALDI-TOF MS in positive reflectron mode and negative mode (F5).....	154
Figure 4.4: Partially labelled molecular structure of compound 4.1'' . Thermal ellipsoids are drawn at 50% probability with hydrogens (except H(2)) and co-crystallized solvent molecule omitted for clarity.....	156
Figure 4.5: Representative crude ^1H NMR spectrum of PCHO in CDCl_3 taken immediately after stopping reaction.....	159

Figure 4.6: Profile for in situ monitored FTIR absorbance at 1089 cm^{-1} with overlaid three-dimensional stacked plot.	160
Figure 4.7: Plot of (A) $[\text{CHO}]$ vs time, (B) $L_n([\text{CHO}]_0/[\text{CHO}]_t)$ vs time and (C) $\{1/[\text{CHO}]_t - 1/[\text{CHO}]_0\}$ vs time for solvent-free ROP of CHO at $40\text{ }^\circ\text{C}$	165
Figure 4.8: (A) Plots of conversion vs. time for linear portion of PCHO formation at different temperatures. $22\text{ }^\circ\text{C}$: $y = 0.0039x$, $R^2 = 0.9823$, $40\text{ }^\circ\text{C}$: $y = 0.0147x$, $R^2 = 0.9944$, $60\text{ }^\circ\text{C}$: $y = 0.1172$, $R^2 = 0.9969$, $80\text{ }^\circ\text{C}$: $y = 0.2866x$, $R^2 = 0.9943$. (B) Arrhenius plot PCHO formation. k_{obs} represent the slopes of first-order plots at various temperatures. Linear regression fit shown with equation: $y = -8249.4x + 21.835$, $R^2 = 9752$	167
Figure 4.9: Plot of number-average molecular weight (M_n) vs % conversion of CHO for ROP using 4.1 at $60\text{ }^\circ\text{C}$	169
Figure 5.1: Various Cr(III) complexes used as catalyst for reactions of CO_2 with epoxides.	183
Figure 5.2: MALDI-TOF mass spectrum of 5.1 collected in positive reflectron mode, showing higher mass region and proposed Cr(III) complex fragments.....	187
Figure 5.3: Partially labelled molecular structure of μ -hydroxo-bridged 5.1a . Thermal ellipsoids are drawn at 50% probability with hydrogens and co-crystallized acetonitrile molecule omitted for clarity.....	189
Figure 5.4: Partially labelled molecular structure of chloride-bridged 5.1b . Thermal ellipsoids are drawn at 50% probability with hydrogens and co-crystallized dichloromethane molecule omitted for clarity.	191
Figure 5.5: Profiles for in situ monitored FTIR absorbances 1749 cm^{-1} (PCHC) and 2339 cm^{-1} (CO_2) with overlaid three-dimensional stack plot.	194

Figure 5.6: Profiles of absorbance vs time at the initial stages of CHO/CO ₂ copolymerization using 5.1 co-catalyzed by PPNN ₃ (solid red), DMAP (dotted green), PPNNCl (dashed blue) and 2 equiv. of PPNN ₃ (long-dashed black).	196
Figure 5.7: Observed fragments of 5.1 /PPNN ₃ using ESI-TOF MS in negative reflectron mode at various ratios.	197
Figure 5.8: Partially labelled molecular structure of 5.2 . Thermal ellipsoids are drawn at 50% probability with hydrogens (except for aquo ligand) and co-crystallized dichloromethane omitted for clarity.....	198
Figure 5.9: Magnified MALDI-TOF mass spectrum (higher mass region, m/z 10350 – 12250) of PCHC obtained from Table 5.1, entry 2. Proposed polymer structure shown.	201
Figure 5.10: Magnified MALDI-TOF mass spectrum (higher mass region, m/z 8040 – 10250) of PCHC obtained from Table 5.1, entry 3. Proposed polymer structures shown.	202
Figure 5.11: Normalized absorbance vs time plots for linear portion of reaction profile showing growth of absorbance of the polycarbonate carbonyl C=O band at 1750 cm ⁻¹ , for copolymerization of CHO/CO ₂ using 5.1 /PPNN ₃ . Best fit linear regression lines produced relative rates (r_{obs}) of 0.00504 (0.05 mol%, X), 0.00795 (0.1 mol%,▲), 0.0147 (0.2 mol%, ■) and 0.0299 (0.4 mol%, ●).....	204
Figure 5.12: Plot of $\ln(r_{\text{obs}})$ against $\ln[\mathbf{5.1}]$ for copolymerization of CHO/CO ₂ . Equation of linear regression: $y = 0.859x + 2.789$, $R^2 = 0.9909$	204
Figure 6.1: Co and Cr amino-bis(phenolate) complexes discussed in this chapter.	215

Figure 6.2: Profiles for in situ monitored FTIR absorbances at 1745 cm^{-1} (PCHC) and 1809 cm^{-1} (CHC) for CHO/CO₂ copolymerization over 24 h using **3.1**/PPNCl.217

Figure 6.3: UV-vis spectra of **4.1** in dichloromethane with various ratios of THF added.
.....220

List of Abbreviations and Units

(°): degrees

[2,4-DNP][−] or DNP: 2,4-dinitrophenolate

1,4-CHDO: 1,4-cyclohexadiene oxide

2,4-DNP: 2,4-dinitrophenol

2,4-DNP-Co-salen: 2,4-dinitrophenolate cobalt salen complex

4-NP: 4-nitrophenol

Å: Ångstrom (10^{-10} m)

AGE: allyl glycidyl ether

ATR: attenuated total reflectance (spectroscopy)

bhqba: bis(hydroxyquinoline)butylamine

BDC: benzenedicarboxylate

BEP: 1-benzyloxycarbonyl-3,4-epoxypyrrolidine

BG: benzyl glycidate

BGE: benzyl glycidyl ether

BINOL: 1,1'-bi-2-naphthol

BO: 1-butene oxide

BPA: 2,2-bis-(4-hydroxyphenyl)propane

Bu₄N⁺: tetrabutylammonium

CDCl₃: deuterated chloroform

CFCs: chlorofluorocarbons

CHC: cyclohexene carbonate

CHDO: cyclohexadiene oxide

CHO: cyclohexene oxide

conv.: conversion

CXO: 3,5,8-trioxabicyclo[5.1.0]octane

\bar{D} : dispersity (M_w/M_n)

DDT: dichlorodiphenyltrichloroethane

DHBA: dihydrobenzoic acid

DHC: dihydrocoumarin

DMAP: 4-(dimethylamino)pyridine

DMC: dimethyl carbonate

DPC: diphenyl carbonate

DSC: differential scanning calorimetry

E_a : activation energy

ECH: epichlorohydrin

ESI: electrospray ionization

EWG: electron-withdrawing groups

FTIR: fourier transform infrared (spectroscopy)

GC: gas chromatography

GHG: greenhouse gases

GPC: gel-permeation chromatography

GWP: Global Warming Potential

h: hour

HKR: hydrolytic kinetic resolution

HMDSO: hexamethyldisiloxane

HPLC: high-performance liquid chromatography

Hz: hertz

K: Kelvin

m/z : mass to charge ratio

MALDI-TOF: matrix-assisted laser desorption/ionization

min: minute

mL: milliliter (10^{-3} L)

M_n : number average molecular weight

MOFs: metal-organic frameworks

MPa: megapascal (10 bar or 145 psi)

MPOAP: modified poly(aniline-co-o-aminophenol)

MS: mass spectrometry

Mt: metric tonne

M_w : weight average molecular weight

NMR: nuclear magnetic resonance (spectroscopy)

NR: not recorded

OBzF₅: pentafluorobenzoate

PA: phthalic anhydride

PAA: poly(acrylic acid)

PC: propylene carbonate

PCHC: poly(cyclohexene carbonate)

PCHO: poly(cyclohexene oxide)

PEG: polyethylene glycol

PEO: polyethylene oxide

PGAC: poly(glyceric acid carbonate)

PGE: phenylglycidyl ether

PO: propylene oxide

PPA: 3-phenyl-1-propanol

PPC: poly(propylene carbonate)

PPG: polypropylene glycol

PPNCl: (bis(triphenylphosphine)iminium chloride)

rac: racemic

ROP: ring-opening polymerization

salan: *N,N'*-bis(phenolato)-1,2-diaminoethane

salen: *N,N'*-bis(salicylidene)-ethylenediamine

salophen: *N,N'*-bis(salicylidene)-1,2-phenylenediamine

SO: styrene oxide

TAML: tetraamidomacrocyclic ligand

TaxEDA: triethylaluminum adduct of (2-dibenzylamino)ethoxydiethylaluminum

TBAB: tetrabutylammonium bromide

TBAF: tetrabutylammonium fluoride

TBD: 1,5,7-triazabicyclo[4.4.0]dec-5-ene

TEA: triethylaluminum

TFA: trifluoroacetate

T_g : glass transition temperature

THF: tetrahydrofuran

TO: turnovers

TOF: turnover frequency

TON: turnover number

TFPP: 5,10,15,20-tetrafluorophenylporphyrin

TPP: 5,10,15,20-tetraphenylporphyrin

Ts: *p*-toluenesulfonyl

TTMAPP-I₄: tetra(trimethylphenylammonium iodide)porphyrin

UV-vis: ultraviolet-visible (spectroscopy)

VCHO: 4-vinylcyclohexene oxide

VIO: vinyl oxide

VOC: volatile organic compound

vs: versus

yr: years

List of Appendices

Figure A - 1: Stacked ^{13}C NMR spectra of 2.6a and proligand H₂L2 in CDCl_3	231
Figure A - 2: Representative ^1H NMR spectrum of 2.8a	232
Figure A - 3: Representative ^1H NMR spectrum of 2.9a in CDCl_3	233
Figure A - 4: Representative ^1H NMR spectrum of 2.6b in CDCl_3	234
Figure A - 5: Representative ^1H NMR spectrum of 2.8b in CDCl_3	235
Figure A - 6: Representative ^1H NMR spectrum in CDCl_3 of aliquot taken immediately after reaction (Table 2.1, entry 5). % Conversion = integration of cyclic carbonate methine multiplet (1.08 at 4.88 ppm) divided by the sum of cyclic carbonate methine multiplet (1.08 at 2.99 ppm) and monomer (1.00 at 2.99 ppm).....	236
Figure A - 7: Representative ^1H NMR spectrum in CDCl_3 of aliquot taken immediately after reaction (Table 2.1, entry 10).	237
Figure A - 8: Representative ^1H NMR spectrum in CDCl_3 of aliquot taken immediately after reaction (Table 2.1, entry 11).	238
Figure A - 9: Representative ^1H NMR spectrum in CDCl_3 of aliquot taken immediately after reaction (Table 2.1, entry 12).	239
Figure A - 10: Representative ^1H NMR spectrum in CDCl_3 of aliquot taken immediately after reaction (Table 2.1, entry 13).	240
Figure A - 11: Representative ^1H NMR spectrum in CDCl_3 of aliquot taken immediately after reaction (Table 2.1, entry 14).	241
Figure A - 12: Representative ^1H NMR spectrum of aliquot taken immediately after reaction (Table 3.1, entry 7) in CDCl_3 . % Conversion = integration of polymer/cyclic	

carbonate peaks (11.37 at 4.89 – 4.52 ppm) divided by the sum of cyclic carbonate/polymers (11.37 at 4.89 – 4.52 ppm) and monomer (1.00 at 3.12 ppm).....242

Figure A - 13: Representative ^{13}C NMR spectrum of aliquot taken immediately after reaction (Table 3.1, entry 1) in CDCl_3 . Syndiotactic and isotactic diads observed at 153.2 and 153.8 ppm respectively. Integration ratios of 1:1 suggests atactic polymer.243

Figure A - 14: Representative ^1H NMR spectrum of isolated cyclohexene carbonate in CDCl_3 . Peak at 4.71 ppm represents methine protons from *cis* isomer whereas multiplet at 4.02-4.07 ppm represents that of *trans* isomer.....244

Figure A - 15: Representative ^{13}C NMR spectrum of isolated cyclohexene carbonate in CDCl_3 . Peaks at 23.14, 28.16 and 83.55 ppm correspond to carbons from *trans*-CHC and the more intense counterparts (19.10, 26.70 and 75.8 ppm) correspond to *cis*-CHC. Signal at 155.4 ppm corresponds to the carbonyl carbon from both isomers.245

Figure A - 16: Representative crude ^{13}C NMR spectrum of PCHO in CDCl_3 from Table 4.1, entry 12 with enlarged area showing characteristic polymer signal (23.28, 30.08, 70.62, 73.48 and 78.77 ppm).246

Figure A - 17: Representative crude ^1H NMR spectrum of PCHC in CDCl_3 from Table 5.1, entry 1 with enlarged area showing characteristic polymer signal (4.66 and 4.61 ppm).247

Figure A - 18: Representative crude ^{13}C NMR spectrum of PCHC in CDCl_3 from Table 5.1, entry 1 with enlarged area showing characteristic polymer syndiotactic and isotactic diads (153.8 and 153.3 ppm respectively).248

Figure B - 1: MALDI-TOF mass spectrum of **2.9a**.249

Figure B - 2: MALDI-TOF mass spectrum of 2.6b	250
Figure B - 3: MALDI-TOF mass spectrum of 2.8b	251
Figure B - 4: MALDI-TOF mass spectrum of 2.6c	252
Figure B - 5: MALDI-TOF mass spectrum of 2.8c	253
Figure B - 6: MALDI-TOF mass spectrum of 2.6d	254
Figure B - 7: MALDI-TOF mass spectrum of 2.8d	255
Figure B - 8: MALDI-TOF mass spectrum of 2.6e	256
Figure B - 9: MALDI-TOF mass spectrum of 2.8e	257
Figure B - 10: MALDI-TOF mass spectrum of 2.6f	258
Figure B - 11: MALDI-TOF mass spectrum of 3.1 and comparison to calculated isotopic pattern.	259
Figure B - 12: MALDI-TOF mass spectrum of polycarbonate obtained from Table 1, entry 1.	260
Figure B - 13: MALDI-TOF mass spectrum of polycarbonate obtained from Table 1, entry 9.	261
Figure B - 14: Expanded MALDI-TOF mass spectrum of polycarbonate obtained from Table 1, entry 9.	262
Figure B - 15: MALDI-TOF mass spectrum of 4.1 in negative reflectron mode.....	263
Figure B - 16: MALDI-TOF mass spectrum of 4.1 /DMAP in positive reflectron mode. Ratio of Cr to DMAP is 1:4.	264
Figure B - 17: MALDI-TOF mass spectrum of 4.2 in positive reflectron mode.....	265
Figure B - 18: MALDI-TOF mass spectrum of 4.2 in negative reflectron mode.....	266
Figure B - 19: MALDI-TOF mass spectrum of 4.3 in positive reflectron mode.....	267

Figure B - 20: MALDI-TOF mass spectrum of 4.3 in negative reflectron mode.....	268
Figure B - 21: MALDI-TOF mass spectrum of 4.4 in positive reflectron mode.....	269
Figure B - 22: MALDI-TOF mass spectrum of 4.4 in negative reflectron mode.....	270
Figure B - 23: MALDI-TOF mass spectrum of 5.1 in positive reflectron mode showing complex monomeric fragments.....	271
Figure B - 24: MALDI-TOF mass spectrum of 5.1 in negative reflectron mode.....	272
Figure B - 25: MALDI-TOF mass spectrum of polycarbonate obtained from Table 5.1, entry 2.	273
Figure B - 26: MALDI-TOF mass spectrum of polycarbonate obtained from Table 5.1 entry 3.	274
Figure B - 27: MALDI-TOF mass spectrum of 4.1 /DMAP in negative reflectron mode. Ratio of Cr to DMAP is 1:4.	275
Figure C - 1: Partially labelled molecular structure of compound 2.9a . Thermal ellipsoids are drawn at 50% probability with hydrogens and co-crystallized dichloromethane molecule omitted for clarity.....	279
Figure C - 2: Partially labelled molecular structure of compound 3.1 . Thermal ellipsoids are drawn at 10% probability. Structure of the asymmetric unit shown, and hydrogens omitted for clarity.	280
Figure C - 3: Hexacobalt cluster of 3.1 showing inner cavity formed by hydrogen bonding.	281
Figure C - 4: Partially labelled molecular structure of compound 4.1'' . Thermal ellipsoids are drawn at 50% probability with hydrogens (except H(2)) and co-crystallized solvent molecule omitted for clarity.....	288

Figure C - 5: Partially labelled molecular structure of 5.1a . Thermal ellipsoids are drawn at 50% probability with hydrogens and co-crystallized acetonitrile molecule omitted for clarity.	289
Figure C - 6: Partially labelled molecular structure of 5.1b . Thermal ellipsoids are drawn at 50% probability with hydrogens and co-crystallized dichloromethane molecule omitted for clarity.....	290
Figure D - 1: Representative DSC second heating curve of polymer produced by 5.1/PPNN₃ for copolymerization of CHO/CO ₂	294
Figure D - 2: Representative DSC second heating curve of polymer produced by 5.1/PPNN₃ for terpolymerization of CHO/PO/CO ₂ (Table 6.2, entry 2).....	295
Figure D - 3: Representative DSC second heating curve of polymer produced by 5.1/PPNN₃ for terpolymerization of CHO/PO/CO ₂ (Table 6.2, entry 3).....	296
Figure D - 4: Representative DSC second heating curve of polymer produced by 5.1/PPNN₃ for terpolymerization of CHO/PO/CO ₂ (Table 6.2, entry 4).....	297
Figure D - 5: Representative DSC second heating curve of polymer produced by 5.1/PPNN₃ for terpolymerization of CHO/ECH/CO ₂ (Table 6.2, entry 6).	298

Chapter 1: Introduction

1.1 Green chemistry

1.1.1 Brief introduction to green chemistry principles

With its inception about 25 years ago, Green Chemistry is essentially the design, manufacture and application of chemical products guided by a set of twelve principles with an overall goal of reducing or eliminating the use or generation of hazardous substances.^{1,2} Several publicized infamous chemical-related disasters resulting in environmental damage and pollution, such as the ‘burning’ Cuyahoga River, Bhopal chemical plant disaster, the Love Canal waste disposal disaster and also bioaccumulation of dichlorodiphenyltrichloroethane (DDT), have led to the development of this initiative, to help prevent future occurrences.³

Since that time, there has been widespread international interest resulting in hundreds of programs and governmental initiatives on Green Chemistry.¹ A few of the leading initiatives have been facilitated by the United States, United Kingdom and Italy.⁴ These initiatives include the US Presidential Green Chemistry Challenge Awards which were established in 1995, the Green Chemistry Institute, which was founded in 1997, and more importantly, the Royal Society of Chemistry journal, *Green Chemistry*, in 1999.¹ Many universities now have programs dedicated to Green Chemistry. According to Paul Anastas, the most important aspect of Green Chemistry is the concept of intentional green design rather than accidental discovery. With a goal of achieving sustainability at a molecular level, Green Chemistry has been applied to many sectors in industry including

the aerospace, automobile, cosmetics, electronics, energy, household product, pharmaceutical, agriculture and other industries.¹ The large impact of Green Chemistry has been realized due to the fact that its principles and advances went beyond the laboratory and influenced industries, education, the environment and the general public.² Because of the significant contribution from Green Chemistry, chemists have shown to potentially design next-generation products and processes which are profitable and simultaneously beneficial for human health and the environment.

There are twelve principles which define Green Chemistry and govern the criteria of the framework for sustainable design of products and processes.¹⁻³ It would be very difficult to simultaneously abide by all twelve principles when designing chemicals or reactions. As a result, there are several principles strongly adhered to in this research which include: (1) prevention, (2) atom economy, (5) safer solvents and auxiliaries, (7) use of renewable feedstocks and (9) catalysis. These will be discussed further throughout this thesis but it is important to note that these principles and other strategies used also lead to reduced waste production. E.g. solvent-free reactions which means less solvent waste for disposal after reaction workup. Atom economy is prevalent in most of the catalytic reactions performed; essentially, 100% of the atoms from reactants end up in useful products and not unwanted products from side reactions. In ligand synthesis within this thesis, solvents such as ethanol and water were used. Apart from the flammability and VOC (volatile organic compound) nature of ethanol, water and ethanol can be generally considered as safe solvents.⁵ The metal-based coordination complexes designed and synthesized in this research were used as catalysts. Often used in low loadings, catalytic

reagents are advantageous of over stoichiometric reagents (equimolar or even excess amounts) and result in less waste generation because they promote increased selectivity to the desired product. Catalyzed processes also generally require less energy input and proceed via different and faster reaction pathways.^{2,6} Renewable feedstocks are a potential alternative to fossil fuel derivatives and also reduce the burden on this limited resource.^{2,3} Common renewable feedstocks include non-animal, land-based biomass such as lignin, while others can be ocean-sourced such as shellfish waste. However, there are non-living renewable feedstocks such as carbon dioxide (CO₂), which is showing and increase in popularity.

1.1.2 Carbon dioxide utilization as a renewable feedstock

The anthropogenic greenhouse effect is essentially an amplification of the natural phenomenon due to increased atmospheric levels of greenhouse gases (GHG) such as CO₂, N₂O, CH₄ and various CFCs. Increased anthropogenic activities such as fossil fuel combustion has led to an increase in atmospheric CO₂ concentrations and is believed to be linked to climate change.³ According to the US National Oceanic & Atmospheric Administration, the concentration of CO₂ in the atmosphere is now above 400 ppm; circa 100 ppm more than the pre-industrial era thus making CO₂ the most abundant greenhouse gas present in the earth's atmosphere (**Figure 1.1**).^{3,7}

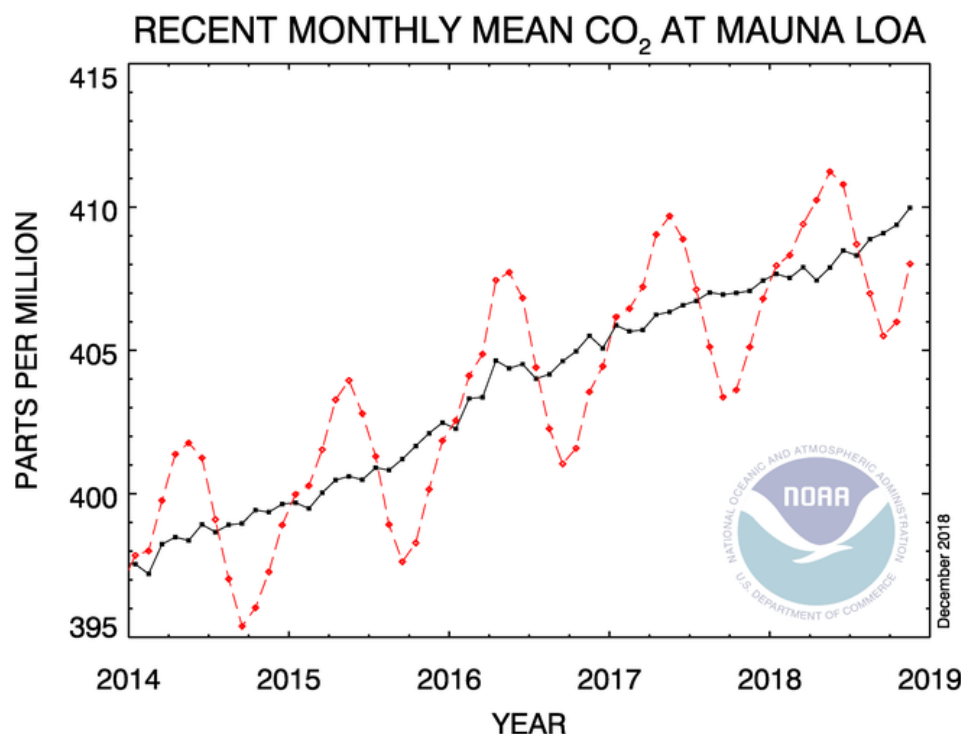


Figure 1.1: Trends in CO₂ atmospheric concentration. Dashed line represents mid-month mean values whereas continuous line represents the same but with correction applied.⁷

With a Global Warming Potential (GWP) of 1, CO₂ (reference GHG for GWP listings) is not the most effective greenhouse gas (compared to methane, GWP of 56) but it is the second most abundant (second to water vapor) and it is this combination that makes it very effective towards increasing the Earth's temperature.³ Due to this fact as well as properties such as non-flammability and non-toxicity (at low concentrations), researchers have targeted the chemical utilization of carbon dioxide.⁸

Carbon dioxide in its natural gaseous state is very stable; it has a highly negative Gibbs Energy of formation (ΔG_f), $-394.01 \text{ kJ mol}^{-1}$.⁹ It also possesses carbon in its highest possible oxidation state.⁹ To overcome this energy barrier and utilize CO₂, either a direct

input of physical energy or the use of reactive chemical species such as catalysts and/or other reagents can be applied.⁹ This research uses transition metal coordination compounds as catalysts for CO₂ activation in reactions with epoxides.

There are several processes that involve the utilization of CO₂, some of which have resulted in industrialization and others, although very promising, have remained in the research phase. Some industrialized processes include urea production (146 Mt produced in 2008), methanol production (20 Mt produced in 2007), salicylic acid production in the Kolbe-Schmitt reaction (170 kt/yr) and inorganic carbonates (30 Mt/yr).⁸ According to De-Falco et al., current research areas for CO₂ utilization fall under three main headings such as inorganic mineralization, organic carboxylation, reduction and biochemical conversion.⁸ A subdivision of organic carboxylation comprises reactions involving the incorporation of whole CO₂ molecules into organic backbones to produce functional groups such as –COOR (carboxylates, esters), –NCO (isocyanates or ureas) and –RO–CO–OR (carbonates), **Figure 1.2**.^{8,10} An area of CO₂ research with increasing popularity is coupling of CO₂ with epoxides to produce either cyclic carbonates via a cycloaddition reaction, or polycarbonates via copolymerization. These reactions are collectively known as coupling reactions.

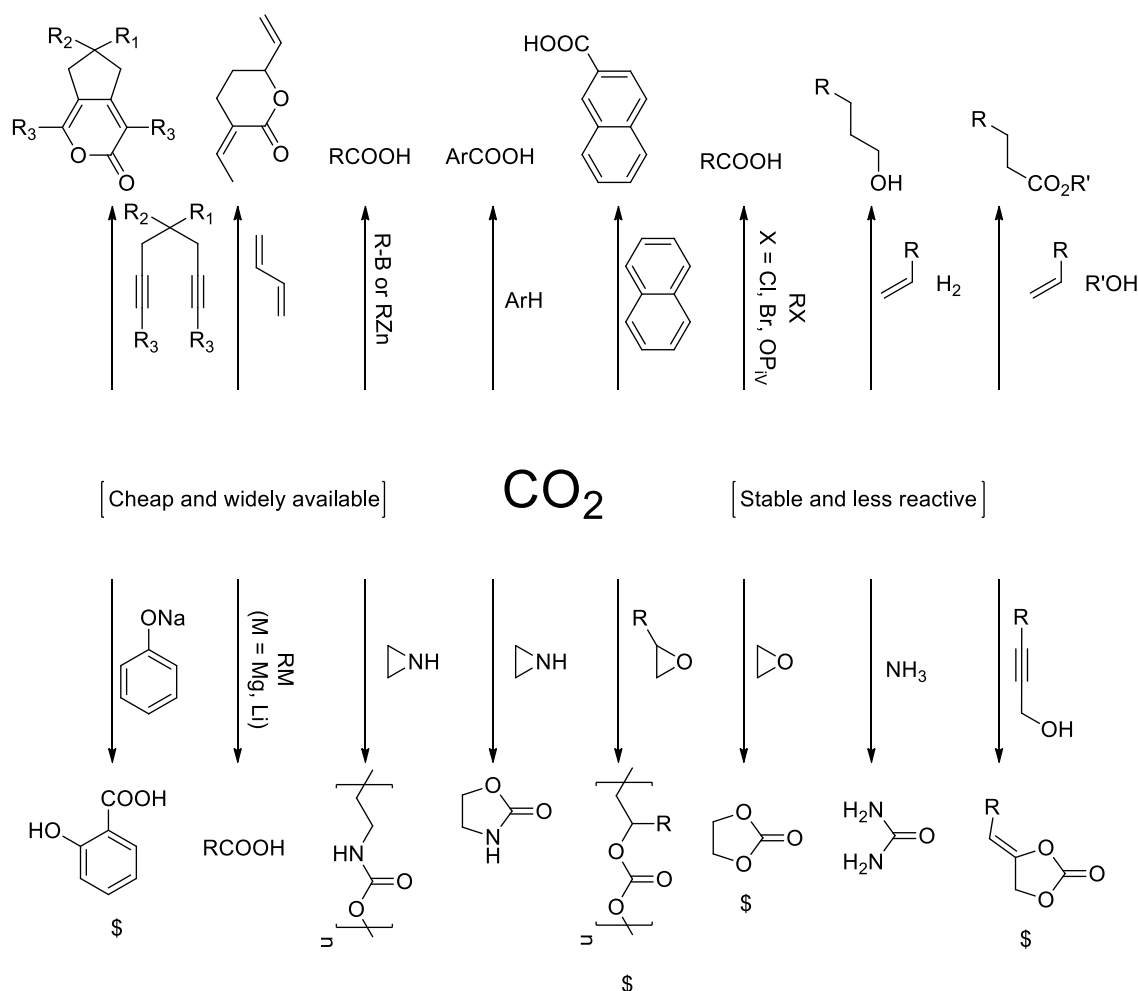
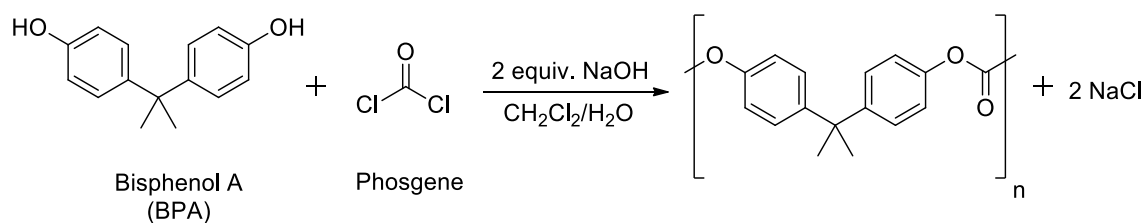


Figure 1.2: Some chemical processes involving CO₂ utilization for synthesis of potentially useful organic molecules.¹⁰ \$ = industrialized processes. Modified from RightsLink®: Springer Nature, Nature Communications, Q. Liu, L. Wu, R. Jackstell and M. Beller, *Nat. Commun.*, 2015, **6**, 5933-5947, Copyright 2015.

1.1.3 Overview on polycarbonate synthesis

First industrialized by Bayer AG in 1958, the phosgene process is used to produce bisphenol-A (BPA) polycarbonate, which is an interfacial polycondensation reaction between phosgene and diols. The trivial name bisphenol-A was derived from the reagents used in its synthesis which are phenol and acetone (“-A” referring to acetone).¹¹ More specifically, the polymerization of 2,2-bis-(4-hydroxyphenyl)propane (BPA) and

phosgene (**Scheme 1.1**) gas is carried out in a biphasic solvent system such as water and dichloromethane where polycondensation happens at the interface of the two phases, which is promoted by strong agitation. There is a preference for the use of dichloromethane as a solvent due to the high solubility of polycarbonate in dichloromethane.¹² The main reaction happens in two steps. The di-sodium salt of BPA (formed from an initial reaction with sodium hydroxide) is phosgenated to form chloroformates of BPA; a catalyzed polycondensation of the BPA-chloroformates produces polycarbonate in a dichloromethane solution.¹² Catalysts such as tertiary amines or quaternary ammonium salts are employed for this process.



Scheme 1.1: Synthesis of polycarbonate using phosgene and BPA.

Like most industrialized processes, this one possesses several drawbacks which raise several environmental and economical concerns with the process and product. Therefore consumer pressure toward sustainable materials is one of many driving forces for an alternative route to polycarbonate synthesis. For example, there are certain endocrine disruptor pathways associated with BPA, and phosgene is so highly toxic (once used as a chemical weapon) that it is severely restricted worldwide.^{12,13} Furthermore, the process is far more complicated than illustrated in **Scheme 1.1**, in terms of product processing and waste treatment before disposal (**Figure 1.3**).

Large amounts of the highly toxic and corrosive phosgene gas (about 2 tons per ton of produced polycarbonate) is used which puts restrictions on the process.¹² Furthermore, copious amounts of dichloromethane are used, which in itself is a potential carcinogen with a low boiling point (39.7 °C), thus making it difficult to contain, especially during solvent evaporation for polymer isolation. The wastewater generated from washing of the dichloromethane/polymer solution contains contaminants such as unreacted di-sodium BPA salts, NaCl, catalyst and low molecular weight polymers. This wastewater also requires treatment before discharging from the factory, which is energetically costly. Quantities of water can reach as high as 100 times the weight of produced pure polycarbonate. There is also an issue of unavoidable chlorinated contaminants in the final polymer product, which is believed to affect the polymer properties¹²

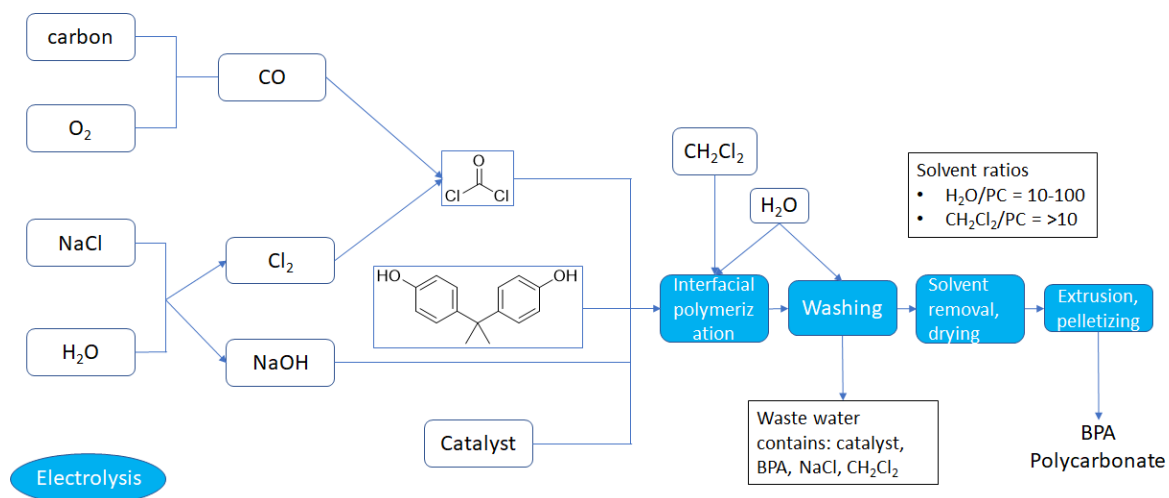


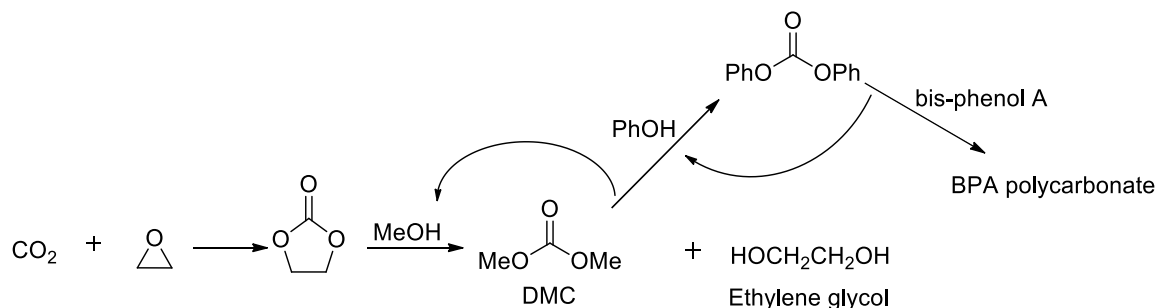
Figure 1.3: Phosgene process for production of polycarbonate (PC).¹²

Despite the few drawbacks above, BPA-polycarbonate possesses properties such as a comfortable usable temperature range of $-40\text{ }^{\circ}\text{C}$ to $135\text{ }^{\circ}\text{C}$ (where it can undergo large plastic deformations before it cracks or breaks) and a glass transition temperature (T_g) of $149\text{ }^{\circ}\text{C}$, which makes it suitable for a wide variety of applications, thus resulting in it being the second largest used thermoplastic.^{12,14,15} This class of thermoplastics has other remarkable properties such as heat resistance, lightness, electrical insulation, transparency and high impact resistance.^{12,14,16,17} For instance, a polycarbonate with the trade name Makrolon® can be used in (1) construction (canopies, facades, security windows, shelter and skylights); especially shapes where glass would not be viable, (2) automotive industry (transparent and colored parts of vehicles), (3) medicine (injection systems and oxygenators) and (4) consumer products (safety goggles, ophthalmic lenses and large water bottles), just to name a few. These account for a worldwide demand of 3.6 million tons per year (as of 2011) for aromatic polycarbonates.^{14,18}

1.1.4 Catalytic coupling of CO₂ with epoxides

A remarkable advancement to the ‘phosgene’ process was developed by the Asahi-Kasei Corporation, which resulted in a novel process where phosgene was replaced with CO₂ to produce the same BPA-based polycarbonate (**Scheme 1.2**).^{8,12,19} A direct dehydration reaction between CO₂ and BPA to produce polycarbonate would be impractical for commercialization therefore Asahi-Kasei developed an indirect route that uses CO₂ and ethylene oxide (EO) as initial reagents followed by a few subsequent steps (final reaction with BPA) to produce BPA-PC (**Scheme 1.2**).¹² A phosgene-free route to high-purity polycarbonate would require diphenyl carbonate, DPC, (made from dimethyl

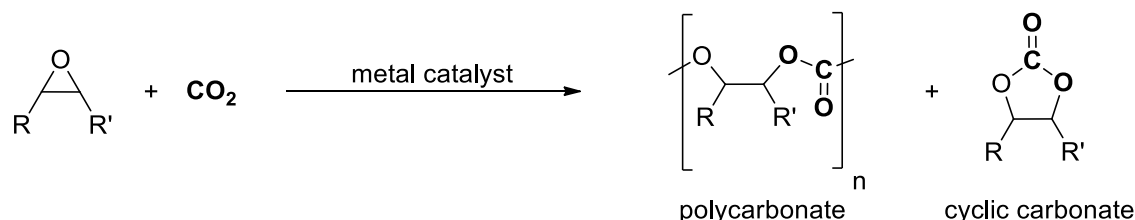
carbonate, DMC, and phenol) as a reagent for the polymerization step. For several years, this phosgene-free process was not industrialized because there lacked a viable procedure for highly pure DMC synthesis on a large scale and DPC was not available commercially. Previous DMC synthesis routes (ethylene carbonate plus methanol) suffered from problems such as requiring high temperature and pressure, and giving low yields due to oligomerization of starting materials and/or low equilibrium constant even at high methanol loading. Asahi-Kasei solved the equilibrium and purity problems associated with synthesis of these precursors. A new but simple catalyst system (Pd/C and NaI) was used for DMC production which solved purity problems (easy removal of catalyst by filtration) and a newly engineered/patented reactor with tandem distillation (of produced DPC), solved the equilibrium problem for DPC synthesis.¹² It is interesting to note that intermediate products are recycled (except for ethylene glycol which is a commonly used chemical hence can be sold). Even the CO₂ generated during ethylene oxidation can be used for carbonate formation).^{8,19} Furthermore, there are claims of no environmental drawbacks, there is no waste water and the molten polycarbonate produced is directly extruded without any purification.¹²



Scheme 1.2: Asahi-Kasei's phosgene free process for BPA-PC production.

Besides increased pressure for CO₂ utilization and consumer pressure for more sustainable polymers, another inspiration for this research is a potential alternative route to polycarbonate synthesis, and not as a replacement to the currently commercialized BPA/phosgene process (**Scheme 1.1**). As mentioned earlier, CO₂ is a very stable molecule, therefore transformations would require reactions with high-energy reagents such as epoxides or other molecules like aziridines (**Figure 1.2**)¹⁹ Contrary to the Asahi-Kasei process, direct coupling of CO₂ with epoxides can yield polycarbonate depending on the catalyst and reaction conditions (**Scheme 1.3**). As mentioned earlier, polycarbonates are useful for a wide variety of applications, but so far polycarbonates made strictly from CO₂ and epoxides have inferior properties compared to BPA-polycarbonate. However, other applications have been proposed such as films and packaging.⁹ There is a need for improvement of these properties and cost of production in order for a bigger impact. These mechanical properties are a result of the stereochemical nature of the linear carbonate linkage in the polycarbonate. Furthermore, the enantioselectivity of the polycarbonate and head-to-tail connectivity (formed from unsymmetrical monomers) are some factors which aid in determining the thermal stability and the mechanical properties which can be tuned when desired.¹⁷ Furthermore, improvement in catalyst activity, efficiency and selectivity are also needed, which in turn offers tremendous potential for polycarbonate production from epoxides and CO₂.⁹ Decreased selectivity affords the formation of cyclic carbonates that were once considered to be an unwanted by-product, but researchers have now found widespread applications for these products (**Scheme 1.3**). They can be used as organic synthetic

intermediates for fine chemicals, polar aprotic solvents for batteries/solar cells, precursor molecules for biomedical applications and raw materials for engineering plastics.^{10,20-22}



Scheme 1.3: Metal-catalyzed coupling of epoxides with CO₂ for polycarbonate or cyclic carbonate formation.

These CO₂ and epoxide coupling reactions are often catalyzed by systems containing metals such as aluminum,²³ chromium,²⁴ cobalt²⁵ and zinc²⁶ just to name a few.⁹ The focus of this thesis lies on cobalt and chromium-based complexes as catalyst for these CO₂ and epoxide coupling reactions. Typically, other species possessing good nucleophilic properties, are also employed and play a crucial role in CO₂/epoxide coupling reactions as co-catalysts; some examples include salts containing bulky cations thus affording a weak interaction with the anion and making it more reactive (e.g. Bu₄NBr and PPNX where X = Cl⁻ and N₃⁻) and 4-dimethylaminopyridine (DMAP).

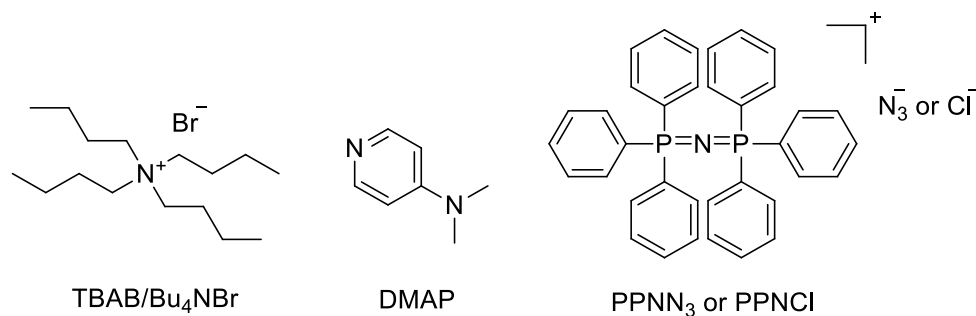
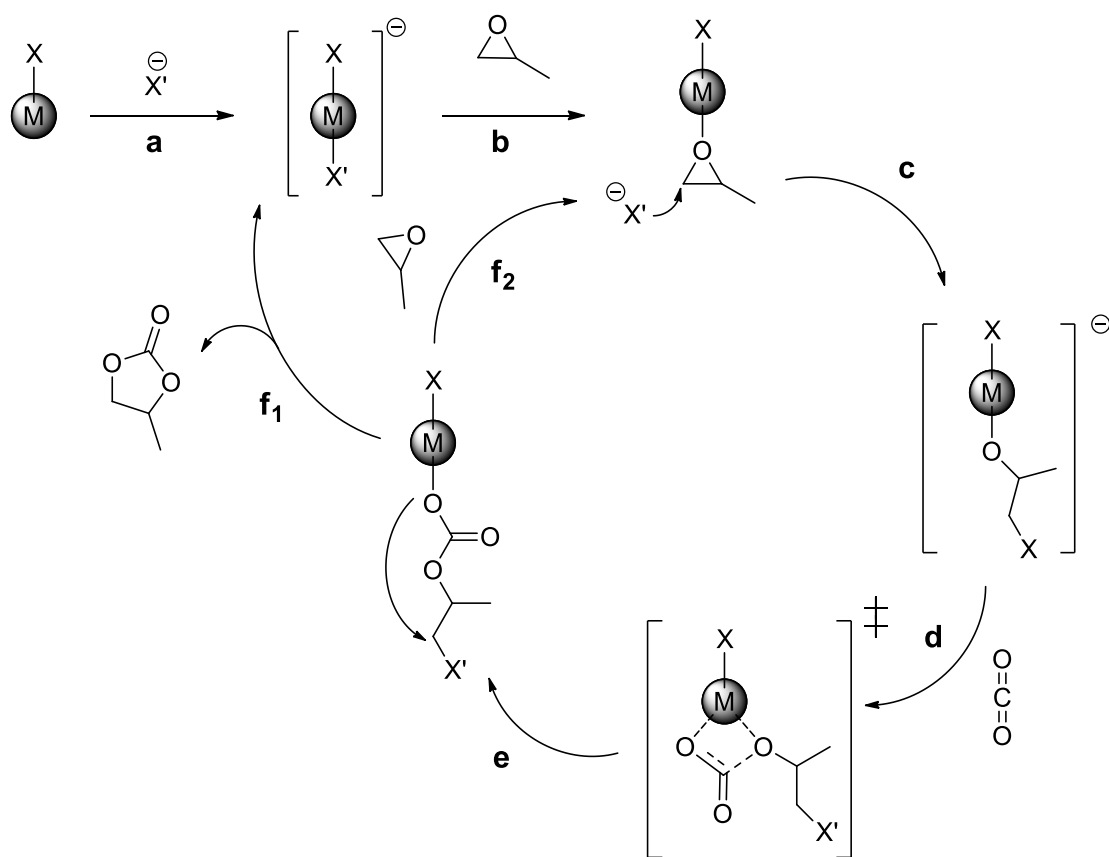
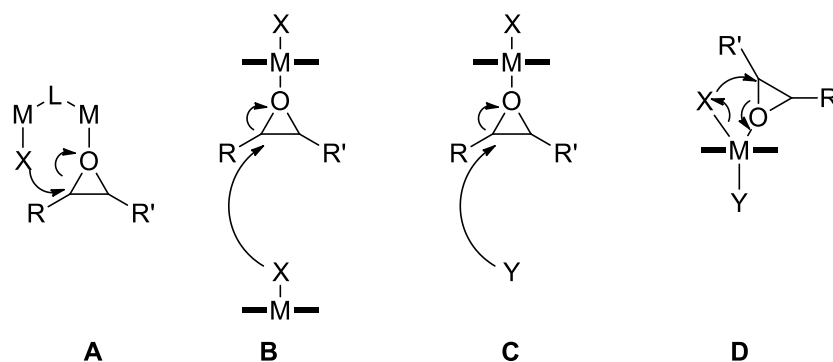


Figure 1.4: Commonly used co-catalysts for CO₂/epoxide coupling reactions.

A generalized mechanism representing the pivotal steps in the coupling of CO₂ and epoxides to yield either polycarbonate or cyclic carbonate is shown in **Scheme 1.4**. It is interesting to note that generally the rate-determining step for these reactions is not the CO₂-insertion step (**Scheme 1.4, step d**) which leads to the transition state, but the epoxide ring opening step (**Scheme 1.4, step c**). Also, the step following CO₂ insertion is crucial to the type of product; propagation (**Scheme 1.4, step f₂**) could occur thus leading to polymer formation or back-biting which leads to the formation of cyclic carbonate (**Scheme 1.4, step f₁**). Back-biting can occur following an S_N2 mechanism with stereochemical inversion, hence generating a specific isomer or an S_N1 mechanism with racemization to generate a mixture of isomers. The initiation step (**Scheme 1.4, steps a and b**) is also widely studied and several mechanisms for initiation have been proposed (**Figure 1.5**).²⁷



Scheme 1.4: General reaction mechanism for coupling epoxides (propylene oxide) with CO₂ to yield either polycarbonate or cyclic carbonate.¹⁹



L = ancillary ligand, co-ligand/initiator (e.g. acetate)
 Y = co-catalyst (e.g. PPNCl)
 —M— = salen/salan/porphyrin metal fragment

Figure 1.5: Different initiation pathways for CO₂/epoxide coupling reactions. (A) Dinuclear intramolecular mechanism. (B) Intermolecular dinuclear mechanism. (C) Metal catalyst/co-catalyst mononuclear mechanism. (D) Mononuclear intramolecular mechanism.²⁷

1.2 Brief history of metal-catalyzed coupling of CO₂ with epoxides

Al-based porphyrin complexes as well as Zn-based compounds were among the first catalysts reported for the co-polymerization of CO₂ with epoxides.²⁸ In the 1960s Inoue and co-workers at Kyoto University first reported the enantioselective homopolymerization of racemic propylene oxide (PO) using a zinc-based catalyst (made from reacting diethyl zinc and an optically active alcohol).¹⁶ Co-polymerization of PO and CO₂ was reported using a poorly defined heterogeneous catalyst system which was a 1:1 mixture of water and diethyl zinc (ZnEt₂) to give polypropylene carbonate (PPC) with a TOF of 0.12 h⁻¹ at 20-50 atm CO₂ and 80 °C; this was the first reported copolymer from CO₂ and epoxides.^{16,29} The first reported use of a homogeneous catalyst was reported by Takeda and Inoue in 1978. Aluminum tetraphenylporphyrin (TPP) complexes (in the presence of EtPh₃PBr as a co-catalyst) were active toward the copolymerization of both

PO and cyclohexene oxide (CHO) with CO₂. Polymers with molecular weights between 3500 and 6000 g mol⁻¹ were produced at a very slow rate over 13 days.⁹ Another major advance surfaced when Coates and co-workers reported a series of zinc β-diiminate complexes which demonstrated very high activity toward CHO and CO₂ copolymerization. One zinc β-diiminate analog demonstrated activity up to 729 TO h⁻¹ at 50 °C and 7 atm CO₂ pressure to produce monodisperse (dispersity, \bar{D} = 1.15) poly(cyclohexene carbonate) (PCHC) with carbonate linkages of 99% and molecular weight of 23.3 kg mol⁻¹. This molecular weight was about 4 times larger than those produced by Takeda and Inoue in 1978 for PCHC. Introduction of electron-withdrawing groups (EWG) on the catalyst increased activity up to 917 TO h⁻¹ at the same temperature and pressure. This was a remarkable improvement over the first reported catalyst system which had activity of 0.12 TO h⁻¹. Further studies with a similar analog produced an exemplary 2290 TO h⁻¹ producing polymer with up to 90% carbonate linkages.⁹ These are just a few chronological advancements in this area of research which is steadily gaining popularity, as evident in the growing number of publications (**Figure 1.6**).

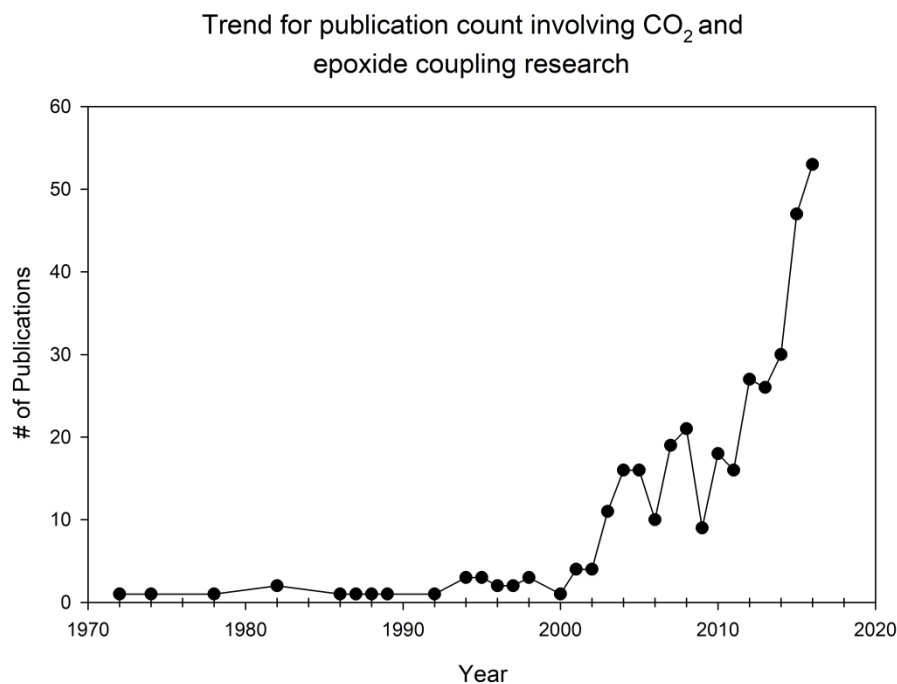


Figure 1.6: Trend in the number of publications on CO₂ and epoxide coupling. Analysis from SciFinder®; search terms “carbon dioxide and epoxide coupling”, April 2018.

1.2.1 Cobalt complexes as catalysts for coupling of CO₂ with epoxides

Catalyst systems using cobalt for CO₂ and epoxide coupling reactions have been reported by many researchers.³⁰⁻³⁴ Most catalyst systems are classified as binary catalysts because they are used in synergy with nucleophilic co-catalysts to facilitate initiation through epoxide ring-opening. The salen-type ligand has been the focus of many researchers and when coordinated to transition metals such as cobalt and chromium they exhibit high catalytic activity.^{9,16} In general the salen-type system comprises an ONNO-tetradentate ligand structure with a metal and axial ancillary ligands that can dissociate in the presence of excess coordinating species (such as epoxides); this combination exhibits both high catalytic activity as well as very good stability.^{9,16,17} Some systems are termed

bifunctional, meaning the nucleophilic “co-catalyst” is incorporated into the ligand structure.^{25,35,36}

1.2.1.1 Binary catalysts

One of the first reported cobalt-based catalysts for epoxide and CO₂ coupling reactions was by Coates and co-workers in 2003 and featured the salen ligand system (**Figure 1.7**).³¹ This catalyst was >99% selective towards PPC formation with 99% carbonate linkages and activity of 71 TO h⁻¹ at 25 °C and 55 bar CO₂ pressure. Narrow polymer dispersity of 1.11 and molecular weights of 6.9 kg mol⁻¹ were reported. Activities were dependent on the nature of X, but it was later discovered that with the addition of a co-catalyst, the activities can be increased.³¹ Furthermore, this catalyst was observed to be more robust than its Cr(III)-salen counterparts; unpurified monomers can be used and reactions set upon the open-bench.³¹ Since then, there have been a vast number of cobalt-based catalyst systems reported in the literature, and key discoveries since 2010 will be mentioned here. Important structural considerations of the catalyst design, conditions of activity and mechanistic insights will be highlighted.

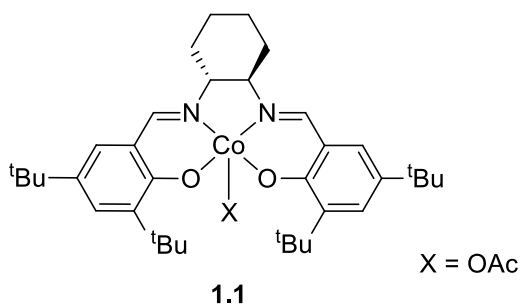


Figure 1.7: First reported cobalt catalyst for CO₂/epoxide copolymerization reactions.³¹

Nozaki and co-workers reported a series of bimetallic Co(III)-salen complexes (**Figure 1.8**) for copolymerization of PO with CO₂.³⁷ These complexes possessed cobalt coordination sites linked by a diester group bearing aliphatic chains of various lengths (**Figure 1.8**). The best activity (180 TO h⁻¹) was observed at a very low catalyst loading of 0.03%, at 22 °C and 50 atm of CO₂ without the use of a co-catalyst. This was more active than its mononuclear counterpart (TOF of 20 h⁻¹) and produced polymers with molecular weight of 36.7 kg mol⁻¹, *D* of 1.07 and 84% carbonate linkages.³⁷ High activity at these low loadings is indicative of a bimetallic propagation mechanism. The addition of a co-catalyst (bis(triphenylphosphine)iminium chloride, PPNCI) shifts the propagation mechanism to monometallic even when the dinuclear catalyst is used.³⁷

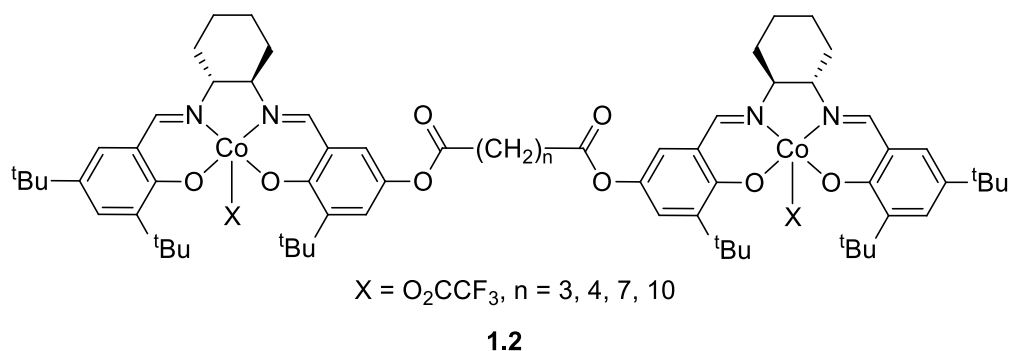


Figure 1.8: Bimetallic Co(III)-salen complex for copolymerization of CO₂ with PO.³⁷

Berry and co-workers reported a highly active catalyst selective towards cyclic carbonate synthesis.³⁸ The catalyst is a Co(III) tetraamidomacrocyclic ligand (TAML) complex (**Figure 1.9**) which is air and moisture stable and capable of producing cyclic carbonate of various epoxides such as PO, CHO, epichlorohydrin (ECH), styrene oxide (SO) and cyclooctene oxide. Highest activity was observed with PO with 100% isolated

yield (cyclic carbonate) and activity of 351 TO h⁻¹ at 120 °C and 2 MPa of CO₂. The structure of this complex is different from the traditional salen complexes in that it is macrocyclic and contains four anionic donors, therefore a lithium counter-ion is present to generate an overall neutral species. Mechanistic studies performed indicate that the reactions proceed via a coordination-insertion mechanism followed by back-biting to yield cyclic carbonate.

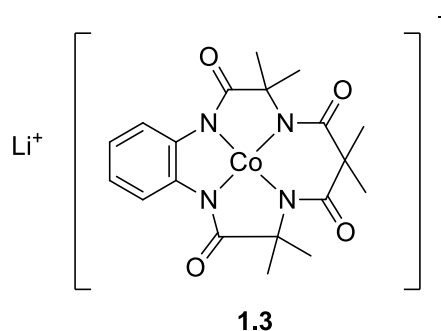


Figure 1.9: Co-TAML metal complex reported by Berry and co-workers as a catalyst for cyclic carbonate synthesis from CO₂ and epoxides.³⁸

A non-traditional Co(II)-salen complex bearing salicylaldimine ligands with bulky straight chain methoxysilyl amine groups on the imino functionality was reported by Ulusoy, Kilic and co-workers for coupling of styrene oxide (SO) with CO₂ to produce cyclic carbonate.³⁹ Essentially, steric bulk affords a symmetrical complex with a center of inversion lying at the metal center. Phenolate substituents of electron donating character were introduced and it was observed that increased electron donation at the *para*-position accelerates CO₂ fixation. High activity of up to 405 TO h⁻¹ and 81% yield was observed for a reaction performed at 100 °C and 1.6 MPa CO₂ pressure, for 2 h.³⁹ In another instance, Kim and co-workers reported a Co(III)-salen chiral complex for cycloaddition

of PO and CO₂. The interesting feature here is that the Co(III)-salen complex is coordinated to a second Co(II) atom (bearing two BF₄ counter-ions) via the phenolate oxygens, which is then immobilized onto an aluminosilicate support by electrostatic interactions (**Figure 1.10**).²¹ In the presence of a catalytic amount of water and 1-hexyl-3-methylimidazolium chloride, optically pure propylene carbonate (PC) was afforded by catalytic resolution resulting from hydrolytic kinetic resolution of the racemic PO followed by coupling with CO₂ in a one-pot reaction.²¹

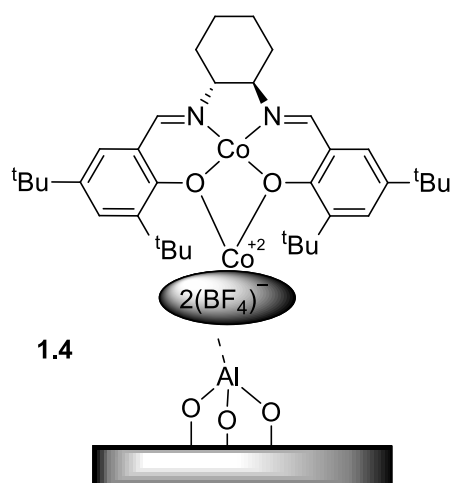


Figure 1.10: Immobilized (*R,R*)-Co(II)-salen complex used as a catalyst for propylene carbonate synthesis from CO₂ and *rac*-PO.²¹

A series of Co(II)/(III) amino-bis(phenolate) tripodal complexes was reported by Kozak, Kerton and co-workers for PO/CO₂ cycloaddition (**Figure 1.11**).³² Ligand, co-catalyst and Co oxidation state effects were investigated. Basically, the stronger electron-donating ability of the pyridyl donor along with its planar nature induced increased cycloaddition selectivity. Furthermore, the Co(II) amino-bis(phenolate) species were more active for coupling reactions compared to their Co(III) analogs and

tetrabutylammonium bromide (TBAB) was the most superior co-catalyst. Best activity came from compound **1.5c**, **Figure 1.11** with TBAB as a co-catalyst and showed a TON of 2025 for a reaction done at 25 °C and 3.4 MPa.³²

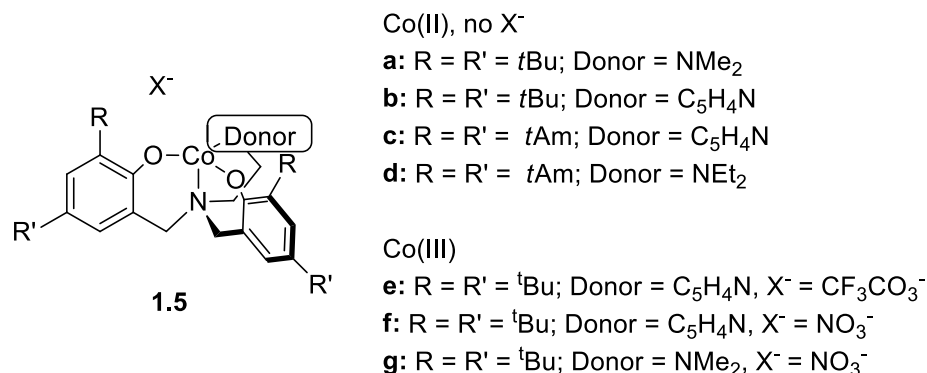
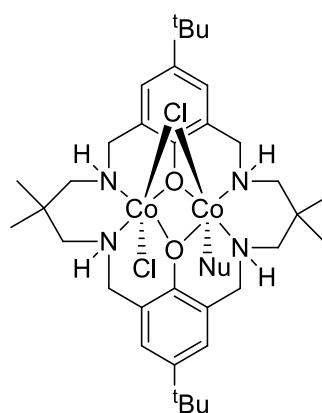


Figure 1.11: Co(II)/(III) amino-bis(phenolate) complex for cycloaddition of CO_2 and PO .³²

Williams and co-workers reported di-cobalt(III) halide macrocyclic complexes for the copolymerization of CHO and CO_2 (the most active species shown in **Figure 1.12**).²⁷ Depending on the procedure used for synthesis (excess halide and/or nucleophiles), the complexes can be either neutral or anionic with hexacoordinate cobalt centers. Several studies were done to determine whether a bimetallic reaction mechanism was followed. For example, analysis of polymer end-group and reaction mixtures (small quantities of nucleophile-opened CHO observed) using MALDI-TOF MS and ESI-MS, showed negligible initiation by the nucleophilic co-catalyst, which is an indication of the bimetallic pathway. The presence of the competing epoxide promotes dissociation of the nucleophile followed by coordination of the epoxide to the vacant site; the halide from the adjacent metal then ring-opens the epoxide followed by CO_2 insertion. Simultaneously,

an epoxide coordinates onto the other metal which is then ring opened by the newly formed carboxylate leading to polymer propagation as the growing chain moves back and forth between metals. These complexes (**1.6a-c**) showed increased activity over the previously reported analog bearing acetate ligands instead of halides and over the Zn-based analogs.^{30,40} At 1 bar, up to 161 TO h⁻¹ was observed with >99% polymer and carbonate linkage selectivity. Molecular weights up to 33.1 kg mol⁻¹ were obtained.²⁷



1.6a: Nu = 1-methylimidazole
1.6b: Nu = DMAP
1.6c: Nu = pyridine

Figure 1.12: Di-cobalt(III) catalyst for copolymerization of CHO and CO₂.²⁷

Porphyrins are another popular class of ligands used to form coordination compounds for use as catalysts in coupling reactions involving CO₂ and epoxides. Rieger and co-workers reported a series of cobaltoporphyrins (**Figure 1.13**) for coupling of PO with CO₂ to produce either polycarbonate or cyclic carbonate, with a PPNCI co-catalyst.⁴¹ They were able to tune the selectivity for cyclic carbonate or polycarbonate by altering the substitution pattern on the ligand framework. Catalysts with electron-withdrawing

nitro groups (compound **1.7f**) produce strictly propylene carbonate while electron-donating isopropoxide (compound **1.7e**) produces primarily PPC with trace amounts of PC and polypropylene oxide. The best activity was observed using **1.7e** and a 103 TO h^{-1} with 90% conversion of PO to polycarbonate and molecular weights of 39.0 kg mol^{-1} at $30 \text{ }^{\circ}\text{C}$ and 3 MPa was observed. Increased temperature ($60 \text{ }^{\circ}\text{C}$) shifted the selectivity towards cyclic carbonate, which is expected as there is a higher activation barrier for the cyclization reaction to occur.⁴¹

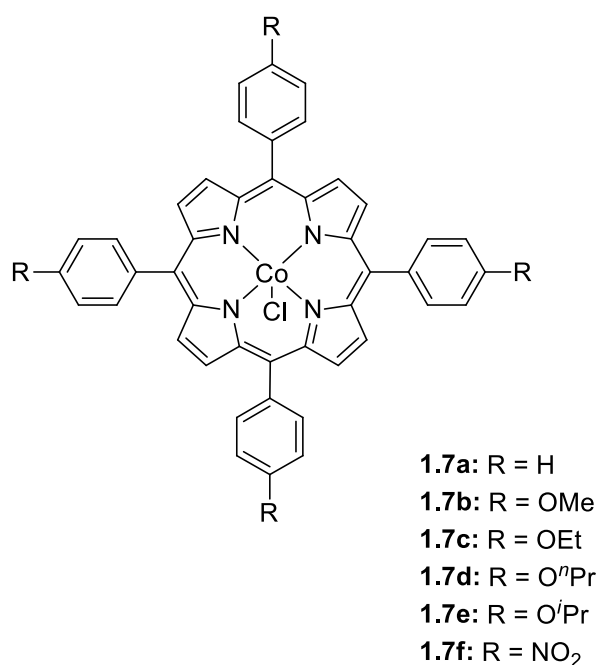
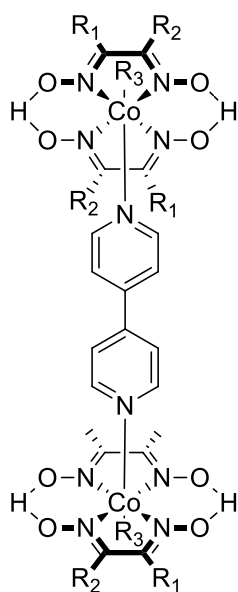


Figure 1.13: Cobaltoporphyryrin complexes used as catalysts for coupling of PO and CO₂.⁴¹

Kilic and co-workers reported a series of cobaloxime complexes for coupling of CO₂ with epichlorohydrin to produce cyclic carbonate (**Figure 1.14**).⁴² Compounds **1.8a** and **1.8b** are only a few of those reported; other variations include replacement of the

hydrogen-bond bridge (O—H---O) with Cu coordinated to the two terminal oxygens and a 2,2'-bipyridine-based ligand (various analogs such as phenanthroline and 4,5-diazofluoren-9-one). The most active catalyst for cyclic carbonate formation from epichlorohydrin and CO₂ was **1.8b** with DMAP as a co-catalyst. Activity of up to 448 TO h⁻¹ was observed, which resulted in gas chromatography (GC) yields of up to 88.9% cyclic carbonate at 100 °C, 1.6 MPa and 0.1% catalyst loading, in only 2 h.⁴² In a later study, mononuclear cobaloximes of those in **Figure 1.14** were reported again for cycloaddition of CO₂ with epichlorohydrin.⁴³ In this case, the 4,4'-bipyridine linker was replaced with 4-*t*-butylpyridine and R₂ = 4-ethylphenyl (**Figure 1.14**). There were also analogs containing Cu coordinated to the two terminal oxygens and a 2,2'-bipyridine-based ligand in replacement of the hydrogen-bond bridge (O—H---O). The catalyst system where R₂ = 4-ethylphenyl and bearing a hydrogen-bond bridge, showed the best activity (75.9% GC yield and 380 TO h⁻¹). Amidst this good activity, there was negligible to no activity when epoxides such as PO, SO, CHO and 1,2-epoxybutane were explored.⁴³ The activity of epichlorohydrin vs others is likely due to epichlorohydrin being an activated epoxide compared with other substrates.



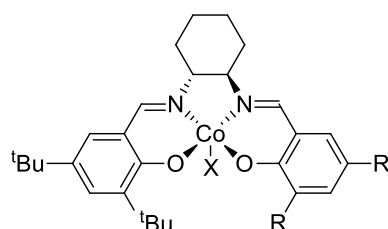
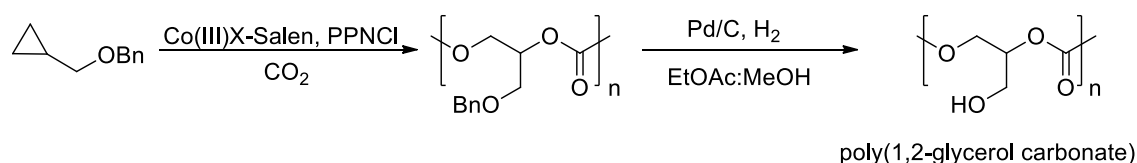
1.8a: $R_1 = R_2 = \text{CH}_3$, $R_3 = \text{Cl}$

1.8b: $R_1 = R_2 = \text{CH}_3$, $R_3 = \text{benzyl}$

Figure 1.14: Cobaloxime complexes for cycloaddition of epoxides and CO_2 .^{42,43}

Many researchers are now designing catalysts for polycarbonate synthesis using specialized epoxides (bearing modifiable functional groups) with the intent of post-functionalization of the polymer to target a specific property. Grinstaff reported a series of chiral Co(III)-salen complexes for use as catalysts in copolymerization of benzyl glycidyl ether (BGE) and CO_2 (**Figure 1.15**).⁴⁴ The aim was to synthesize a degradable polymer for potential biomedical applications. The protected epoxyalcohol BGE was copolymerized with CO_2 with each of compounds **1.9a-f** to investigate the effect of the axial ligand. Compounds **1.9a-e** were able to produce atactic polycarbonate from copolymerization of *rac*-BGE and CO_2 with >99% carbonate linkages when reactions were done at 22 °C and 1.52 MPa but differences in polymer selectivity were observed; bromide produced lowest selectivity (73%) whereas [2,4-DNP]⁻ produced the highest

(>99%). This is one of the many cases in the literature where [2,4-DNP]⁻ has demonstrated increased activity compared to other ancillary ligands hence it is an area of focus for catalyst modification to tune catalyst activity. It is interesting to note that this study presents an immortal polymerization which is indicated by a linear M_n versus conversion plot.⁴⁴ Compound **1.9f**/PPN-DNP showed very high activity with *rac*-BGE; up to 620 TO h⁻¹ at 60 °C, 1.52 MPa and extremely low catalyst loading (0.01 mol%), producing molecular weights of 32.2 kg mol⁻¹ was observed. With the intent of producing an isotactic polymer, Jacobsen's catalyst was used for hydrolytic kinetic resolution (HKR) of *rac*-BGE to produce the R-enantiomer which was then coupled with CO₂ to produce isotactic poly(1,2-glycerolcarbonate) using **1.9f**/PPN-DNP. Ultimately, the isotactic poly(1,2-glycerolcarbonate) degraded significantly faster than poly(1,3-glycerolcarbonate), which is a currently investigated polymer for biomaterials.⁴⁴



- 1.9a:** X = NO₃, R = ^tBu
- 1.9b:** X = Cl, R = ^tBu
- 1.9c:** X = Br, R = ^tBu
- 1.9d:** X = OOCCH₃, R = ^tBu
- 1.9e:** X = [2,4-DNP]⁻, R = ^tBu
- 1.9f:** X = 2,4-DNP, R = ⁿPr-TBD, PPN-DNP

Figure 1.15: Copolymerization reaction of CO₂ and BGE using a variety of Co(III)X-salen complexes.⁴⁴

Merna and co-workers reported a series of Co(III)X-salphen complexes for copolymerization reactions of CHO/CO₂ and PO/CO₂.⁴⁵ The structure of this Co(III)X-

salphen complex is like the ones shown in **Figure 1.7** but a 1,2-phenylene backbone instead of 1,2-cyclohexylene (hence no chirality) and the X ancillary ligand was varied ([2,4-DNP]⁻, trichloroacetate, pentafluorobenzoate, acetate and chloride). Polycarbonates with >99% carbonate linkages were produced and molecular weights ranged from 15.0 to 30.0 kg mol⁻¹. Analogs bearing the weakest nucleophile (trichloroacetate) displayed the highest activity for PO/CO₂ copolymerization. Cyclic carbonate formation was also observed for PO/CO₂ reactions. According to the authors, the activity of these complexes is attributed to the rigid geometry which allows for efficient influence of the Lewis acidity of the metal center.⁴⁵

Terpolymerization offers an avenue for introducing more than one epoxide into the polycarbonate for a desired purpose. Williams and co-workers reported a chiral Co(III)Cl-salen complex bearing a cyclohexylene backbone for CO₂/1,4-cyclohexadiene oxide (1,4-CHDO) copolymerization and CO₂/CHO/1,4-CHDO terpolymerization.¹³ 1,4-CHDO is an unsaturated epoxide, hence there is potential for post-functionalization of the polycarbonate. At a pressure of 0.2 MPa and 28 °C, the highest conversion was 78% with molecular weights of 12.9 kg mol⁻¹. It is interesting to note that the epoxides from this study were bio-derived and hence considered to be renewable.¹³

Lu and co-workers reported dinuclear Co(III)X-salen complexes for stereoselective CHO/CO₂ and 3,5,8-trioxabicyclo[5.1.0]octane (CXO)/CO₂ copolymerization (**Figure 1.16**).⁴⁶ This presents a unique case in terms of mechanism, and the type of polymer produced. When a racemic mixture of **1.10a** and **1.10b** was used in the presence of PPN-DNP for coupling of a *meso*-CHO (for example) and CO₂, **1.10b** formed (*S,S*)-

polycarbonate chains whereas **1.10a** forms (*R,R*)-chains but the presence of a chain transfer agent such as adventitious water allowed for chain exchange (also referred to as chain-shuttling) resulting in **1.10a**-(*S,S* chain) and **1.10b**-(*R,R* chain). Polymer propagation resumed at each metal center with the desired stereoisomer thus yielding a diblock structure until this exchange happens again; this occurred repeatedly, thus giving an isotactic multiblock polycarbonate. The result is a stereocomplexed, highly crystalline polycarbonate. The best catalytic activity observed was 333 TO h⁻¹ at ambient temperature and 1.5 MPa CO₂ pressure, which produced polymers with 35.1 kg mol⁻¹.⁴⁶

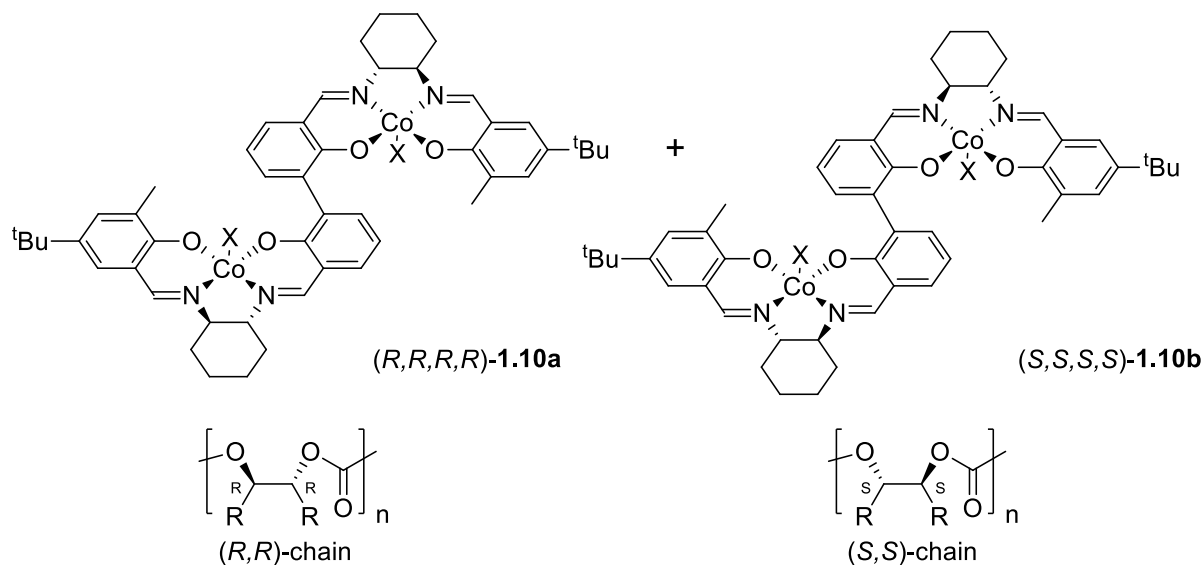


Figure 1.16: Racemic dinuclear Co(III)X-salen complex for copolymerization of CO₂ and *meso*-epoxides.⁴⁶

Derivatives of the salen ligands which contain cyclohexylene backbones are sometimes referred to as salcy ligands. Nozaki and co-workers reported a study where Co(III)-salcy complexes were generated in situ and used for copolymerization of PO and

CO₂.⁴⁷ Various analogs were reported with different substituents at the *para*-phenolic position on the ligand; pre-catalysts were Co(II)-(*t*Bu-salcy), Co(II)-(OMe-salcy) and Co(II)-(NMe₂-salcy). Essentially, the Co(III)X-salcy compounds were generated via oxidation using FcPF₆ (ferrocenium hexafluorophosphate), therefore X = [PF₆]⁻ for the active species. Using PPNCl as a co-catalyst, activity (TON) was nearly identical when compared to their Co(III) isolated counterparts, for copolymerization of PO/CO₂. An interesting observation is that when AgPF₆ was used as an oxidant there was no catalytic activity and this was attributed to the generated Ag solid, which inhibited the reaction. The use of PPN-DNP increased activity (TON) and selectivity towards polycarbonate; the better leaving ability of chloride promoted backbiting thus favoring cyclic carbonate formation. The best activity of 488 TO h⁻¹ was observed with Co(II)-(OMe-salcy)/PPN-DNP at 22 °C, 1.5 MPa CO₂ pressure and produced polypropylene carbonate (100% selectivity) with a molecular weight of 32.1 kg mol⁻¹.⁴⁷

1.2.1.2 Bifunctional catalysts

Some catalysts can perform epoxide/CO₂ coupling reactions without the use of a co-catalyst or initiator counterion. These types of catalysts represent a large portion of Co-based systems reported in the literature and are commonly known as bifunctional catalysts; also referred to as two-component catalysts (Williams).⁹

Lu and co-workers reported a series of highly active bifunctional Co(III)-salen complexes and compared them to the binary analogs for copolymerization reactions of CHO and CO₂ (**Figure 1.17**).²⁵ Compound **1.11a** was used in the presence of a co-catalyst ([Bu₄N][DNP]) but compounds **1.11b** and **c** function without a co-catalyst. It is

commonly believed that the ionic moiety on the structure serves as an initiator, which being attached to the complex, allows for increased activity. The length of the alkyl linker is also important. Compound **1.11b** had the highest observed activity with 6105 TO h⁻¹ at 120 °C and 2.5 MPa (still active at 1 bar and ambient temperature). Compared to the first reported Co-salen catalyst systems, this is about 85 times more active in terms of TOF.

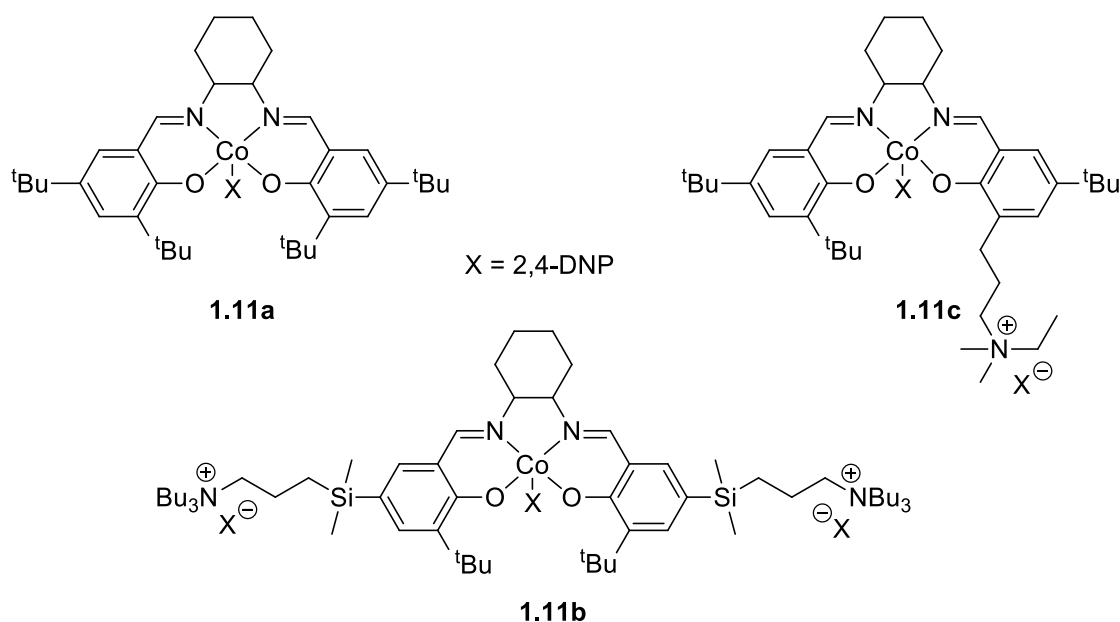


Figure 1.17: Mono and bifunctional Co(III)-salen catalysts.²⁵

Another highly active (likely one of the most active in the literature) bifunctional Co(III)-salen catalyst system was reported by Lee and co-workers for terpolymerization of various epoxides with CO₂ (**Figure 1.18**).⁴⁸ Previous work involved variation of the anion on the Co(III) complex to generate different complexes for PO and CO₂ copolymerization.⁴⁹ Compound **1.12** was one of the most active species which produced a very impressive 16000 TO h⁻¹ with molecular weights up to 300 kg mol⁻¹ and >99%

polymer selectivity. This species adopts a rather unusual coordination mode with cobalt where the imine nitrogens of the ligand do not coordinate, but instead the counterions from the tethered quaternary ammonium salts. In this study **1.12** was used for terpolymerization of PO/1-hexene oxide (HO)/CO₂, PO/CHO/CO₂, and PO/1-butene oxide (BO)/CO₂. Reactions were typically done for 1 h at 70 – 75 °C with 20 bar CO₂ pressure and at a catalyst loading of 0.001 mol%. In the case of CHO/PO/CO₂ terpolymerization, activity ranged from 5100 – 9700 TO h⁻¹ with >99% polycarbonate selectivity and molecular weights up to 210 kg mol⁻¹. A noteworthy observation is an increase in glass-transition temperature, T_g , (increase ranged from 52 – 93 °C) with an increase in mole fraction of CHO (F_{CHO}), in the polymer. For HO/PO/CO₂ terpolymerization, activity of up to 9100 TO h⁻¹ with >99% polycarbonate selectivity and M_n up to 198 kg mol⁻¹ was observed. There was a decrease in T_g with increased F_{HO} (32 to -15 °C). BO/PO/CO₂ terpolymerization showed a smaller change in T_g (33 – 9 °C). Contrary to PCHC, pure poly-1-hexene carbonate (PHC) and poly-1-butene carbonate (PBC) both have T_g s lower than that of PPC, hence the decrease in T_g with increase F_{HO} or F_{BO} in the terpolymers. BO/PO/CO₂ showed activity of up to 14000 TO h⁻¹ with >99% polycarbonate selectivity and M_n up to 264 kg mol⁻¹. A remarkable advantage from this study is the ease of polymer purification (removal of catalyst residue) by filtration through a short silica plug where the catalyst can be recovered from the silica and reused.

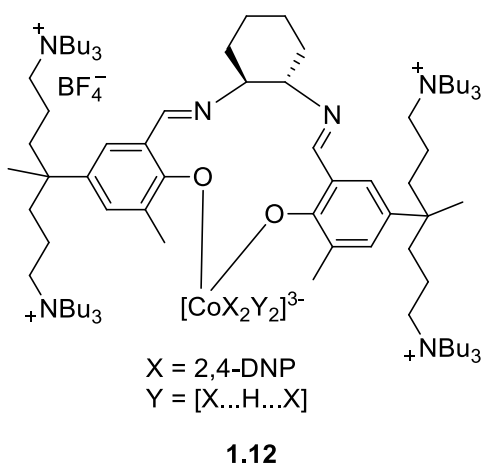


Figure 1.18: Co(III) complex of salen-type ligand tethered by four quaternary ammonium salts for terpolymerization of CO₂, PO and other epoxides.⁴⁸

Lu and co-workers reported a series of asymmetric multichiral Co(III)-salen complexes bearing 1,5,7-triazabicyclo[4.4.0]dec-5-ene (TBD) and binaphthol (BINOL) substituents for copolymerization of CO₂ and PO (**Figure 1.19**).⁵⁰ When a racemic mixture of PO was used in the presence of compound **1.13c**, regioregular polymer with more than 99% head-to-tail linkages was produced.⁵⁰ Highest activity (236 TO h⁻¹) was achieved with **1.13c** and produced polymer with a molecular weight of 98.7 kg mol⁻¹ and *D* of 1.09. Polymer selectivity and carbonate linkages of 99% were obtained in 6 h at 20 °C and 10 bar CO₂ pressure.

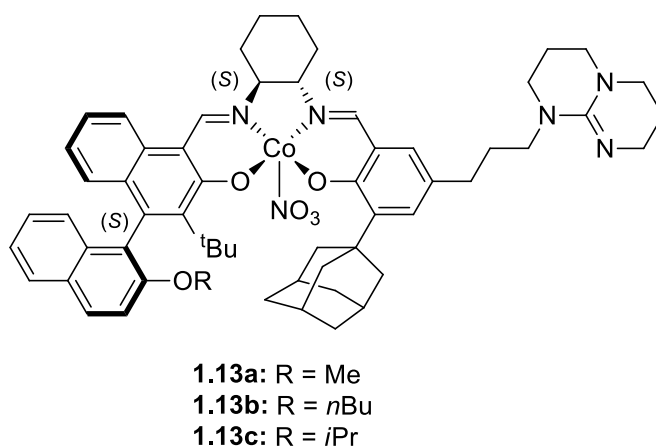


Figure 1.19: Multichiral Co(III)-salen asymmetric catalyst used for copolymerization of PO and CO₂.⁵⁰

Niu and Li reported a bifunctional 2,4-DNP-Co(III)-salen complex bearing *para* substituted methylene-tethered morpholinyl groups for copolymerization of PO/CO₂ and terpolymerization of PO/CHO/CO₂ (**Figure 1.20**).⁵¹ The complex did not possess the typical tethered ionic groups and did not require a co-catalyst, therefore it is considered bifunctional. The methylene-tethered morpholinyl groups are believed to stabilize (due to their Lewis basicity) the salen-Co(III) 2,4-dinitrophenolate complex and prevent decomposition to inactive salen-Co(II).⁵¹ High activity with up to 673 TO h⁻¹ was achieved for CO₂/CHO copolymerization with >97% polycarbonate selectivity and molecular weights up to 110 kg mol⁻¹ for reactions done at 15 bar and 25 °C. Terpolymerization of PO/CHO/CO₂ however, produced lower activity (100 TO h⁻¹) and molecular weights up to 76.5 kg mol⁻¹. It is interesting to note that the proposed mechanism involved CO₂-insertion firstly into the C-O bond of the Schiff base to produce

a carbonate followed by epoxide insertion to produce an alkoxide followed by alternating enchainment of PO and CO₂ to produce polycarbonate.

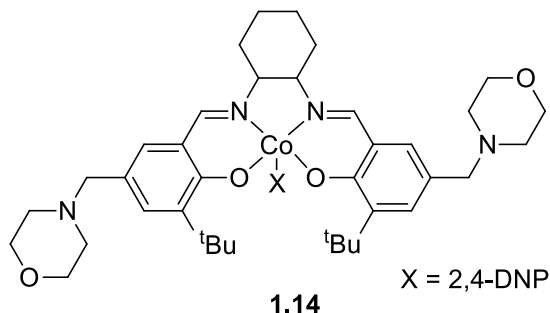


Figure 1.20: 2,4-DNP-Co(III)-salen complex bearing Lewis basic substituents for PO/CO₂ copolymerization and CHO/PO/CO₂ terpolymerization.⁵¹

A series of bifunctional cobaltoporphyrins (tetra(trimethylphenylammonium iodide)porphyrin or TTMAPP-I₄) (**Figure 1.21**) was reported by Jing and co-workers for coupling of epoxides and CO₂ to produce cyclic carbonates.⁵² Temperature effects (using **1.15a**), counterion effects (**1.15a** – **1.15g**), and recycling studies were performed for PO/CO₂ coupling reactions. The order of reactivity for counterions was observed to be OAc[−] > I[−] > Cl[−] > Br[−] > OTs[−] > CF₃COO[−] > CCl₃COO[−] for solvent-free reactions. Due to poor solubility of some of the catalyst species in PO, methanol was used, and the new order of reactivity was CF₃COO[−] > CCl₃COO[−] > OAc[−] > I[−] > Br[−] > Cl[−] > OTs[−]. Five successive recycling attempts showed a decrease in yield from 95.4% to 81.3%. Reactions were typically done at 80 °C, 6.6 bar CO₂ pressure and 0.1 mol% catalyst loading. Epoxide screening was performed with compound **1.15a**. The best overall activity was observed with PO giving a yield of 95.4% cyclic carbonate at 190.8 TO h^{−1}.

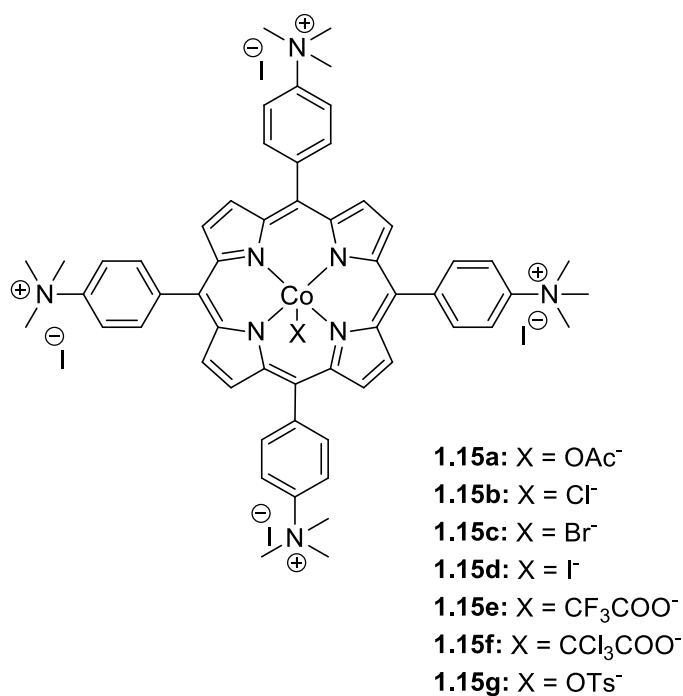


Figure 1.21: Co-TTMAPP-I₄ bifunctional complexes used as catalysts for PO/CO₂ coupling to produce cyclic carbonate.⁵²

Lu and co-workers reported two Co(III)-salen complexes for copolymerization of phenyl-glycidyl ether (PGE) and CO₂.⁵³ One species was essentially compound **1.11c** and the other (referred to as single-component) was similar but contained an *ortho* appended propyl-tethered TBD group instead. In a previous work by Darensbourg and Lu, these compounds showed high activity for copolymerization of epichlorohydrin (ECH) and CO₂ with activity up to 640 TO h⁻¹ from the TBD-based Co(III)-salen species.⁵⁴ Lu and co-workers, observed perfectly alternating polycarbonate with regiochemical control and up to >99% head-to-tail arrangement. In comparison to the binary analog (**1.11a**/PPNDNP), the bifunctional species were more efficient at CO₂/PGE copolymerization even at low catalyst loading and/or enhanced temperature. Activation

energies, E_a , for copolymer formation versus cyclic carbonate were found to be largely different for both types of catalyst systems (up to 74.4 kJ mol^{-1}) hence the high selectivity for polycarbonate formation. It is interesting to note that it has been observed that the TBD group is capable of ring-opening the epoxide to form a carbonate ligand after CO_2 -insertion and this labile adduct is believed to stabilize the Co(III) species against deactivation to inactive Co(II) species.⁹

In 2013, Darensbourg and co-workers reported Co(III)-salen complexes (**Figure 1.22**) with appended *n*-propyl- NEt_2Me^+ , **1.16a**, and *n*-propyl- NCy_2Me^+ , **1.16b**, quaternary ammonium salts for copolymerization of CO_2 and indene oxide.⁵⁵ Compared to their binary analog **1.11a**/PPNDNP, **1.16a** and **1.16b** exhibit higher activity (TOF) and selectivity for poly(indene carbonate) production. With average reactions times of 2 days and conversions of up to 62%, TOFs were low ($1.7 - 11.5 \text{ TO h}^{-1}$). Reactions were typically done at 0°C in dichloromethane (for **1.11a**/PPNDNP) or toluene (for both **1.16a** and **1.16b**) at a concentration of 1 g/mL and 34 bar CO_2 pressure. Low temperature was necessary to favor the production of polycarbonate as the cyclic carbonate is known to be the thermodynamic product of the coupling reaction. At catalyst loadings of 0.1 mol%, only 60% polycarbonate selectivity was achieved with **1.11a**/PPNDNP whereas up to >99% selectivity for **1.16a** and **1.16b** with narrow dispersities (average of 1.02). It is interesting to note that the observed molecular weights (9.7 kg mol^{-1}) were much lower than the theoretical (106 kg mol^{-1}) and is attributed to rapid and reversible chain transfer processes. The highest T_g observed for the polycarbonate reported therein was 138°C , which represents the highest glass-transition temperature reported for polycarbonate

formed from catalytic copolymerization of CO₂ and epoxides. The high T_g is likely due to the presence of aromatic groups within the structure of the polymer.

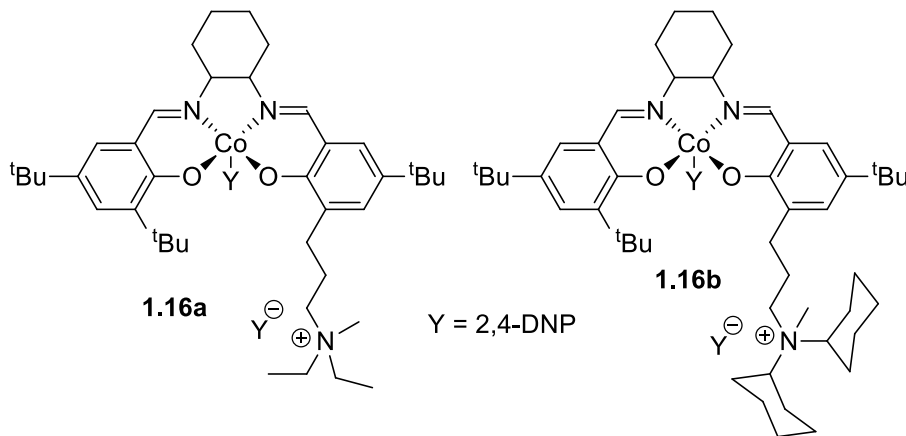


Figure 1.22: Bifunctional Co(III)-salen complexes with appended ⁿpropyl-NEt₃Me⁺ and *n*-propyl-NCy₂Me⁺ quaternary ammonium salts.⁵⁵

Lu and co-workers reported a kinetic study on the comparison in activation energies between **1.11a**/ⁿBu₄-DNP and **1.16a** for copolymerization of PO or CHO with CO₂ using in situ infrared spectroscopy.⁵⁶ **1.11a**/ⁿBu₄N-DNP represents intermolecular epoxide activation whereas **1.16a** represents intramolecular activation via a nucleophilic onium salt co-catalyst (**Figure 1.23**). All reactions were performed solvent-free at 25 °C and 20 bar CO₂ pressure and catalyst loadings ranging from 0.2 – 0.01 mol%. An increase in induction period was observed for the binary system (**1.11a**/ⁿBu₄N-DNP) with a decrease in catalyst loading, but no induction period was observed for the bifunctional system (**1.16a**). This difference is attributed to a bimolecular synergistic effect taking place in the binary system whereas in the bifunctional system, an intramolecular cooperative process takes place. A reaction pathway consistent with first order dependence on catalyst

concentration was observed for the bifunctional system whereas an order of 1.61 for the binary system which suggests more complexity in the copolymerization process. In terms of E_a , **1.16a** displayed 77.0 and 29.5 kJ mol⁻¹ activation barriers for PO/CO₂ cyclic carbonate and polycarbonate respectively, whereas **1.11**/ⁿBu₄N-DNP displayed corresponding values of 50.1 and 33.8 kJ mol⁻¹. For CHO/CO₂ coupling, the E_a was 47.9 kJ mol⁻¹ for polymer formation using **1.11a**/ⁿBu₄-DNP, and for **1.16a** it was 31.7 kJ mol⁻¹. These numbers account for increased selectivity and activity of the bifunctional system to produce polycarbonate compared to the binary analog.

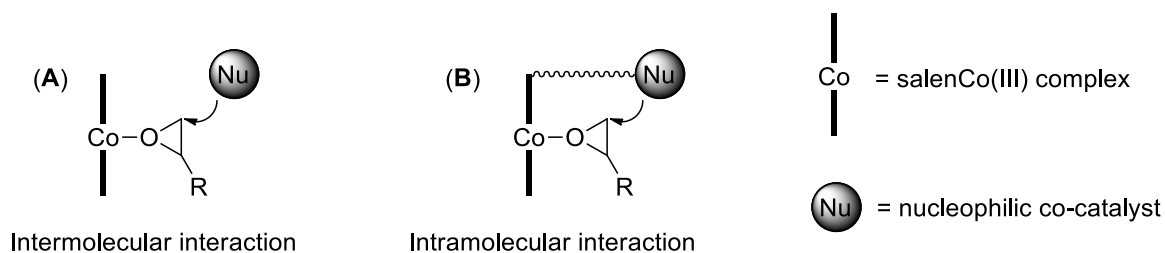


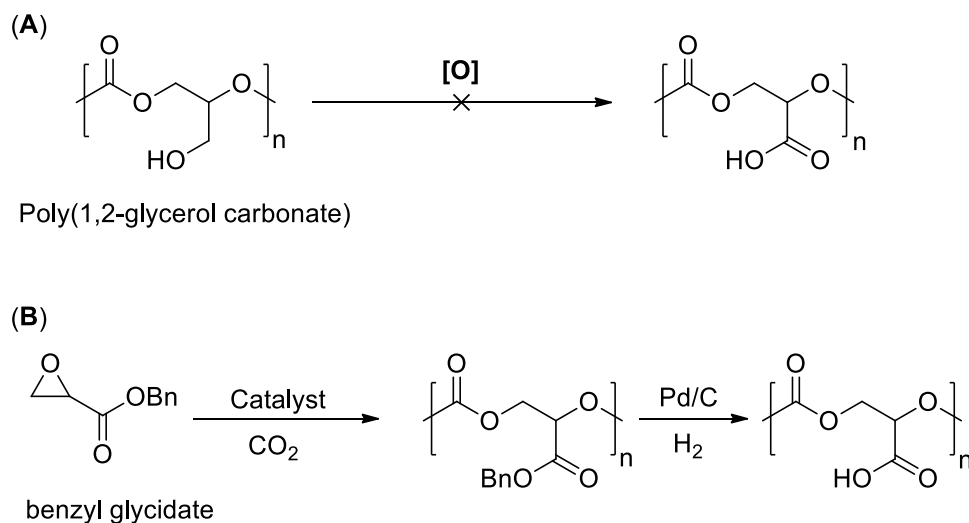
Figure 1.23: Proposed epoxide activation pathways by a nucleophilic co-catalyst for binary (A) and bifunctional (B) catalyst systems.

Darensbourg and co-workers reported a study where **1.16b** was employed as a catalyst for terpolymerization of vinyl oxide (VIO)/PO/CO₂ to produce polycarbonate compared to terpolymerization of allylglycidyl ether (AGE)/PO/CO₂ using **1.11a**/PPN-DNP, which was then post-functionalized by cross-linking via thiol-ene click chemistry (**Scheme 1.7**) to produce polymers with potential biomedical applications.⁵⁷ Only the AGE/PO/CO₂ terpolymer was chosen for cross-linking due to its more randomized distribution of vinyl groups. A noteworthy insight is that **1.11a**/PPN-DNP and **1.16b** were

used in conditions to favor 100% selectivity toward completely alternating copolymer but **1.16b** was purposely chosen to avoid cyclic carbonate production specifically for VIO/PO/CO₂ coupling.

Co(III)X-salen complexes with appended *ortho* phenolate substituents has been the focus for many researchers to be used as bifunctional catalyst for CO₂/epoxide coupling reactions. In 2015, Grinstaff and co-workers reported the use of **1.16a** (*rac*- and *S,S*) while comparing it to the binary analog (**1.11a**/PPN-DNP) and another bifunctional species (**1.11a** but with an *ortho* appended propyl-tethered TBD group) for coupling reactions of *rac*-benzyl glycidate or (*R*)-benzyl glycidate (BG)/CO₂ (**Scheme 1.5**).⁵⁸ The overall goal was to produce poly(glyceric acid carbonate), PGAC, which is a degradable analog to poly(acrylic acid) (PAA). This study represents the first report of PGAC synthesis using BG and CO₂. Direct oxidation of poly(1,2-glycerol carbonate) to PGAC was unsuccessful hence an alternate route using the benzyl-protected carbonate monomer, BG, was employed for polycarbonate synthesis, followed by Pd/C-catalyzed deprotection (**Scheme 1.5**). Coupling reactions were typically done at 25 °C and 15 bar CO₂ pressure with catalyst loadings of 0.2 mol% and lower. Both **1.11a**/PPN-DNP and the bifunctional analog (with propyl-tethered TBD group) produced cyclic carbonate for BG/CO₂ coupling reactions. On the other hand, *rac*-**1.16a** produced atactic PGAC with up to >90% polymer selectivity, >99% carbonate linkages and head-to-tail connectivity of 92%. Catalyst activity was up to 18 TO h⁻¹, which is low compared to a similar epoxide, BGE (~150 TO h⁻¹). This observation was attributed to the electron-withdrawing effect of the carbonyl group on BG. After HKR of *rac*-BG using (*R,R*)-salcy-Co(III)-OTs, the

resulting (*R*)-BG was copolymerized with CO₂ using (*S,S*)-**1.16a** to produce purely isotactic PGAC with >99% head-tail linkages. Ultimately, studies in deionized water showed significant degradation of PGAC (in about 12 days over a 26-day period) while PAA did not.



Scheme 1.5: Attempted synthesis of PGAC via oxidation of poly(1,2-glycerol carbonate) (A) and successful synthesis via BG/CO₂ copolymerization followed by Pd/C-catalyzed deprotection (B).⁵⁸

Liu and co-workers reported a study involving the terpolymerization of 4-VCHO/PO/CO₂ using **1.17**, **Figure 1.24**, followed by post-epoxidation of the C=C double bond then cyclic carbonate formation.⁵⁹ Temperature, time, VCHO/PO ratio and catalyst loading effects were investigated on the catalytic activity (TOF) towards the terpolymerization process. Increasing the VCHO mole fraction in the epoxide feed showed the most significant impact, which was a steady decrease in TOF. Best activity was 936 TO h⁻¹ for a reaction done at 70 °C and 30 bar CO₂ pressure, producing polycarbonate with molecular weight of 40.4 kg mol⁻¹ (highest was 80.5 kg mol⁻¹) and

88% polymer selectivity. A terpolymer sample with 0.27 molar fraction of VCHC units in the polymer chain was employed for oxidation by *m*-CPBA (*meta*-chloroperoxybenzoic acid) to generate epoxide-functionalized polycarbonate. Subsequent reaction with CO₂/LiBr generated cyclic carbonate-functionalized polycarbonate. Essentially, there was a linear dependence of T_g on mole fraction of vinyl, cyclic carbonate and epoxide functionalities; the highest T_g observed was 196 °C, which is now the highest T_g reported for a CO₂-based polycarbonate.

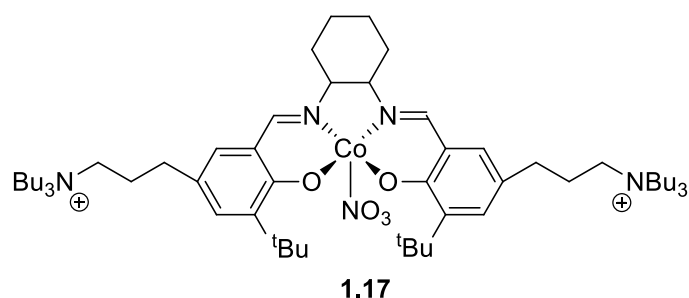
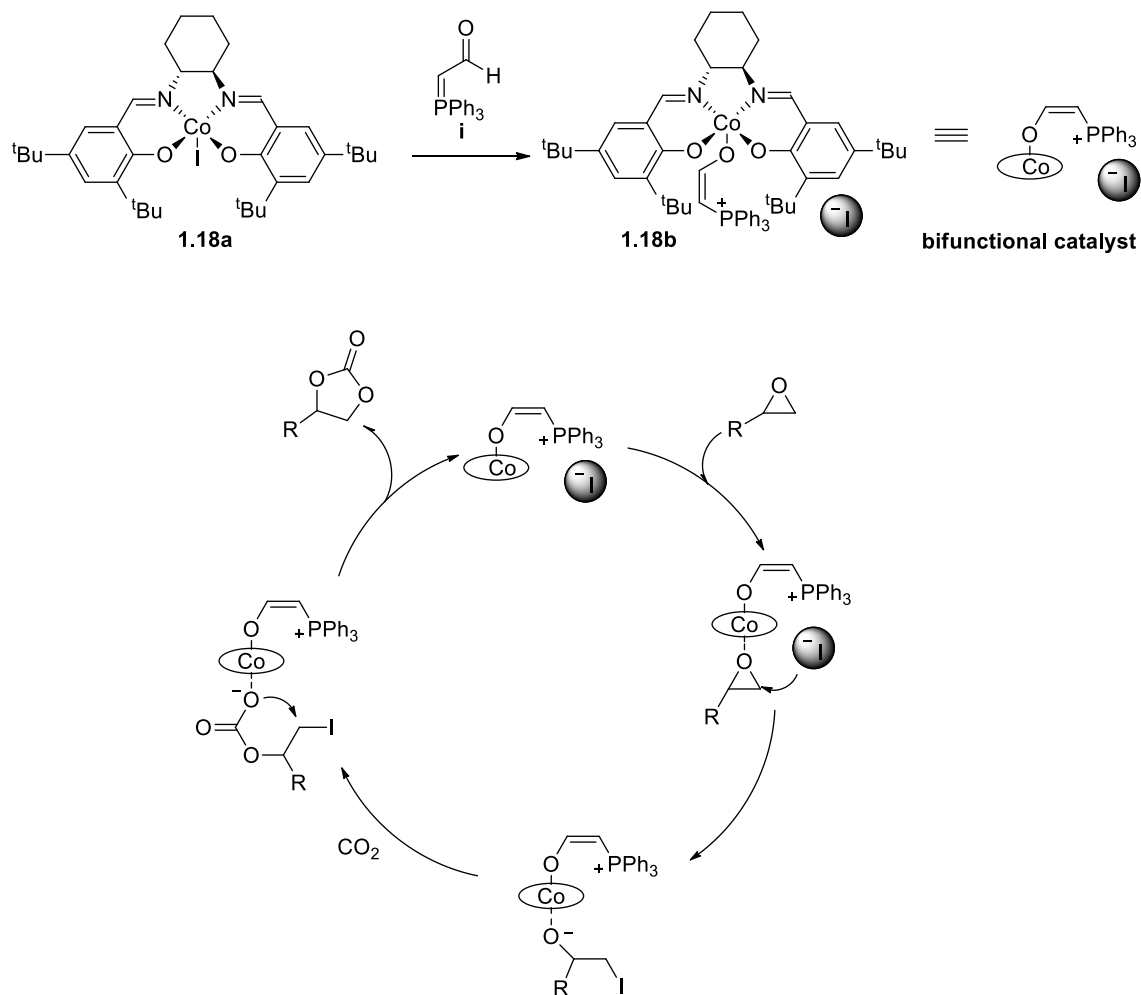


Figure 1.24: *Rac*-salen-Co(III)-NO₃ complex used as a catalyst for terpolymerization of 4-vinylcyclohexene oxide (VCHO)/PO/CO₂.⁵⁹

In a recent study, a catalyst system where salen-Co(III)I is first activated by a phosphorane to generate the active bifunctional catalyst species was reported (**Scheme 1.6**).⁶⁰ This process represents a conceptually new catalyst system for coupling of terminal epoxides with CO₂ under ambient condition (25 °C, 1 bar CO₂ pressure). Pivotal to the efficiency of the process is the coordination of the phosphorane which enhances the Lewis acidity of the Co(III) center and simultaneously generates an I[−] nucleophile which ring-opens the epoxide. The influence of different phosphoranes (**i**, **Scheme 1.6** was the most effective) and substrate scope experiments were investigated. With a dozen different

epoxides explored, isolated yields ranged from 80 – 95% for reactions performed between 24 and 36 h.



Scheme 1.6: Salen-Co(III)I complex activated by phosphorane to generate a bifunctional catalyst system (top). The proposed reaction mechanism (bottom).⁶⁰

1.3 Chromium complexes for coupling of CO₂ with epoxides

1.3.1 Salan, salen and related catalyst systems

Chromium catalysts for coupling and copolymerization of CO₂ and epoxides have been discussed in several excellent reviews.^{9,16,61,62} This section will focus primarily on advancements since 2011. By far the dominant ligand used in these systems exhibit [ONNO] chelation to the metal, as exemplified by the salen, salan and salophen ligands.⁶²

Darensbourg and colleagues developed a (salan)CrCl complex, **Figure 1.25**, that displays moderate to high activity towards CO₂ and cyclohexene oxide (CHO) copolymerization reactions with up to 405 TO h⁻¹, M_n of 27.2 kg mol⁻¹ and $\bar{D} = 1.19$. Di- and tri-block copolymers of polypropylene carbonate (PPC)/polycyclohexene carbonate (PCHC) and PPC/PCHC/polyvinyl cyclohexene carbonate (PVCHC) respectively were also obtained.⁶³ Further studies into mechanistic aspects indicate that the use of toluene presents a higher activation barrier for polycarbonate formation due to its non-polar nature compared to the ring-opened metal-alkoxide transition state. Eyring plot data show an increased activation barrier in toluene compared to the solvent-free process. In the absence of added solvent, the activation energy for CHO/CO₂ copolymerization from Arrhenius plots gave $E_a = 46.9$ kJ mol⁻¹.⁶⁴ In toluene, the enthalpy of activation (ΔH^\ddagger) was found to be 73.9 kJ mol⁻¹ and the entropy of activation (ΔS^\ddagger) was -68.8 J mol⁻¹ K⁻¹; the magnitude of ΔS^\ddagger is consistent with the previously proposed associative mechanism.⁶⁴ Furthermore, the presence of a polar cosolvent enhances the rate of cyclic carbonate formation especially for epoxide monomers which are prone to produce cyclic carbonate.⁶⁵

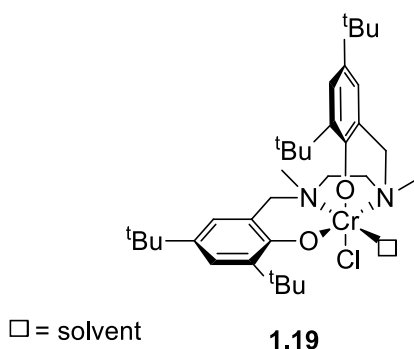


Figure 1.25: Chromium-salen complexes for coupling of epoxides and CO₂.⁶³

A less rigid and unsymmetrical form of the salen ligand structure was reported by Darensbourg, Liu and co-workers which presents an [ONSO]-type coordination to chromium (**Figure 1.26**). This semi-rigid ligand bears a thio-ether and imine bridged backbone and affords less electrophilicity at the metal center compared to its saturated N-donor counterpart which is believed to disfavor polymer chain growth initially during the reaction.⁶⁶ Substituent effects on CO₂/CHO copolymerization using [ONSO]CrX (**1.20a-d**) were studied. Essentially, there was an increase in activity when electron-withdrawing groups were introduced into the ligand (**1.20a** vs **1.20b**). **1.20c** displayed the highest overall activity, with up to 100 TO h⁻¹ and 64% PCHC selectivity. Co-catalyst optimization showed the best activity occurred with PPnCl, therefore it was used for further optimization. Compound **1.20a** showed up to 90% PCHC but gave only 20% conversion of CHO when TBACl was used as a co-catalyst. The highest conversion was observed with **1.20c**/PPnCl, which produced PCHC at 10.9 kg mol⁻¹ and *D* of 1.28.⁶⁶

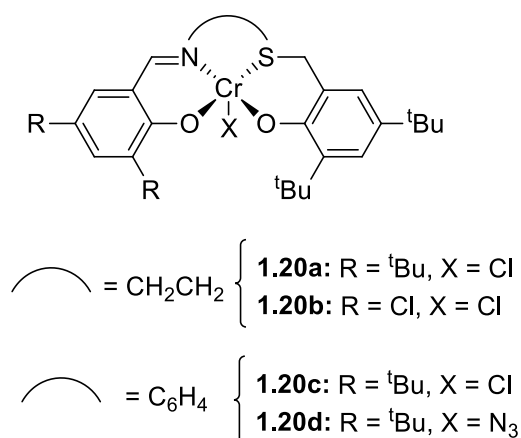


Figure 1.26: [ONSO]-Cr(III) complexes for copolymerization of CO₂ and CHO.⁶⁶

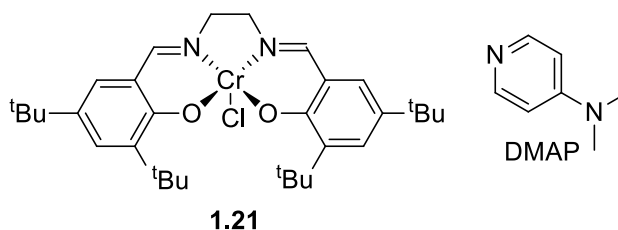


Figure 1.27: Original salen-Cr(III)/DMAP binary catalyst system.

The mechanism behind the formation of PC from CO₂ and propylene oxide (PO) coupling was investigated by computational methods for the salen-CrCl/DMAP system binary system (**Figure 1.27**). A reaction profile diagram for the formation of PC, showing relative energies of various species throughout the reaction pathway was constructed (**Figure 1.28**).⁶⁷ Major findings include the absence of a bimetallic pathway and activation of solely the epoxide by the metal center, rather than simultaneous activation of the epoxide and CO₂. A similar computational study was reported by Darensbourg and co-workers where a salen-Cr(III) compound was compared to the salen-Co(III) analog for

coupling reactions involving epoxides and CO₂.⁶⁸ Polymeric carbonate displacement and subsequent epoxide ring-opening were found to be the rate-determining step ($\Delta G^\ddagger = 92 - 113 \text{ kJ mol}^{-1}$), whereas CO₂ insertion was found to be fast ($\Delta G^\ddagger = 25 - 33 \text{ kJ mol}^{-1}$). Compared to the salen-Co(III) catalysts, salen-Cr(III) systems generally have a higher free energy barrier, which is consistent with the overall higher temperatures needed for Cr(III)-catalyzed systems. Another major finding was that CO₂ is not activated by the metal center before insertion; this is in agreement with Baik and co-workers.^{67,68} Darensbourg and co-workers also reported computational studies to support experimental observations for differences in reactivity among CHO, 1,3-cyclohexadiene oxide (1,3-CHDO) and 1,4-cyclohexadiene oxide (1,4-CHDO), **Figure 1.29**, toward copolymerization reactions with CO₂ using **1.25a**/PPNN₃ (**Figure 1.31**) as the catalyst system. The degree of activity was found to be 1,3-CHDO > CHO > 1,4-CHDO for monomer conversion in copolymerization reactions with CO₂.⁶⁹ This was validated computationally where the relative free energy barrier for copolymers of 1,3-CHDO, CHO and 1,4-CHDO were 11, 14 and 25 kJ mol⁻¹ respectively.⁶⁹ In cases where small amounts of cyclic carbonate were produced, *trans*-1,3-CHDC was never observed; it is the least thermodynamically stable product based on computational studies. Polycarbonate from 1,3-CHDO was produced in molecular weight ranges of 8.9 – 11.4 kg mol⁻¹ with \bar{D} 1.10 – 1.25. It is interesting to note that **1.25a**/PPNN₃ showed lower selectivity towards polycarbonate (40.8 – 69.2%) compared to the Co analog (100%).

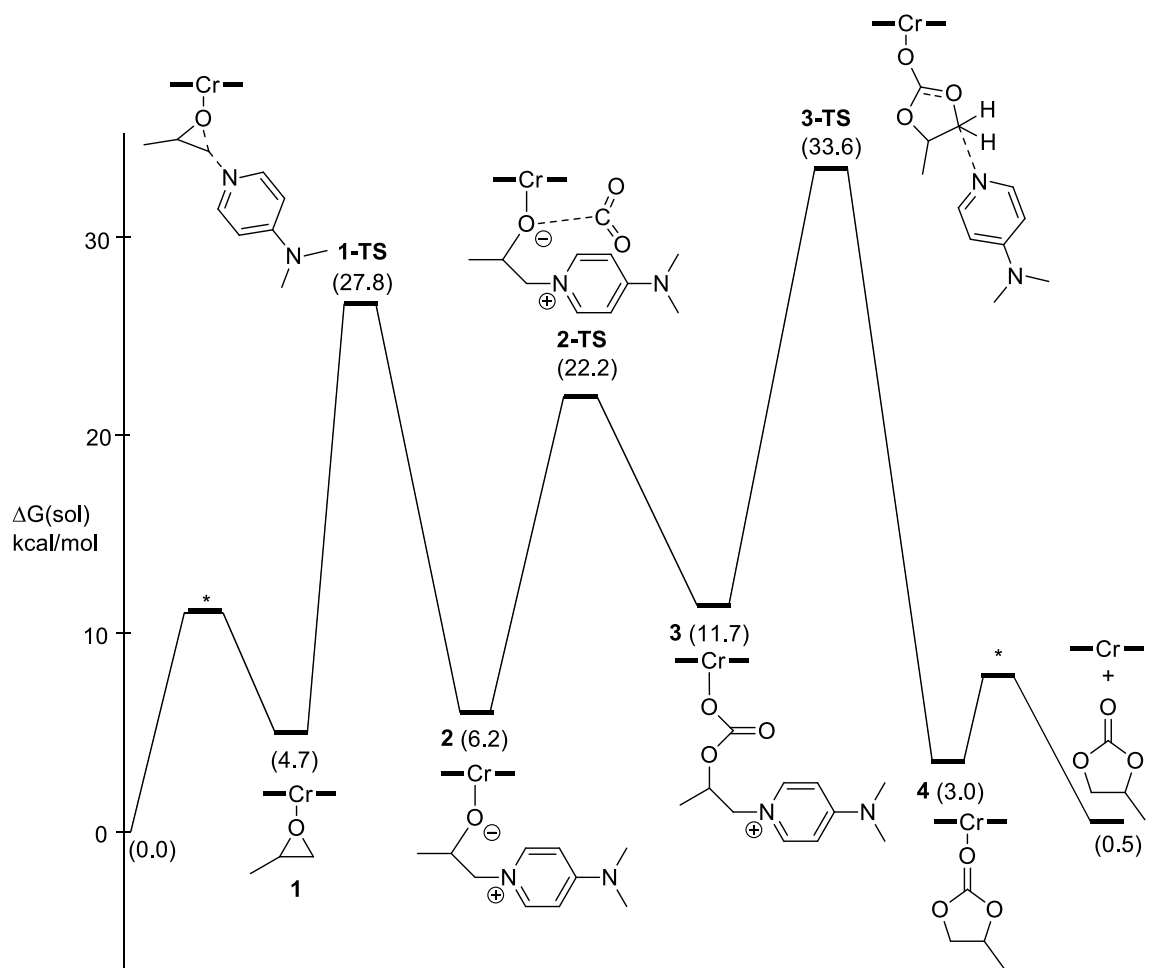


Figure 1.28: Reaction profile for production of PC from CO₂ and propylene oxide.⁶⁷

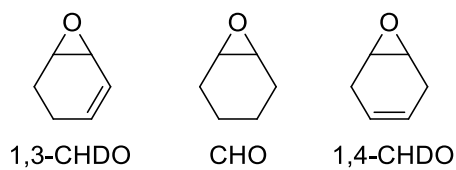


Figure 1.29: Epoxides compared by Darensbourg and co-workers for reactivity in copolymerization reactions with CO₂.⁶⁹

Salen chromium complexes bearing only the bis(imine)-ethylene backbone are often modified with substituents such as phenylene (salophen) and cyclohexylene (to induce chirality). Darensbourg and co-workers compared the activities of a salen-Cr(III)-N₃ bifunctional catalyst (**1.22b**, **Figure 1.30**) and its binary counterpart, (**1.23b**, **Figure 1.30**) for coupling reactions involving CO₂ and isobutene oxide, 2,3-epoxy-2-methylbutane and *cis* and *trans* 2-butene oxide. Further comparison of **1.22b** and **1.23b** to the salen-Co(III)-DNP bifunctional (**1.22a**, **Figure 1.30**) and binary analogs, (**1.23a**, **Figure 1.30**) were also reported. *Cis*-2-butene oxide was the most active for coupling reactions (and the only substrate to produce polycarbonate) which is a result of less steric hindrance for the incoming nucleophile by the methyl on the carbon adjacent to the one undergoing nucleophilic attack during epoxide ring-opening. Both systems were able to produce polycarbonate but only the bifunctional system showed up to 100% polymer selectivity.⁷⁰

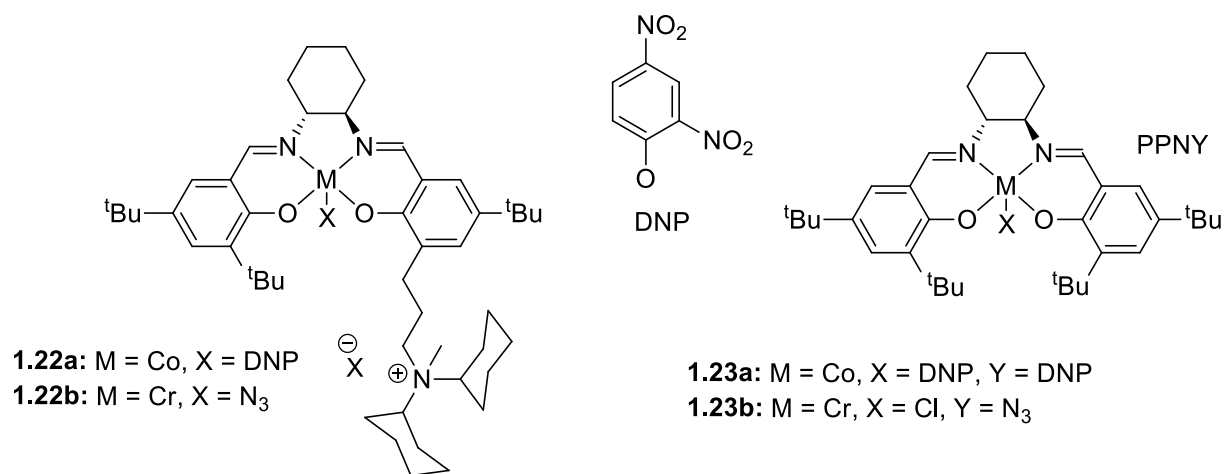
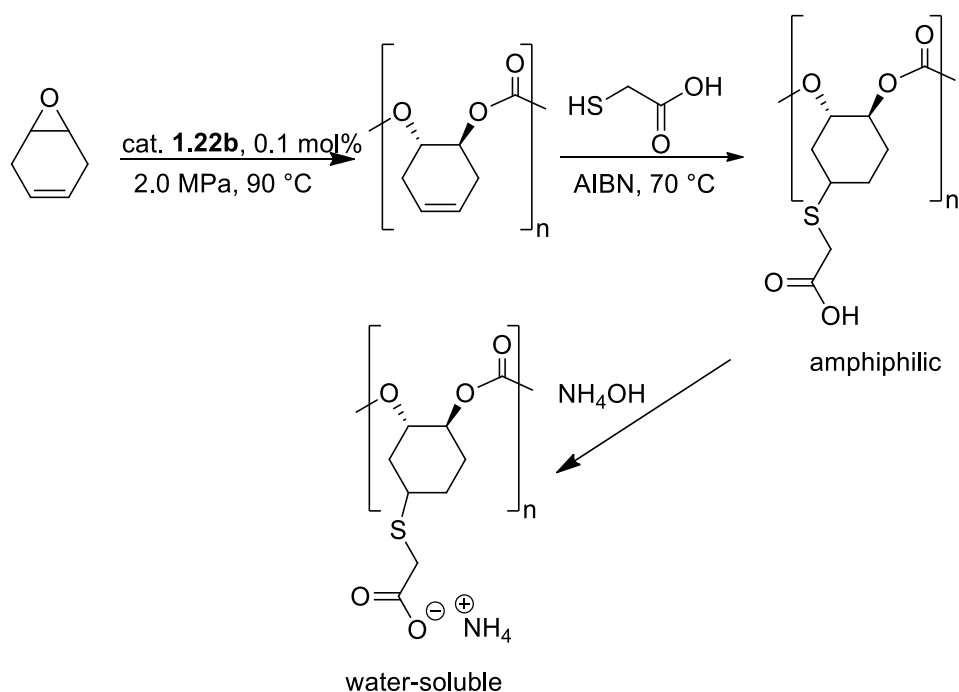


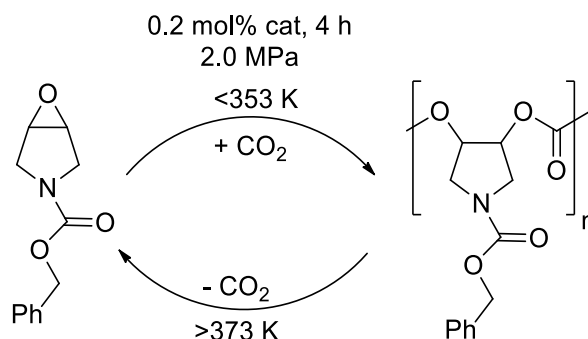
Figure 1.30: Bifunctional (**1.22b**) salen-Cr(III) and binary (**1.23b**) salen-Cr(III) complexes used as catalyst for coupling reactions of isobutene oxide, 2,3-epoxy-2-methylbutane and *cis* and *trans* 2-butene oxide with CO₂.⁷⁰

Catalyst systems **1.22b** and **1.23b** were used to catalyze the copolymerization reactions of CO₂ and 1,4-CHDO. Catalyst **1.22b** demonstrated high polycarbonate selectivity of >99% whereas compound **1.23b** showed up to 77.8% (under ideal conditions) polymer selectivity, along with small amounts of *cis* and *trans* cyclic carbonates.⁷¹ However, monomer conversions were drastically different, showing 69.6% and 9.5% for **1.22b** and **1.23b**, respectively. Molecular weights ranged from 2.1 – 7.6 kg mol⁻¹ and *Đ* from 1.1 – 1.5. With the intent of producing amphiphilic polycarbonate, Darensbourg and co-workers post-functionalized the unsaturated moiety in the polymer backbone with thioglycolic acid via a thiol-ene click reaction (**Scheme 1.7**) using AIBN as a radical initiator followed by deprotonation to produce a water-soluble polymer.



Scheme 1.7: Post-functionalization of poly-3,4-cylcohexadiene carbonate using thioglycolic acid via a thiol-ene click reactions.

Lu and co-workers reported a sustainable approach to polymer synthesis using a dinuclear salen-Cr(III)-X complex **1.24a**, **Figure 1.31**, in the presence of PPNF for copolymerization of 1-benzyloxycarbonyl-3,4-epoxy pyrrolidine (BEP) and CO₂.⁷² This was a specifically designed novel epoxide, which once copolymerized with CO₂ would completely depolymerize to its starting monomeric form when heated to >373 K with quantitative yields (**Scheme 1.8**). These polycarbonates possessed molecular weights ranging from 2.7 – 10.2 kg mol⁻¹ with moderate dispersities averaging to about 1.32.⁷²



Scheme 1.8: Recycling of BEP from polycarbonate using heat.

With the intent of synthesizing degradable polycarbonates Lu and co-workers used *racemic* mono- and dinuclear salen-Cr(III)-X catalysts in the presence of PPN salts for copolymerization of CHO/CO₂ and terpolymerization of CHO/CO₂/phthalic anhydride (PA) or dihydrocoumarin (DHC).⁷³ For CO₂/CHO copolymerization **1.24a** was superior with activity up to 483 TO h⁻¹ and >99% carbonate linkages with no cyclic carbonate detected. Even at extremely low catalyst loading (0.002%), high activity of 390 TO h⁻¹ was observed without sacrificing polymer selectivity. In the case of terpolymerization

(PA/CHO/CO₂), an interesting stepwise polymerization occurred where PA and CHO copolymerized until all PA was consumed, (yielding a polyester) followed by copolymerization of CHO/CO₂ to produce an overall polyester-*b*-polycarbonate terpolymer (**Table 1.1**).

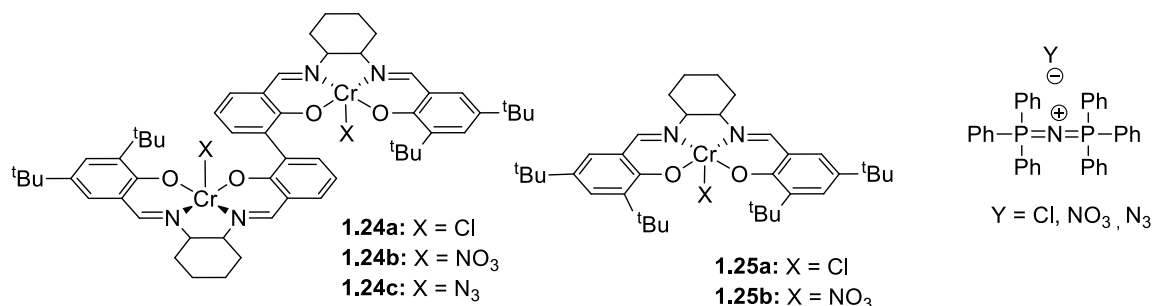
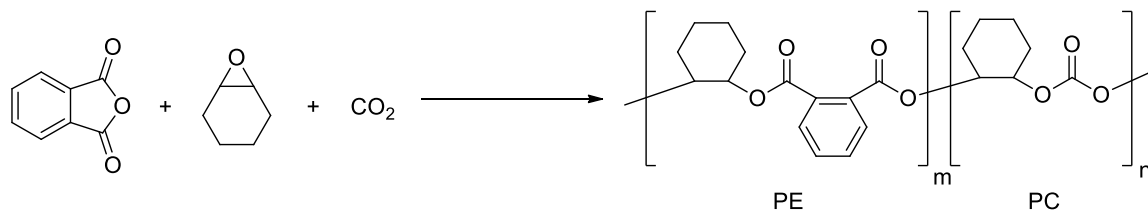


Figure 1.31: Mono- and dinuclear salen-Cr(III)-X catalyst used for synthesis of polycarbonates from CHO/CO₂ copolymerization and CHO/CO₂/PA terpolymerization.⁷³

Table 1.1: CHO/PA/CO₂ terpolymerization catalyzed by **1.24a**/PPNCl.⁷³

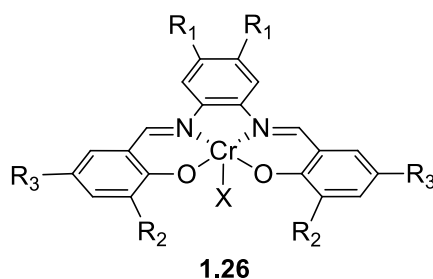


Entry ^[a]	Time (h)	PA conv. ^[b] (%)	PE content ^[c] (%)	PC content ^[d] (%)	<i>M_n</i> ^[e] (kg mol ⁻¹)	<i>Đ</i> ^[e]
1	0.5	43	100	0	3.73	1.19
2	1.0	78	100	0	5.45	1.21
3	1.5	90	100	0	6.87	1.22
4	2.0	>99	100	0	7.32	1.22
5	2.5	>99	78	22	7.43	1.15
6	3.0	>99	73	27	7.93	1.18
7	3.5	>99	68	32	8.56	1.21
8	4.0	>99	63	36	8.91	1.20
9	6	>99	55	46	10.2	1.20

[a] Reaction was performed in neat CHO (30 mmol) in 20 mL autoclave at 80 °C and a 1.0 MPa CO₂ pressure. **1.24a**/PPNCl/PA/CHO = 1/2/500/1000, molar ratio. [b]

Conversion of PA, determined by ^1H NMR spectroscopy. [c] PE (Polyester) content in the resultant polymer, determined by ^1H NMR spectroscopy. [d] PC (Polycarbonate) content in the resultant polymer, determined by ^1H NMR spectroscopy. [e] Determined by gel permeation chromatography in THF, calibrated with polystyrene.

Jia and co-workers reported a novel salen-Cr(III)Cl immobilized on a modified poly(aniline-co-o-aminophenol), MPOAP, for copolymerization of CHO and CO_2 .⁷⁴ Enhanced activity over the homogeneous analog was observed as well as increased molecular weights and narrower dispersity. The best result was observed in a 10 h reaction at 348 K and 50 bar which produced polycarbonate (isotactic and syndiotactic) with molecular weight of 10.9 kg mol^{-1} and \bar{D} of 1.08. Catalyst activity was displayed in $\text{g}_{\text{poly}} \cdot \text{g}_{\text{cat}}^{-1} \cdot \text{h}^{-1}$ where MPOAP-salen-Cr(III)Cl and salen-Cr(III)Cl (homogeneous analog) displayed $15.01 \text{ g}_{\text{poly}} \cdot \text{g}_{\text{cat}}^{-1} \cdot \text{h}^{-1}$ and $12.97 \text{ g}_{\text{poly}} \cdot \text{g}_{\text{cat}}^{-1} \cdot \text{h}^{-1}$ respectively. The believed benefits of the MPOAP support are selectivity, where no cyclic carbonate was observed, and increased thermal stability compared to its unsupported counterpart.⁷⁴



- a:** $R_1 = H, R_2 = R_3 = tBu$,
b: $R_1 = H, R_2 = R_3 = H$,
c: $R_1 = H, R_2 = tBu, R_3 = H$,
d: $R_1 = H, R_2 = H, R_3 = tBu$,
e: $R_1 = H, R_2 = tBu, R_3 = MeO$,
f: $R_1 = H, R_2 = tBu, R_3 = NO_2$,
g: $R_1 = CH_3, R_2 = R_3 = H$,
h: $R_1 = Me, R_2 = R_3 = H$,
i: $R_1 = Cl, R_2 = R_3 = H$,
j: $R_1 = Cl, R_2 = tBu, R_3 = H$,
k: $R_1 = Cl, R_2 = tBu, R_3 = MeO$
a-k: $X = Cl$, **(i):** $X = Br$, **(ii):** $X = I$, **(iii):** $X = OAc$, **(iv):** $X = OTs$

Figure 1.32: (Salophen)Cr(III)X analogs reported by North and co-workers.⁷⁵

North and co-workers reported an exhaustive study on (Salophen)-Cr(III)-X complexes used for mostly cyclic carbonate production from CO₂ and epoxides **Figure 1.32**.⁷⁵ A variety of epoxides, co-catalyst, ligand aromatic substituents (R_1, R_2, R_3), and the ancillary ligand, X were screened. The reactions done in this work were performed primarily at ambient temperature and pressure with high activity where compound **1.26e(i)** was the most active. Kinetics studies showed that [(salophen)CrBr₂][−] was the active species and a mechanism was proposed. Dissociation of one bromide ligand occurs in the presence of competing epoxide, followed by intermolecular ring-opening, CO₂ insertion and subsequent back-biting to yield the cyclic carbonate.⁷⁵ North and co-workers had previously reported an analogous catalyst system, **1.26b** with an NEt₂

substituent in the *ortho* position, for similar reactions.⁷⁶ Substrate and co-catalyst screenings were also done and TBAB was shown to be the most active co-catalyst. Compared to its Al analog, **1.26b**, showed less activity at ambient temperature and pressure. However, at higher temperature and pressure, **1.26b** was more efficient when sterically congested disubstituted substrates were used; consistent with Darensbourg and co-workers' computational study.^{68,76}

1.3.2 Other catalyst systems bearing tetradentate ligands

With a slight alteration in ligand trend, Dinjus and co-workers reported a study using Cr(III) N₄-pyridine-carboxamide complexes for coupling of CO₂ with epoxides (**Figure 1.33**). A comparison was performed with Co and Fe analogs, but the Cr species were only active toward cyclic carbonate production from PO/CO₂ and very low conversion (>9%) for CHO/CO₂. However, there was 100% selectivity towards polymer production for compounds **1.27a** and **1.27b** but carbonate linkages were only 21% and 38% respectively.⁷⁷

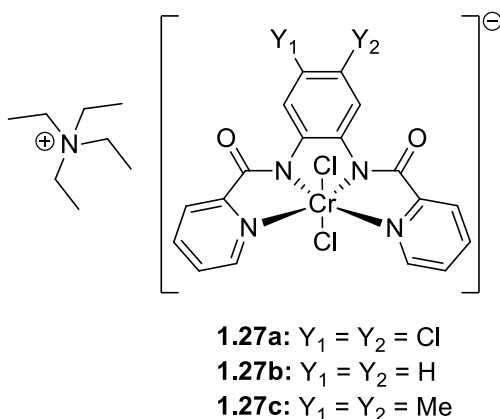


Figure 1.33: Cr(III) N₄-pyridine-carboxamide complexes for coupling of CO₂ with CHO or PO.⁷⁷

Another approach to the N_4 ligand type is a Cr(III) complex reported by Bulto and co-workers, bearing bis(aniline) rather than bis(phenolate).⁷⁸ The complex consists of a Cr(III) center with two neutral imine and two neutral amine donors (from aniline) with two axial chloride (one may dissociate) ligands and a chloride counter-ion. Another analog featured anionic amine donors where the Cr(III) center has one axial chloride ligand. Generally, the cationic species showed increased activity over the neutral species for CO_2/SO coupling reactions to give cyclic styrene carbonate. In contrast, polycarbonate production was afforded when CO_2 was coupled with CHO using the former catalyst system. With reaction conditions such as 5 MPa CO_2 pressure, 0.2 mol% catalyst/co-catalyst (DMAP, PPNCl and Py were investigated) loading, low activities of up to 17 TO h^{-1} were achieved but with good conversion (80%). Polycarbonate selectivity and CO_2 incorporation of 80% and 92% respectively, were observed.⁷⁸

A different class of Schiff base containing Cr(III) complexes were reported by Bulto and co-workers, **Figure 1.34**, which possessed a combination of tri- and bidentate ligands as well as an axial chloride ancillary ligand.⁷⁹ After catalyst screening, the Cr(III) complex formed from **1.28b** was the most successful for coupling of CHO/ CO_2 to produce a mixture of polycarbonate and cyclic carbonate; the ratio of the two depended on the co-catalyst used. For 12 h reactions done at 353 K and 5 MPa CO_2 , high conversions (up to 93%) with 62% polymer selectivity and 96% CO_2 incorporation were observed. MALDI-TOF MS studies indicate the presence of chain-transfer (chloride chain-ends) and water acting as a terminating agent (hydroxide chain-end). On the other

hand, when SO or PO were used as substrates, strictly cyclic carbonate was observed with PPNCl as a co-catalyst; up to 97% conversion for 24 h.⁷⁹

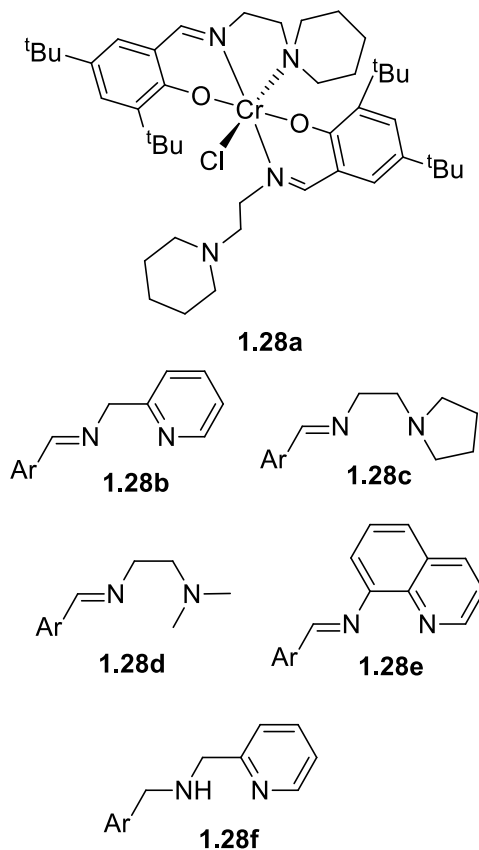


Figure 1.34: Cr(III) hexacoordinate complexes reported by Bulto and co-workers for coupling CO₂ and CHO. Ar = 2,4-di-tert-butyl phenol.⁷⁹

Gambarotta, Duchateau and co-workers also reported Cr(III) catalysts bearing mono-, bi- or tridentate ligands with aminopyrrole, iminopyrrole, pyridine-aminophosphine and acetylacetonate functionalities (**Figure 1.35**).⁸⁰ With a total of eight complexes, screenings showed that **1.29a** and **1.29b** were the most active when coupled with PPNCl as a co-catalyst. It is interesting to note that these coupling reactions were also possible in

toluene with conversions up to 99% and high carbonate linkages (93%) but over long reaction times and therefore moderate TOFs.

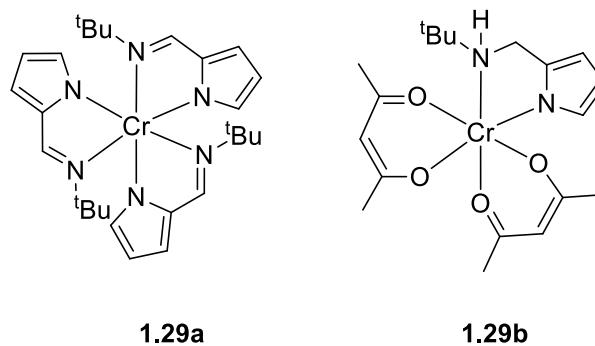
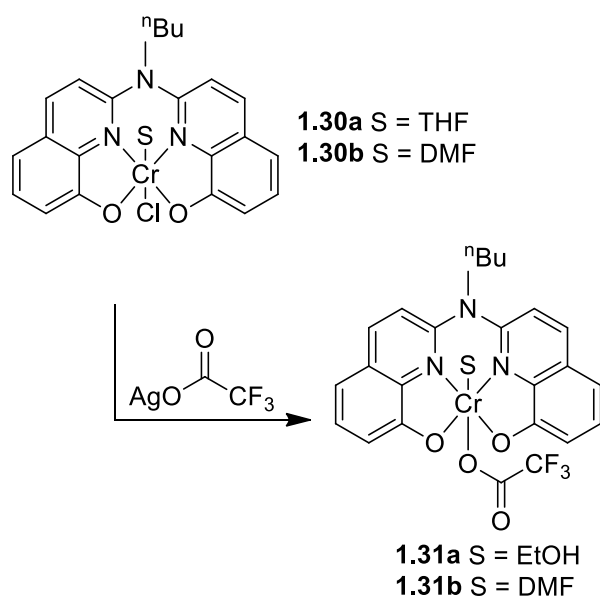


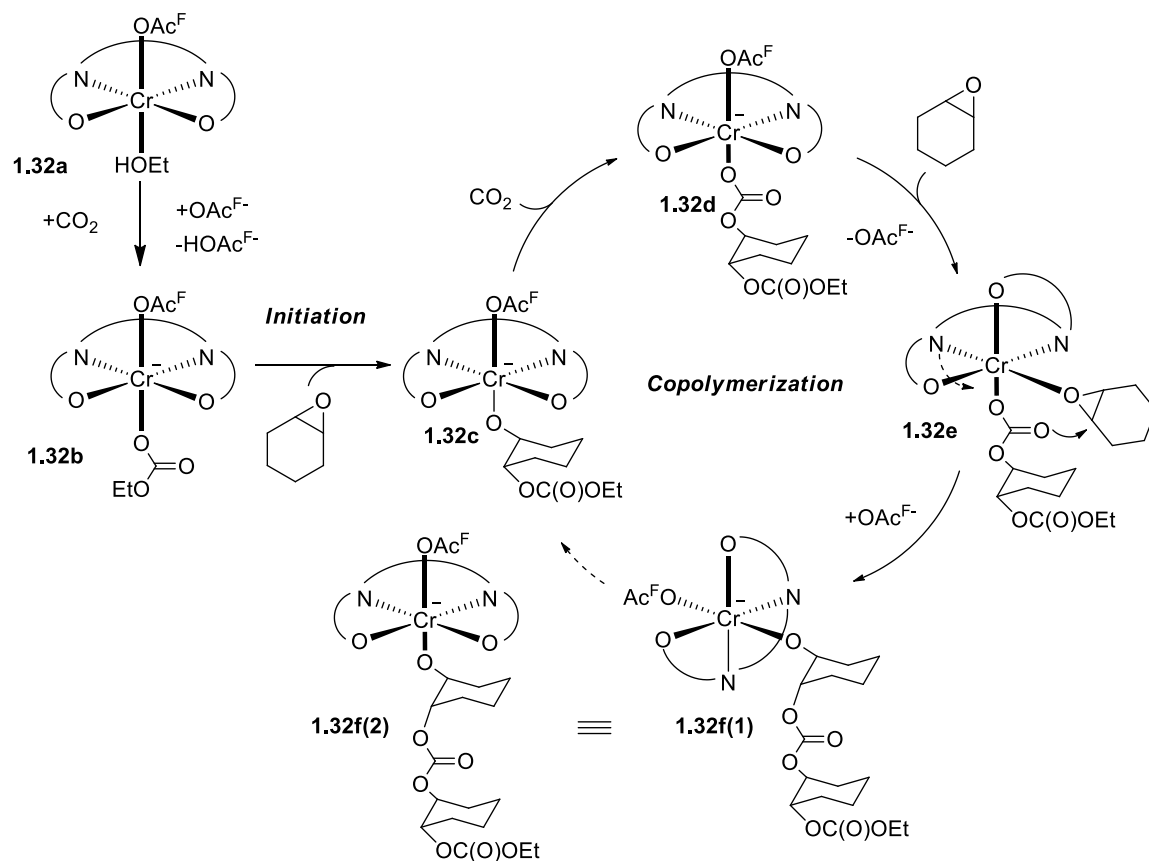
Figure 1.35: Most active Cr(III)-iminopyrrole and Cr(III)-acac-aminopyrrole complexes reported by Duchateau and co-workers for CHO/CO₂ coupling reactions.⁸⁰

Müller, Sundermeyer and co-workers reported a Cr(III) complex supported by a bis(hydroxyquinoline)butylamine, bhqba, possessing an [ONNO] chelating pattern (**Scheme 1.9**).⁸¹ The active species **1.31a** and **1.31b** were synthesized via ligand exchange using silver trifluoroacetate. Compound **1.31a** was highly active toward CO₂/CHO coupling, producing a mixture of polycarbonate and cyclic carbonate with conversions of up to 76% after only 3 h; for PO/CO₂, up to >99% conversion in 4.5 h but only cyclic carbonate was detected.⁸¹

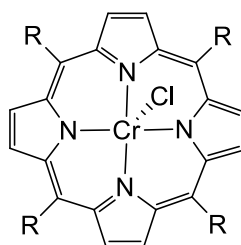


Scheme 1.9: Bis(hydroxyquinoline)Cr(III)-OAc^F complexes used by Müller, Sundermeyer and co-workers for reactions involving CO₂ and CHO.⁸¹

Based on kinetics studies, a mechanism was proposed and referred to as inner-sphere mechanism because of the ligand's ability to rearrange its coordination geometry with the metal center and promote intramolecular epoxide insertion into the growing polymer chain (**Scheme 1.10**). An interesting feature of this mechanism is pre-initiation where CO₂ inserts into the Cr-ethanol bond (in **1.32a**) right before epoxide insertion; a rarely proposed phenomenon. Subsequent steps after CHO insertion include CO₂ insertion into the metal alkoxide bond of **1.32c** to produce **1.32d** bearing a metal-carboxylate. Incoming coordinating CHO promotes dissociation of the trifluoroacetate ligand, which triggers rearrangement of the ligand thus producing **1.32e**. This unique arrangement along with the ligand's preference for an equatorial arrangement promotes intramolecular epoxide insertion to produce **1.32f(1)** which is equivalent to **1.32f(2)**.⁸¹



Scheme 1.10: Inner-sphere mechanism proposed by Müller and co-workers for CO_2/CHO coupling reactions using a bis(hydroxyquinoline)Cr(III)- OAc^{F} .⁸¹



- 1.33a:** R = phenyl (TPP)
1.33b: R = pentafluorophenyl (TFPP)

Figure 1.36: Porphyrin-Cr(III) complexes used as catalyst in $\text{CO}_2/\text{epoxide}$ coupling reactions.⁸²⁻⁸⁴

Chisholm and co-workers reported porphyrin-derived ligands (TPP)Cr(III)Cl, **1.33a**, and (TFPP)Cr(III)Cl, **1.33b** (Figure 1.36), in comparison to their Al and Co counterparts in coupling reactions involving PO and CO₂.⁸² Some key findings include **1.33a** being two orders of magnitude faster than the Al analog for ROP of PO at room temperature and double chain-growth per metal in the presence of PPnCl for CO₂/PO copolymerization. An increased loading of Cl⁻ appears to induce polymer backbiting by displacing the growing polymer chain, thus leading to PC formation. A later reported study using **1.33a** for coupling reactions involving SO and CO₂ showed products such as polystyrene oxide, polystyrene carbonate and cyclic styrene carbonate.⁸³ NMR, polarimetry and chiral HPLC were used to investigate the stereochemistry of the ring-opening step. Essentially, ring-opening was detected at both the methine and methylene carbons but preferentially at the methine with stereochemical inversion also occurring.⁸³ Chukanova and colleagues reported a kinetic study on the PO/CO₂ coupling reactions using (TPP)Cr(III)Cl in comparison to its Co analog to determine the effect of reaction conditions on the reaction rate.⁸⁴ Essentially, the rate is constant until 20% conversion of PO and activity up to 130 TO h⁻¹ was observed. Contrary to the Co catalyst, the reaction rate is pressure dependent in the range of 0.4 – 1.0 MPa for (TPP)Cr(III)Cl. The most significant difference was product selectivity; (TPP)Cr(III)Cl produced strictly PC but the (TPP)Co(III)Cl produces a mixture of PC and PPC.⁸⁴

Kozak and co-workers reported a series of Cr(III)Cl amine-bis(phenolate) complexes (**1.34a-e**) for copolymerization of CO₂ with CHO in the presence of DMAP (in most cases) as a co-catalyst.⁸⁵ It is interesting to note that **1.34a** adopts a chloride-bridged

dimer conformation in the solid state, that possesses the phenolate rings in a *cis* configuration rather than *trans* (**Figure 1.37**). This dimer is believed to dissociate in solution, especially in the presence of coordinating species such as CHO.⁸⁶⁻⁸⁸ MALDI-TOF MS was used to study the various binding modes of a Cr(III) amino-bis(phenolate) complex with DMAP under influence of the pendent arm. Some cases showed two DMAP molecules binding (displacing the chloride) and others showed no DMAP coordination even at high DMAP loading. DMAP end-groups in the polymer at high loading suggests intermolecular nucleophilic attack mechanism but at one equivalent, chloride end-groups were more prominent suggesting a non-competing DMAP mechanism for ring opening.⁸⁵

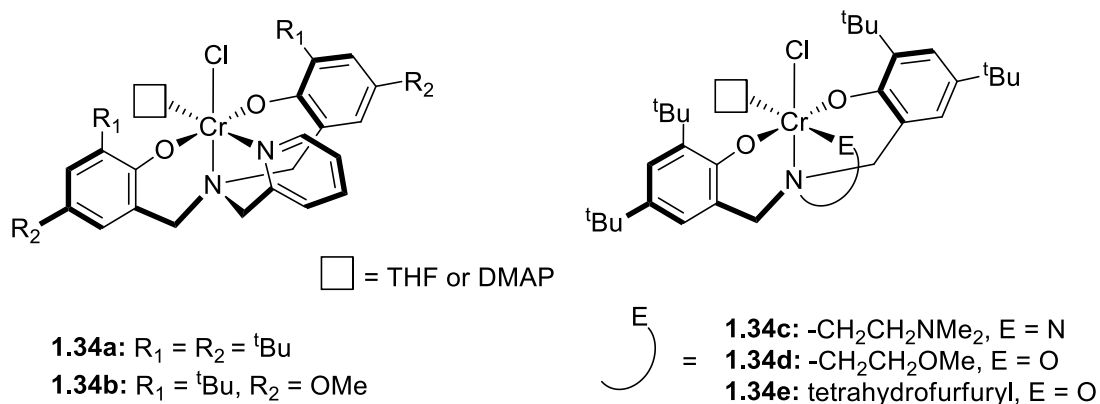


Figure 1.37: Various Cr(III) amino-bis(phenolate) complexes used for copolymerization of CO_2 and CHO.⁸⁵

In another study, compounds **1.34b·THF** and **1.34b·DMAP** showed increased catalytic activity over its predecessor, **1.34a** (chloride-bridged dimer), for copolymerization of CHO and CO_2 .²⁴ However, **1.34c-THF** showed increased initial activity (reaction rates via in situ infrared monitoring) over **1.34b·THF** and chloride

bridged, dimeric **1.34a**.⁸⁶ Polymer end-group analysis using MALDI-TOF MS indicated that initiation takes place via ring opening of the epoxide by the anion of the co-catalyst. However, when **1.34b·DMAP** was used in the presence of PPnCl, it was proposed that DMAP dissociation is promoted which then ring-opens the epoxide; this is based on observed DMAP polymer end-groups.²⁴ When **1.34c·THF** was used in the presence of DMAP, chloride end-groups were observed which indicates chloride displacement followed by ring-opening of the newly coordinated epoxide.⁸⁶ Based on these and other findings two pathways for initiation were proposed; a cationic pathway in the absence of PPnCl and neutral in the presence of PPnCl for compound **1.34b·DMAP**. Further studies on **1.34b·DMAP** show a first order dependence on catalyst loading which is similar to the findings from a bifunctional catalyst bearing a quaternary ammonium salt.⁸⁹ Varying the co-catalyst (DMAP) concentration showed an increase in the concentration of DMAP end-groups and also increased reaction rate without sacrificing selectivity of polycarbonate synthesis. These new findings brought forth a proposal for possible intramolecular epoxide ring-opening initiation step at higher (more than 1 equivalent) DMAP concentrations.⁸⁹ Kozak and co-workers have also explored other epoxides for coupling with CO₂. Chloride bridged, dimeric **1.34a** was used for copolymerization of PO and CO₂ to produce polycarbonate at 295 – 298 K, primarily when PPnCl (highest selectivity) was used as the co-catalyst. Cyclic carbonate was produced at higher temperatures particularly when TBAB was used.⁸⁷ For SO/CO₂ coupling, strictly cyclic carbonate was produced.

Liu and co-workers reported an [OSSO]Cr(III)X complex for copolymerization of 4-vinylcyclohexene oxide and CO₂. This ligand is dianionic and analogous to the [ONNO]-salan ligands and affords a tetradentate coordination mode with chromium.⁹⁰ Reported compounds had backbones/X ligand such as cyclohexylene/Cl or N₃, ethylene/Cl, and phenylene/Cl (**Figure 1.38**). Catalyst screening showed the cyclohexylene/Cl combination in the presence of PPNCl, to be the most active with 73% PVCHC selectivity, 97.5% carbonate linkages and M_n of 15000 g mol⁻¹. Using this [OSSO]Cr(III)Cl complex, reaction optimizations showed activity up to 134 TO h⁻¹ and 79% selectivity to PVCHC.⁹⁰

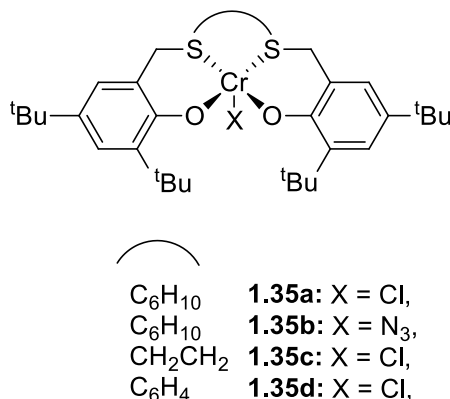


Figure 1.38: [OSSO]Cr(III)X complexes used for copolymerization of 4-vinylcyclohexene oxide and CO₂.⁹⁰

1.3.3 Other types of catalyst systems

A Cr(III) catalyst system using a metal-organic framework (MOF) known as **FJI-C10** was reported by Cao and co-workers for coupling of epoxides and CO₂ to produce cyclic carbonates. The MOF contains Cr₃O clusters are held together by 1,4-benzenedicarboxate (BDC) and ethylimidazolium-BDC (with halide counter-ion)

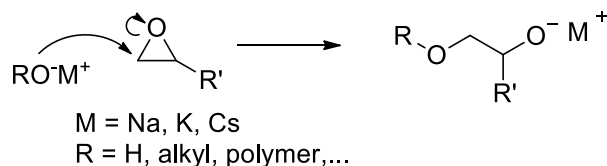
linkers.⁹¹ Cyclic carbonates were produced from CO₂ and epoxides such as epichlorohydrin, styrene oxide and allylglycidyl ether to name a few. Reactions were performed at 1 bar CO₂ and no co-catalyst with yields up to 93%. Qiang and co-workers reported a Zn and Cr DMC catalyst system, synthesized by ball milling, for alternating copolymerization of CO₂ and PO (PPC), PO/ PA and CO₂/PO/PA (PPCPA). Molecular weights for PPC and PPCPA of 68.6 kg mol⁻¹ and 15.9 kg mol⁻¹, respectively, and selectivity up to 82.5 % were obtained, which is impressive for PPC.

1.4 Ring-opening polymerization of epoxides

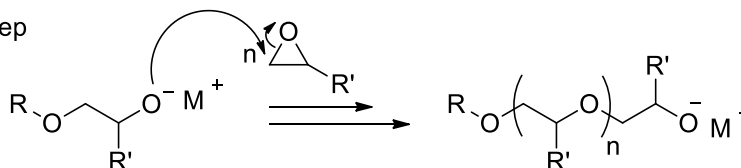
1.4.1 Types of ROP mechanisms

According to Coates and co-workers, epoxide ring-polymerizations generally follow one of these three main mechanisms (1) cationic, (2) anionic and (3) metal-mediated.⁹² The cationic mechanism is one that affords little control during the polymerization process, leads to stereo-irregular polymer and is usually coupled with a metal-based mediator hence a coordination-insertion mechanism is followed. During the polymerization process a common occurrence is the generation of a cation which leads to scrambling of the stereocenter therefore affording stereo-irregular polymer. Anionic ROP is more common and is often observed with metal-free initiators. However, initiation by an alkoxide species (for example an alkali metal alkoxide) involves nucleophilic-S_N2-type substitution to form a new alkoxide, which propagates by further attacking monomer molecules thus resulting in polymer. Termination is usually done using a protic compound like water or an alcohol (**Scheme 1.11**)

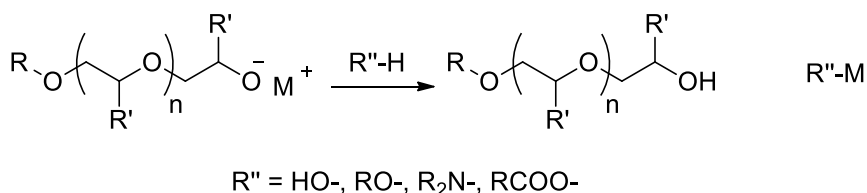
Initiation Step



Propagation Step

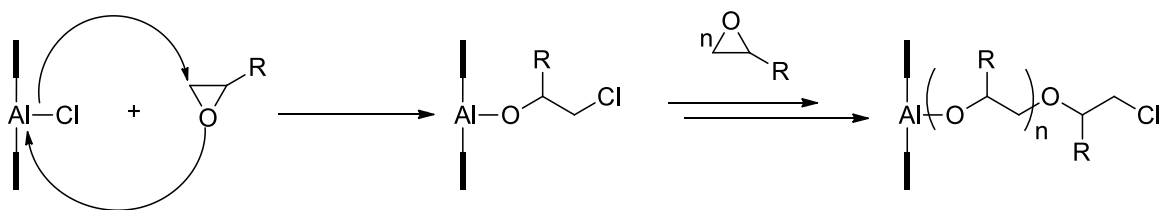


Termination Step



Scheme 1.11: Anionic ROP mechanism initiated by alkali metal alkoxides.

The metal-mediated mechanism, also referred to as the coordination-insertion mechanism is the sort seen when a coordination complex with a Lewis acidic metal center is used as a catalyst, such as (TPP)AlCl used by Inoue and co-workers for ROP of epoxides.^{93,94} Metal-mediated and anionic mechanisms are related as their active species may consist of metal/alkoxide species ($L_n\text{M-OR}$). The difference is that alkali and alkaline-earth metals form a more ionic interaction with the alkoxide species whereas transition and main-group metals form a more covalent bond (coordinate covalent). An incoming epoxide coordinates to the metal-center and is ring-opened by the dissociated nucleophile in a concerted fashion to generate a metal-alkoxide species which ring-opens new epoxide to propagate and generate polyether (**Scheme 1.12**).



Scheme 1.12: Illustration of metal-mediated ROP of epoxides using aluminum-based species.

1.4.2 Selected catalysts for ROP of epoxides

Many catalysts, which can contain metals or be metal-free, are capable of ring-opening polymerization reactions of epoxides to produce polyethers.^{92,94} Metal-based systems can contain Co, Al, Zn, or alkali/alkaline-earth metals, whereas metal-free systems include amines and N-heterocyclic carbenes.^{92,94}

Coates and co-workers used a bimetallic salen-Co(III)-Cl complex for ROP of propylene oxide in the presence of an organic ionic compound (**Figure 1.39**).⁹⁵ Substrate variation and co-catalyst (**1.37a – i**, and **1.38**) screening studies were performed (using *R,R,R,R*-**1.36a** as the catalyst) to determine their influence on ROP reactions. For the acetate-based co-catalysts, alkali metal salts showed no activity (conversion) after 24 h whereas TBAOAc (tetrabutylammonium acetate) showed low activity (10.2%) that was attributed to its instability to bases. The phosphazaniums (**1.37a-i**) and phosphonium (**1.38**) were further explored to due to the poor activity of the acetates. Phosphazanium, **1.37b**, showed good activity and selectivity whereas PPnCl (for comparison), showed no activity which demonstrated the utility of the phosphazanium co-catalyst. Compounds **1.37c**, **1.37d** and **1.37i** showed no activity at all whereas **1.37f** showed moderate activity

and selectivity. Ultimately, the best activity came from **1.36a/1.37e** combination with conversion of 49.9% and 8000 TO min⁻¹ with molecular weight of 157 kg mol⁻¹ ($\bar{M}_n = 1.9$). Reactions were typically done at 0 °C with a catalyst loading of 0.025% in dimethoxyethane (DME) as a solvent (1M [PO]). It is interesting to note that only the (*R*)-PO was consumed when **1.36a/1.37e** was used (producing (*S*)-polypropylene oxide) while *rac*-**1.36b/1.37e** produced a mixture of both (*R*)- and (*S*)-polypropylene oxide.

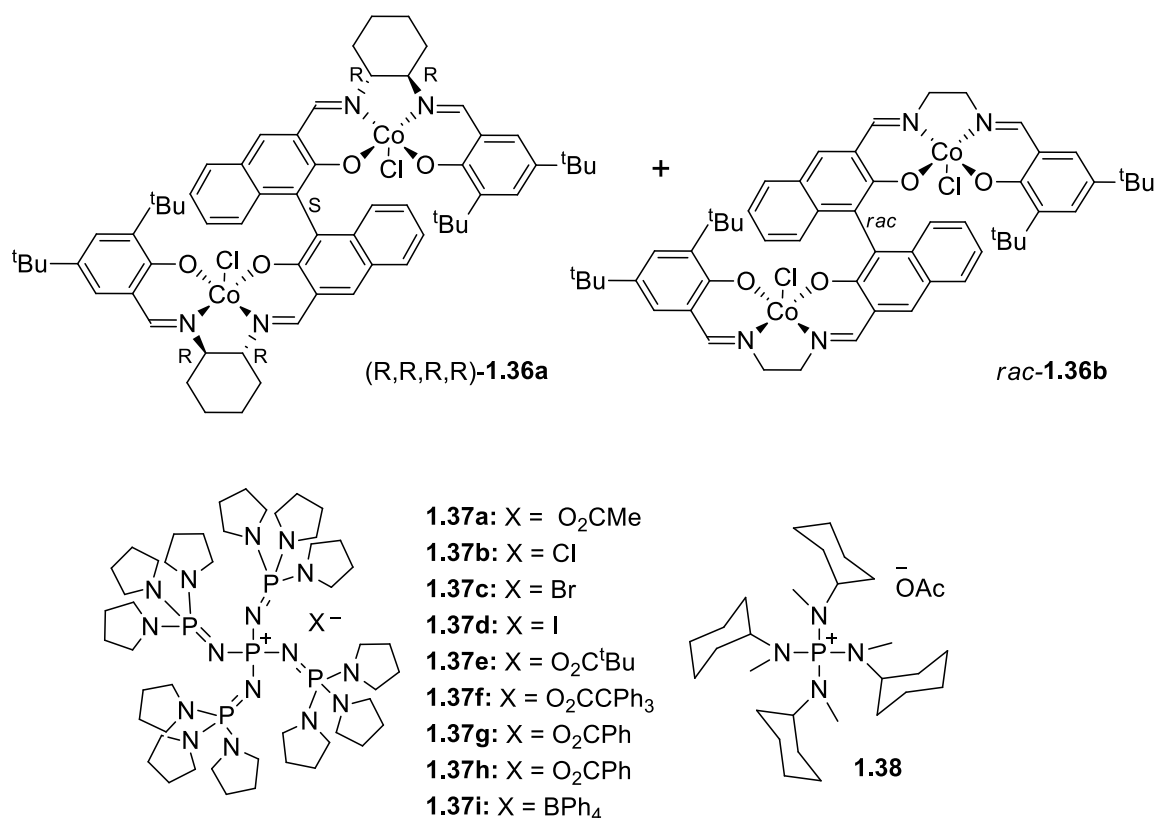


Figure 1.39: Bimetallic salen-Co(III)Cl complexes and co-catalysts used for ROP of propylene oxide.⁹⁵

Aluminum has been a very common metal of choice for metal-based catalyst systems (**Figure 1.40**) for ROP of epoxides and an early report of epoxide ROP reactions by Inoue

and co-workers entailed the use of a (TPP)AlCl catalyst (**1.40**).^{92,93} Inoue performed ring-opening copolymerisation reactions using two epoxides simultaneously such as PO/1,2-epoxybutane (1BO) and PO/EO. In both cases, a linear increase in molecular weight with an increase in conversion was observed, while maintaining narrow dispersities. This was classified as a living polymerization due to block copolymers and controlled chain lengths.

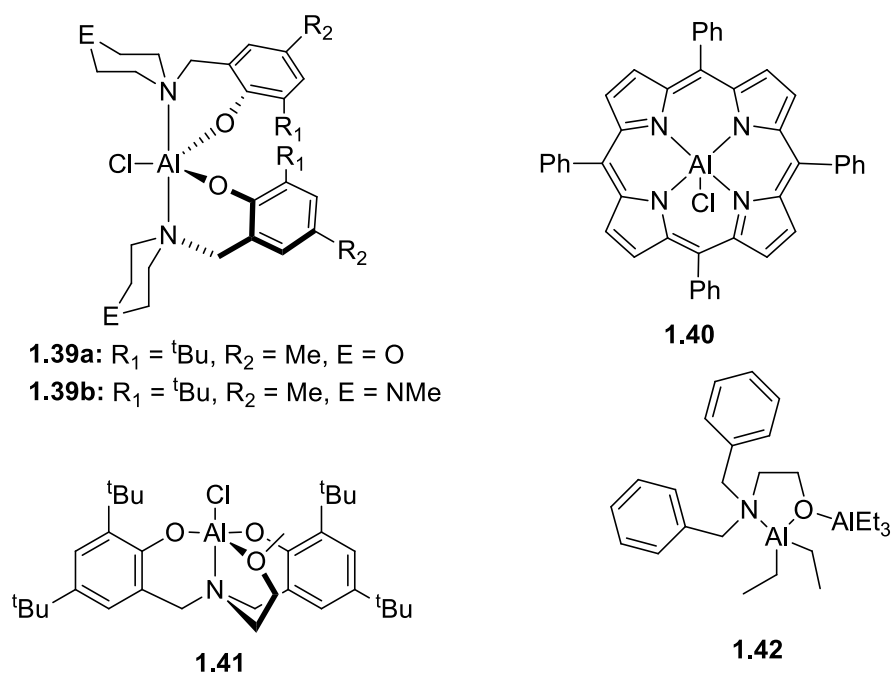


Figure 1.40: Aluminium-based metal complexes used as catalyst for ROP of epoxides.^{92,93,96,97}

Kerton and co-workers reported highly active aluminum amine-bis(phenolate) complexes for ROP of CHO (**1.39a-b** and **1.41**).⁹⁶ The chloride ancillary ligand is believed to be the initiator through nucleophilic attack of coordinated epoxide which was evidenced by MALDI-TOF MS analysis of the resulting polymer, polycyclohexene oxide

(PCHO). Furthermore, these reactions were done neat because of the general inhibition in the presence of solvents such as tetrahydrofuran (THF). Reactions were done neat at room temperature with catalyst loadings ranging from 0.001 – 0.5 mol% and generated PCHO with molecular weights up to 500 kg mol⁻¹ and narrow dispersities. The best activity came from **1.39a** with 580 TO min⁻¹ in a 1 min reaction. Kinetic studies show that the reactions were first order in [Al].

Another aluminum based species is compound **1.42**, **Figure 1.40**, which was reported by Lynd and co-workers for the ROP of PO, BO, ECH and AGE.⁹⁷ The catalyst was a (2-dibenzylamino) ethoxydiethylaluminum (TAXEDA) complex bearing a triethylaluminum (TEA) adduct. In the presence of epoxide, there was concerted dissociation of the TEA adduct and coordination of the epoxide. Nucleophilic attack of TAXEDA ring-opens the epoxide (via its ethoxy oxygen) which generated a new alkoxide bridging both aluminium centers. An incoming epoxide promoted the same process therefore the propagating polyether chain moves along both aluminum metal centers resulting in a (2-dibenzylamino) ethoxy end-group. The “livingness” of this polymerization was investigated by chain extension. AGE was polymerized to completion after 46 h, then subsequent addition of a new monomer showed polymerization continued, thus generating a diblock copolymer. Reactions were typically done at 80 °C for 2 days giving conversions of >99% with high catalyst loadings of up to 1.1 mol%. The highest molecular weight was 95 kg mol⁻¹ with an average *D* of 1.27 for a 5 h reaction using ECH as the monomer.

A report by Kakuchi and co-workers represents a metal-free catalyst system comprised of an alcohol and a phosphazene base for ROP of styrene oxide to produce polystyrene oxide (PSO).⁹⁸ The active initiator is generated by reacting 3-phenyl-1-propanol (PPA) with the phosphazene species to produce **1.43**, **Figure 1.41**. Reactions were performed at room temperature with catalyst loadings ranging from 0.5 – 2 mol% for more than 20 h, with observed conversions of >90 %. Molecular weights ranged from 5.2 – 20.5 kg mol⁻¹, \bar{D} averaging about 1.1 and the theoretical M_n value agreed with the experimental values. PPA end-groups were clearly observed using MALDI-TOF MS therefore experiments to develop end-functionalized PSO using other alcohols such as 4-vinylbenzyl alcohol, 5-hexen-1-ol, 6-azido-1-hexanol, and 3-(hydroxymethyl)-3-methyloxetane (possess well-known clickable and polymerizable groups) were investigated. Kinetic experiments showed a linear increase in PSO molecular weight with reaction all the way up to 100% monomer conversion, and chain extension experiments indicated that this was a living polymerization.

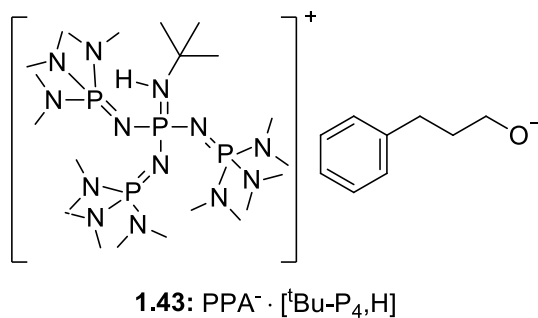


Figure 1.41: Alcohol/phosphazene active species for ROP of styrene oxide.⁹⁸

Another metal-free study was reported by Morinaga and co-workers where tetra-*n*-butylammonium fluoride (TBAF) in the presence of water or ethanol was used for ROP of glycidyl phenyl ether (GPE) to produce poly(GPE).⁹⁹ Polymerizations were typically done at 50 °C for 21 h and conversions of >99% were achieved. This catalyst system demonstrated a very controlled polymerization as the theoretical M_n values were consistent with the experimental values (1400 g mol⁻¹ and 1200 g mol⁻¹ for observed and theoretical respectively) and \bar{D} averages about 1.25. A proposed mechanism for ROP of GPE started with ring-opening of the epoxide by fluoride which generated an alkoxide with an ionic interaction with tetra-*n*-butylammonium cation (Bu₄N⁺). The alkoxide of the ionic species was then protonated by the alcohol thus yielding [Bu₄N⁺ ·OR]. Propagation took place with either the fluoride ring-opened species or [Bu₄N⁺ ·OR] as initiators to react with unreacted GPE to produce poly(GPE) bearing a tetrabutylammonium alkoxide.

1.5 Objectives of this thesis

Previous work in the Kozak group has shown success in developing Co(II)/(III) amino-bis(phenolate) complexes for use as catalysts in coupling CO₂ and epoxides in the presence of co-catalysts. The selectivity of these reactions was primarily towards cyclic carbonates. One goal of this research was to modify current Co(II)/(III) amino-bis(phenolate) coordination complexes by introducing various monodentate and/or bidentate ancillary ligands with the aim of tuning catalyst selectivity toward polycarbonate synthesis. Modification and characterization of a series of Co(III) amino-bis(phenolate) complexes bearing various ancillary ligands such as acetate,

trifluoroacetate (TFA) and 2,4-dinitrophenolate yielded selectivity toward cyclic carbonate synthesis and is discussed in Chapter 2.

Another goal was to modify the electronic properties of the metal center by varying functional groups on the phenolate O-donors of the tetradentate ligand. Making the Co center more Lewis acidic allowed for polycarbonate synthesis to be preferred over cyclic carbonate formation. This is discussed in Chapter 3. The resulting polycarbonate presented challenges in purification (removal of residual catalyst) therefore, avenues for optimization of polymer purification are also discussed. The structure of the metal complex (active catalyst) was elucidated by X-ray crystallography which allowed for explanation of observed polymer end-groups, as determined by MALDI-TOF MS.

Cr(III)-amino bis(phenolate) coordination complexes developed in the Kozak group in the past have shown very good activity as catalysts for CO₂/epoxide copolymerization reactions. The goal of this project was to develop a different Cr(III)-based catalyst system for CO₂/epoxide copolymerization reactions with the potential for increased activity and/or a wider substrate scope. Chapter 4 describes the synthesis and characterization of a new Cr(III) amino-bis(phenolate) coordination complex related to studies with an iron complex of the identical ligand.¹⁰⁰ This ligand is also based on reported salan-type ligands and the nitrogens in the backbone are tethered together therefore it is more rigid. This led to the following discoveries: (1) An “ate” Cr(III) complex with a structure that depends on its environment in solution; (2) High catalytic activity toward ROP of CHO; (3) An unusual polymerization process which yields high molecular weight polymer. Kinetic

studies performed, provide insight into activity and characteristics of the polymerization process.

With a goal of further modifying the above-mentioned Cr(III) complex, selectivity was tuned toward polycarbonate synthesis by modifying the substituents on the phenolate O-donors and the results are presented in Chapter 5. To investigate the substrate scope and produce terpolymers, further experiments involving the terpolymerization PO/CHO/CO₂, CHO/ECH/CO₂ and Glycidol/CHO/CO₂ are discussed in Chapter 6. Moreover, miscellaneous experiments with the aim of understanding various mechanistic aspects are also presented in Chapter 6.

1.6 References

1. P. Anastas and N. Eghbali, *Chem. Soc. Rev.*, 2010, **39**, 301-312.
2. P. T. Anastas and J. C. Warner, *Green chemistry: theory and practice*, Oxford University Press, Oxford, 1998.
3. M. Lancaster, *Green chemistry: an introductory text*, Royal Society of Chemistry, Cambridge, 2002.
4. P. T. Anastas, *Green Chem.*, 2003, **5**, G29-G34.
5. R. K. Henderson, C. Jiménez-González, D. J. C. Constable, S. R. Alston, G. G. A. Inglis, G. Fisher, J. Sherwood, S. P. Binks and A. D. Curzons, *Green Chem.*, 2011, **13**, 854-862.
6. G. Rothenberg, *Catalysis: concepts and green applications*, Wiley-VCH, Chichester, 2008.
7. P. Tans and R. Keeling, Global Trends in Atmospheric Carbon Dioxide, <https://www.esrl.noaa.gov/gmd/ccgg/trends/>, (accessed January, 2019).
8. M. De-Falco, G. Iquianello and G. Centi, *CO₂: A Valuable Source of Carbon*, Springer-Verlag, London, 1st edn., 2013.
9. M. R. Kember, A. Buchard and C. K. Williams, *Chem. Commun.*, 2011, **47**, 141-163.
10. Q. Liu, L. Wu, R. Jackstell and M. Beller, *Nat. Commun.*, 2015, **6**, 5933-5947.
11. Z. Prokop, L. Hanková and K. Jeřábek, *React. Funct. Polym.*, 2004, **60**, 77-83.
12. S. Fukuoka, M. Tojo, H. Hachiya, M. Aminaka and K. Hasegawa, *Polym. J.*, 2007, **39**, 91-114.

13. M. Winkler, C. Romain, M. A. R. Meier and C. K. Williams, *Green Chem.*, 2015, **17**, 300-306.
14. J. Artz, T. E. Müller, K. Thenert, J. Kleinekorte, R. Meys, A. Sternberg, A. Bardow and W. Leitner, *Chem. Rev.*, 2018, **118**, 434-504.
15. M. Parvin and J. G. Williams, *J. Mater. Sci.*, 1975, **10**, 1883-1888.
16. D. J. Darensbourg, *Chem. Rev.*, 2007, **107**, 2388-2410.
17. X. Zhuang, K. Oyaizu, Y. Niu, K. Koshika, X. Chen and H. Nishide, *Macromol. Chem. Phys.*, 2010, **211**, 669-676.
18. Covestro-AG, Material solutions for application innovations, <https://www.plastics.covestro.com/Applications/Overview.aspx>, (accessed May 1st, 2018).
19. D. J. Darensbourg, *Adv. Inorg. Chem.*, 2014, **66**, 1-23.
20. M. Taherimehr and P. P. Pescarmona, *J. Appl. Polym. Sci.*, 2014, **131**, 41141-41157.
21. D. Y. Jang, H. G. Jang, G. R. Kim and G.-J. Kim, *Catal. Today*, 2012, **185**, 306-312.
22. F. M. Al-Qaisi, M. Nieger, M. L. Kemell and T. J. Repo, *ChemistrySelect*, 2016, **1**, 545-548.
23. C. Chatterjee and M. H. Chisholm, *Chem. Rec.*, 2013, **13**, 549-560.
24. K. Devaine-Pressing, L. N. Dawe and C. M. Kozak, *Polym. Chem.*, 2015, **6**, 6305-6315.
25. W.-M. Ren, X. Zhang, Y. Liu, J.-F. Li, H. Wang and X.-B. Lu, *Macromolecules*, 2010, **43**, 1396-1402.

26. P. K. Saini, C. Romain and C. K. Williams, *Chem. Commun.*, 2014, **50**, 4164-4167.
27. M. R. Kember, F. Jutz, A. Buchard, A. J. P. White and C. K. Williams, *Chem. Sci.*, 2012, **3**, 1245-1255.
28. M. Aresta, A. Dibenedetto and A. Angelini, *Chem. Rev.*, 2014, **114**, 1709-1742.
29. S. J. Poland and D. J. Darensbourg, *Green Chem.*, 2017, **19**, 4990-5011.
30. M. R. Kember, A. J. P. White and C. K. Williams, *Macromolecules*, 2010, **43**, 2291-2298.
31. Z. Qin, C. M. Thomas, S. Lee and G. W. Coates, *Angew. Chem. Int. Ed.*, 2003, **42**, 5484-5487.
32. L. N. Saunders, N. Ikpo, C. F. Petten, U. K. Das, L. N. Dawe, C. M. Kozak and F. M. Kerton, *Catal. Commun.*, 2012, **18**, 165-167.
33. E. K. Noh, S. J. Na, S. S. S.-W. Kim and B. Y. Lee, *J. Am. Chem. Soc.*, 2007, **129**, 8082-8083.
34. C. M. Kozak, K. Ambrose and T. S. Anderson, *Coord. Chem. Rev.*, 2018, **376**, 565-587.
35. D. J. Darensbourg, W.-C. Chung and S. J. Wilson, *ACS Catal.*, 2013, **3**, 3050-3057.
36. J. Y. Jeon, J. J. Lee, J. K. Varghese, S. J. Na, S. Sujith, M. J. Go, J. Lee, M.-A. Ok and B. Y. Lee, *Dalton Trans.*, 2013, **42**, 9245-9254.
37. K. Nakano, S. Hashimoto and K. Nozaki, *Chem. Sci.*, 2010, **1**, 369-373.
38. A. Ghosh, P. Ramidi, S. Pulla, S. Z. Sullivan, S. L. Collom, Y. Gartia, P. Munshi, A. S. Biris, B. C. Noll and B. C. Berry, *Catal. Lett.*, 2010, **137**, 1-7.

39. M. Ulusoy, A. Kilic, M. Durgun, Z. Tasci and B. Cetinkaya, *J. Organomet. Chem.*, 2011, **696**, 1372-1379.
40. M. R. Kember, A. J. P. White and C. K. Williams, *Inorg. Chem.*, 2009, **48**, 9535-9542.
41. C. E. Anderson, S. I. Vagin, W. Xia, H. Jin and B. Rieger, *Macromolecules*, 2012, **45**, 6840-6849.
42. A. Kilic, M. Ulusoy, M. Durgun and E. Aytar, *Inorg. Chim. Acta*, 2014, **411**, 17-25.
43. A. Kilic, M. Ulusoy, M. Durgun, E. Aytar, A. Keles, M. Dagdevren and I. Yilmaz, *J. Coord. Chem.*, 2014, **67**, 2661-2679.
44. H. Zhang and M. W. Grinstaff, *J. Am. Chem. Soc.*, 2013, **135**, 6806-6809.
45. Z. Hošťálek, R. Mundil, I. Císařová, O. Trhlíková, E. Grau, F. Peruch, H. Cramail and J. Merna, *Polymer*, 2015, **63**, 52-61.
46. Y. Liu, W.-M. Ren, W.-P. Zhang, R.-R. Zhao and X.-B. Lu, *Nat. Commun.*, 2015, **6**, 8594.
47. M. Hatazawa, K. Nakabayashi, S. Ohkoshi and K. Nozaki, *Chem. Eur. J.*, 2016, **22**, 13677-13681.
48. J. E. Seong, S. J. Na, A. Cyriac, B.-W. Kim and B. Y. Lee, *Macromolecules*, 2010, **43**, 903-908.
49. J. Yoo, S. J. Na, H. C. Park, A. Cyriac and B. Y. Lee, *Dalton Trans.*, 2010, **39**, 2622-2630.
50. R. Wei-Min, L. Ye, W. Guang-Peng, L. Jie and L. Xiao-Bing, *J. Polym. Sci., Part A: Polym. Chem.*, 2011, **49**, 4894-4901.

51. H. Li and Y. Niu, *Appl. Organomet. Chem.*, 2011, **25**, 424-428.
52. D. Bai, X. Wang, Y. Song, B. Li, L. Zhang, P. Yan and H. Jing, *Chin. J. Catal.*, 2010, **31**, 176-180.
53. W.-M. Ren, M.-W. Liang, Y.-C. Xu and X.-B. Lu, *Polym. Chem.*, 2013, **4**, 4425-4433.
54. G.-P. Wu, S.-H. Wei, W.-M. Ren, X.-B. Lu, T.-Q. Xu and D. J. Darensbourg, *J. Am. Chem. Soc.*, 2011, **133**, 15191-15199.
55. D. J. Darensbourg and S. J. Wilson, *Macromolecules*, 2013, **46**, 5929-5934.
56. J. Liu, W.-M. Ren, Y. Liu and X.-B. Lu, *Macromolecules*, 2013, **46**, 1343-1349.
57. D. J. Darensbourg and Y. Wang, *Polym. Chem.*, 2015, **6**, 1768-1776.
58. H. Zhang, X. Lin, S. Chin and M. W. Grinstaff, *J. Am. Chem. Soc.*, 2015, **137**, 12660-12666.
59. H. Zhang, B. Liu, H. Ding, J. Chen and Z. Duan, *Polymer*, 2017, **129**, 5-11.
60. F. Zhou, S.-L. Xie, X.-T. Gao, R. Zhang, C.-H. Wang, G.-Q. Yin and J. Zhou, *Green Chem.*, 2017, **19**, 3908-3915.
61. G. W. Coates and D. R. Moore, *Angew. Chem. Int. Ed.*, 2004, **43**, 6618-6639.
62. S. Klaus, M. W. Lehenmeier, C. E. Anderson and B. Rieger, *Coord. Chem. Rev.*, 2011, **255**, 1460-1479.
63. D. J. Darensbourg, M. Ulusoy, O. Karroonnirum, R. R. Poland, J. H. Reibenspies and B. Çetinkaya, *Macromolecules*, 2009, **42**, 6992-6998.
64. D. J. Darensbourg, J. C. Yarbrough, C. Ortiz and C. C. Fang, *J. Am. Chem. Soc.*, 2003, **125**, 7586-7591.

65. D. J. Darensbourg, R. R. Poland and A. L. Strickland, *J. Polym. Sci., Part A: Polym. Chem.*, 2012, **50**, 127-133.
66. B. Han, L. Zhang, S. J. Kyran, B. Liu, Z. Duan and D. J. Darensbourg, *J. Polym. Sci., Part A: Polym. Chem.*, 2016, **54**, 1938-1944.
67. D. Adhikari, S. T. Nguyen and M.-H. Baik, *Chem. Commun.*, 2014, **50**, 2676-2678.
68. D. J. Darensbourg and A. D. Yeung, *Polym. Chem.*, 2015, **6**, 1103-1117.
69. D. J. Darensbourg, W.-C. Chung, A. D. Yeung and M. Luna, *Macromolecules*, 2015, **48**, 1679-1687.
70. D. J. Darensbourg and W.-C. Chung, *Macromolecules*, 2014, **47**, 4943-4948.
71. D. J. Darensbourg, W.-C. Chung, C. J. Arp, F.-T. Tsai and S. J. Kyran, *Macromolecules*, 2014, **47**, 7347-7353.
72. Y. Liu, H. Zhou, J.-Z. Guo, W.-M. Ren and X.-B. Lu, *Angew. Chem. Int. Ed.*, 2017, **56**, 4862-4866.
73. Y. Liu, J.-Z. Guo, H.-W. Lu, H.-B. Wang and X.-B. Lu, *Macromolecules*, 2018, **51**, 771-778.
74. J. Wang, X. Shan, S. Shan, H. Su, S. Wu and Q. Jia, *Catal. Commun.*, 2015, **59**, 116-121.
75. J. A. Castro-Osma, K. J. Lamb and M. North, *ACS Catal.*, 2016, **6**, 5012-5025.
76. J. A. Castro-Osma, M. North and X. Wu, *Chem. Eur. J.*, 2016, **22**, 2100-2107.
77. M. Adolph, T. A. Zevaco, C. Altesleben, O. Walter and E. Dinjus, *Dalton Trans.*, 2014, **43**, 3285-3296.

78. L. Cuesta-Aluja, M. Djoufak, A. Aghmiz, R. Rivas, L. Christ and A. M. Masdeu-Bultó, *J. Mol. Catal. A: Chem.*, 2014, **381**, 161-170.
79. S. Iksi, A. Aghmiz, R. Rivas, M. D. González, L. Cuesta-Aluja, J. Castilla, A. Orejón, F. El Guemmout and A. M. Masdeu-Bultó, *J. Mol. Catal. A: Chem.*, 2014, **383-384**, 143-152.
80. J. Gurnham, S. Gambarotta, I. Korobkov, L. Jasinska-Walc and R. Duchateau, *Organometallics*, 2014, **33**, 4401-4409.
81. S. Elmas, M. A. Subhani, M. Harrer, W. Leitner, J. Sundermeyer and T. E. Müller, *Catal. Sci. Technol.*, 2014, **4**, 1652-1657.
82. C. Chatterjee and M. H. Chisholm, *Inorg. Chem.*, 2012, **51**, 12041-12052.
83. N. D. Harrold, Y. Li and M. H. Chisholm, *Macromolecules*, 2013, **46**, 692-698.
84. O. M. Chukanova and G. P. Belov, *Kinet. Catal.*, 2017, **58**, 397-401.
85. C. M. Kozak, A. M. Woods, C. S. Bottaro, K. Devaine-Pressing and K. Ni, *Faraday Discuss.*, 2015, **183**, 31-46.
86. K. Ni and C. M. Kozak, *Inorg. Chem.*, 2018, **57**, 3097-3106.
87. R. K. Dean, K. Devaine-Pressing, L. N. Dawe and C. M. Kozak, *Dalton Trans.*, 2013, **42**, 9233-9244.
88. R. K. Dean, L. N. Dawe and C. M. Kozak, *Inorg. Chem.*, 2012, **51**, 9095-9103.
89. K. Devaine-Pressing and C. M. Kozak, *ChemSusChem*, 2017, **10**, 1266-1273.
90. G. Si, L. Zhang, B. Han, H. Zhang, X. Li and B. Liu, *RSC Adv.*, 2016, **6**, 22821-22826.
91. J. Liang, Y.-Q. Xie, X.-S. Wang, Q. Wang, T.-T. Liu, Y.-B. Huang and R. Cao, *Chem. Commun.*, 2018, **54**, 342-345.

92. M. I. Childers, J. M. Longo, N. J. Van Zee, A. M. LaPointe and G. W. Coates, *Chem. Rev.*, 2014, **114**, 8129-8152.
93. T. Aida, K. Wada and S. Inoue, *Macromolecules*, 1987, **20**, 237-241.
94. A.-L. Brocas, C. Mantzaridis, D. Tunc and S. Carlotti, *Prog. Polym. Sci.*, 2013, **38**, 845-873.
95. P. C. B. Widger, S. M. Ahmed and G. W. Coates, *Macromolecules*, 2011, **44**, 5666-5670.
96. H. Plommer, I. Reim and F. M. Kerton, *Dalton Trans.*, 2015, **44**, 12098-12102.
97. C. G. Rodriguez, R. C. Ferrier, A. Helenic and N. A. Lynd, *Macromolecules*, 2017, **50**, 3121-3130.
98. H. Misaka, R. Sakai, T. Satoh and T. Kakuchi, *Macromolecules*, 2011, **44**, 9099-9107.
99. M. Hisatoyo, U. Yusuke, Y. Naho, N. Daisuke and E. Takeshi, *J. Polym. Sci., Part A: Polym. Chem.*, 2011, **49**, 5210-5216.
100. D. Alhashmialameer, J. Collins, K. Hattenhauer and F. M. Kerton, *Catal. Sci. Technol.*, 2016, **6**, 5364-5373.

Co-Authorship Statement

The results in Chapters 2 and 3 have been submitted for publication.

Authors: Kenson Ambrose, Katherine N. Robertson and Christopher M. Kozak.

The first author (Kenson Ambrose) contributed 90% of the content of the article as the main researcher including performing the experiments, analyzing and collecting data, and writing the manuscript.

The co-author (Katherine N. Robertson) was the crystallographer who collected the data and solved the molecular structure of **3.1**.

The corresponding author (Christopher M. Kozak), my supervisor, was the principal investigator of this research who suggested initial experiments, assisted with analyzing data, revised and submitted the manuscript.

Chapter 2: Synthesis and Characterization of Co(III) Amino-bis(phenolate) Complexes as Catalysts for Cyclic Carbonate Production from CO₂ and Epoxides

2.1 Introduction

Cyclic carbonates are useful materials with potential for a wide variety of applications such as solvents in lithium ion batteries, polar aprotic solvents with low vapor pressure, precursor compounds for manufacture of plastics, intermediates for production of pharmaceuticals and other compounds (for example polymers, acyclic carbonates and diols).^{1,2} Cycloaddition reactions involving carbon dioxide (CO₂) and epoxides can be used to produce cyclic carbonates and have been well represented in the literature.² A wide variety of epoxides have been explored for cyclic carbonate production by coupling with CO₂ and a few examples are shown in **Figure 2.1**. Most epoxides used are synthesized from fossil fuel derivatives but others such as limonene, pinene and ethylene oxides can be synthesized from renewable resources.³

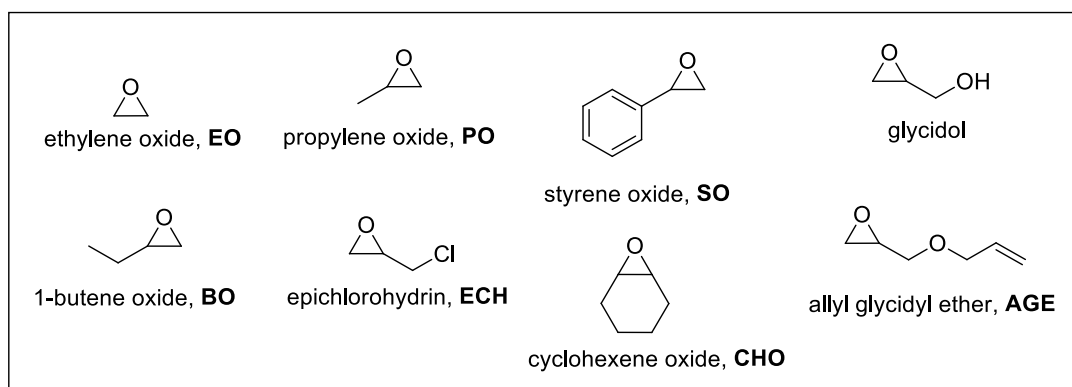


Figure 2.1: Examples of epoxides used in CO₂/epoxide cycloaddition reactions for cyclic carbonate synthesis and their commonly used abbreviations.

Reactions for cyclic carbonate production from CO₂/epoxide coupling can be catalyzed by complexes containing metals such as Fe,^{4,5} Al,^{6,7} Cr,⁸⁻¹¹ and Co.¹²⁻¹⁹ Some of these metal complexes involve chelation of the metal by ligands such as salens (giving mono- and bimetallic complexes),⁸ porphyrins,¹⁸⁻²⁰ amino-bis(phenolates)^{12,21} and even various organic linkers for formation of metal-organic frameworks (MOFs).¹⁰ An additional anionic ligand (often termed an ancillary ligand or counterion) is often introduced to enhance catalytic activity by aiding with initiation for both cycloaddition and polymerization reactions. These ancillary ligands include Cl⁻, Br⁻, I⁻, OAc⁻, OTs⁻, ⁻O₂CCl₃ (trichloroacetate) and [2,4-DNP]⁻ (2,4-dinitrophenolate) where the latter four may demonstrate a bidentate coordination mode.^{19,22} Although the majority of chromium and cobalt catalysts reported in the literature are selective towards polycarbonate synthesis (from CO₂/epoxide copolymerization), cyclic carbonate selectivity is afforded via various back-biting mechanisms of either a growing polymer chain or the initially formed metal-carbonate.²³ Furthermore, higher reaction temperature is often associated with selectivity toward cyclic carbonate production as its activation barrier is higher than that of polycarbonate production.^{24,25}

An early report of CO₂/epoxide coupling by Nguyen and Paddock in 2001 showed the use of a robust and air-stable Cr(III)-salen complex bearing a Cl⁻ ligand for cyclic carbonate production when co-catalyzed by 4-(dimethylamino)pyridine (DMAP).²⁶ The catalyst system was highly active for cycloaddition reactions of a variety of terminal epoxides, performed at 75 °C and 3.5 bar CO₂ pressure, producing yields (by ¹H NMR) of 94 – 100%. A proposed mechanism shows the dissociation of the Cl⁻ ligand generates a

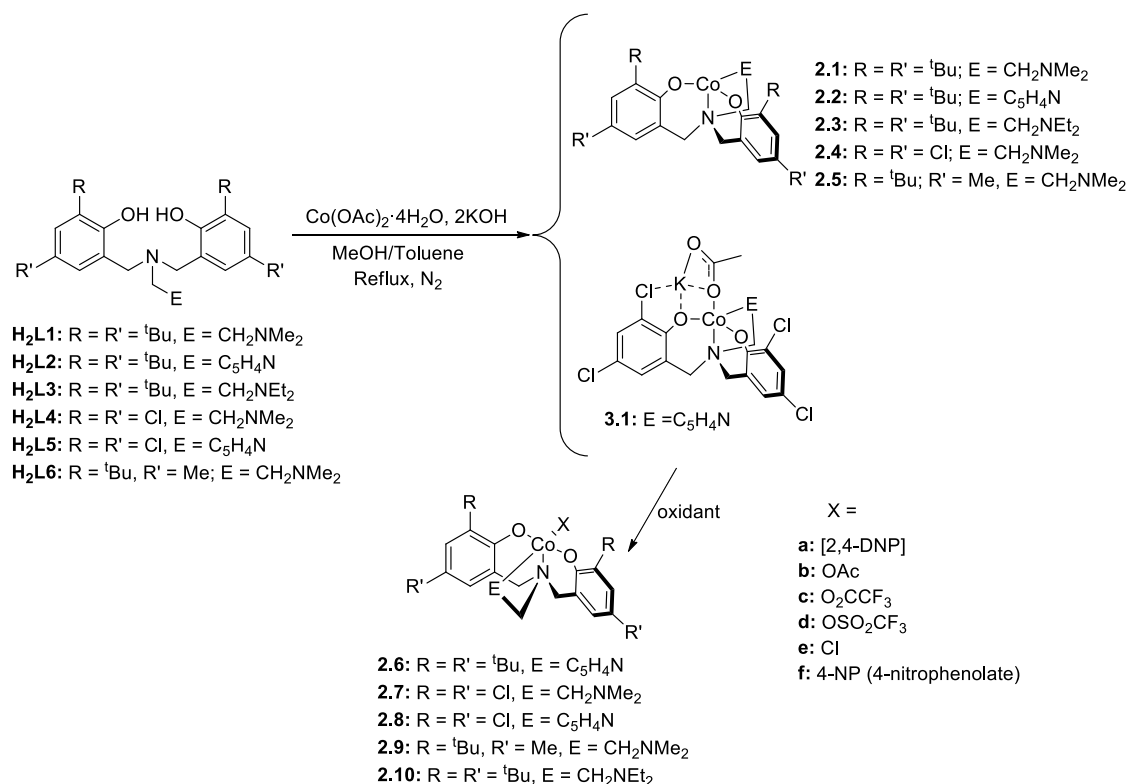
vacant coordination site in the presence of DMAP to form a Cr(III)-DMAP adduct as one of the active species. This demonstrates one of the roles of a potentially labile ancillary ligand in these catalyst systems.

Merna has shown that varying the ancillary ligand on a salphen-Co(III)-Y (where Y = OAc⁻, [2,4-DNP]⁻, ⁻OBzF₅ or ⁻O₂CCl₃) metal complex had a significant effect on catalytic activity toward PO/CO₂ coupling reactions to produce both polycarbonate and cyclic carbonate.²² The Co complex bearing the ligand with the weakest nucleophilic character (⁻O₂CCl₃) and co-catalyst PPNCl, demonstrated the highest activity for PO/CO₂ coupling with a TOF of up to 456 h⁻¹. Polymer analysis by MALDI-TOF MS showed ⁻O₂CCl₃ end-capped polymer fragments, which suggest initiation by ⁻O₂CCl₃ ion. Complexes bearing [2,4-DNP]⁻ showed the second highest catalytic activity of 391 TO h⁻¹. This demonstrates the potential of the ancillary ligand to act as an initiator during CO₂/epoxide coupling reactions. The Jing group has demonstrated the effect of various counterions on the activity of metalloporphyrin complexes for PO/CO₂ cycloaddition reactions.¹⁹ ⁻O₂CCF₃ showed the best activity (TOF) among all the counterions explored and the order of activity was found to be ⁻O₂CCF₃ > ⁻O₂CCl₃ > OAc⁻ > I⁻ > Br⁻ > Cl⁻ > OTs⁻. Electron-withdrawing fluorine substituents in ⁻O₂CCF₃ mean it is most likely the weakest binding ligand, and this correlates to higher activity. Various epoxides were explored including PO, SO and ECH with up to 191 TO h⁻¹ for reactions performed at 80 °C and 6.6 bar CO₂.

Co complexes with [2,4-DNP]⁻ ancillary ligands or counterions have been widely reported in the literature for CO₂/epoxide coupling.²⁷⁻³¹ However, only a few have been

structurally characterized to show the bidentate coordination mode of [2,4-DNP]⁻,^{28,29} otherwise denoted as Co bonded to an “X” ligand (where X = [2,4-DNP]⁻). Chen has shown that [2,4-DNP]⁻ plays a major role in the initiation mechanism where in the presence of Bu₄NBr, it generates a vacant coordination site via dissociation of its nitro-group and simultaneously promotes intramolecular ring-opening of the newly bound epoxide.²⁹ This behaviour has also been observed with an OAc⁻ ancillary ligand with a Co(III)-salen/PPNCl catalyst system for copolymerization of CHO/CO₂.³²

In this chapter, the synthesis and characterization of various Co(III) amino-bis(phenolate) complexes (**Scheme 2.1**) through modification of previously reported Co(II) complexes, by oxidation and chelation of various ancillary ligands will be discussed. Also presented is the catalytic activity of several of these complexes toward cyclic carbonate production from epoxide/CO₂ coupling where cocatalyst and temperature effects were observed.



Scheme 2.1: General synthetic route for Co(II)/(III) complexes used in this work.

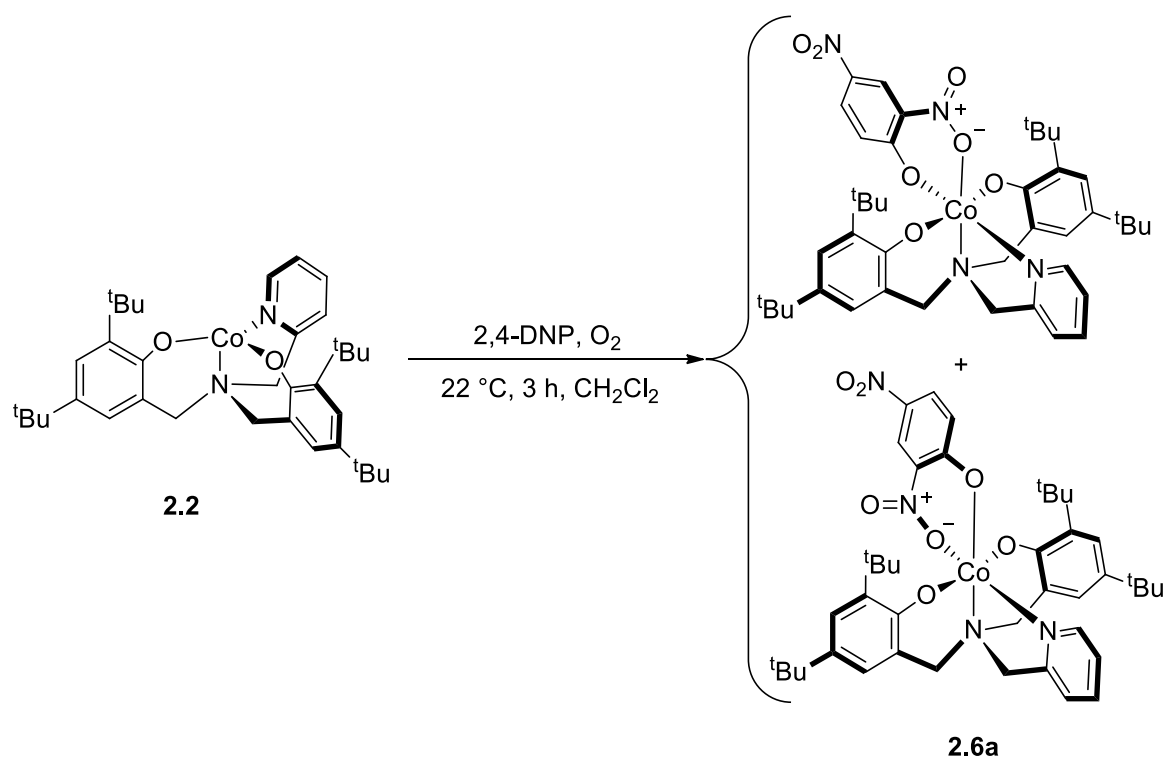
2.2 Results and discussion

2.2.1 Synthesis of Co(III) amino-bis(phenolate) complexes

2.2.1.1 Co(2,4-DNP) amino-bis(phenolate) complexes

Complex **2.6a** was synthesized via oxidation of **2.2** using oxygen in the presence of 2,4-dinitrophenol (2,4-DNP) in dichloromethane at 22 °C to yield a black crystalline solid (**Scheme 2.2**). This synthetic route is consistent with the synthesis of similar reported structures.^{22,27,29,33} Characterization of **2.6a** via ^1H NMR spectroscopy (**Figure 2.2**) showed three different environments of methylene proton signals in the 2.70 – 5.03 ppm region. The CH_2Ar methylenes are diastereotopic and appear as doublets whereas the

CH_2Py methylene resonance occurs as a singlet. This is consistent with a *trans* orientation of the phenolate groups resulting in a C_s symmetry of a six-coordinate complex **2.6a** in solution. Each of these signals shows the existence of major and minor isomers, which are believed to result from two possible orientations of a bidentate $[2,4-DNP]^-$ ligand. Namely, the phenolate O-donor of the ligand may also occupy a site *trans* to the apical (central) or pendent N-donors of the amino-bis(phenolate) ligand. Bidentate binding of $[2,4-DNP]^-$ to Co(III)salen derivatives has been previously observed.³⁴ The aromatic region is complicated as expected for protons of the $[2,4-DNP]^-$ ligand, the phenolate environments and the pyridyl pendent donor, as well as their major and minor variants. ^{13}C NMR shows an increase in the number of aromatic carbon signals compared to the proligand **H₂L2** (see Appendix A, Figure A-1), which is indicative of an additional aromatic species $[2,4-DNP]^-$ in the structure of the complex. The purity of complex **2.6a** was confirmed by elemental analysis.



Scheme 2.2: Synthetic route for complex **2.6a**.

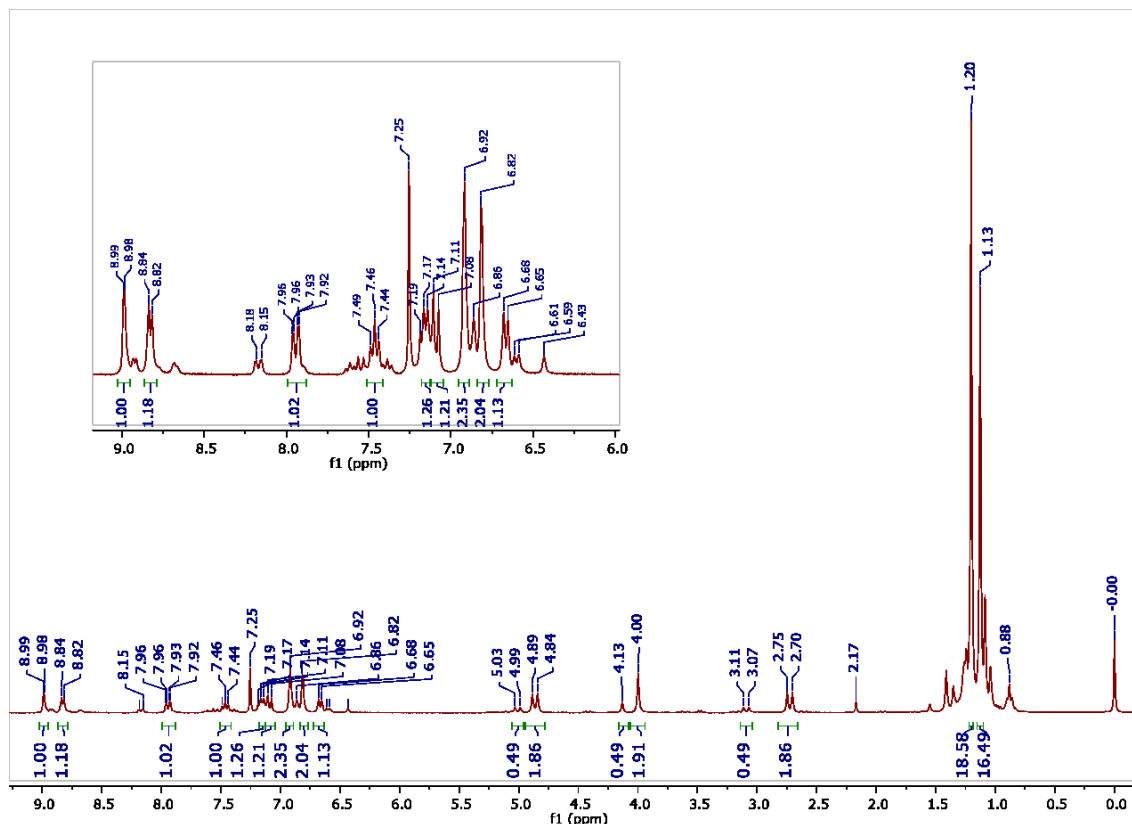


Figure 2.2: ^1H NMR spectrum of complex **2.6a** with expanded aromatic region (insert).

Compound **2.8a** was afforded via a similar procedure to **2.6a** yielding an orange-brown crystalline solid. The ^1H NMR spectrum (see Appendix A, Figure A-2) shows two different signals corresponding to methylene protons, namely a doublet at 3.0 ppm (2H) and a broad resonance at 4.2 ppm (4H). This is indicative of phenolate groups in *trans* position to each other thus generating diastereotopic CH_2Ar methylenes. The broad resonance at 4.2 ppm is a coincident peak of the CH_2Ar methylene doublet overlapping a CH_2Py singlet. Interestingly, unlike **2.6a**, no minor isomer were observed. Seven aromatic signals each integrated to 1H correspond to the pyridyl pendent donor and 2,4-dinitrophenolate ligand. Two further aromatic H resonances were observed each

integrating to 2H correspond to the symmetrically equivalent phenolate groups of a complex having C_s symmetry. The ^{13}C NMR spectrum shows 19 carbons, which is consistent with the number of different carbon environments in the complex. The composition of complex **2.8a** as [2,4-DNP-CoL5] with 1.1 equiv. of co-crystallized CH_2Cl_2 was confirmed by elemental analysis.

Complex **2.9a** was synthesized using a similar procedure to **2.6a** and **2.8a**, but oxidized using air to produce a yellow-green solid. The use of pure oxygen led to decomposition of the product, as shown by the presence of free proligand **H₂L6** by NMR spectroscopy. Characterization of **2.9a** by ^1H NMR spectroscopy (see Appendix A, Figure A-3) showed three diagnostic aromatic signals at 6.26, 7.61 and 8.77 ppm each integrating to 1H, and are consistent with $[\text{2,4-DNP}]^-$ aromatic protons. The phenolate protons are consistent again with a *trans*-oriented complex similar to those proposed for **2.6a** and **2.8a**. Characterization of **2.9a** via MALDI-TOF MS (see Appendix B, Figure B-1) showed a peak at m/z 497.3 corresponding to $[\text{CoL6}]^+$ resulting from loss of the $[\text{2,4-DNP}]^-$ ligand, and another at m/z 680.3 corresponding to $[\text{M}]^+$. Elemental analysis confirmed the composition of **2.9a** as [2,4-DNP-CoL6] with 0.15 equiv. CH_2Cl_2 .

Unfortunately, single crystals of **2.6a** and **2.8a** suitable for X-ray diffraction analysis were not obtained, however single crystals of **2.9a** were acquired by slow evaporation of a solvent system containing dichloromethane and 50:50 hexanes/diethyl ether. The molecular structure of **2.9a** and selected bond lengths and angles are shown in **Figure 2.3**. Structural data are given in Appendix C, Table C-1. The complex exhibits a distorted octahedral geometry around the Co(III) metal center where the $[\text{O}_2\text{NN}']$ ligand occupies

four coordination sites. The phenolate oxygens are oriented *trans* to each other consistent with the ^1H NMR spectrum (see Appendix A, Figure A-3). The other two coordination sites are occupied by a bidentate $[2,4\text{-DNP}]^-$ ligand with its phenolate oxygen *trans* to the pendent dimethylamino group and a nitro-group oxygen donor *trans* to the central amino group. When investigating related structures of similar ligands to amino-bis(phenolates), only two other structurally authenticated examples of 2,4-DNP-Co(III) salen complexes were found.^{28,29} As mentioned earlier, in complex **2.9a**, the $[2,4\text{-DNP}]^-$ phenolate O donor resides *trans* to the pendent dimethylamino arm of the diamino-bis(phenolate) ligand. Interestingly, the two reported salen complexes demonstrate differing arrangements depending on the length of the linker between the imine groups. Where a salcy-type ligand is employed (having a cyclohexyl linker, thus forming a 5-membered chelate), the $[2,4\text{-DNP}]^-$ phenolate O donor sits *trans* to an imino N donor.²⁹ When a 2,2-dimethyl-1,3-propylene linker is used (resulting in a 6-membered chelate) the $[2,4\text{-DNP}]^-$ phenolate O donor sits *trans* to another phenolate O donor of the salen ligand.²⁸ This results in differences in the Co–O bond lengths of the $[2,4\text{-DNP}]^-$ ligands. Complex **2.9a** shows the shortest distance of 1.877(2) Å, whereas the salcy compound has a slightly longer distance of 1.8964(16) Å and the propylene salen complex is even longer at 1.918(2) Å. Where the role of the $[2,4\text{-DNP}]^-$ group is important in the catalytic cycle of CO_2 /epoxide coupling and copolymerization,³⁴ these structural differences may influence the activity of the catalysts.

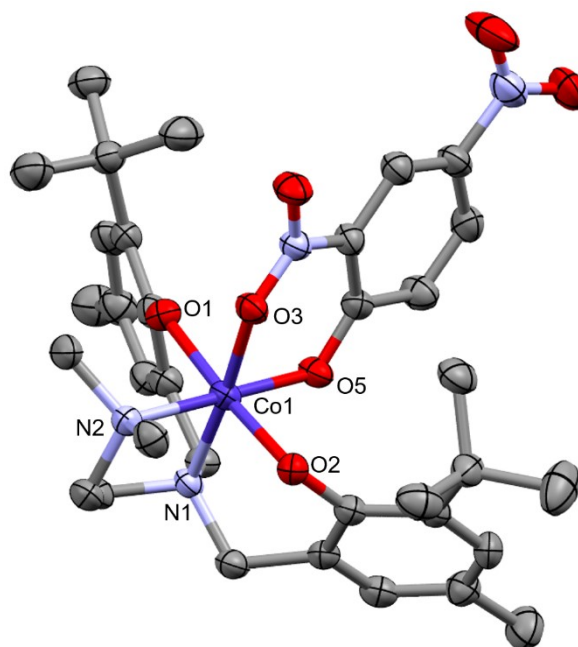
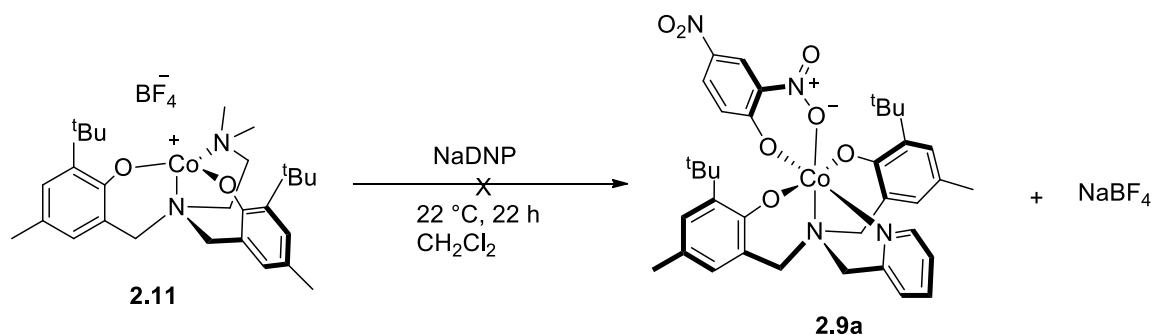


Figure 2.3: Partially labelled molecular structure of compound **2.9a**. Thermal ellipsoids are drawn at 50% probability with hydrogens and co-crystallized dichloromethane molecule omitted for clarity. Selected bond distances (Å) and angles (deg): Co(1) – O(5), 1.877(2); Co(1) – O(1), 1.903(2); Co(1) – O(3), 1.926(2); Co(1) – O(2), 1.931(2) Co(1) – N(1), 1.950(3); Co(1) – N(2), 2.029(3); O(5) – Co(1) – O(1), 88.97(10); O(5) – Co(1) – O(3), 93.21(9); O(5) – Co(1) – O(2), 89.89(9); O(5) – Co(1) – (N), 91.42(10); O(5) – Co(1) – N(2), 179.60(9); O(1) – Co(1) – O(3), 86.36(9); O(1) – Co(1) – O(2), 174.83(9); O(1) – Co(1) – N(1), 92.06(10); O(1) – Co(1) – N(2), 90.87(10); O(3) – Co(1) – O(2), 88.67(9); O(3) – Co(1) – N(1), 175.08(9); O(3) – Co(1) – N(2), 87.14(10); O(2) – Co(1) – N(1), 93.01(10); O(2) – Co(1) – N(2), 90.30(10); N(1) – Co(1) – N(2), 88.23(11).

Analysis of the other 2,4-dinitrophenolate species were inconclusive in terms of characterization. The compounds bearing a pyridyl (**2.6a** and **2.8a**) pendent appear to be more stable under oxidative conditions of pure oxygen than the dialkylamine-containing pendent group species. As mentioned earlier, **2.9a** was synthesized using a milder oxidant (air) because the use of pure oxygen as an oxidant led to complex decomposition as shown by NMR spectroscopy of the product being consistent with that of the proligand,

H₂L6. This was also observed with compounds **2.7a** and **2.10a** and was not further pursued. An alternative method using silver salts was attempted for oxidation of Co(II) complexes to Co(III) for subsequent coordination of the 2,4-dinitrophenolate ligand. Specifically, **2.5** was reacted with silver tetrafluoroborate (AgBF₄) in the absence of light (to prevent decomposition of AgBF₄) to produce the ionic complex **2.11**. Subsequent reaction of **2.11** with sodium 2,4-dinitrophenolate (NaDNP) would ideally produce **2.9a**, **Scheme 2.3**. Characterization by ¹H NMR produced a complicated spectrum therefore this synthetic route was not pursued further. Compounds **2.6a**, **2.8a**, and **2.9a** were adequately characterized and therefore employed as catalysts for CO₂/epoxide coupling reactions discussed later.

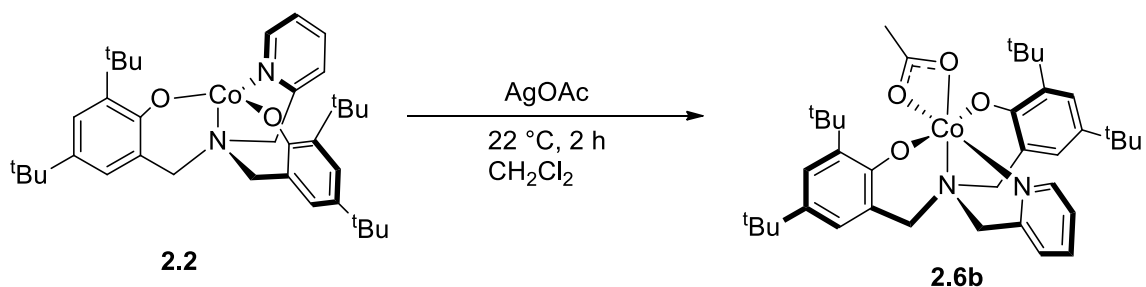


Scheme 2.3: Unsuccessful synthetic route for complex **2.9a**.

2.2.1.2 Co(OAc) amino-bis(phenolate) complexes

Complexes **2.6b** and **2.8b** were afforded via reaction of the respective [CoL_n] precursor with silver acetate in dichloromethane while wrapped in aluminum foil at 22 °C (**Scheme 2.4**), resulting in a dark brown solution with a dark grey precipitate. Removal of the precipitate via gravity filtration afforded a dark brown solution where the volatiles

were removed and the resulting dark brown solid dried to produce yields of 66.7% (**2.6b**) and 95.8% (**2.8b**). The Co(II) center is converted to Co(III) using silver acetate as an oxidant resulting in an amorphous silver solid precipitate observed after reaction. This is a less commonly used but established procedure^{35,36} compared to the more commonly used method where acetic acid is used with pure oxygen or air as an oxidant.³⁷⁻³⁹



Scheme 2.4: Synthetic route to compound **2.6b**.

2.6b was characterized via ¹H NMR spectroscopy (see Appendix A, Figure A-4). The spectrum showed a diagnostic singlet at 1.96 ppm integrated to 3 protons which corresponds to the methyl in the acetate ligand. Furthermore, three different signals for methylene protons (doublet at 3.05, singlet at 3.98 and doublet at 4.58) means that there are three different methylene proton environments where the singlet corresponds to identical methylene protons from the pyridyl pendent and the doublets correspond to two sets of diastereotopic methylene protons adjacent to the phenolate groups, which was confirmed by identical coupling constants (13.1 Hz). This suggests that the phenolate groups may be in a *trans* position to each other. *Cis* phenolates would produce 4 diastereotopic protons. Characterization of **2.6b** by MALDI-TOF MS shows multiple peaks which corresponds to various complex adducts (see Appendix B, Figure B-2) some

of which were identified. A peak at m/z 601.4 corresponds to $[\text{CoL2}]^+$ and m/z 660.4 corresponds to $[\text{OAc-CoL2}]^+$. Moreover, peaks at m/z 699.3 and 708.3 correspond to $[\text{CoL2+K}]^+$ and $[\text{CoL2+Ag}]^+$ respectively. Compound **2.8b** represents an analog with a more Lewis acidic Co(III) center resulting from the electron-withdrawing chlorine *ortho* and *para*-phenolate substituents thus a stronger coordination of the acetate ligand to the Co(III) center is expected. This is evidenced by the observed cleaner ^1H NMR spectrum (compared to compound **2.6b**) and the MALDI-TOF mass spectrum having $[\text{M}]^+$ as the most intense peak. The ^1H NMR spectrum shows clearer signals including a diagnostic signal (at 1.89 ppm) which corresponds to the methyl protons of the acetate ligand (see Appendix A, Figure A-5). The MALDI-TOF mass spectrum of **2.8b** (see Appendix B, Figure B-3) shows a peak with the largest relative intensity at m/z 573.9, which corresponds to $[\text{OAc-CoL5}]$ and the theoretical isotopic pattern is in good agreement with the experimental pattern.

2.2.1.3 Co(O₂CCF₃) amino-bis(phenolate) complexes

Trifluoroacetate (TFA)-containing Co(III) complexes were also synthesized but with limited characterization (**2.6c** and **2.8c**). Complexes **2.6c** and **2.8c** were synthesized via reaction of the respective Co(II)L_n complex with silver trifluoroacetate (AgTFA) at 22 °C for 2 h while wrapped in aluminum foil, which resulted in a dark brown solution containing a grey precipitate. AgTFA served as an oxidant for converting the Co(II) metal center to Co(III). The use of silver acetate salts bearing electron-withdrawing substituents as oxidants for conversion of Co(II) to Co(III) has been reported.⁴⁰ Treatment of the mixture after reaction involved removal of the grey precipitate by gravity filtration

followed by removal of volatiles from the resulting filtrate and drying *in vacuo*, thus producing a dark brown solid at yields of 12.8% and 66.4% for compounds **2.6c** and **2.8c**, respectively. Other oxidative methods for addition of the TFA (and analogs such as trichloroacetate) ancillary ligand and conversion of Co(II) to Co(III) involve the use of the respective acetic acid and pure O₂ as an oxidant.^{19,22} Characterization of **2.6c** and **2.8c** was only successful via MALDI-TOF MS and inconclusive via NMR spectroscopy. The MALDI-TOF mass spectrum of **2.6c** showed a peak at *m/z* 714.4 which corresponds to the [Co(TFA)L2]⁺ but at only 10% relative intensity. This suggests that either coordination of the TFA ligand was incomplete or that TFA is weakly bound (due to electron-withdrawing fluorine substituents) and dissociates under MALDI-TOF conditions. The MALDI-TOF mass spectrum of **2.8c** however, showed a peak at *m/z* 666.9 which corresponds to [Co(TFA)L5+KH] at a relative intensity of 89%. This indicates stronger binding of the TFA ligand to the Co(III) center due to its increased Lewis acidity compared to **2.6c**. Due to inadequate characterization, compounds **2.6c** and **2.8c** were not employed as catalysts for CO₂/epoxide coupling reactions.

2.2.1.4 Other attempted syntheses of Co(III) amino-bis(phenolate) complexes

Synthesis of Co(III) complex **2.6d** was attempted by reacting **2.2** with silver triflate in dichloromethane while wrapped in aluminum foil for 22 h, which resulted in a brown solution containing a grey precipitate (solid Ag). Treatment by gravity filtration then removal of volatiles from the filtrate and drying *in vacuo* produced a dark brown solid at a yield of 41.4%. This method is representative of early reports for conversion of Co(II) to Co(III) and addition of a triflate (⁻OSO₂CF₃) ligand using AgOSO₂CF₃.⁴¹ Synthesis of

compound **2.8d** was also attempted using this procedure. Characterization of **2.6d** by MALDI-TOF MS (see Appendix B, Figure B-6) showed peaks of m/z 750.2 at 10% relative intensity and 100% intensity at m/z 601.3 which corresponds to $[\text{CoL2}]^+$ and $[\text{Co}(\text{OSO}_2\text{CF}_3)\text{L2}]^+$ respectively. Like **2.6c**, this may suggest weak coordination of the triflate ligand, thus the low intensity of the molecular ion peak under MALDI-TOF conditions. For compound **2.8d**, the molecular ion peak was not observed (m/z 663.7) when characterized by MALDI-TOF-MS (see Appendix B, Figure B-7). At 100% relative intensity, m/z 463.0 was observed, which corresponds to lithium ion-containing **L5** ($[\text{LiL5}]^+$) and m/z 514.8 corresponds to $[\text{CoL5}]^+$. It is interesting to note that a peak at m/z 680.7 with 40% relative intensity was observed and corresponds to $[\text{CoOSO}_2\text{CF}_3(\text{OH})\text{L5}]^+$ and the calculated isotopic pattern is in good agreement with the observed pattern. This suggests the presence of a Co-**L5** adduct bearing monodentate $^-\text{OSO}_2\text{CF}_3$ and OH^- ligands.

The preparation of CoClL_n complexes was also attempted using a well-represented method using CoCl_2 as the metal starting material.⁴²⁻⁴⁴ **H₂L2** and cobalt(II) chloride in a toluene/methanol solvent system was heated to reflux while exposed to air for 24 h (for compound **2.8e**). Volatiles were removed from the resulting dark brown solution, which was dried to produce a dark green solid in a 78.8% yield. A modification for compound **2.8e** involved the use of triethylamine for ligand deprotonation and tetrahydrofuran (THF)/methanol as solvents due to **H₂L5** being more soluble in THF than toluene. Compounds **2.6e** and **2.8e** were both characterized by MALDI-TOF MS (see Appendix B, Figures B-8 and B-9 respectively). The MALDI-TOF mass spectrum of **2.6e** shows the

molecular ion peak, m/z 638.4 at 10% relative intensity while the highest intensity peaks, m/z 545.5 and m/z 601.4, correspond to **H₂L2** and **CoL2** respectively. Compound **2.8e** however, favors the formation of a dimeric complex. More specifically, a proposed sodium ion-containing chloride-bridged dimer (**Figure 2.4**) and a phenolate-bridged dimer as evidenced by the MALDI-TOF mass spectrum (see Appendix B, Figure B-9). When this procedure was used previously in the Kozak group with a bulkier (bearing *t*-amyl phenolate substituents and a diethylamine pendent donor) amino-bis(phenolate) ligand, a tetracobaltate(II) ion having two amino-ammonium bis(phenol) counterions was observed.⁴⁵

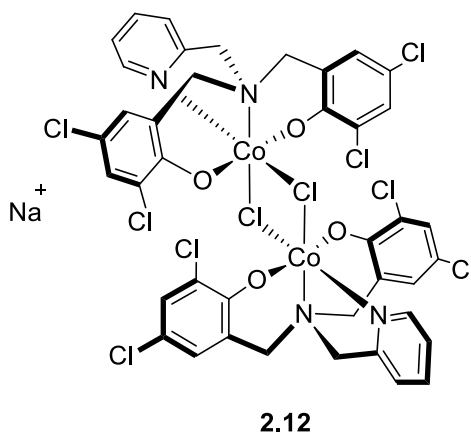


Figure 2.4: Chloride-bridged dimer of **2.8e** observed by MALDI-TOF MS analysis (m/z 1123.7).

Lastly, coordination of a 4-nitrophenol (4-NP) was explored via the same method for synthesis of compound **2.6a**. A black solid was achieved in a 29.3% yield. Characterization by MALDI-TOF MS analysis showed the presence of $[\text{CoL2}]^+$ which corresponds to a peak at m/z 601.3 with 100% relative intensity. Closer inspection shows

a peak at only 1% intensity corresponding to $[\text{Li} + \text{Co}(\text{4NP})\text{L2}]^+$ (see Appendix B, Figure B-10). Preparation of related Co compounds of 4-NP has been done using a similar procedure⁴⁶ and others have generated a Co-4NP complex in situ during a CO_2 /epoxide coupling reaction.⁴⁷ Another report has shown that a longer reaction time (4 days) is needed for complete oxidation of Co(II) to Co(III) and coordination of 4-NP.⁴⁸ This suggests either low stability of the desired product under MALDI-TOF conditions or an incomplete reaction. As mentioned earlier, compounds with inconclusive characterization were not employed in catalytic studies.

2.2.2 Coupling of epoxides with CO_2 using Co(III) amino-bis(phenolate) complexes

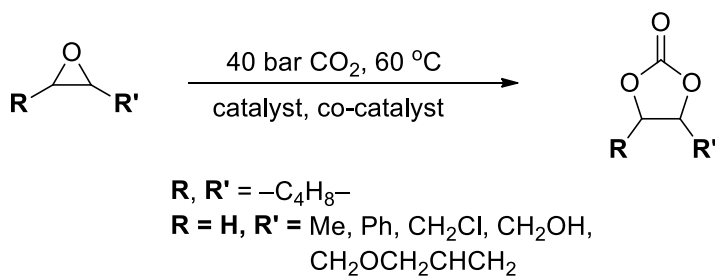
A selection of the Co(III) complexes synthesized were used as catalysts for cycloaddition of epoxides and CO_2 in the presence of TBAB, PPNCl and PPNN_3 as co-catalysts (**Table 2.1**). These co-catalysts were chosen based on their wide use for cyclic carbonate formation as well as their solubility in the epoxides studied. The Kerton and Kozak groups have previously reported the catalytic activity of Co(II)/(III) complexes bearing tripodal amino-bis(phenolate) ligands toward CO_2 /PO cycloaddition reactions,¹ and subsequently explored further by Rieger and co-workers.⁹ Therefore Co(III) amino-bis(phenolate) complexes specifically with a 2,4-dinitrophenolate (**2.6a**, **2.8a** and **2.9a**), an acetate (**2.8b**) and a trifluoroacetate (**2.8c**) ancillary ligand were studied for epoxide/ CO_2 cycloaddition reactions. Compound **2.6a** was investigated for CHO/ CO_2 and PO/ CO_2 coupling and showed little to no conversion of the epoxide (entries 1 vs 2) when co-catalyzed by PPNN_3 . **2.6a**/TBAB and **2.8a**/TBAB (entries 3 and 4) also showed little to no conversion with CHO. However, when PO is used, moderate conversion was

observed for cycloaddition with CO₂ using compounds **2.6a**, **2.8a** and **2.9a**. A control reaction was not performed as it is known that in the absence of a catalyst, PPN-based salts do not appear to promote cyclic carbonate formation whereas small amounts of cyclic carbonate formation from epoxides/CO₂ have been observed with TBAB.^{12,21,22,49,50} A very small increase was observed when **2.8a** was employed co-catalyzed with TBAB but **2.9a**, however, showed the lowest conversion of the three (entries 5, 6 and 7). The presence of a pyridyl donor (compared to a dimethylethylamino donor) appears to favor cycloaddition. In terms of electronic and steric properties, the pyridyl group is less sterically demanding and is a stronger σ -donor, thus making the cobalt center less electron-rich and less hindered for epoxide binding. A decrease in temperature resulted in a significant decrease in conversion for PO/CO₂ coupling (**Table 2.1**, entry 8). Cyclic propylene carbonate production is thermodynamically favored whereas poly(propylene carbonate) is the kinetic product, therefore PO/CO₂ coupling reactions are often performed at temperatures of 22 °C or lower to favor polycarbonate formation,^{4,29,51} but this was not the case here. Compounds **2.6a** and **2.8a** share the same donor arrangement, octahedral geometry, and 18e⁻ configuration, which means the complexes are kinetically inert. However, altering the electronic properties of the amino-bis(phenolate) ligand by introducing electron-withdrawing chlorines in **2.8a** in the *ortho* and *para*-positions of the phenolate donors instead of *tert*-butyl groups (**2.6a**), makes the Co-center more Lewis acidic. With the higher conversion showed by **2.8a** for PO/CO₂ coupling, compared to **2.6a** and **2.9a**, it was employed with TBAB for CO₂ coupling with other epoxides. Results show conversions up to 95% when **2.8a**/TBAB is used for epoxide coupling reactions (entries 10 – 14, **Table 2.1**). Compound **2.8b** (contains an OAc ligand) when

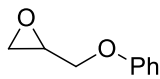
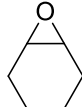
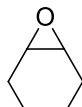
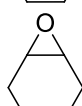
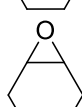
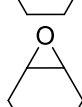
employed with DMAP or TBAB (at a higher catalyst loading) showed very low conversion for CHO/CO₂ coupling. However, **2.8b**/PPNOAc showed a slightly higher conversion (entries 16 versus 17) which suggests that the OAc nucleophile coupled with the bulky PPN⁺ cation, presents a marginally more active catalyst system. When **2.8c**/PPNCl was used, an increase in conversion was observed at elevated temperature (entries 18 and 19) which demonstrates the ability to overcome larger energies (compared to polycarbonate) needed for cyclic carbonate production.

The catalyst system described in this work may not have displayed high activity (up to 26 TO h⁻¹) but it does demonstrate some degree of functional group tolerance as seen in **Table 2.1**. Activity of other reported catalyst systems toward cyclic carbonate formation from CO₂ and epoxide coupling have been shown to be as high as 36 000 TO h⁻¹ for homogeneous systems⁶, at high temperatures, (90 °C) which is known to promote cyclic carbonate formation. The most attractive catalyst systems are those which demonstrate high activity toward epoxides of various functionalities, under mild conditions such as $T \leq 60\text{ °C}$ and $\leq 10\text{ bar CO}_2$ or even near ambient conditions.

Table 2.1: Cycloaddition of various epoxides and CO₂ using compounds Co(III)X amino-bis(phenolate) complexes (where X is [2,4-DNP], OAc, or ⁻O₂CCF₃).^a



Entry	Catalyst/co-cat	Substrate	Conversion ^b (%)	TON
1	2.6a/PPNN ₃		0	0
2	2.6a/PPNN ₃		3	15
3	2.6a/TBAB		3 ^c	15
4	2.8a/TBAB		0	0
5	2.6a/TBAB		52	260
6	2.8a/TBAB		55	275
7	2.9a/TBAB		32	160
8 ^d	2.6a/TBAB		4	20
9	2.6a/TBAB		14	70
10	2.8a/TBAB		64	320
11	2.8a/TBAB		95	475
12	2.8a/TBAB		93	465
13	2.8a/TBAB		27	135

14	2.8a/TBAB		78	390
15	2.8b/DMAP		0	0
16 ^e	2.8b/TBAB		4	8
17 ^e	2.8b/PPNOAc		12	24
18	2.8c/PPNCl		10	50
19 ^f	2.8c/PPNCl		42	210

^aReaction conditions: 60 °C, 40 bar CO₂, 24 h, 0.2 mol% catalyst loading. Reactions were performed in neat epoxide using the co-catalyst stated. ^bConversions to cyclic carbonate were calculated using ¹H NMR (see Appendix A, Figure A-6). ^cTrace amounts of polycarbonate detected. ^dReaction performed at 22 °C. ^e0.5 mol% catalyst loading used here. ^fReaction performed at 100 °C.

2.3 Conclusions

A series of Co(III) amino-bis(phenolate) complexes bearing various counterions (or ancillary ligands) such as [2,4-DNP]⁻, OAc, ⁻O₂CCF₃, Cl⁻, ⁻OSO₂CF₃ and [4-NP]⁻ were synthesized and characterized. It is interesting to note that **2.6a** showed the presence of a minor isomer by NMR spectroscopy while none of the other Co(2,4-DNP) complexes demonstrated this. Furthermore, single crystal X-ray diffraction analysis was used to structurally characterize compound **2.9a** which showed the preferred orientation of the [2,4-DNP]⁻ ligand. Some of the complexes were employed as catalysts for CO₂/epoxide coupling reactions where selectivity toward cyclic carbonates was observed.

Temperature, co-catalyst and ligand phenolate substituent (*t*-butyl vs Cl) effects were observed and the best activity was demonstrated by **2.8a**/TBAB, which produced a TON of 475 under the following conditions: 60 °C, 40 bar CO₂, 24 h and 0.2 mol% catalyst loading.

2.4 Experimental

2.4.1 General experimental procedures and instrumentation

Unless otherwise stated, all reagents were used as received. Inert atmosphere syntheses were conducted under N₂ using Schlenk techniques. Dry, degassed toluene and dichloromethane were acquired from an MBraun Solvent Purification System. NMR spectra were recorded using Bruker AVANCE III 300 MHz and Bruker AVANCE 500 MHz spectrometers with chemical shifts in ppm, referenced relative to residual solvent protons and ¹³C signal of solvent. NMR solvents were purchased from Cambridge Isotope Laboratories and used without further purification. Mass spectrometry analysis was performed using an Applied Biosystems 4800 MALDI TOF/TOF Analyzer equipped with a reflectron, delayed ion extraction and high-performance nitrogen laser (200 Hz operating at 355 nm). Anthracene was used as a matrix for analysis of Co complexes. Anthracene and respective complex were dissolved in dichloromethane at a ratio of 2:1 and overall concentration of 6 mg mL⁻¹. Aliquots of 0.5 – 1 µL of these samples were spotted and solvent allowed to evaporate. MALDI-TOF MS data were processed and images prepared using mMass software (www.mmass.org).

Elemental analysis was performed at Guelph Chemical Laboratories LTD in Guelph, Ontario Canada or at the Centre for Environmental Analysis and Remediation at Saint

Mary's University, Halifax, Nova Scotia, Canada. The X-ray structure of **2.9a** was acquired using a Rigaku AFC8-Saturn 70 single crystal X-ray diffractometer equipped with an X-Stream 2000 low temperature system and a SHINE optic. CO₂ (99.998% pure) and epoxide cycloaddition reactions were performed in a 100 mL stainless-steel Parr 5500 equipped with a Parr 4836 control unit. The prolignands **H₂L1** – **H₂L6**^{12,52} and compounds **2.1** – **2.5**⁴⁵ were prepared as previously reported.

2.4.2 Synthesis of cobalt complexes

2.4.2.1 Synthesis of complex 2.6a

Compounds **2.6a** – **2.10a** were synthesized according to the following optimized procedure. **2.2** (0.500 g, 0.831 mmol) and 2,4-dinitrophenol (0.175 g, 0.972 mmol) were dissolved in dichloromethane (50.0 mL). The resulting brown mixture stirred under 1 atmosphere of pure oxygen (99.5% pure, using a balloon) for 3 h at room temperature. The dark brown solution was cooled to –20 °C forming a green precipitate that was removed by gravity filtration. The filtrate was collected, and volatiles removed under reduced pressure. The resulting dark brown solid was washed with a 50:50 mixture of diethyl ether and hexanes then cooled to –20 °C. The resulting precipitate was dried *in vacuo* to give a black crystalline solid; 0.470 g, 72.5% yield. Compound **2.6a**: ¹H NMR (CDCl₃, 300 MHz) (minor isomer in brackets): δ 1.13 (s, 18H, C(CH₃)₃), 1.20 (s, 18H, C(CH₃)₃), 2.725 (3.09) (d, *J* = 13.1 Hz, 2H, CH₂Ar), 4.00 (4.13) (s, 2H CH₂Py), 4.865 (5.01) (d, *J* = 13.1 Hz 2H, CH₂Ar), 6.65-6.68 (d, *J* = 8.0 Hz, 1H ArH), 6.82 (s, 2H ArH), 6.92 (s, 2H ArH), 7.08-7.17 (m, 2H ArH), 7.44-7.49 (t, *J* = 7.6 Hz, 1H ArH), 7.94 (dd, *J* = 2.5, 9.6 Hz, 1H ArH), 8.82-8.84 (d, *J* = 6.1 Hz, 1H ArH), 8.98-8.99 (d, *J* = 2.5 Hz, 1H

ArH). ^{13}C NMR (CDCl_3 , 75.0 MHz): δ 29.79, 31.71, 33.92, 35.25, 63.57, 64.24, 118.55, 119.47, 120.69, 122.12, 123.59, 124.04, 124.21, 128.82, 129.16, 136.41, 136.74, 138.56, 140.94, 149.68, 160.97, 161.97, 173.32. *Anal.* Calc. for $\text{C}_{42}\text{H}_{53}\text{CoN}_4\text{O}_7$: C, 64.28; H, 6.81; N, 7.14. Found: C, 64.39; H, 7.05; N, 7.12.

Compound **2.8a**: ^1H NMR (Acetone- d_6 , 500 MHz) δ 2.98-3.01 (d, J = 13.8 Hz, 2H CH_2Ar), 4.18 (m, 4H $\text{CH}_2\text{Ar}/\text{CH}_2\text{Py}$), 6.95-6.96 (d, J = 2.3 Hz, 2H ArH), 7.00-7.02 (d, J = 9.7 Hz, 1H ArH), 7.05-7.06 (d, J = 2.0 Hz, 2H), 7.41-7.43 (d, J = 7.1 Hz, 1H ArH), 7.62-7.64 (t, J = 6.3 Hz, 1H ArH), 7.81-7.84 (dd, J = 9.1, 1.8 Hz, 1H ArH), 7.95-7.98 (t, J = 7.3 Hz, 1H ArH), 8.76-8.77 (d, J = 2.5 Hz, 1H ArH), 8.83-8.84 (d, J = 5.5 Hz, 1H ArH). ^{13}C NMR (Acetone- d_6 , 125 MHz): 61.49, 66.39, 119.56, 122.92, 124.28, 125.34, 126.26, 127.60, 128.28, 129.00, 129.53, 130.30, 133.92, 141.19, 150.07, 160.20, 162.04, 173.03. *Anal.* Calc. for $\text{C}_{26}\text{H}_{17}\text{CoCl}_4\text{N}_4\text{O}_7 \cdot 1.1\text{CH}_2\text{Cl}_2$: C, 41.12; H, 2.44; N, 7.08. Found: C, 41.33; H, 2.37; N, 6.88.

Compound **2.9a**: ^1H NMR (CDCl_3 , 300 MHz) δ 1.15 (s, 18H $\text{ArC}(\text{CH}_3)_3$), 2.17 (s, 6H ArCH_3), 2.28 (d, J = 22.7 Hz, 2H $\text{CH}_2\text{CH}_2\text{N}(\text{CH}_3)_2$), 2.47 (s, 6H $\text{N}(\text{CH}_3)_2$), 2.64 (d, J = 23.0 Hz, 4H CH_2Ar), 2.81 (d, J = 13.7 Hz, 2H $\text{CH}_2\text{CH}_2\text{N}(\text{CH}_3)_2$), 6.26 (d, J = 9.6 Hz, 1H ArH), 6.70 (s, 2H ArH), 6.81 (s, 2H ArH), 7.61 (d, J = 7.7 Hz, 1H ArH), 8.77 (s, 1H ArH). ^{13}C NMR (CDCl_3 , 75.0 MHz) δ 15.28, 20.77, 30.14, 35.04, 50.30, 58.25, 60.39, 61.04, 65.85, 122.19, 122.31, 123.19, 123.72, 127.07, 127.62, 127.91, 128.31, 136.59, 136.84, 159.34. *Anal.* Calc. for $\text{C}_{34}\text{H}_{45}\text{CoN}_4\text{O}_7 \cdot 0.15\text{CH}_2\text{Cl}_2$: C, 59.15; H, 6.58; N, 8.08. Found: C, 59.29; H, 6.46; N, 8.03. MALDI-TOF MS positive mode, anthracene: m/z (%) = 497.3 (100) $[\text{M} - 2,4\text{-DNP}]^+$; 680.3 $[\text{M}]^+$.

2.4.2.2 Synthesis of 2.6b

2.2 (0.250 g, 0.415 mmol) and silver acetate (0.069 g, 0.413 mmol) were dissolved in dichloromethane (30.0 mL) and stirred within an aluminum foil-wrapped flask at 22 °C for 2 h. The evolved dark grey precipitate was removed by filtration resulting in a dark brown filtrate. Volatiles were removed under reduced pressure to leave a dark brown solid which was dried *in vacuo* giving 0.180 g, 66.7% yield. **2.6b**: ^1H NMR (CDCl_3 , 300 MHz,) δ 1.20 (s, 18H C(CH_3)₃), 1.31 (s, 18H C(CH_3)₃) 1.96 (s, 3H CH_3COO), 3.05 (d, J = 13.1 Hz, 2H NCH_2Ar), 3.98 (s, 2H NCH_2Py), 4.58 (d, J = 13.1 Hz 2H NCH_2Ar), 6.63 (d, J = 8.0 Hz, 1H ArH), 6.80 (s, 2H 2x ArH), 6.94 (s, 2H ArH), 7.39 (t, J = 7.8 Hz, 1H ArH), 8.56 (d, J = 5.6 Hz, 1H ArH). MALDI-TOF MS positive mode, anthracene: m/z (%) = 601.4 (76) $[\text{CoL2}]^+$; 660.4 (100) $[\text{M}]^+$; 699.3 (33) $[\text{M} + \text{K}]^+$; 708.3 (69) $[\text{Ag} + \text{CoL2}]^+$

Compound **2.8b** was also synthesized using this method: ^1H NMR (CDCl_3 , 300 MHz) δ 1.89 (s, 3H CH_3COO), 3.04 (d, J = 13.9 Hz, 2H NCH_2Ar), 3.64 (d, J = 13.8 Hz, 2H NCH_2Ar), 4.01 (s, 2H NCH_2Py), 6.88 (d, J = 2.5 Hz, 2H ArH), 7.14 (d, J = 2.5 Hz, 2H ArH), 7.29 (d, J = 7.7 Hz, 1H ArH), 7.42 – 7.35 (m, 1H ArH), 7.80 (t, J = 7.2 Hz, 1H ArH), 8.84 (d, J = 4.9 Hz, 1H ArH). ^{13}C NMR (CDCl_3 , 75 MHz,) δ 23.54, 60.46, 64.72, 119.53, 122.01, 123.93, 124.39, 124.44, 127.02, 128.01, 129.42, 139.51, 152.18, 160.82, 193.79. MALDI-TOF MS positive mode, anthracene: m/z (%) = 573.9 (100) $[\text{M}]^+$.

2.4.2.3 Synthesis of 2.6c

2.2 (0.500 g, 0.831 mmol) and silver trifluoroacetate (0.184 g, 0.831 mmol) were mixed in dichloromethane (20.0 mL) and stirred within an aluminum foil-wrapped flask for 2 h at 22 °C. The resulting precipitate was removed via gravity filtration and the brown filtrate collected. Volatiles were removed under reduced pressure resulting in a brown solid which was dried *in vacuo*; 0.076g, 12.8% yield. Compound **2.6c**: MALDI-TOF MS positive mode, anthracene: m/z (%) = 601.3 (100) [CoL2]⁺; 714.4 (10) [M]⁺.

Compound **2.8c** was also synthesized using this method (0.202g): MALDI-TOF MS positive mode, anthracene: m/z (%) = 514.9 (100) [CoL5]⁺; 666.9 (89) [M + KH]⁺

2.4.2.4 Attempted synthesis of 2.6d

2.2 (0.250 g, 0.415 mmol) and silver trifluoromethanesulfonate (0.107 g, 0.415 mmol) were mixed in dichloromethane (30.0 mL) then stirred within an aluminum foil-wrapped flask for 24 h at 22 °C resulting in a brown solution with a dark grey precipitate. The precipitate was removed via gravity filtration resulting in a brown filtrate. Volatiles were removed from the filtrate under reduced pressure and dried *in vacuo* resulting in a dark brown solid; 0.128g, 41.1% yield. Compound **2.6d**: MALDI-TOF MS positive mode, anthracene: m/z (%) = 601.3 (100) [CoL2]⁺; 750.2 (10) [M]⁺.

The synthesis of compound **2.8d** was also attempted using this procedure: MALDI-TOF MS positive mode, anthracene: m/z (%) = 463.0 (100) [L5 + Li]⁺; 514.8 (24) [CoL5]⁺; 680.7 (40) [M + OH]⁺.

2.4.2.5 Attempted synthesis of [CoClL_n] complexes (2.6e and 2.8e)

Compound **2.6e**: **H₂L2** (0.500 g, 0.918 mmol) was dissolved in toluene (10.0 mL). CoCl₂ was dissolved in degassed methanol (10.0 mL) then added to the ligand solution and the mixture was heated to reflux open to air using a condenser fitted with a drying tube for 24 h. Upon cooling, the resulting dark brown solution was collected, and volatiles removed under reduced pressure resulting in a dark green solid once dried *in vacuo*; 0.462 g, 78.8% yield. MALDI-TOF MS positive mode, anthracene: *m/z* (%) = 545.5 (100) [H₃L2]⁺; 601.4 (99) [CoL2]⁺; 638.4 (8) [M]⁺.

Compound **2.8e**: **H₂L5** (0.500 g, 1.09 mmol), triethylamine (152 μL, 1.09 mmol) and CoCl₂·6H₂O (0.259 g, 1.09 mmol) were dissolved in tetrahydrofuran (10.0 mL) and stirred at 22 °C under a balloon of O₂ (1 atm) for 2 h. The resulting purple solution with a white precipitate was filtered and the filtrate collected. Volatiles were removed under reduced pressure then dried *in vacuo* resulting in a black crystalline solid; 0.457 g, 76.2% yield. MALDI-TOF MS positive mode, anthracene: *m/z* (%) = 459.0 (100) [H₃L5]⁺; 1123.8 (13) [2(M) + Na]⁺.

2.4.2.6 Attempted synthesis of 2.6f

2.2 (0.500 g, 0.830 mmol) and 4-nitrophenol (0.116 g, 0.830 mmol) were mixed in dichloromethane (30.0 mL) and stirred at 22 °C under a balloon of O₂ for 3 h. The resulting mixture was filtered and the filtrate collected. Volatiles were removed under reduced pressure then dried *in vacuo* to produce a black solid; 0.185 g, 29.3%. MALDI-TOF MS positive mode, anthracene: *m/z* (%) = 601.3 (100) [CoL2]⁺.

2.4.3 Representative CO₂/epoxide coupling procedure

Compound **2.6a** (0.0368 g, 0.240 mmol) and tetrabutylammonium bromide, TBAB, (0.0158 g, 0.0491 mmol) were dissolved in propylene oxide (1.425 g, 24.0 mmol), and were mixed in a vial resulting in a dark brown solution. The solution was injected via syringe into a pre-dried (under vacuum at 80 °C overnight) pressure reactor and pressurized to 40 bar CO₂ and stirred at 60 °C for 24 h; special precautions were taken when pressurizing the reactor due to increased risks involved at greater than atmospheric pressure. Upon cooling to room temperature, the reactor was vented into the fume hood and opened, revealing a dark brown solution. An aliquot was taken for ¹H NMR spectroscopy to calculate the conversion.

2.4.4 X-ray crystallography procedure

Compound **2.9a**: Crystallography was performed by Julie Collins of the C-CART X-ray Diffraction Laboratory, Memorial University of Newfoundland, St. John's, Newfoundland, A1B 3X7, Canada. Single crystals of C₃₅H₄₇Cl₂CoN₄O₇, **2.9a**, were crystallized from a mixture of hexane, diethyl ether and dichloromethane. A suitable crystal was selected and mounted in Paratone N on a MiTeGen MicroMount on a Rigaku Saturn70 (2x2 bin mode) diffractometer. The crystal was kept at 158 K during data collection. Using Olex2⁵³, the structure was solved with the olex2.solve⁵⁴ structure solution program using Charge Flipping and refined with the ShelXL⁵⁵ refinement package using Least Squares minimization.

2.5 References

1. A. Decortes, A. M. Castilla and A. W. Kleij, *Angew. Chem. Int. Ed.*, 2010, **49**, 9822-9837.
2. R. R. Shaikh, S. Pornpraprom and V. D'Elia, *ACS Catal.*, 2018, **8**, 419-450.
3. S. J. Poland and D. J. Darensbourg, *Green Chem.*, 2017, **19**, 4990-5011.
4. D. Alhashmialameer, J. Collins, K. Hattenhauer and F. M. Kerton, *Catal. Sci. Technol.*, 2016, **6**, 5364-5373.
5. A. Buonerba, A. De Nisi, A. Grassi, S. Milione, C. Capacchione, S. Vagin and B. Rieger, *Catal. Sci. Technol.*, 2015, **5**, 118-123.
6. C. J. Whiteoak, N. Kielland, V. Laserna, E. C. Escudero-Adán, E. Martin and A. W. Kleij, *J. Am. Chem. Soc.*, 2013, **135**, 1228-1231.
7. M. North, P. Villuendas and C. Young, *Chem. Eur. J.*, 2009, **15**, 11454-11457.
8. J. A. Castro-Osma, K. J. Lamb and M. North, *ACS Catal.*, 2016, **6**, 5012-5025.
9. J. A. Castro-Osma, M. North and X. Wu, *Chem. Eur. J.*, 2016, **22**, 2100-2107.
10. J. Liang, Y.-Q. Xie, X.-S. Wang, Q. Wang, T.-T. Liu, Y.-B. Huang and R. Cao, *Chem. Commun.*, 2018, **54**, 342-345.
11. L. Cuesta-Aluja, M. Djoufak, A. Aghmiz, R. Rivas, L. Christ and A. M. Masdeu-Bultó, *J. Mol. Catal. A: Chem.*, 2014, **381**, 161-170.
12. L. N. Saunders, N. Ikpo, C. F. Petten, U. K. Das, L. N. Dawe, C. M. Kozak and F. M. Kerton, *Catal. Commun.*, 2012, **18**, 165-167.
13. A. Ghosh, P. Ramidi, S. Pulla, S. Z. Sullivan, S. L. Collom, Y. Gartia, P. Munshi, A. S. Biris, B. C. Noll and B. C. Berry, *Catal. Lett.*, 2010, **137**, 1-7.

14. M. Ulusoy, A. Kilic, M. Durgun, Z. Tasci and B. Cetinkaya, *J. Organomet. Chem.*, 2011, **696**, 1372-1379.
15. A. Kilic, M. Ulusoy, M. Durgun and E. Aytar, *Inorg. Chim. Acta*, 2014, **411**, 17-25.
16. A. Kilic, M. Ulusoy, E. Aytar and M. Durgun, *Ind. Eng. Chem. Res.*, 2015, **24**, 98-106.
17. H. G. Sogukomerogullari, E. Aytar, M. Ulusoy, S. Demir, N. Dege, D. S. Richeson and M. Sönmez, *Inorg. Chim. Acta*, 2018, **471**, 290-296.
18. C. E. Anderson, S. I. Vagin, W. Xia, H. Jin and B. Rieger, *Macromolecules*, 2012, **45**, 6840-6849.
19. D. Bai, X. Wang, Y. Song, B. Li, L. Zhang, P. Yan and H. Jing, *Chin. J. Catal.*, 2010, **31**, 176-180.
20. D. Bai, Q. Wang, Y. Song, B. Li and H. Jing, *Catal. Commun.*, 2011, **12**, 684-688.
21. M. Reiter, P. T. Altenbuchner, S. Kissling, E. Herdtweck and B. Rieger, *Eur. J. Inorg. Chem.*, 2015, **2015**, 1766-1774.
22. Z. Hošťálek, R. Mundil, I. Císařová, O. Trhlíková, E. Grau, F. Peruch, H. Cramail and J. Merna, *Polymer*, 2015, **63**, 52-61.
23. D. J. Darensbourg, *Adv. Inorg. Chem.*, 2014, **66**, 1-23.
24. D. J. Darensbourg, J. C. Yarbrough, C. Ortiz and C. C. Fang, *J. Am. Chem. Soc.*, 2003, **125**, 7586-7591.
25. G.-P. Wu, S.-H. Wei, W.-M. Ren, X.-B. Lu, B. Li, Y.-P. Zu and D. J. Darensbourg, *Energy Environ. Sci.*, 2011, **4**, 5084-5092.
26. R. L. Paddock and S. T. Nguyen, *J. Am. Chem. Soc.*, 2001, **123**, 11498-11499.

27. Y. Niu, W. Zhang, X. Pang, X. Chen, X. Zhuang and X. Jing, *J. Polym. Sci., Part A: Polym. Chem.*, 2007, **45**, 5050-5056.
28. Y. Niu, H. Li, X. Chen, W. Zhang, X. Zhuang and X. Jing, *Macromol. Chem. Phys.*, 2009, **210**, 1224-1229.
29. X. Zhuang, K. Oyaizu, Y. Niu, K. Koshika, X. Chen and H. Nishide, *Macromol. Chem. Phys.*, 2010, **211**, 669-676.
30. G.-P. Wu, S.-H. Wei, W.-M. Ren, X.-B. Lu, T.-Q. Xu and D. J. Darensbourg, *J. Am. Chem. Soc.*, 2011, **133**, 15191-15199.
31. H. Li and Y. Niu, *Polym. J.*, 2010, **43**, 121.
32. Y. Niu and H. Li, *Colloid. Polym. Sci.*, 2013, **291**, 2181-2189.
33. X.-B. Lu, L. Shi, Y.-M. Wang, R. Zhang, Y.-J. Zhang, X.-J. Peng, Z.-C. Zhang and B. Li, *J. Am. Chem. Soc.*, 2006, **128**, 1664-1674.
34. S. Elmas, M. A. Subhani, H. Vogt, W. Leitner and T. E. Müller, *Green Chem.*, 2013, **15**, 1356-1360.
35. J. Y. Jeon, J. J. Lee, J. K. Varghese, S. J. Na, S. Sujith, M. J. Go, J. Lee, M.-A. Ok and B. Y. Lee, *Dalton Trans.*, 2013, **42**, 9245-9254.
36. W.-M. Ren, Z.-W. Liu, Y.-Q. Wen, R. Zhang and X.-B. Lu, *J. Am. Chem. Soc.*, 2009, **131**, 11509-11518.
37. A. Cyriac, J. Y. Jeon, J. K. Varghese, J. H. Park, S. Y. Choi, Y. K. Chung and B. Y. Lee, *Dalton Trans.*, 2012, **41**, 1444-1447.
38. C. T. Cohen, T. Chu and G. W. Coates, *J. Am. Chem. Soc.*, 2005, **127**, 10869-10878.

39. K. L. Peretti, H. Ajiro, C. T. Cohen, E. B. Lobkovsky and G. W. Coates, *J. Am. Chem. Soc.*, 2005, **127**, 11566-11567.
40. H. Zhang and M. W. Grinstaff, *J. Am. Chem. Soc.*, 2013, **135**, 6806-6809.
41. G.-J. Kim, H. Lee and S.-J. Kim, *Tetrahedron Lett.*, 2003, **44**, 5005-5008.
42. G. Li, Y. Liu, K. Zhang, J. Shi, X. Wan and S. Cao, *J. Appl. Polym. Sci.*, 2013, **129**, 3696-3703.
43. A. R. Silva, T. Mourão and J. Rocha, *Catal. Today*, 2013, **203**, 81-86.
44. Y. Wei, T. Pang, J. Liu, M. Li and L. Liang, *Acta Crystallogr. Sect. E*, 2012, **68**, m455-m456.
45. L. N. Saunders, M. E. Pratt, S. E. Hann, L. N. Dawe, A. Decken, F. M. Kerton and C. M. Kozak, *Polyhedron*, 2012, **46**, 53-65.
46. X. Zhuang, H. Yu, Z. Tang, K. Oyaizu, H. Nishide and X. Chen, *Chin. J. Polym. Sci.*, 2011, **29**, 197-202.
47. X.-B. Lu and Y. Wang, *Angew. Chem. Int. Ed.*, 2004, **43**, 3574-3577.
48. J. Yoo, S. J. Na, H. C. Park, A. Cyriac and B. Y. Lee, *Dalton Trans.*, 2010, **39**, 2622-2630.
49. R. K. Dean, K. Devaine-Pressing, L. N. Dawe and C. M. Kozak, *Dalton Trans.*, 2013, **42**, 9233-9244.
50. A. Sibaouih, P. Ryan, K. V. Axenov, M. R. Sundberg, M. Leskelä and T. Repo, *J. Mol. Catal. A: Chem.*, 2009, **312**, 87-91.
51. D. J. Darensbourg and S. J. Wilson, *Macromolecules*, 2013, **46**, 5929-5934.
52. A. M. Reckling, D. Martin, L. N. Dawe, A. Decken and C. M. Kozak, *J. Organomet. Chem.*, 2011, **696**, 787-794.

53. O. V. Dolomanov, L. J. Bourhis, R. J. Gildea, J. A. K. Howard and H. Puschmann, *J. Appl. Crystallogr.*, 2009, **42**, 339-341.
54. L. J. Bourhis, O. V. Dolomanov, R. J. Gildea, J. A. K. Howard and H. Puschmann, *Acta Crystallogr. Sect. A*, 2015, **71**, 59-75.
55. G. Sheldrick, *Acta Crystallogr. Sect. A*, 2008, **64**, 112-122.

Chapter 3: Synthesis and Characterization of Co(II) Amino-bis(phenolate) complexes as Catalysts for Copolymerization of CO₂ and Cyclohexene Oxide

3.1 Introduction

CO₂ is an abundant greenhouse gas in the Earth's atmosphere with its concentration at approximately 400 ppm.^{1,2} It is non-toxic and non-flammable, therefore CO₂ activation has become appealing for its utilization as a renewable C-1 feedstock.³⁻⁵ Coupling or copolymerization of CO₂ and epoxides is a growing area of research for a number of reasons. Cyclic carbonates are used as a component in electrolytes in lithium-ion batteries,⁶ precursors for polymer synthesis⁶ and as alternative polar aprotic solvents because they are non-toxic, biodegradable and non-corrosive.^{5,7-10} The optical transparency and impact resistant properties of polycarbonates make them ideal for CDs, DVDs and aircraft windows.¹¹

Along with the advantage of using ring-strained, high energy epoxides, an efficient catalyst system is needed to perform CO₂/epoxide coupling reactions.¹² Catalyst systems containing metals such as Co,¹³⁻²⁸ Al,²⁹⁻³¹ Cr,^{9,32-37} and Fe³⁸⁻⁴² have been shown to catalyze the formation of organic carbonates from CO₂/epoxide coupling reactions. In this research, we describe Co-amino-bis(phenolate) catalyst systems for CO₂/epoxide coupling. Cobalt coordination complexes of different ligand classes have been reported by Williams using "Robson"-type macrocyclic ligands,⁴³ Coates using salen ligands,¹⁸ and Lee using salen ligands containing quaternary ammonium salt units.⁴⁴ Salen ligands containing neutral nucleophiles such as propylene-tethered TBD units (where TBD =

1,5,7-triazabicyclo[4.4.0]dec-5-ene) have also been reported.⁴⁵ The salen catalyst system when paired with cobalt or chromium exhibits high catalytic activity for CO₂/epoxide copolymerization.^{3,46} It exhibits an [ONNO] chelation pattern at the metal center coupled with axial (often labile) ancillary ligands, which promote high catalytic activity and adequate stability.^{3,46,47} Typically, some catalyst systems require an additional nucleophilic species (neutral or ionic) such as 4-(dimethylamino)pyridine (DMAP) or onium salts such as tetrabutylammonium bromide (TBAB) or bis(triphenylphosphine)-iminium halide (PPNX) to facilitate initiation. These catalyst systems are termed “binary”. Other catalyst systems may be bifunctional because they have the nucleophilic co-catalyst incorporated into the ligand structure (either covalently tethered neutral or ionic groups) and these have shown exemplary catalytic activity.^{16,48,49}

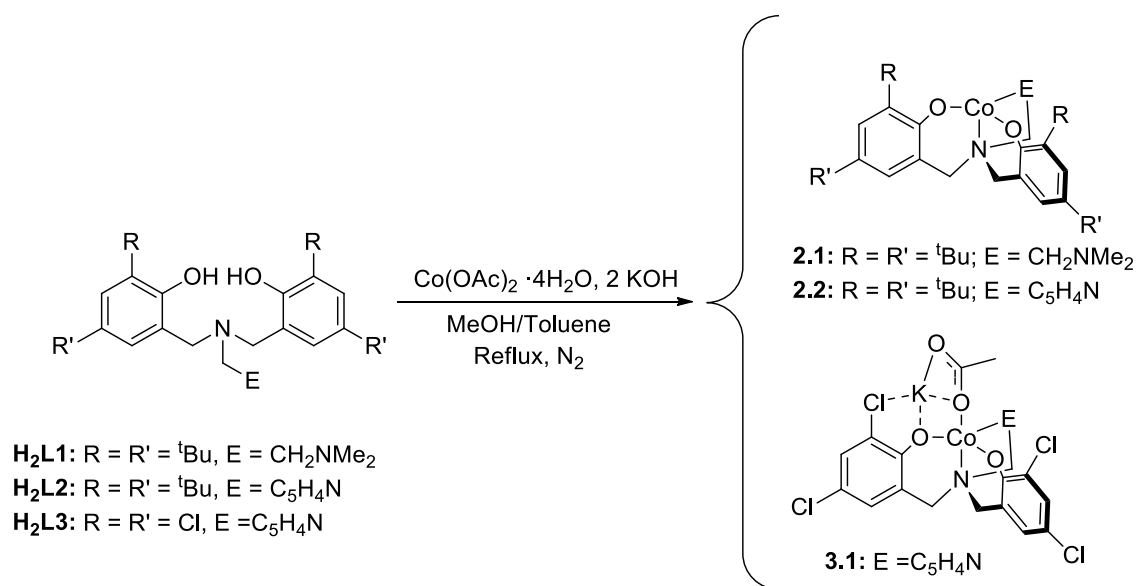
The Kozak group has developed binary catalyst systems based on the amine-bis(phenolate) ligand system.^{32,33,50-59} Unlike typical equatorial and planar tetradentate salen ligands, the amino-bis(phenolate) ligands are tripodal, can be either tridentate or tetradentate (depending on the nature of the pendent arm) and have non-planar [ONNO] coordination pattern.^{53,55} The electronic and steric properties can be tuned by varying the type of pendent arm and substituents on the phenolate groups.⁵⁵ Furthermore, they have potentially stronger donor ability via amines donors, than salen (imine donors) and the phenolate donors can occupy a *cis* or *trans* arrangement thus allowing for different environments for an incoming nucleophile when a vacant site is generated during a reaction.⁵⁵

The Kozak group has previously shown that amino-bis(phenolate) ligands can be coordinated to cobalt using $\text{Co}(\text{OAc})_2 \cdot 4\text{H}_2\text{O}$ under basic conditions to afford Co(II) or Co(III) complexes when the reaction is performed under an inert or oxidative atmosphere (air or pure oxygen), respectively.^{56,58} Catalytic activity for cycloaddition reactions of CO_2 with propylene oxide (PO) show up to 2025 turnovers using a Co(II) complex (0.046 mol% catalyst loading) at 25 °C, 35 bar CO_2 and co-catalyzed by TBAB.⁵⁶ Studies investigating the effect of cobalt oxidation state on PO/ CO_2 coupling show significantly higher turnovers with Co(II) compared to Co(III) complexes. Although good activity was exhibited by these catalysts for CO_2 /PO coupling, the production of polycarbonate was not achieved.⁵⁶ However, Rieger and co-workers have since shown selectivity towards polycarbonate synthesis when CO_2 /cyclohexene oxide (CHO) coupling reactions were explored using a similar Co catalyst having a dimethylaminoethyl pendent donor.⁶⁰ This was facilitated by making the Co center more Lewis acidic by using electron-withdrawing chlorine substituents in the *ortho*- and *para*-positions of the phenolate donors. The active Co(II) species was isolated in the solid state as a methanol adduct. Poly(cyclohexene carbonate) (PCHC) production was observed when co-catalyzed by DMAP giving yields up to 25% and high CO_2 incorporation for reactions performed at 80 °C and 50 bar CO_2 . Herein the work in this chapter describes the modification of sterics and electronics at Co(II) centers by varying both phenolate and pendent *N*-donors amino-bis(phenolate) complexes, and the effects on activity for CO_2 and epoxide copolymerization reactions. Specifically, the use of dichlorophenolate donors with pyridyl pendent arms were found to be superior to the more electron-donating dialkylphenolate and tertiary amino donor groups.

3.2 Results and discussion

3.2.1 Synthesis of Co(II) complex

Co(II) complexes **2.1**, **2.2** and **3.1** were prepared as described in **Scheme 3.1**. The Kozak group has previously reported the detailed syntheses of **2.1** and **2.2**,⁵⁷ but their catalytic activity for CO₂/epoxide coupling/copolymerization was not reported. Compounds **2.1** and **2.2** possess electron donating alkyl groups in the *ortho* and *para* positions of the phenolate groups and were isolated as solvento (methanol, acetone, aquo and propylene oxide) adducts in the solid state.⁵⁷ The work in this thesis involved the preparation of a more electron-deficient complex, **3.1**, which is related to pyridyl donor-containing complex **2.2**, but possessing chloro-functionalities in the *ortho* and *para* positions of the phenolate ligand. Related Co(II) complexes of similar ligands, although bearing dimethylamino and diethylamino pendent groups, have been reported by Rieger⁶⁰ and Wang,⁶¹ respectively. Complex **3.1** was characterized by MALDI-TOF MS, which showed *m/z* 514.9 corresponding to a [CoL3]⁺ ion and a peak at *m/z* 612.9 corresponding to [CoL3·KOAc]⁺ (see Appendix B, Figure B-11). The simulated isotopic patterns are in good agreement with the observed patterns. Elemental analysis of **3.1** confirmed the presence of KOAc and the observed composition was consistent with a formula possessing 1.65 equiv. KOAc per Co[L3] unit. Attempts at removing residual KOAc by recrystallization were ineffective and the persistence of the impurity can be explained through structure determination in the solid state by X-ray diffraction.



Scheme 3.1: Synthesis of Co(II) amino-bis(phenolate) complexes **2.1**, **2.2** and **3.1**.

Single crystals of **3.1** suitable for X-ray diffraction were acquired via slow evaporation of a solution of **3.1** in acetone and toluene at $-20\text{ }^{\circ}\text{C}$. The molecular structure is shown in **Figure 3.1**, structural data given in Table C-1, Appendix C and selected bond lengths and angles in Tables C-4 and C-5, respectively. Unfortunately, the crystal data were poor due to weak diffractions, therefore, problems were encountered and SQUEEZE was used to remove excess electron density that was likely due to the presence of solvent that could not be accurately modelled.

The complex exists as a hexacobalt cluster where six $\text{Co}[\text{L3}]$ units are linked via bridging acetate ligands, potassium ions and aquo ligands in a complex arrangement. The asymmetric unit possesses three $\text{Co}[\text{L3}]$ units, three potassium ions, three acetate ligands and one water molecule, hence formulated as $\text{K}_3[(\text{Co}[\text{L3}])_3(\text{OAc})_3(\text{H}_2\text{O})]$. The $\text{Co}[\text{L3}]$ fragments exist in two geometric forms: two contain trigonal bipyramidal Co(II) sites and

one contains an octahedral Co(II) center. The acetate ligands are monodentate and bridging. The central Co[L3] fragment (identified for clarity as Co[L3]₁) is trigonal bipyramidal having one acetate O-donor in the apical position. The two phenolate groups each bind to potassium ions, which are in turn coordinated by the *ortho* chloro groups of the phenolate donors, hence forming an O–Cl chelate at the potassium. The two potassium ions are bridged by a water molecule. The acetate ligand serves to bridge to the six-coordinate Co(II) center, Co[L3]₂. The third Co(II) site, Co[L3]₃ is trigonal bipyramidal and is connected to the central Co[L3]₁ fragment via another monodentate acetate group which bridges the third Co(II) site to a potassium ion chelated by the O–Cl of the central Co[L3]₁ site. A simplified illustration of the bonding is shown in **Figure 3.1**. In addition to the tetradentate amino-bis(phenolate) ligand, six-coordinate Co[L3]₂ contains two monodentate acetate ligands in a *cis* arrangement and *trans*-oriented phenolate donors. Bond distances between the Co center and the amino-bis(phenolate) ligand (L3) are comparable to previously reported Co(II) structures with similar geometries.^{60,61} The asymmetric unit expands to give a hexacobalt cluster through extensive bridging manifested through coordination of the potassium and acetate fragments, as well as hydrogen bonding between the O–H of the aquo ligands and acetate O sites. This results in the formation of a saddle-like cavity within the cluster. Furthermore, the packing of the unit cell shows a left-handed helical arrangement of the hexacobalt clusters translating along the c-axis.

Structures having chloro-functionalized phenolate donors in multidentate *N,O* ligands have been reported for iron,^{62,63} aluminum^{64,65} and cobalt.^{57,60,61,66} Most relevant is the

report of an amino-tris(phenolate) complex of cobalt(III) with two NaOAc bridging ligands.⁶⁶ The structure shows a dimetallic Co(III) amino-tris(phenolate) complex with chlorine-containing phenolate donors, and two sodium ions are bridged via the phenolate oxygen and chlorine substituents. The acetate ligands are monodentate μ_3 -bridges between a single cobalt center and two sodium ions. An earlier example has been reported of a manganese complex bearing a trianionic pentadentate Schiff base ligand with *ortho* chlorinated phenolate groups.⁶⁷ This complex exhibits sodium ion interactions with bridging acetates and phenolate oxygens to produce a 1-D supramolecular array of alternating manganese “ate” complexes and Na^+ ions. However, there are no structures reported bearing phenolato carbon-halogen-potassium and metal-X-potassium (or other group 1 element, where X is an anionic ligand) interactions.

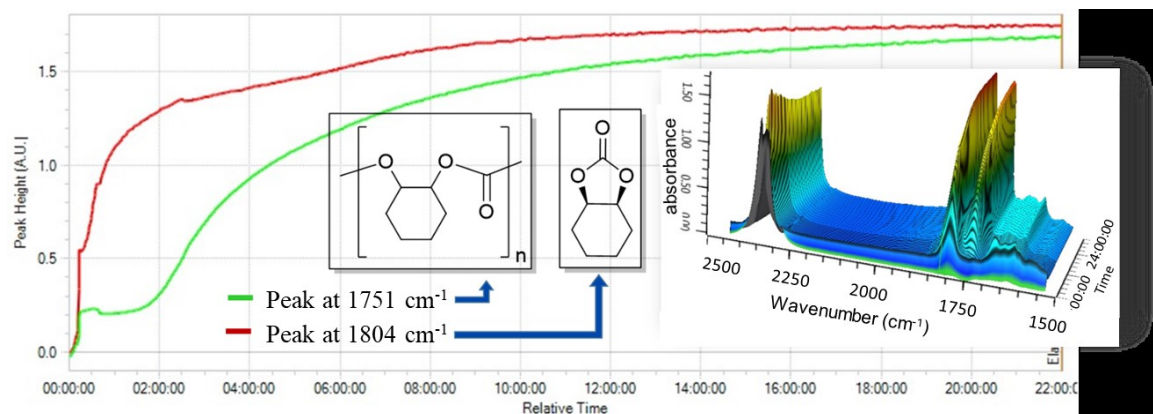


Figure 3.2: In situ FTIR reaction profile of polycarbonate (green) and cyclic carbonate (red) formation resulting from bands at 1751 cm^{-1} and 1804 cm^{-1} , respectively. Inset: three-dimensional stack plot collected every 60 s for Table 3.1 entry 7.

The use of DMAP and **3.1** at 1% catalyst loading afforded 98% conversion of CHO, of which 76% was PCHC with the remaining product being cyclohexene carbonate, CHC, (Table 3.1, entry 1). A decreased catalyst loading to 0.5 mol% resulted in decreased conversion of 65% while maintaining high CO_2 incorporation (Table 3.1, entry 2). Selectivity for polycarbonate formation also decreased. Increasing the temperature to $100\text{ }^\circ\text{C}$ had a marginal effect on conversion compared to results at $80\text{ }^\circ\text{C}$, but the polycarbonate formation decreased significantly instead favoring CHC formation. At $120\text{ }^\circ\text{C}$ epoxide conversion increased to 94% with 88% selectivity for CHC formation (Table 3.1, entry 8). Characterization by ^1H , ^{13}C NMR (see Appendix A, Figures A-14 and A-15) and IR spectroscopies (Figure 3.2) showed the *cis* isomer of CHC was produced, which requires a double stereochemical inversion.⁴⁰ The more common *trans* isomer usually results from polymer backbiting under thermodynamic control and is believed to be enhanced by the presence of excess anionic co-catalyst.^{42,68} Cyclic carbonates formed

from CO₂ and epoxides (such as propylene oxide and cyclohexene oxide) are thermodynamically favored products but possess a higher activation barrier compared to polycarbonate formation, which can be overcome by increasing temperature.^{69,70}

Increasing the pressure of CO₂ to 60 bar at 80 °C and 0.5 mol% catalyst and co-catalyst loading shows much improved ($\geq 97\%$) selectivity for polycarbonate formation with 95% or higher carbonate linkages (**Table 3.1**, entries 4 – 6). The reaction, while slow, shows excellent stability over time with conversions increasing from 47% after 24 h to 94% after 72 h. This finding reveals a dependence of reaction rate on CO₂ pressure and similar observations have been reported by the Kozak group for chromium(III) amino-bis(phenolate) complexes, but the reaction rates were much faster than for cobalt complex **3.1**.³² CO₂ does not require prior coordination to the coordinatively saturated metal center for incorporation into carbonates and epoxide ring-opening is often found to be the rate-determining step in many catalyst systems for this reaction.⁷¹⁻⁷⁵ CO₂ pressure has been showed by Ghosh and co-workers to affect catalyst activity (TOF) for propylene carbonate production from CO₂/PO coupling using Co(III) amidoamine complexes.⁷⁶ TOFs increased from approximately 200 to 500 TO h⁻¹ when the CO₂ pressure increased from 7 to 20 bar, but decreased as pressure was increased beyond 20 bar. This behavior was also observed with a Co(III)-TAML (TAML = tetraamidomacrocyclic ligand) complex for PO/CO₂ coupling where an increase in TOF was observed as CO₂ pressures increased from 7.5 to 20 bar, but decreased significantly at higher pressures.⁷⁷ Other Co-containing catalyst systems also demonstrated an initial enhanced activity with increased CO₂ pressure, but decreased beyond a particular pressure threshold.^{78,79}

Employing tetrabutylammonium bromide (TBAB) and bis(triphenylphosphine)-iminium chloride (PPNCl) (entries 7 and 9, respectively) at 80 °C showed high conversions in 24 h reaction times but decreased selectivity for polycarbonate synthesis. At 120 °C and 40 bar CO₂, high conversions were obtained but 88% yield of CHC was produced, and the small amount of PCHC produced had a high degree of ether linkages (entry 8). Increasing CO₂ pressure to 60 bar (entries 10 and 11) showed similar conversion when performed at 40 bar using TBAB and PPNCl co-catalysts (entries 7 and 9, respectively), although TBAB proved more selective for PCHC formation at the higher pressure. This differs from the report of Rieger and co-workers who observed no conversion of CHO when TBAB was used with related Co(II) amino-bis(phenolate) systems.⁶⁰ The increased basicity of DMAP makes the polymerization process more favorable over PPNCl and TBAB.⁷⁷ Furthermore, increased selectivity for *cis* CHC (when TBAB or PPNCl are used) suggests that once CHO is ring-opened by the halide nucleophile, followed by subsequent CO₂ insertion (forming a cobalt-carboxylate species), the carboxylate dissociates to form a charge-separated carboxylate species. This new anionic carbonate can now undergo an intramolecular nucleophilic substitution, halide elimination and formation of *cis* CHC.⁴⁰

Complexes **2.1** and **2.2** have been previously shown to produce cyclic propylene carbonate (PC) from PO/CO₂ coupling reactions in the presence of TBAB and PPNN₃, with up to 950 turnovers at 25 °C and 34 bar CO₂ pressure.⁵⁶ Complex **2.2** showed higher activity than **2.1** due to its stronger-donating, planar pyridyl group. When employed in this study, **2.1** and **2.2** showed no activity for conversion of CHO after 24 hours (entries

12 and 13 respectively) hence were not pursued further. This suggests that altering the electronics of the ligand through introduction of electronegative chlorine atoms on the phenolate groups increased the Lewis acidity at the metal center, thus increasing activity toward copolymerization reactions by promoting epoxide activation and/or ring opening and lowers the tendency for polymer chain (growing) dissociation.⁶⁰ The possibility that the potassium acetate found in the structure of **3.1** could serve as co-catalyst by providing acetate as a nucleophile was investigated. A 0.5 mol% loading of **3.1** in CHO at 40 bar CO₂ at 80 °C showed a small growth in infrared bands at 1750, 1804 and 1827 cm⁻¹ (corresponding to poly(cyclohexene carbonate) and cyclohexene carbonates), but only traces of products could be observed by ¹H NMR spectroscopy after 24 h. Compound **3.1** is a rare example of epoxide/CO₂ copolymerization by a Co(II) catalyst system. Nozaki and co-workers reported selectivity toward polycarbonate formation from PO/CO₂ using a Co(II)-salen complex. In that case the precursor catalyst was oxidized in situ during the copolymerization reaction.²⁶ Other Co(II) catalyst systems, however, are shown to be selective toward cyclic carbonate production.^{56,79,80}

Table 3.1: Copolymerization of CO₂ and CHO using **2.1**, **2.2** and **3.1**.^a

Entry	Compound: [Cat.]/ [Co-cat]/[CHO]	CO ₂ pressure (bar)	Time (h)	conv. (%) ^b	selectivity (% PCHC)	% carbonate
1	3.1 : 1:100:1(DMAP)	40	72	98	76	92
2	3.1 : 1:200:1(DMAP)	40	72	65	57	94
3 ^c	3.1 : 1:200:1(DMAP)	40	72	61	15	93
4	3.1 : 1:200:1(DMAP)	60	24	47	97	95
5	3.1 : 1:200:1(DMAP)	60	48	66	98	97
6	3.1 : 1:200:1(DMAP)	60	72	94	97	97
7	3.1 : 1:200:1(TBAB)	40	24	92	21	97
8 ^d	3.1 : 1:200:1(TBAB)	40	24	94	6	71
9	3.1 : 1:200:1(PPNCl)	40	24	85	60	96
10	3.1 : 1:200:1(PPNCl)	60	24	78	62	96
11	3.1 : 1:200:1(TBAB)	60	24	92	40	90
12	2.1 : 1:200:1(DMAP)	40	24	0	-	-
13	2.2 : 1:200:1(DMAP)	40	24	0	-	-

^a Reactions were performed in neat CHO at 80 °C using catalyst loadings shown, 40 bar CO₂ and DMAP as a co-catalyst unless otherwise stated. ^b Conversion calculated by ¹H NMR (Figure S7). ^c Reaction performed at 100 °C. ^d Reaction performed at 120 °C.

3.2.3 Polycarbonate end group analysis

Characterization of the polycarbonates using MALDI-TOF MS allows for end group analysis, which provides an insight into the polymerization initiation step. The mass spectrum of polycarbonate obtained under the conditions in **Table 3.1**, entry 1 shows a bimodal distribution of masses separated by m/z 142 corresponding to the cyclohexene carbonate repeat unit (see Appendix B, Figure B-12). Multiple fragments are often observed for polycarbonates formed from CO₂/epoxide copolymerization which may result from various initiation and termination mechanisms, and chain transfer during the polymerization process.^{19,32,33} A magnification of the mass spectrum is given in **Figure 3.3**. The major series (blue triangle) corresponds to polymer chains having hydroxide and DMAP end groups, possibly resulting from a DMAP-initiated polymer chain which was then terminated by protonolysis of the metal-alkoxide. The minor series (red square) corresponds to lithium ion-containing polymer chains having methoxy and hydroxide end groups. The source of lithium likely occurs via contamination from the instrument because no lithium-containing cationizing additives were used in preparation of MALDI-TOF samples.

In light of the inactivity towards CO₂/CHO copolymerization exhibited by **2.1** and **2.2** as well as the related amino-bis(phenolate) Co(II) complexes reported by Rieger,⁶⁰ the presence of acetate appears to be advantageous toward polycarbonate formation, but as described above, is insufficient on its own to give high catalytic activity. The minor series (red square, **Figure 3.3**) corresponds to polymer chains having hydroxide and methoxy end groups where the methoxy end group likely results from HCl-catalyzed methanolysis.

Cold acidified methanol was used for polymer purification and removal of residual Co catalyst; therefore, fragments containing methoxy end groups may result during this procedure.

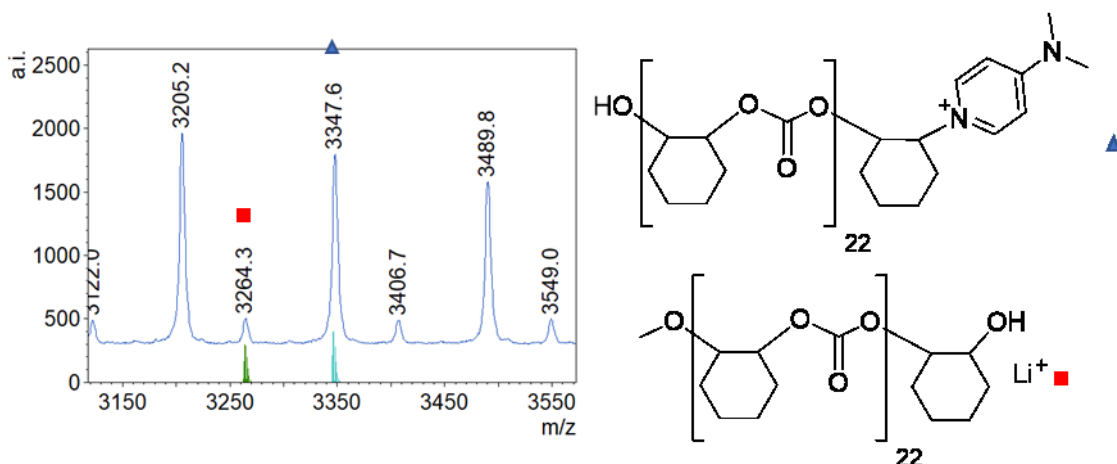


Figure 3.3: Magnified section (m/z 3120 – 3570) of the MALDI-TOF mass spectrum of PCHC obtained in Table 3.1, entry 1.

When **3.1** was used with PPNCl as a co-catalyst for CHO/CO₂ copolymerization (Table 3.1, entry 9), five polymer chain types were observed in the low mass region (Figure 3.4), whereas two polymer chain types were observed in a higher mass region (Figure 3.5). The higher mass polymers correspond to methoxy group and chloride-terminated polymers (Figure 3.5). These two chains are also visible in the low mass region. This suggests that initiation by added chloride from PPNCl is more effective at polycarbonate production, consistent with its poorer leaving group ability compared with bromide. Acetate end-group-containing polymers were only observed in lower mass fragments. The presence of acetate end groups suggests the polymer results from the linking of two chains (acetate-initiated) via chain transfer mechanisms. The acetate-end

group results from the presence of KOAc coordinated to the amino-bis(phenolate) Co(II) fragment as identified in the molecular structure of **3.1**, **Figure 3.1**. The chloride end-capped polymer is again likely to result from chain transfer mechanisms involving two chloride-initiated polymer chains and the large variety of polymer end groups suggests extensive chain transfer processes are occurring. This is supported further by the presence of dihydroxyl end-capped polycarbonate chains (giving polycarbonate diols) which is likely due to chain transfer by adventitious water.³²

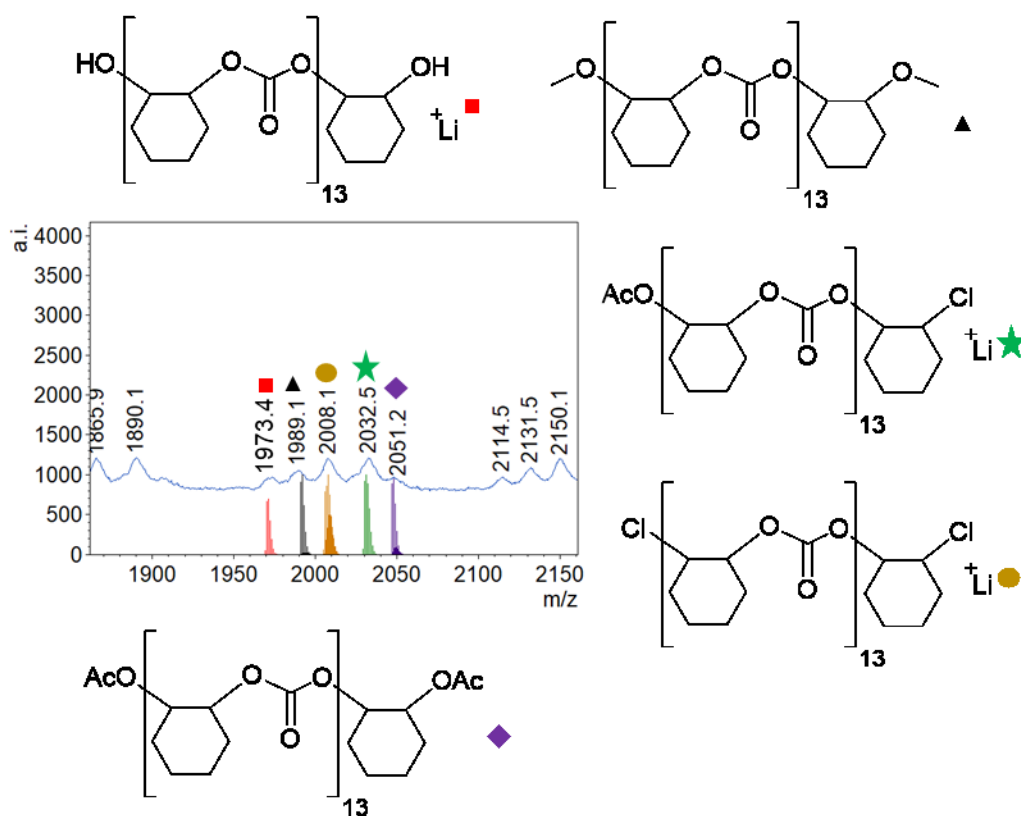


Figure 3.4: Magnified MALDI-TOF mass spectrum (low mass region, m/z 1860 – 2160) of PCHC obtained from Table 3.1, entry 9. Calculated mass fragments (below observed spectrum) and proposed polymer structures shown.

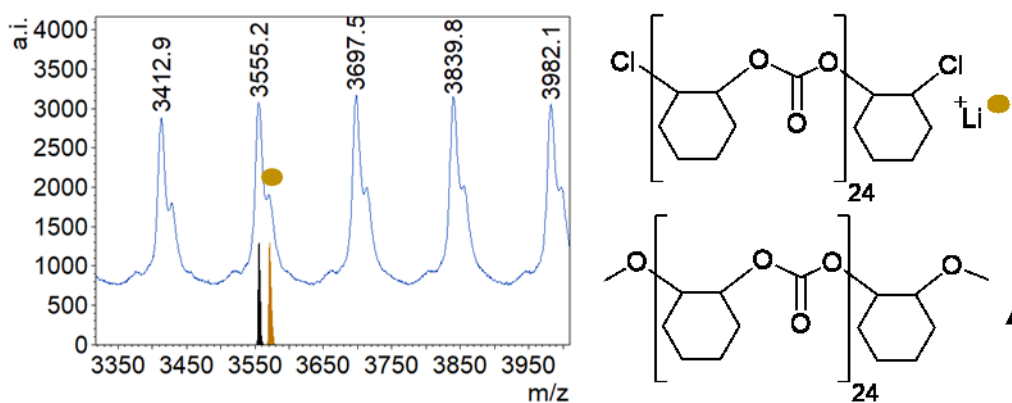


Figure 3.5: Magnified MALDI-TOF mass spectrum (higher mass region, m/z 3310 – 4010) of PCHC obtained from Table 3.1, entry 9. Calculated mass fragments (below observed spectrum) and proposed polymer structures shown.

3.3 Conclusions

The electronic and steric influence of varying the phenolate and *N*-donors in Co(II) amino-bis(phenolate) complexes was investigated in terms of their catalytic activity toward epoxide/ CO_2 coupling reactions. Increasing Lewis acidity at the Co(II) metal center by introducing electron-withdrawing chlorine substituents in **3.1** afforded selectivity towards polycarbonate synthesis from CHO/ CO_2 with moderate conversions, selectivity and high CO_2 incorporation. It is worth noting that compound **3.1** also afforded the production of the unusual *cis* isomer of cyclohexene carbonate at elevated temperatures. Structural characterization of **3.1** showed the presence of Co·KOAc adducts in the solid state. The acetate ions served as minor initiators during the polymerization reaction as shown by end group analysis using MALDI-TOF MS.

3.4 Experimental

3.4.1 General experimental considerations

Unless otherwise stated, all reagents were used as received. Inert atmosphere syntheses were conducted under N₂ using Schlenk techniques or using an MBraun DP glove box. Dry toluene and dichloromethane were acquired from an MBraun Solvent Purification System. NMR spectra were recorded using Bruker AVANCE III 300 MHz or Bruker AVANCE 500 MHz spectrometers with chemical shifts in ppm relative to TMS or residual solvent signal as an internal standard. NMR solvents were purchased from Cambridge Isotope Laboratories and used without further purification. Mass spectrometry was performed using an Applied Biosystems 4800 MALDI TOF/TOF Analyzer equipped with a reflectron, delayed ion extraction and high-performance nitrogen laser (200 Hz operating at 355 nm). Anthracene was used as a matrix for analysis of **2.1**, **2.2** and **3.1** and dihydrobenzoic acid (DHBA) was used as a matrix for polymer analysis. Anthracene and complex were dissolved in dichloromethane at a ratio of 2:1 and overall concentration of 6 mg mL⁻¹. DHBA and polymer were combined at a ratio of 4:1 in THF at an overall concentration of 12 mg mL⁻¹. Aliquots of 0.5 – 1 µL of these samples were spotted and solvent allowed to evaporate. MALDI-TOF MS data were processed and images prepared using mMass software (www.mmass.org).

Elemental analyses were performed at Guelph Chemical Laboratories in Guelph, Ontario, Canada or at the Centre for Environmental Analysis and Remediation at Saint Mary's University, Halifax, Nova Scotia, Canada. The X-ray structure of **3.1** was acquired using a Bruker diffractometer equipped with an APEXII CCD detector.

Copolymerization reactions with in situ monitoring were performed using a 100 mL Parr 4560 reactor equipped with a Mettler Toledo SiComp ATR Sentinel sensor connected to a ReactIR 15 base unit through a silver-halide Fiber-to-Sentinel conduit. Profiles for absorbance height at 1750 cm^{-1} (for polycarbonate) and 1804 cm^{-1} (cyclic carbonate) were measured every 60 s. Gel permeation chromatography (GPC) for polymer molecular weight and dispersity determination was performed using an Agilent 1260 Infinity HPLC coupled with Wyatt Technologies multi-angle light scattering, viscometry and refractive index detectors. The proligands **H₂L1** – **H₂L3**^{56,81} and compounds **2.1** and **2.2**⁵⁷ were prepared as previously reported.

3.4.2 Synthesis of **3.1**

H₂L3 (1.00 g, 2.18 mmol) was dissolved in toluene (10.0 mL) under an N₂ atmosphere. Co(OAc)₂·4H₂O (0.543 g, 2.18 mmol) was dissolved in degassed methanol (20.0 mL) in a separate flask. Potassium hydroxide (0.244 g, 4.36 mmol) was added under N₂ to the ligand solution followed by the methanolic Co(OAc)₂·4H₂O solution. The mixture was stirred under N₂ for 24 h resulting in a pink precipitate, which was collected, washed and dried *in vacuo* to give 271 mg of pink product. The filtrate was collected, the solvent evaporated and more of the pink product extracted into acetone resulting in a white precipitate, which was removed by filtration and removal of volatiles from the filtrate gave an additional 719 mg of pink solid. Total yield 990 mg (74%). Single crystals suitable for X-ray diffraction were obtained from a solution of **3.1** in acetone and toluene and cooling to $-20\text{ }^{\circ}\text{C}$ over 4 d. MALDI-TOF MS positive mode, anthracene: m/z (%) = 514.9141 (39) [M]⁺; 612.9060 (100) [M+KOAc]⁺. *Anal.* Calc. for

$\text{C}_{20}\text{H}_{14}\text{Cl}_4\text{CoN}_2\text{O}_2 \cdot 1.65(\text{KOAc}) \cdot \text{CH}_3\text{OH}$ C, 41.16; H, 3.26; N, 3.95. Found: C, 41.11; H, 3.29; N, 3.87%. Note: Elemental analysis data represents the pink solid and not recrystallized material therefore, the methanol observed in elemental analysis may have been removed when SQUEEZE was applied to excess electron density during crystal data analysis or methanol may not have co-crystallized with **3.1**.

3.4.3 Representative procedure for CO_2 /epoxide copolymerization

Cyclohexene oxide (4.70 g, 47.9 mmol), DMAP (29.2 mg, 0.240 mmol) and **3.1** (0.123 g, 0.240 mmol) were mixed in a vial to give a purple solution. This mixture was injected via syringe into a pressure vessel, (pre-dried under vacuum at 80 °C overnight) and pressurized to 40 bar CO_2 (99.998%) and stirred at 80 °C for 72 h. Upon cooling to room temperature, the reactor was vented into the fume hood and opened. A brown solid was obtained, and a sample was taken for characterization and quantification by ^1H NMR spectroscopy.

3.4.4 X-ray crystallography procedure

Crystallography for compound **3.1** was performed by Katherine N. Robertson of the Department of Chemistry, Saint Mary's University, Halifax, Nova Scotia B3H 3C3, Canada. Single crystals of $\text{C}_{66}\text{H}_{53}\text{Cl}_{12}\text{Co}_3\text{K}_3\text{N}_6\text{O}_{13}$, **3.1**, were crystallized from acetone and toluene. A suitable crystal was selected and placed in Paratone N oil, mounted in a nylon loop and data collected on a Bruker diffractometer equipped with an APEXII CCD detector. The crystal was kept at 125(2) K during data collection. Using Olex2,⁸² the structure was solved with the SIR2004⁸³ structure solution program using Direct Methods

and refined with the XH⁸⁴ refinement package using CGLS minimisation. SQUEEZE was applied to excess electron density during crystal data analysis.

3.5 References

1. M. Lancaster, *Green chemistry: an introductory text*, Cambridge: Royal Society of Chemistry, Cambridge, Eng., 2002.
2. P. Tans and R. Keeling, Global Trends in Atmospheric Carbon Dioxide, <https://www.esrl.noaa.gov/gmd/ccgg/trends/>, (accessed March, 2018).
3. D. J. Darensbourg, *Chem. Rev.*, 2007, **107**, 2388-2410.
4. M. Aresta, A. Dibenedetto and A. Angelini, *Chem. Rev.*, 2014, **114**, 1709-1742.
5. M. Taherimehr and P. P. Pescarmona, *J. Appl. Polym. Sci.*, 2014, **131**, 41141-41157.
6. M. Aresta, A. Dibenedetto and E. Quaranta, *J. Catal.*, 2016, **343**, 2-45.
7. D. Y. Jang, H. G. Jang, G. R. Kim and G.-J. Kim, *Catal. Today*, 2012, **185**, 306-312.
8. F. M. Al-Qaisi, M. Nieger, M. L. Kemell and T. J. Repo, *Chemistry Select*, 2016, **1**, 545-548.
9. Y. Liu, J.-Z. Guo, H.-W. Lu, H.-B. Wang and X.-B. Lu, *Macromolecules*, 2018, **51**, 771-778.
10. B. Schöffner, F. Schöffner, S. P. Verevkin and A. Börner, *Chem. Rev.*, 2010, **110**, 4554-4581.
11. Y. Wang and D. J. Darensbourg, *Coord. Chem. Rev.*, 2018, **372**, 85-100.
12. S. Klaus, M. W. Lehenmeier, C. E. Anderson and B. Rieger, *Coord. Chem. Rev.*, 2011, **255**, 1460-1479.

13. H. Zhang, X. Lin, S. Chin and M. W. Grinstaff, *J. Am. Chem. Soc.*, 2015, **137**, 12660-12666.
14. G.-P. Wu, S.-H. Wei, W.-M. Ren, X.-B. Lu, T.-Q. Xu and D. J. Darensbourg, *J. Am. Chem. Soc.*, 2011, **133**, 15191-15199.
15. X. Jiang, F. Gou, F. Chen and H. Jing, *Green Chem.*, 2016, **18**, 3567-3576.
16. W.-M. Ren, X. Zhang, Y. Liu, J.-F. Li, H. Wang and X.-B. Lu, *Macromolecules*, 2010, **43**, 1396-1402.
17. D. J. Darensbourg and S. J. Wilson, *Macromolecules*, 2013, **46**, 5929-5934.
18. Z. Qin, C. M. Thomas, S. Lee and G. W. Coates, *Angew. Chem. Int. Ed.*, 2003, **42**, 5484-5487.
19. M. R. Kember, F. Jutz, A. Buchard, A. J. P. White and C. K. Williams, *Chem. Sci.*, 2012, **3**, 1245-1255.
20. K. Nakano, S. Hashimoto and K. Nozaki, *Chem. Sci.*, 2010, **1**, 369-373.
21. Y. Liu, W.-M. Ren, W.-P. Zhang, R.-R. Zhao and X.-B. Lu, *Nat. Commun.*, 2015, **6**, 8594.
22. M. Winkler, C. Romain, M. A. R. Meier and C. K. Williams, *Green Chem.*, 2015, **17**, 300-306.
23. D. J. Darensbourg and Y. Wang, *Polym. Chem.*, 2015, **6**, 1768-1776.
24. R. Wei-Min, L. Ye, W. Guang-Peng, L. Jie and L. Xiao-Bing, *J. Polym. Sci., Part A: Polym. Chem.*, 2011, **49**, 4894-4901.
25. C. E. Anderson, S. I. Vagin, W. Xia, H. Jin and B. Rieger, *Macromolecules*, 2012, **45**, 6840-6849.

26. H. Masahiro, N. Koji, O. Shin-ichi and N. Kyoko, *Chem. Eur. J.*, 2016, **22**, 13677-13681.
27. H. Zhang, B. Liu, H. Ding, J. Chen and Z. Duan, *Polymer*, 2017, **129**, 5-11.
28. F. Zhou, S.-L. Xie, X.-T. Gao, R. Zhang, C.-H. Wang, G.-Q. Yin and J. Zhou, *Green Chem.*, 2017, **19**, 3908-3915.
29. C. Chatterjee and M. H. Chisholm, *Chem. Rec.*, 2013, **13**, 549-560.
30. L. Peña Carrodegua, J. González-Fabra, F. Castro-Gómez, C. Bo and A. W. Kleij, *Chem. Eur. J.*, 2015, **21**, 6115-6122.
31. C. J. Whiteoak, N. Kielland, V. Laserna, E. C. Escudero-Adán, E. Martin and A. W. Kleij, *J. Am. Chem. Soc.*, 2013, **135**, 1228-1231.
32. K. Ni and C. M. Kozak, *Inorg. Chem.*, 2018, **57**, 3097-3106.
33. K. Devaine-Pressing, L. N. Dawe and C. M. Kozak, *Polym. Chem.*, 2015, **6**, 6305-6315.
34. B. Han, L. Zhang, S. J. Kyran, B. Liu, Z. Duan and D. J. Darensbourg, *J. Polym. Sci., Part A: Polym. Chem.*, 2016, **54**, 1938-1944.
35. Y. Liu, H. Zhou, J.-Z. Guo, W.-M. Ren and X.-B. Lu, *Angew. Chem. Int. Ed.*, 2017, **56**, 4862-4866.
36. J. A. Castro-Osma, K. J. Lamb and M. North, *ACS Catal.*, 2016, **6**, 5012-5025.
37. D. J. Darensbourg, W.-C. Chung, A. D. Yeung and M. Luna, *Macromolecules*, 2015, **48**, 1679-1687.
38. D. Alhashmialameer, J. Collins, K. Hattenhauer and F. M. Kerton, *Catal. Sci. Technol.*, 2016, **6**, 5364-5373.

39. A. Buonerba, A. De Nisi, A. Grassi, S. Milione, C. Capacchione, S. Vagin and B. Rieger, *Catal. Sci. Technol.*, 2015, **5**, 118-123.
40. A. Buchard, M. Kember, K. Sandeman and C. K. Williams, *Chem. Commun.*, 2011, **47**, 212-214.
41. K. Nakano, K. Kobayashi, T. Ohkawara, H. Imoto and K. Nozaki, *J. Am. Chem. Soc.*, 2013, **135**, 8456-8459.
42. M. Taherimehr, S. M. Al-Amsyar, C. J. Whiteoak, A. W. Kleij and P. P. Pescarmona, *Green Chem.*, 2013, **15**, 3083-3090.
43. M. R. Kember, A. J. P. White and C. K. Williams, *Macromolecules*, 2010, **43**, 2291-2298.
44. E. K. Noh, S. J. Na, S. S. S-W. Kim and B. Y. Lee, *J. Am. Chem. Soc.*, 2007, **129**, 8082-8083.
45. W.-M. Ren, M.-W. Liang, Y.-C. Xu and X.-B. Lu, *Polym. Chem.*, 2013, **4**, 4425-4433.
46. M. R. Kember, A. Buchard and C. K. Williams, *Chem. Commun.*, 2011, **47**, 141-163.
47. X. Zhuang, K. Oyaizu, Y. Niu, K. Koshika, X. Chen and H. Nishide, *Macromol. Chem. Phys.*, 2010, **211**, 669-676.
48. D. J. Darensbourg, W.-C. Chung and S. J. Wilson, *ACS Catal.*, 2013, **3**, 3050-3057.
49. J. Y. Jeon, J. J. Lee, J. K. Varghese, S. J. Na, S. Sujith, M. J. Go, J. Lee, M.-A. Ok and B. Y. Lee, *Dalton Trans.*, 2013, **42**, 9245-9254.
50. K. Ni, V. Paniez-Grave and C. M. Kozak, *Organometallics*, 2018, **37**, 2507-2518.

51. K. Devaine-Pressing and C. M. Kozak, *ChemSusChem*, 2017, **10**, 1266-1273.
52. C. M. Kozak, A. M. Woods, C. S. Bottaro, K. Devaine-Pressing and K. Ni, *Faraday Discuss.*, 2015, **183**, 31-46.
53. H. Chen, L. N. Dawe and C. M. Kozak, *Catal. Sci. Technol.*, 2014, **4**, 1547-1555.
54. R. K. Dean, K. Devaine-Pressing, L. N. Dawe and C. M. Kozak, *Dalton Trans.*, 2013, **42**, 9233-9244.
55. R. K. Dean, L. N. Dawe and C. M. Kozak, *Inorg. Chem.*, 2012, **51**, 9095-9103.
56. L. N. Saunders, N. Ikpo, C. F. Petten, U. K. Das, L. N. Dawe, C. M. Kozak and F. M. Kerton, *Catal. Commun.*, 2012, **18**, 165-167.
57. L. N. Saunders, M. E. Pratt, S. E. Hann, L. N. Dawe, A. Decken, F. M. Kerton and C. M. Kozak, *Polyhedron*, 2012, **46**, 53-65.
58. U. K. Das, J. Bobak, C. Fowler, S. E. Hann, C. F. Petten, L. N. Dawe, A. Decken, F. M. Kerton and C. M. Kozak, *Dalton Trans.*, 2010, **39**, 5462-5477.
59. F. M. Kerton, C. M. Kozak, K. Lüttgen, C. E. Willans, R. J. Webster and A. C. Whitwood, *Inorg. Chim. Acta*, 2006, **359**, 2819-2825.
60. M. Reiter, P. T. Altenbuchner, S. Kissling, E. Herdtweck and B. Rieger, *Eur. J. Inorg. Chem.*, 2015, **2015**, 1766-1774.
61. J. Zhang, B. Wang, L. Wang, J. Sun, Y. Zhang, Z. Cao and Z. Wu, *Appl. Organomet. Chem.*, 2018, **32**, e4077.
62. L. E. N. Allan, J. P. MacDonald, G. S. Nichol and M. P. Shaver, *Macromolecules*, 2014, **47**, 1249-1257.
63. I. Saberikia, E. Safaei, M. H. Kowsari, Y.-I. Lee, P. Cotic, G. Bruno and H. A. Rudbari, *J. Mol. Struct.*, 2012, **1029**, 60-67.

64. S. L. Hancock, M. F. Mahon and M. D. Jones, *Dalton Trans.*, 2013, **42**, 9279-9285.
65. H. Du, A. H. Velders, P. J. Dijkstra, J. Sun, Z. Zhong, X. Chen and J. Feijen, *Chem. Eur. J.*, 2009, **15**, 9836-9845.
66. C. Martín, A. Pizzolante, E. C. Escudero-Adán and A. W. Kleij, *Eur. J. Inorg. Chem.*, **2018**, 1921-1927.
67. L. Stelzig, B. Chansou, J.-P. Tuchagues, L. Stelzig and A. Steiner, *Chem. Commun.*, 1998, 771-772.
68. D. J. Darensbourg, P. Bottarelli and J. R. Andreatta, *Macromolecules*, 2007, **40**, 7727-7729.
69. D. J. Darensbourg, J. C. Yarbrough, C. Ortiz and C. C. Fang, *J. Am. Chem. Soc.*, 2003, **125**, 7586-7591.
70. J. Liu, W.-M. Ren, Y. Liu and X.-B. Lu, *Macromolecules*, 2013, **46**, 1343-1349.
71. W. K. Offermans, C. Bizzarri, W. Leitner and T. E. Müller, *Beilstein J. Org. Chem.*, 2015, **11**, 1340-1351.
72. D. Darensbourg, *Personal Adventures in the Synthesis of Copolymers from Carbon Dioxide and Cyclic Ethers*, Elsevier, 2014.
73. X.-B. Lu, W.-M. Ren and G.-P. Wu, *Acc. Chem. Res.*, 2012, **45**, 1721-1735.
74. S. J. Poland and D. J. Darensbourg, *Green Chem.*, 2017, **19**, 4990-5011.
75. D. J. Darensbourg and A. D. Yeung, *Polym. Chem.*, 2015, **6**, 1103-1117.
76. P. Ramidi, N. Gerasimchuk, Y. Gartia, C. M. Felton and A. Ghosh, *Dalton Trans.*, 2013, **42**, 13151-13160.

77. A. Ghosh, P. Ramidi, S. Pulla, S. Z. Sullivan, S. L. Collom, Y. Gartia, P. Munshi, A. S. Biris, B. C. Noll and B. C. Berry, *Catal. Lett.*, 2010, **137**, 1-7.
78. A. Kilic, S. Akdag, E. Aytar, M. Durgun and M. Ulusoy, *New J. Chem.*, 2016, **40**, 7901-7910.
79. H. G. Sogukomerogullari, E. Aytar, M. Ulusoy, S. Demir, N. Dege, D. S. Richeson and M. Sönmez, *Inorg. Chim. Acta*, 2018, **471**, 290-296.
80. M. Ulusoy, A. Kilic, M. Durgun, Z. Tasci and B. Cetinkaya, *J. Organomet. Chem.*, 2011, **696**, 1372-1379.
81. A. M. Reckling, D. Martin, L. N. Dawe, A. Decken and C. M. Kozak, *J. Organomet. Chem.*, 2011, **696**, 787-794.
82. O. V. Dolomanov, L. J. Bourhis, R. J. Gildea, J. A. K. Howard and H. Puschmann, *J. Appl. Crystallogr.*, 2009, **42**, 339-341.
83. L. J. Bourhis, O. V. Dolomanov, R. J. Gildea, J. A. K. Howard and H. Puschmann, *Acta Crystallogr. Sect. A*, 2015, **71**, 59-75.
84. G. Sheldrick, *Acta Crystallogr. Sect. A*, 2008, **64**, 112-122.

Chapter 4: Chromium Amino-bis(phenolate) Complexes as Catalysts for Ring-Opening Polymerization (ROP) of Cyclohexene Oxide

4.1 Introduction

There exist many metal-based catalyst systems reported in the literature for CO₂/epoxide coupling reactions showing selectivity toward polycarbonate synthesis.¹⁻³ At some points during the propagation stage of the CO₂/epoxide copolymerization process, epoxides can be inserted consecutively thus producing ether linkages. This demonstrates tunability for these catalysts to produce polyethers. Other metal and non-metal-based catalysts however, are strictly selective toward ring-opening polymerization (ROP) of epoxides in the absence of CO₂ thus producing polyethers.^{4,5} Polyethers such as polyethylene glycol (PEG) represent the benchmark in terms of biocompatible polymers for cosmetic, pharmaceutical and medical applications.⁵ PEG and polypropylene glycol (PPG) are among the most mass produced polyethers at several million tons per year due to their demand in a range of applications.^{4,5} The targeted application depends highly on the molecular weight and at lower molecular weights (less than 30 kg mol⁻¹) the designation “glycol” is used, otherwise the polymers are called polyethylene oxide (PEO).⁵ At low molecular weights, PEG and PEO are liquids or low melting solids. This property can be tuned by blending/co-crystallizing different molecular weights of PEG; this is important for formulation of skin creams and ointments.⁵ PPG however, is a flexible, non-crystalline polymer with a low glass transition temperature (T_g), making it suitable for applications such as lubricants, antifoaming agents, softeners and flexible poly(urethane) foams.

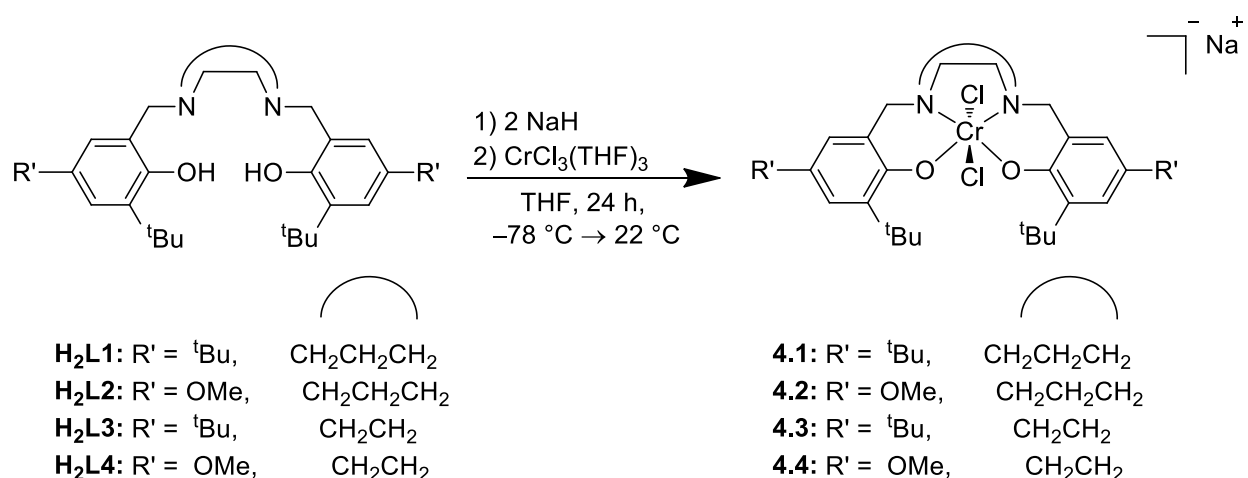
Since first reported in 1859, production of PEG involved the polymerization of ethylene oxide (EO) using an alkali metal hydroxide or zinc chloride.⁶ Polyether from PO (polypropylene oxide) was first reported in 1949 using an iron(III) chloride catalyst for stereoselective ring-opening polymerization of PO which produced amorphous and semi crystalline material, separated using solvent fractionation.⁷ High ring strain (110 – 115 kJ/mol)⁸ present in the three-membered cyclic ethers is one of the driving forces for these ROP reactions. ROP of epoxides (also termed homopolymerization) has been identified to follow three predominant classes of polymerization mechanisms: (a) anionic (base-catalyzed), (b) cationic (acid catalyzed) and (c) metal-mediated (coordination polymerization), where the anionic and coordination polymerization mechanisms are believed to be linked.^{5,7,9} Each mechanism bears different synonyms and this depends on the publication period and author; for example, metal-mediated ROP is also referred to as catalytic ring-opening polymerization (CROP) by Lynd and co-workers.¹⁰ The metal-mediated/coordination ROP mechanism is often employed to achieve higher molecular weight ($>50 \text{ kg mol}^{-1}$) polyethers whereas anionic ROP is suitable for lower molecular weight polyethers (poly-glycols) with controlled chain-end functionality and narrow molecular weight distribution.^{10,11} Moreover, anionic ROP of epoxides suffers from functional group intolerance (substituted epoxides) making it suitable for epoxides such as PO and EO. This chapter focuses on metal-mediated ROP of cyclohexene oxide (CHO).

Among the many metal-based catalyst systems for coordination ring-opening polymerization of epoxides, those containing metals such as Al^{10,12-16} and Zn^{7,17} appear to

be the most established.⁵ Zn-based systems normally exist in the form of alkoxides and alkyl compounds whereas aluminum-based systems exist as complexes bearing ligands such as porphyrins^{13,18} and phenolates^{12,14}. Aluminum systems represent a large part of metal-mediated epoxide ROP reactions in the literature. Throughout the development of epoxide ROP using Al-porphyrin complexes, Inoue reported both living¹⁸ and “immortal”¹⁹ polymerization processes. The living system denoted as TPP-AlCl (where TPP = 5,10,15,20-tetraphenylporphine and various analogs) showed polymerization of PO which took up to 6 days for 100% conversion and gave a molecular weights up to 10.2 kg mol^{-1} and narrow dispersities. The observed molecular weights were in good agreement with the calculated ones. The immortal system was more active producing PPO at 100% conversion in 48 h with molecular weights up to 10 kg mol^{-1} and narrow dispersities. There exist transition metal-based catalysts, namely Ti²⁰ and Co,²¹ but based on a literature search, detailed reports of highly active Cr(III)-containing complexes are rarely reported for ROP of epoxides. Chen and co-workers reported a study which showed ROP of PO using Cr(III)-salen mono- and dinuclear complexes. A dinuclear cationic ROP mechanism was proposed based on ESI-MS studies where various Cr(III)-salen/PO oligomer adducts were observed. The dinuclear catalyst, [Cr(III)Cl-salen]₂, showed conversions up to 62% (TON of 1005) for reactions at 80 °C/16 h, when reactions were performed neat and cocatalyzed by DMAP, whereas the mononuclear Cr(III)Cl-salen catalyst was slightly slower with a conversion of 46% (TON of 690).²² Chen, Chisholm and co-workers also showed ROP of PO using a CrCl-TPP catalyst system which produced PPO at 76% conversion and molecular weight of 61 kg mol^{-1} and \bar{D} of 1.53 over 120 h.²³ A later report by the Chisholm group showed the use of CrCl-TPP

and CrCl-OEP (where OEP = octaethylporphyrin) for ROP of PO when co-catalyzed by PPNC1, with activity up to 2000 TO h⁻¹ and molecular weights of up to 40 kg mol⁻¹.²⁴

In this Chapter, the synthesis and characterization of a series of Cr(III) amino-bis(phenolate) complexes is discussed (**Scheme 4.1**). Also presented are their structures, which afford high activity and selectivity toward ROP of cyclohexene oxide without the use of a co-catalyst, and their reaction kinetics.



Scheme 4.1: Synthetic route to Cr(III) amino-bis(phenolate) complexes **4.1** – **4.4**.

4.2 Results and discussion

4.2.1 Synthesis and characterization of Cr(III) complexes

Cr(III) amino-bis(phenolate) complex **4.1** was afforded via reaction of the proligand with sodium hydride in THF at -78 °C, followed by reaction with CrCl₃(THF)₃ in THF at -78 °C to produce a reddish-brown solid in a yield of 99%. Preparation of Cr(III) complexes via this salt metathesis route is common.²⁵⁻²⁹ Characterization of

paramagnetic **4.1** was performed by MALDI-TOF MS, elemental analysis and single crystal X-ray diffraction. A MALDI-TOF mass spectrum of **4.1** in positive reflectron mode produced m/z 586.4 corresponding to $[\text{CrL1}]^+$ and another peak at m/z 621.4 corresponding to $[\text{CrClL1}]^+$ (**Figure 4.1**). In negative reflectron mode, the MALDI-TOF mass spectrum showed m/z 621.3 corresponding to $[\text{CrClL1}]^-$ and a peak at m/z 656.3 corresponding to $[\text{CrCl}_2\text{L1}]^-$ (see Appendix B, Figure B-15). The calculated isotopic distribution patterns are in good agreement with the experimental patterns, for spectra acquired by both positive and negative reflectron mode. Complex fragments $[\text{CrL}_n]^+$, $[\text{CrClL}_n]^+$ and $[\text{CrCl}_2\text{L}]^-$ (where L_n is an amino-bis(phenolate) ligand) have been previously observed in the Kozak group.^{25,30}

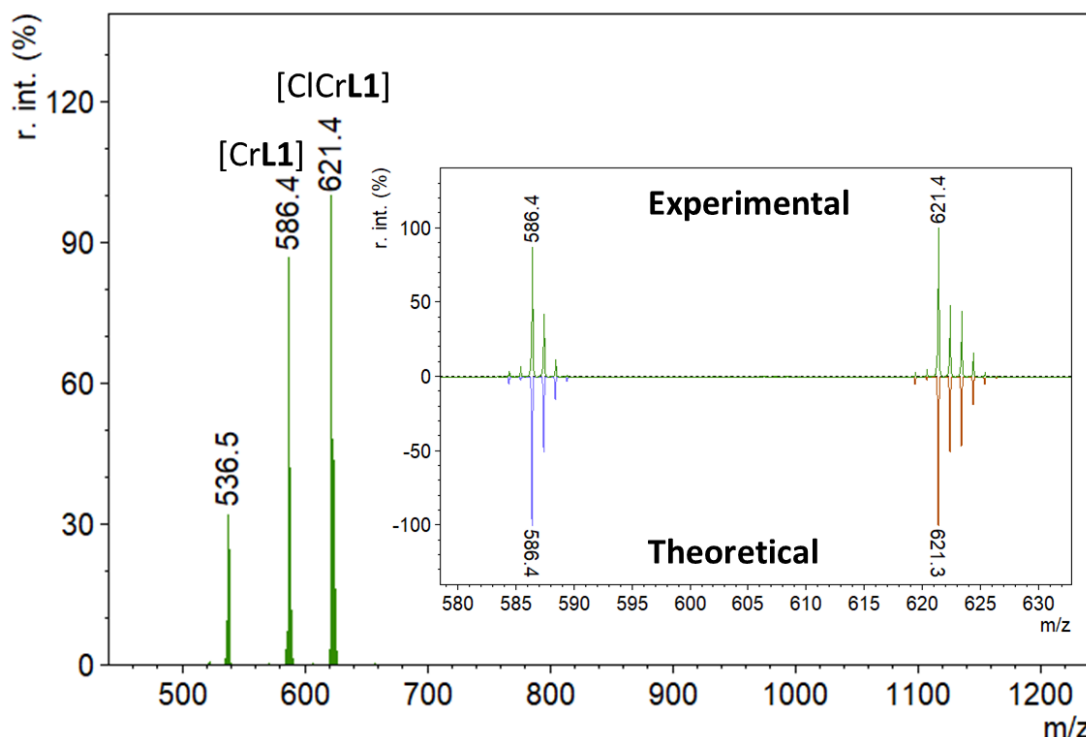


Figure 4.1: MALDI-TOF mass spectrum of **4.1** in positive reflectron mode showing a comparison between experimental and calculated isotopic patterns.

Based on the observed $[\text{CrCl}_2\text{L}_n]^-$ anion in MALDI-TOF MS, **4.1** was theorized to be a chromium “ate” or ionic complex. Furthermore, initial calculation of reaction yield for **4.1** was >100%, which suggested the presence of impurities, therefore, adjustment to the molecular weight as 680.5 g/mol (corresponding to $\{\text{Na}^+[\text{CrCl}_2\text{L1}]^-\}$) produced a yield of 99%. Elemental analysis of **4.1** was consistent with a chemical composition of $(\text{Na}^+[\text{CrCl}_2\text{L1}]^-) \cdot 1.4(\text{THF}) \cdot 1.5\text{H}_2\text{O}$, which further supports this theory. Complexes of Co(III), Fe(III) and Cr(III) bearing a tetradentate chelating ligand and two anionic axial ligands (Cl^- , Br^- or OAc^-) thus producing an ionic complex (with a tetraalkylammonium counterion) have been previously reported.³¹⁻³³ Complex **4.1** is also believed to undergo an equilibrium in the presence of coordinating species such as solvent (THF) or DMAP. When dissolved in toluene (which is non-coordinating), the complex exhibits an orange-brown color (corresponding to **4.1**) whereas in THF, a green color is observed (**4.1'**), **Figure 4.2**. This suggests that coordination of a THF molecule potentially displaces a chloride ligand, resulting in the formation of a neutral complex (**4.1'**) and NaCl.

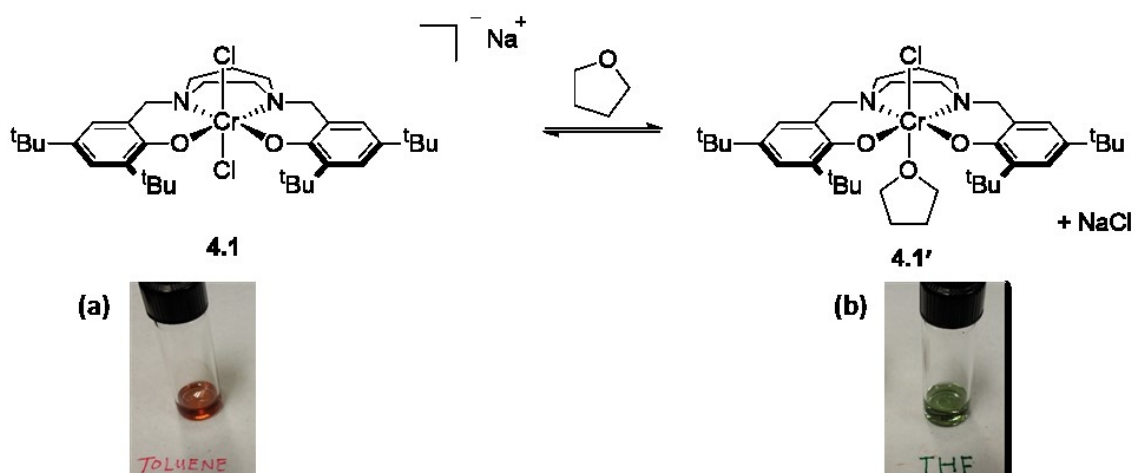


Figure 4.2: Proposed equilibrium for **4.1**. (a) orange-brown color shown in toluene which is most likely the ionic complex and (b) a green color shown in THF for the neutral complex.

When a stronger coordinating species was used (DMAP), the evolution of a white crystalline solid (proposed to be NaCl) was observed after cooling to $-20\text{ }^{\circ}\text{C}$, with dichloromethane as the solvent. Mass spectra were obtained in positive reflectron mode for **4.1** with various amounts of DMAP (DMAP to Cr(III) ratios of 1:1, 1:2 and 1:4) where a series of complex fragments were observed (for 1:4 ratio, see Appendix B, Figure B-16). Masses of m/z 536.4, 586.3, 621.3 and 708.4 correspond to $[\text{H}_2\text{L1}]^+$ (**F1**), $[\text{CrL1}]^+$ (**F2**), $[\text{CrClL1}]^+$ (**F3**) and $[\text{Cr(DMAP)L1}]^+$ (**F4**) respectively (**Figure 4.3**). Surprisingly, a $[\text{CrCl(DMAP)L1}]^+$ adduct was not observed in either positive or negative reflectron mode. Negative reflectron mode however, showed a species at m/z 803.4 (see Appendix B, Figure B-27) corresponding to $\{[\text{CrCl(DMAP)L1}](\text{NaCl})\}^-$ (**F5**). It is worth noting the ratio of DMAP to Cr only influenced the relative abundances of **F4**, which increased and **F3**, which decreased.

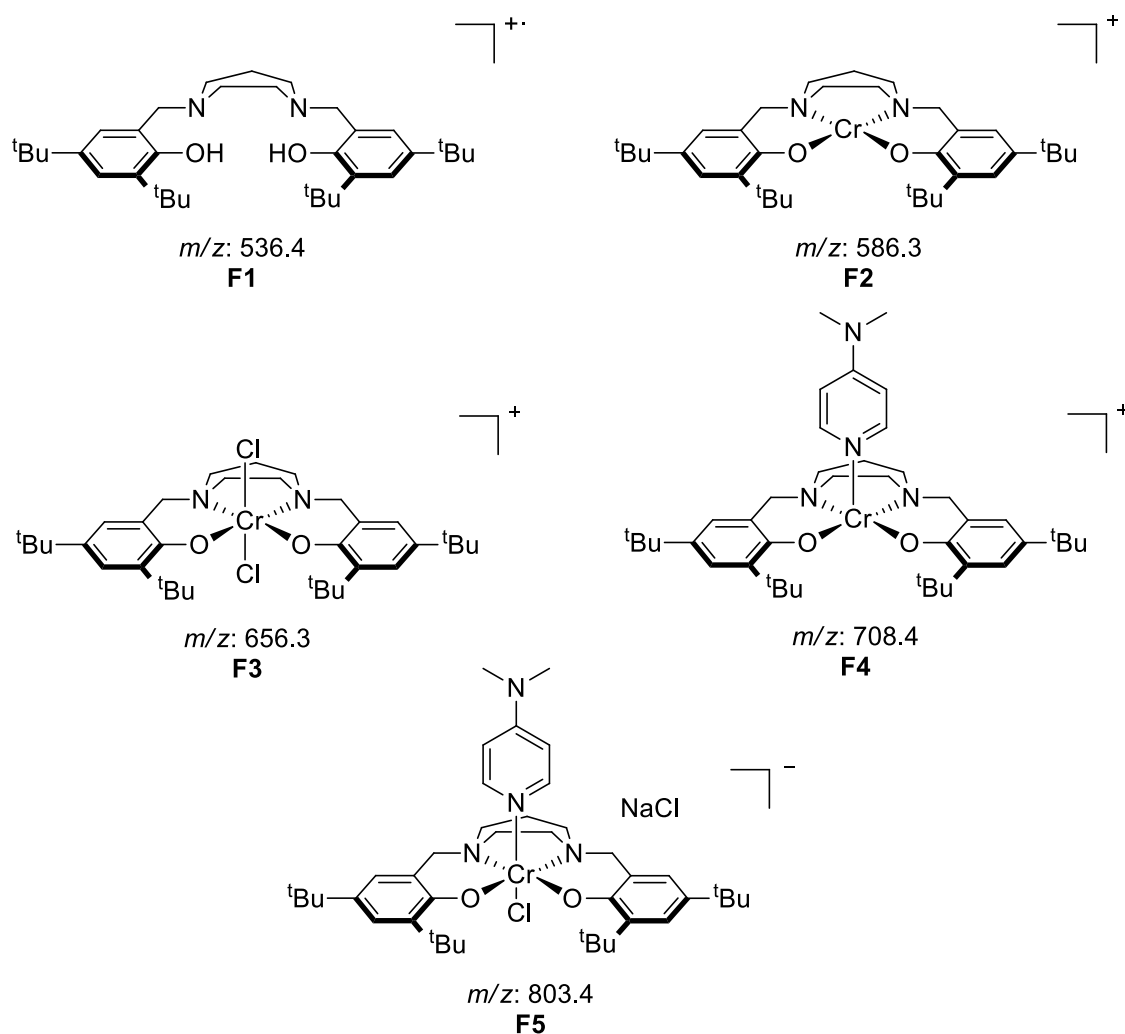


Figure 4.3: Observed fragments of **4.1** and DMAP using MALDI-TOF MS in positive reflectron mode and negative mode (**F5**).

Single crystals suitable for X-ray diffraction of **4.1** were acquired via slow evaporation of the complex dissolved in dichloromethane and hexamethyldisiloxane (HMDSO) at 22 °C in an N₂-containing glove box. The related molecular structure **4.1''** and selected bond lengths and angles are shown in **Figure 4.4**, and additional structural information is reported in Appendix C. It is interesting to note that the X-ray structure

shows that one of the phenolate O-donors is protonated thus formulated as $\{\text{CrCl}_2\text{HL1}\}$, and undergoes intermolecular hydrogen-bonding with an axial chloride and vice versa. That is, complex molecules are paired by two H---Cl hydrogen bonds. Furthermore, Cr(1)–O(1) and Cr(1)–O(2) bond distances of 1.8979(18) and 2.0946(17) Å respectively, show unsymmetrical O-donor bond distances, where the Cr(1)–O(2) bond may be lengthened due to intermolecular hydrogen bonding⁴² or more likely because it is a coordinate covalent bond from a neutral O-donor rather than an anionic donor such as O(1). This data shows a slight inconsistency with the proposed structure of **4.1**, $\{\text{CrCl}_2\text{L1}\}^+\text{Na}^+$, where the Cr(III) complex no longer has a charge separated cation (Na^+) due to the protonated neutral O-donor. This is likely due to the presence of a protic species such as adventitious water, protonating a phenolate oxygen during the crystallization process. Cr(III) complexes with neutral phenol donors,^{43,44} and also with one phenol donor (and anionic phenolate donors) have been reported previously.⁴²

The structure exhibits a distorted octahedral geometry around the Cr(III) metal center where the [ONNO] ligand chelates in a *trans*-meridional fashion and occupies four coordination sites. There are also two *trans* oriented, axial anionic Cl donors as well. This coordination arrangement is typical for more rigid salen ligands (with imine functionalities having sp^2 N donors) but in **4.1**, the homopiperazine backbone also makes **H₂L1** rigid although it contains more flexible sp^3 N-donors. Darensbourg reported a similar [ONNO] chelating ligand (with sp^3 hybridized N donors) but with a *cis-β*-octahedral coordination pattern instead.^{34,35} Cr(III) “ate” complexes containing a tetradentate ligand and *trans* Cl donors have been reported by the Zevaco group. The

complexes contained an N₄-chelating ligand coordinated to Cr(III)Cl₂, thus affording an “ate” complex with a tetraethylammonium counterion.³² From X-ray structural data of **4.1**, the Cr(1)–Cl(1) and Cr(1)–Cl(2) bond distances of 2.3870(7) and 2.3208(7) Å respectively, are in good agreement with a similar Cr(III) amino-bis(phenolate) structure reported by Darensbourg, (Cr–Cl distances of 2.396 and 2.323 Å),³⁶ and other reported Cr(III) complexes with *trans*-axial chloride ligands.^{37–39} Other examples of Cr(III) complexes with *trans*-oriented, axial anionic donors such as azide (N₃)⁴⁰ and isothiocyanate (NCS)⁴¹ have also been reported.

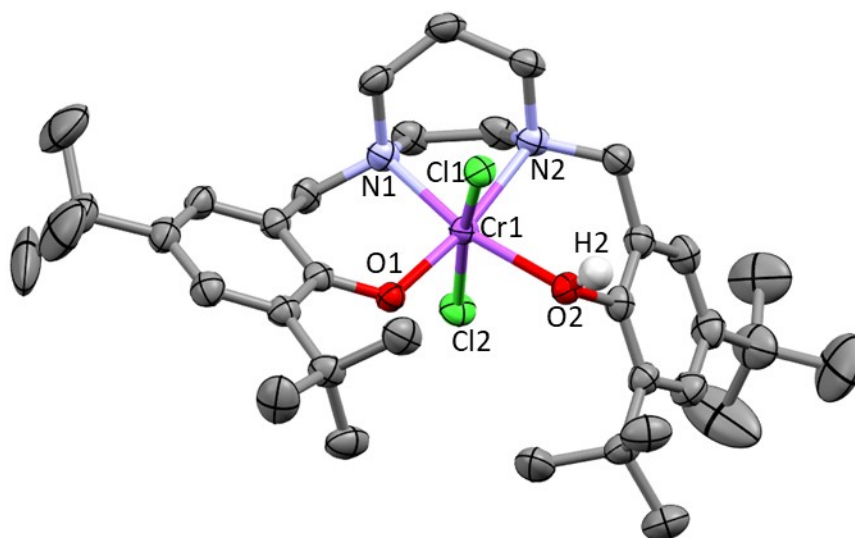


Figure 4.4: Partially labelled molecular structure of compound **4.1''**. Thermal ellipsoids are drawn at 50% probability with hydrogens (except H(2)) and co-crystallized solvent molecule omitted for clarity. Selected bond distances (Å) and angles (deg): Cr(1) – Cl(1), 2.3870(7); Cr(1) – Cl(2), 2.3208(7); Cr(1) – O(1), 1.8979(18); Cr(1) – O(2), 2.0946(17); Cr(1) – N(1), 2.067(2); Cr(1) – N(2), 2.150(2); Cl(2) – Cr(1) – Cl(1), 168.59(3); O(1) – Cr(1) – Cl(1), 86.79(5); O(1) – Cr(1) – Cl(2), 87.78(6); O(1) – Cr(1) – O(2), 99.55(7); O(1) – Cr(1) – N(1), 95.98(8); O(1) – Cr(1) – N(2), 171.16(8); O(2) – Cr(1) – Cl(1), 83.60(5); O(2) – Cr(1) – Cl(2), 87.41(5); O(2) – Cr(1) – N(2), 88.85(8); N(1) – Cr(1) – Cl(1), 110.25(6); N(1) – Cr(1) – Cl(2), 90.29(6); N(1) – Cr(1) – O(2), 164.20(8); N(1) – Cr(1) – N(2), 75.79(8); N(2) – Cr(1) – Cl(1), 91.47(6); N(2) – Cr(1) – Cl(2), 95.38(6); C(7) – O(1) – Cr(1), 125.36(16).

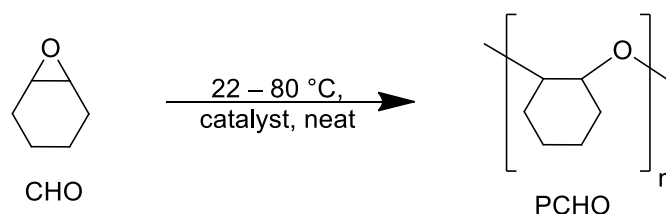
Compound **4.2** was synthesized using a similar procedure to **4.1**, to produce a purple-brown solid at a yield of 56.9%. Characterization of **4.2** by MALDI-TOF MS analysis (in positive reflectron mode) showed peaks at m/z 534.1 and 569.1 corresponding to $[\text{CrL2}]^+$ and $[\text{CrCIL2}]^+$ respectively (see Appendix B, Figure B-17). The calculated isotopic distributions are in good agreement with the observed isotopic distributions. The MALDI-TOF mass spectrum in negative reflectron mode showed m/z 569.2 corresponding to $[\text{CrCIL2}]^-$ and m/z 604.2 corresponding to $[\text{CrCl}_2\text{L2}]^-$. Like **4.1**, the complex fragment corresponding to $[\text{CrCl}_2\text{L2}]^-$ suggests the presence of an “ate” complex. Unfortunately, crystals suitable for X-ray diffraction analysis were not obtained for **4.2**.

Cr complexes **4.3** and **4.4** were synthesized using a slightly modified procedure to **4.1** and **4.2**. Complex **4.3** and **4.4** were synthesized via reaction of H_2L_n with NaH at -78°C to afford ligand deprotonation followed by reaction with $\text{CrCl}_3(\text{THF})_3$ at -78°C to afford red/brown solids in 94% (**4.3**) and 67.4% (**4.4**) yields. The ligand deprotonation step normally involves removal of excess NaH (insoluble in THF) by filter cannula but in this case, the deprotonated ligands ($\text{Na}_2\text{L3}$ and $\text{Na}_2\text{L4}$) precipitated in THF, therefore the reaction with $\text{CrCl}_3(\text{THF})_3$ occurred in the presence of excess NaH. Characterization of **4.3** by MALDI-TOF MS showed peaks at m/z 572.2, 589.2 and 607.2 corresponding to $[\text{CrL3}]^+$, $[\text{CrOHL3}]^+$ and $[\text{CrCIL3}]^+$ respectively in positive reflectron mode and m/z 642.2 corresponding to $[\text{CrCl}_2\text{L3}]^-$ in negative reflectron mode. In positive reflectron mode, Cr complex **4.4** showed m/z 520.1 and 555.1 corresponding to $[\text{CrL4}]^+$ and $[\text{CrCIL4}]^+$ respectively whereas in negative mode m/z 590.1 corresponding to $[\text{CrCl}_2\text{L4}]^-$ was observed (see Appendix B, Figures B-21 and B-22). As mentioned earlier, the exact

structures of **4.1** – **4.4** are ambiguous without structural characterization by single crystal X-ray diffraction but catalytic activity towards CHO ROP reactions strongly suggests that “ate” complexes are quite possible for all four species, which is discussed later.

4.2.2 ROP of cyclohexene oxide using **4.1** – **4.4**

Cr(III) complex **4.1** was employed as a catalyst in most of the ROP reactions discussed in this chapter. ROP reactions were performed neat in CHO, primarily at 22 °C, with higher temperatures used for kinetics experiments, in a N₂-filled glove box to produce poly(cyclohexene oxide), PCHO (**Scheme 4.2**) and the results are summarized in **Table 4.1**.



Scheme 4.2: ROP of CHO producing PCHO.

CHO ROP reactions were terminated by exposing the reaction mixture to air. Aliquots taken immediately after reaction were characterized by ¹H NMR spectroscopy (**Figure 4.5**) and showed a broad multiplet between 3.20 – 3.60 ppm corresponding to methine protons of PCHO. The PCHO methine protons appear to form three main signals (3.37, 3.34 and 3.53 ppm) corresponding to isotactic (*mm*), heterotactic (*mr* and *rm*) and syndiotactic (*rr*) triads respectively, thus making the polymer atactic.^{20,45,46} The ¹³C NMR

spectrum shows weak signals which are consistent with different regions of tacticity in the polymers (see Appendix A, Figure A-16).⁴⁶

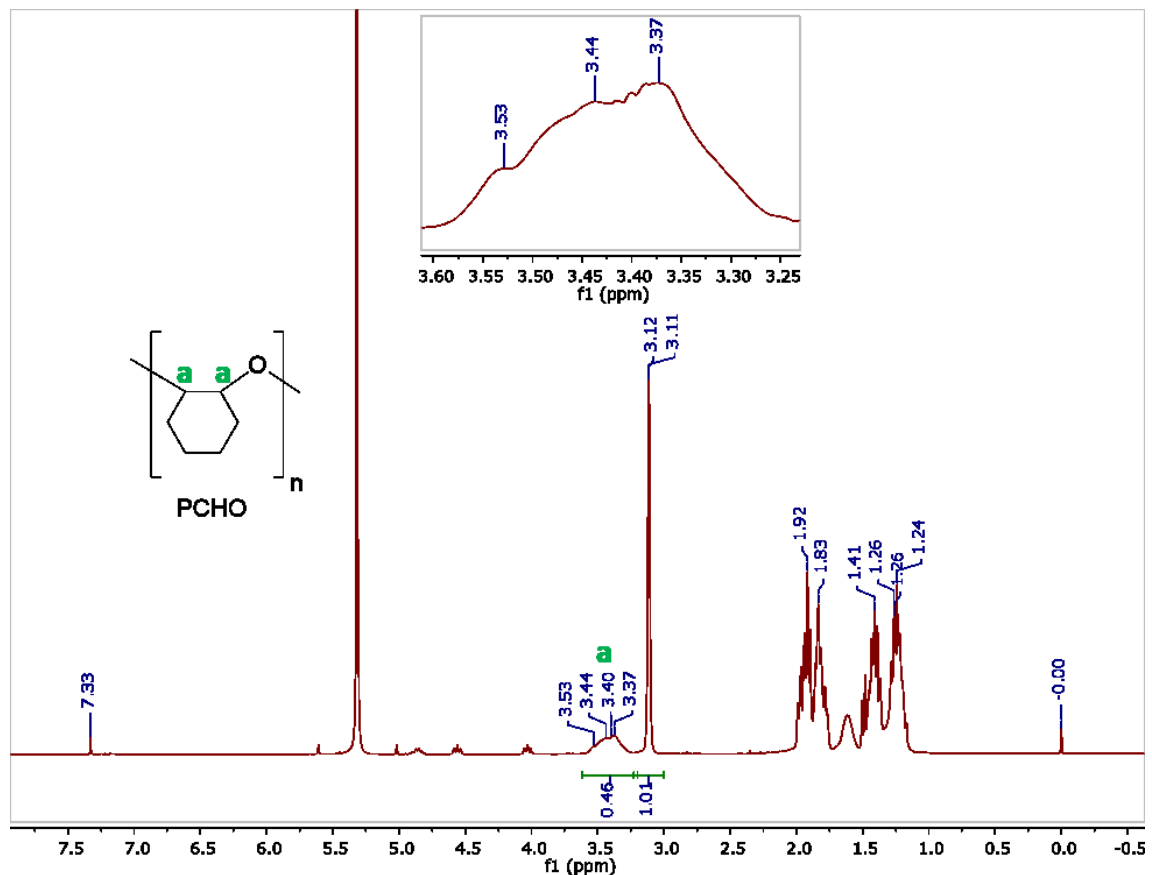


Figure 4.5: Representative crude ^1H NMR spectrum of PCHO in CDCl_3 taken immediately after stopping reaction.

Several reactions were monitored using in situ FTIR spectroscopy, which recorded the formation of PCHO as the only product (**Figure 4.6**). Absorbance height at 1089 cm^{-1} were measured at 60 s intervals thus generating a reaction profile. This absorbance corresponds to the C-O linkage in the polymer backbone.

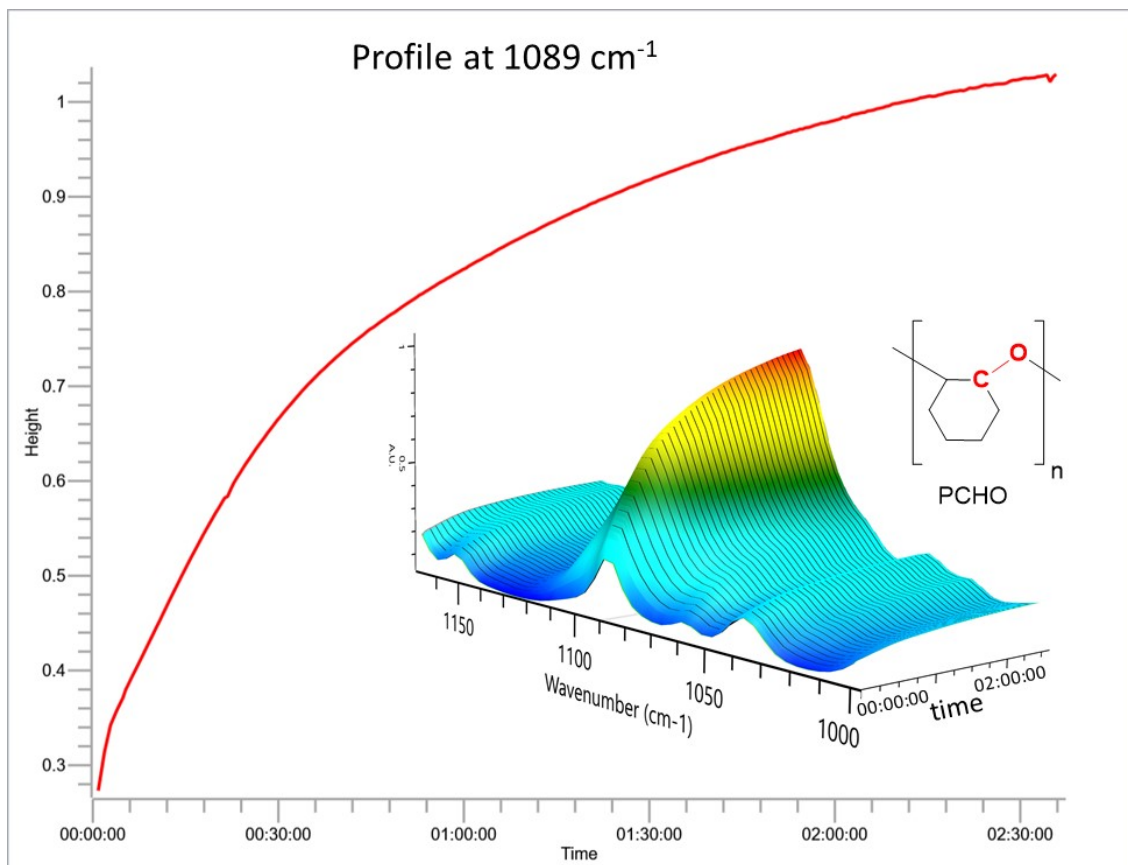


Figure 4.6: Profile for in situ monitored FTIR absorbance at 1089 cm⁻¹ with overlaid three-dimensional stacked plot.

Cr(III) complex **4.1** was first employed for CHO ROP at 22 °C at a catalyst loading of 0.2 mol% (**Table 4.1**, entry 1). The formation of PCHO occurs rapidly and results in a viscous solution therefore ROP reactions were performed until they could no longer be stirred magnetically (34 mins for entry 1). The observed molecular weight (M_w) of 93.2 kg mol⁻¹ is much higher than the expected (38.3 kg mol⁻¹). Higher than expected molecular weights have previously been observed for ROP of CHO.¹² This suggests either the occurrence of chain-transfer mechanisms or the presence of inactive catalyst molecules thus affording a higher monomer to catalyst ratio. To determine the effect of

catalyst loading, ROP reactions were performed at 0.1 and 0.02 mol% (entries 2 and 3), and showed a decrease in polymer yield, but an expected increase in polymer molecular weight. At the lowest catalyst loading however, the polymerization process appears to be most controlled and showed the lowest \bar{D} of 1.2. The effect of temperature was investigated and showed a drastic increase in yield going from 0 °C to 22 °C, however, from 40 °C to 80 °C, reaction yield was approximately the same (**Table 4.1**, entries 5, 6 and 7). Cr complex **4.1** was most active at 60 °C with activity of 644 TO h⁻¹. ROP yield was expected to increase drastically at elevated temperatures due to less inhibition by viscosity but this was not the case here. It can be deduced that **4.1** is highly air sensitive as exposure to air briefly at the beginning of the reaction produced a yield of only 6% after stirring **4.1**/CHO for 38 mins (entry 8). This relates to entry 12 where the DiComp insertion probe was used to monitor the ROP reaction in situ using FTIR spectroscopy (**Figure 4.6**); the modified rubber septum used for insertion of the probe may have allowed minimal exposure to air due to an imperfect seal thus affording a lower than expected yield and a longer reaction time. It is interesting to note that when **4.1** was prepared via a slightly modified method (KH instead of NaH), the reaction was most rapid, showing activity of 1010 TO h⁻¹. Furthermore, when synthesized using an alternative method, (i.e. reacting **H₂L1** with CrCl₂ under N₂ then oxidation of Cr(II) to Cr(III) in air³⁴) no ROP of CHO was observed. This suggests the “ate” complex which bears *trans*-axial chloride ligands may be required for epoxide ring-opening. This catalyst system represents one of the highest reported activity (TOF) for Cr(III)-containing catalyst systems used in epoxide ROP reactions^{22,23,47} where the highest observed was reported by the Coates group (3400 TO h⁻¹), involving ROP of PO to produce isotactic

PPO.⁴⁸ In an effort to avoid the limitation of viscosity and increase reaction yields, polymerizations with **4.1** was attempted using dichloromethane as a reaction medium (entries 10 and 11). Separate reactions performed at 0.1 mol% catalyst loading for 120 min, where 1.00 mL (entry 10) and 0.25 mL (entry 11) of dichloromethane was used, had approximately the same yields of PCHO formation. This was slightly less than the solvent-free equivalent (entry 2) and was expected due to dilution. A decrease in activity with solvent use as a medium has also been reported.¹² Other catalyst systems however, have shown good activity in solvent such as hexane.¹⁴ It is interesting to note that when PO was employed, no conversion to polypropylene oxide (PPO) was observed. Although epoxides are reactive due to 3-membered cyclic ether ring strain, this observation (**Table 4.1**, entry 12) demonstrates the increased reactivity of CHO compared to PO resulting from ring strain in its bicyclic fused ring system.

Of importance is the fact that no ROP of CHO was observed when DMAP was employed as co-catalyst (**Table 4.1**, entry 14). The inactivity of **4.1**/DMAP suggests either the formation of an inactive coordinatively saturated Cr(III) species or displacement of a chloride ligand thus forming solid NaCl (as suggested by the observation of a white precipitate), therefore, epoxide ring-opening is inhibited. Compounds **4.2** – **4.4** were also employed for CHO ROP reactions (entries 15, 16 and 17) where **4.3** was the most active, showing 443 TO h⁻¹, which is nearly half of the observed value for **4.1**. Characterization of produced PCHO by MALDI-TOF mass spectrometry was attempted for end-group analysis but were unsuccessful due to high molecular weights.

Table 4.1: Results from ROP reactions of CHO using complexes **4.1** – **4.4**^a.

Entry	[Cat]:[CHO]	Temperature (°C)	Time (min)	Yield ^b (%)	TOF (h ⁻¹)	<i>M</i> _w (kg mol ⁻¹)	<i>Đ</i>
1	1:500	22	34	54	473	93.2	1.4
2	1:1000	22	60	47	470	208	1.5
3	1:5000	22	114	15	392	193	1.2
4	1:500	0	120	12	NA	42.3	1.5
5	1:500	40	51	61	359	89.4	1.4
6	1:500	60	27	59	644	93.1	1.6
7	1:500	80	44	64	436	78.3	1.5
8 ^c	1:500	22	38	6	ND	ND	ND
9 ^d	1:500	22	19	64	1010	44.4	1.6
10 ^e	1:1000	22	120	41	215	141	1.3
11 ^f	1:1000	22	120	42	185	132	1.4
12 ^g	1:500	22	180	0	NA	NA	NA
13 ^h	1:500	22	180	24	66	65.2	1.4
14 ⁱ	1:500	22	180	0	NA	NA	NA
15	(4.2)1:500	22	45	17.7	118	46.4	1.8
16	(4.3)1:500	22	23	34	443	32.3	2.1
17	(4.4)1:500	22	96	34.5	108	80.8	1.6

^a Unless otherwise stated, reaction conditions were 22 °C, neat CHO, 0.2 mol% catalyst loading. ^b Isolated yield. ^c Reaction was briefly exposed to air before proceeding. ^d **4.1** was prepared with KH instead of NaH. ^e Reaction mixture was dissolved in 1.00 mL or ^f 0.25 mL of dichloromethane. ^g PO was used. ^h In situ FTIR monitoring using DiComp probe. ⁱ DMAP was used as a co-catalyst.

4.2.3 Kinetic studies

Cr complex **4.1** was employed to further investigate the effect of temperature on the homopolymerization process. Initial reaction rates were monitored by following conversion of CHO into PCHO, using ^1H NMR spectroscopy at 5 min intervals for 22 °C and 40 °C and 1 min intervals for 60 °C and 80 °C. Initial reaction rates were faster at 60 °C and 80 °C and a deviation from linearity (in a conversion vs time plot) was observed after 5 mins therefore 1 min intervals were chosen for monitoring reactions at those temperatures. On the other hand, at 22 °C and 40 °C the reaction rate remained linear to at least 30 mins of reaction time. The deviation from linearity is due to a decreased rate of conversion which is from a decrease in CHO concentration as PCHO is produced.

Reaction order in [CHO] was investigated by analysis of kinetic data acquired at 40 °C. Zero, first and second-order plots were generated and are shown in **Figure 4.7**. The R^2 value for the zero-order plot is 0.9971, which decreases slightly in the first order plot but drastically in the second-order plot. Analysis of data at higher temperature shows an enhancement in this trend; that is, the zero-order plot is the most linear. This suggest that the reaction is first-order in [CHO] at lower temperatures but approaches zero-order kinetics at higher temperature. However, a true zero-order reaction would produce a linear conversion vs time plot throughout the reaction, indicating that the rate is independent of CHO concentration, but a deviation from linearity was observed for every temperature therefore kinetics data was analyzed assuming first-order dependence. Furthermore, first-order dependence on [CHO] has previously been shown for ROP of CHO using an Al(III)-piperidyl-phenolato complex¹⁴ and ROP of ϵ -caprolactone.²⁰ The

rate constant was extracted from the slope of the straight line in the first-order plot (Figure 4.7, (B)) and found to be 0.012 min^{-1} when converted (from s^{-1} to min^{-1}). This was slightly higher than that reported for the Al(III)-piperidyl-phenolato system, which was 0.004 min^{-1} , performed at 30°C .

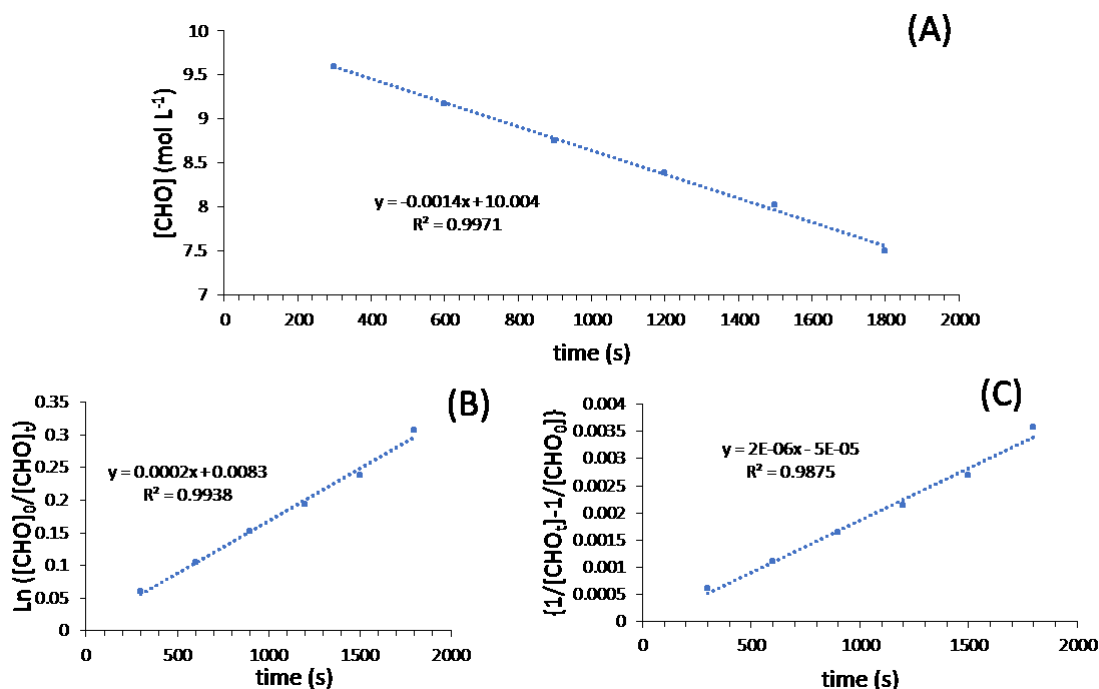


Figure 4.7: Plot of (A) $[\text{CHO}]$ vs time, (B) $\text{Ln}([\text{CHO}]_0/[\text{CHO}]_t)$ vs time and (C) $\{1/[\text{CHO}]_t - 1/[\text{CHO}]_0\}$ vs time for solvent-free ROP of CHO at 40°C .

Plots of CHO conversion vs time showing the linear portion of the initial progress for 22°C , 40°C , 60°C and 80°C are shown in Figure 4.8(A). Using the slope from first-order plots of reaction profiles in Figure 4.8(A), an Arrhenius plot for PCHO formation using 4.1 was generated and is shown in Figure 4.8(B). The activation barrier for PCHO formation was calculated to be 68.6 kJ/mol . Activation data for ROP of epoxides are rarely reported and given the rarity of Cr-based catalyst systems, activation data for

comparison was not found. However, Atwood, McKee and co-workers reported a computational study showing the activation barrier for ring-opening of PO to be 67.3 kJ/mol using an Al-salen catalyst system.⁴⁸ On the other hand, Ishii and co-workers reported an activation barrier of 45.9 kJ/mol for ROP of PO using an Al(III)-[OSSO]-type bis(phenolate) complex by the method of variable temperature ¹H NMR spectroscopy in C₇D₈.¹⁶

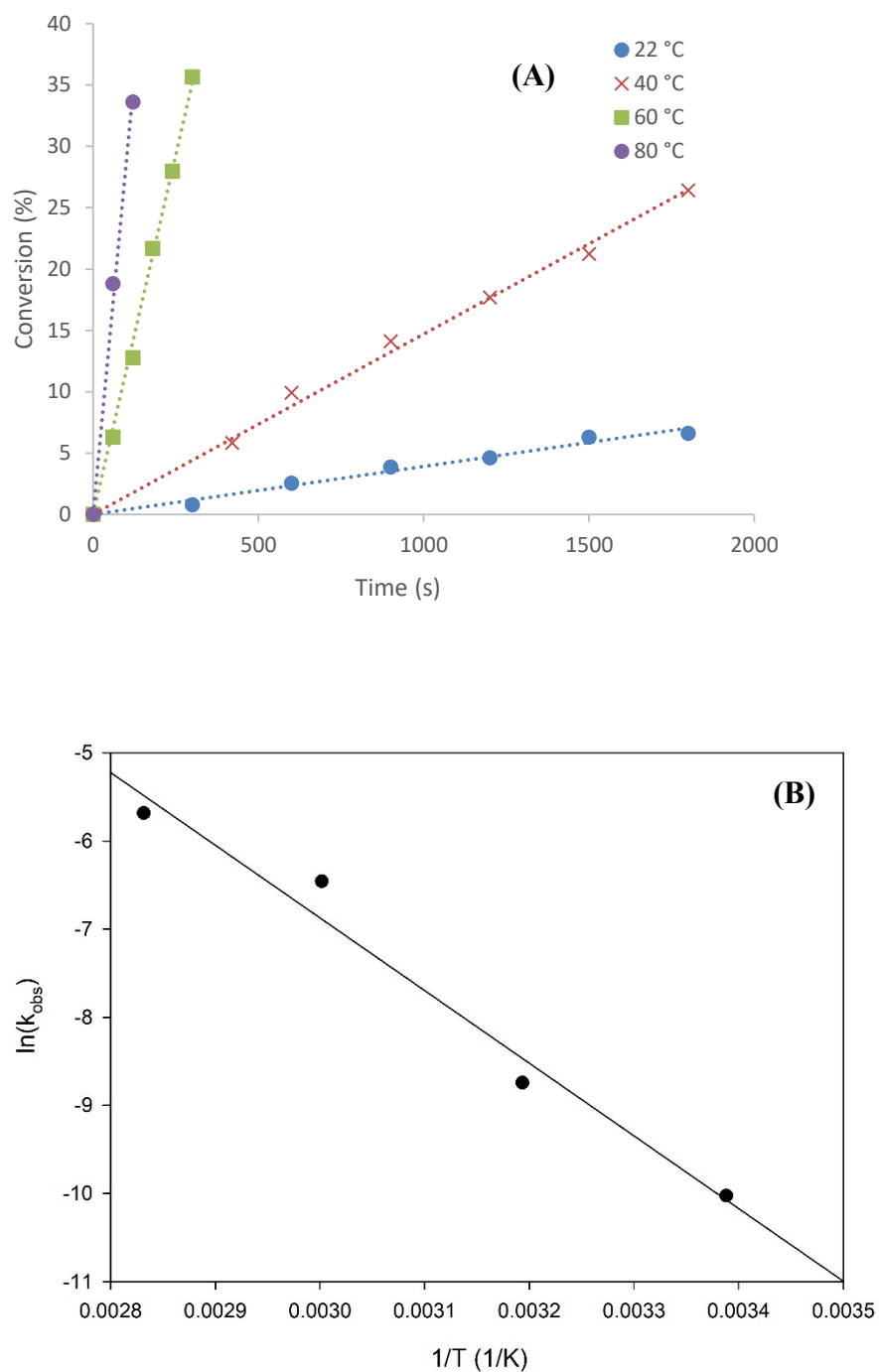


Figure 4.8: (A) Plots of conversion *vs.* time for linear portion of PCHO formation at different temperatures. 22 °C: $y = 0.0039x$, $R^2 = 0.9823$, 40 °C: $y = 0.0147x$, $R^2 = 0.9944$, 60 °C: $y = 0.1172x$, $R^2 = 0.9969$, 80 °C: $y = 0.2866x$, $R^2 = 0.9943$. (B) Arrhenius plot PCHO formation. k_{obs} represent the slopes of first-order plots at various temperatures. Linear regression fit shown with equation: $y = -8249.4x + 21.835$, $R^2 = 0.9752$.

Further inspection of the polymerization kinetic data can be used to gain insight into the type of polymerization process occurring with **4.1**/CHO via a plot of molecular weight vs % conversion. There are three general plot profiles which correspond to three main types of polymerization.⁴⁹ A plot with an upward concave profile normally corresponds to free radical polymerization in which high molecular weight polymer is formed in the initial stages of polymerization. A downward concave profile corresponds to condensation-type polymerization in which high molecular weight polymer is formed as conversion reaches its maximum. In contrast, a linear profile corresponds to a “living”-type polymerization where molecular weight is directly proportional to % monomer conversion. Some metal-based catalyst systems for epoxide ROP reactions have been shown to be “living”.^{10,50} Very recently, Coates and co-workers reported the use of a bimetallic Cr-salen complex for enantioselective polymerization of PO with characteristics (narrow \bar{D} and linear M_n vs conversion plot) comparable to a “living” polymerization process.⁵¹ In the case of **4.1**/CHO a plot of number-average molecular weight (M_n) vs monomer conversion was generated and is shown in **Figure 4.9**. The observed downward concave profile is consistent with a condensation-type polymerization but there is no evolution of small molecules during the propagation step of the polymerization process therefore, **4.1**/CHO ROP system is better classified as chain-growth polymerization.^{52,53}

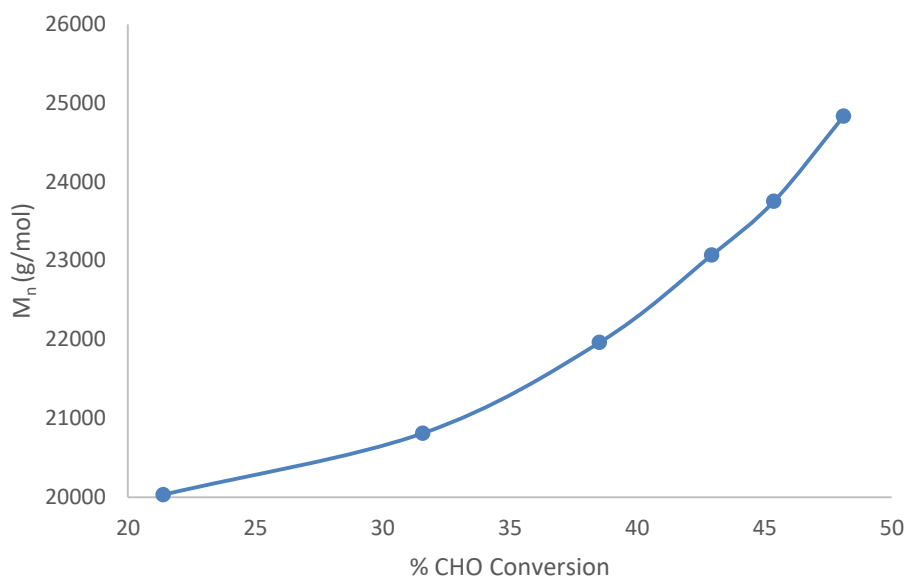


Figure 4.9: Plot of number-average molecular weight (M_n) vs % conversion of CHO for ROP using **4.1** at 60 °C.

4.3 Conclusions

A series of new Cr(III) amino-bis(phenolate) complexes, **4.1** – **4.4** were synthesized and characterized by MALDI-TOF mass spectrometry (**4.1** – **4.4**) and **4.1** further by elemental analysis and X-ray diffraction. The Cr(III) complexes showed high activity toward ring-opening polymerization of cyclohexene oxide resulting in high molecular weight polycyclohexene oxide without the use of a co-catalyst. These Cr(III) amino-bis(phenolate) complexes were proposed to exist as “ate” complexes with bis-axial chloride ligands which serve as nucleophiles for epoxide ring-opening to initiate the ROP process. Kinetic studies of **4.1** revealed an activation barrier for PCHO formation to be 68.6 kJ/mol. Further data analysis indicates a polymerization process similar to that of condensation-polymerization, more specifically, chain-growth polymerization.

4.4 Experimental

4.4.1 General experimental considerations

CHO was dried using CaH_2 and purified by distillation under N_2 before use. Inert atmosphere syntheses were conducted under N_2 using Schlenk techniques or using an MBraun Labmaster DP glove box. Dry toluene and dichloromethane were acquired from an MBraun Solvent Purification System. Anhydrous tetrahydrofuran (THF) was acquired via distillation from sodium/benzophenone ketyl under nitrogen. $\text{CrCl}_3(\text{THF})_3$ was prepared according to a commonly recommended procedure.⁵⁴ NMR spectra were recorded using Bruker AVANCE III 300 MHz and Bruker AVANCE 500 MHz spectrometers with chemical shifts in ppm relative residual solvent signals or TMS. NMR solvents were purchased from Cambridge Isotope Laboratories and used without further purification. Mass spectrometry analysis was performed using an Applied Biosystems 4800 MALDI TOF/TOF Analyzer equipped with a reflectron, delayed ion extraction and high-performance nitrogen laser (200 Hz operating at 355 nm). Anthracene was used as a matrix for analysis of **4.1** – **4.4** and dihydrobenzoic acid (DHBA) was used as a matrix for polymer analysis. Anthracene and complex were dissolved in dichloromethane at a ratio of 2:1 and overall concentration of $6 \text{ mg} \cdot \text{mL}^{-1}$. DHBA and polymer were combined at a ratio of 4:1 in THF at an overall concentration of 12 mg mL^{-1} . Aliquots of $0.5 - 1 \text{ } \mu\text{L}$ of these samples were spotted and solvent allowed to evaporate. MALDI-TOF MS data was processed and images prepared using mMass software (www.mmass.org).

Elemental analysis was performed on a Perkin Elmer 2400 CHN analyzer at the Department of Ocean Sciences, Memorial University, Newfoundland, Canada. The X-ray

structure of **4.1** was acquired using a Rigaku AFC8-Saturn 70 single crystal X-ray diffractometer equipped with an X-Stream 2000 low temperature system and a SHINE optic. Ring-opening polymerization reactions with in situ monitoring were performed using a Mettler Toledo ReactIR 15 spectrometer equipped with a silver-halide Fiber Conduit dip-probe containing a DiComp sensor fitted to a vial via a modified rubber septum. Profiles for absorbance height at 1089 cm^{-1} (polycyclohexene oxide). Gel permeation chromatography (GPC) for polymer molecular weight and dispersity determination was performed using an Agilent 1260 Infinity HPLC with THF as an eluent at a flow rate of 0.30 mL min^{-1} . The HPLC was coupled to triple detectors manufactured by Wyatt technologies (along with Astra 6 software package); Multi-angle Light Scattering (MALS), ViscoStar II viscometer and Optilab T-rEX refractometer. The prolignands **H₂L1** – **H₂L4** were prepared using a previously described procedure and dried in anhydrous THF using MgSO_4 under N_2 .^{55,56}

4.4.2 Synthesis of **4.1**

H₂L1 (2.00 g, 3.73 mmol) and NaH (0.358 g, 14.9 mmol) were added to a Schlenk tube and cooled to $-78\text{ }^\circ\text{C}$. THF (60 mL) was added, resulting in an off-white suspension, which was warmed to $22\text{ }^\circ\text{C}$ and stirred under N_2 for 24 h. The mixture was transferred via filter cannula to a Schlenk flask containing a purple suspension of $\text{CrCl}_3(\text{THF})_3$ (1.40 g, 3.73 mmol) in THF cooled to $-78\text{ }^\circ\text{C}$ then warmed to $22\text{ }^\circ\text{C}$ and stirred under N_2 for 48 h. Volatiles from the resulting green solution were removed under reduced pressure to produce a reddish-brown solid. This solid was dissolved in toluene and the resulting brown mixture was filtered over a Celite bed and the reddish-brown filtrate collected.

Volatiles were removed under reduced pressure and dried *in vacuo* to a yield 2.548 g (99%) of a reddish-brown solid. Crystals suitable for X-ray diffraction were obtained via slow evaporation of **4.1** in a mixture of dichloromethane and HMDSO at 22 °C under N₂. MALDI-TOF MS positive mode, anthracene: m/z (%) = 586.4 (87) [CrL1]⁺; 621.4 (100) [CrCIL1]⁺; MALDI-TOF MS negative mode, anthracene: m/z (%) = 621.4 (46) [CrCIL1]⁻; 656.3 (24) [CCl₂L1]⁻. *Anal.* Calc. for C₃₅H₅₄Cl₂CrN₂NaO₂·1.4(THF)·1.5H₂O: C, 60.30; H, 8.50; N, 3.46. Found: C, 60.00; H, 8.88; N, 3.84.

4.4.3 Synthesis of **4.2**

H₂L2 (1.00 g, 2.06 mmol) and NaH (0.198 g, 8.25 mmol) were added to a Schlenk tube and cooled to -78 °C. THF (30 mL) was added, resulting in an off-white suspension, which was warmed to 22 °C and stirred under N₂ for 16 h. The mixture was transferred via filter cannula to a Schlenk flask containing a purple suspension of CrCl₃(THF)₃ (0.773 g, 2.06 mmol) in THF cooled at -78 °C then warmed to 22 °C and stirred under N₂ for 24 h. Volatiles from the resulting green solution were removed under reduced pressure to produce a reddish-brown solid. This solid was dissolved in toluene and the resulting brown mixture was filtered over a Celite bed. The resulting reddish-brown filtrate was collected, and volatiles were removed under reduced pressure then dried *in vacuo* to yield 0.737 g (56.9%) of a purple-brown solid. MALDI-TOF MS positive mode, anthracene: m/z (%) = 534.1 (87) [CrL2]⁺; 569.1 (43) [CrCIL2]⁺; MALDI-TOF MS negative mode, anthracene: m/z (%) = 569.2 (100) [CrCIL2]⁻; 604.2 (37) [CrCl₂L2]⁻.

4.4.4 Synthesis of 4.3

H₂L3 (2.00 g, 3.83 mmol) and NaH (1.43 g, 3.83 mmol) were added to a Schlenk tube and cooled to -78 °C. THF (60 mL) was added, resulting in an off-white suspension, which was warmed to 22 °C and stirred under N₂ for 24 h. A purple suspension of CrCl₃(THF)₃ in THF cooled at -78 °C was transferred via cannula to the resulting ligand/NaH mixture, warmed to 22 °C and stirred under N₂ for 24 h. The resulting brown mixture was filtered via cannula into another Schlenk flask then volatiles were removed under reduced pressure to produce a reddish-brown solid. The residue was dissolved in toluene then filtered over a Celite bed, filtrate collected and volatiles removed under reduced pressure resulting in a reddish-brown solid; yield 2.49 g (94%) MALDI-TOF MS positive mode, anthracene: m/z (%) = 572.2 (100) [CrL3]⁺; 589.2 (10) [CrOHL3]⁺ 607.2 (80) [CrClL3]⁺; MALDI-TOF MS negative mode, anthracene: m/z (%) = 607.2 (64) [CrClL3]⁻; 642.2 (11) [Cr Cl₂L3]⁻.

4.4.5 Synthesis of 4.4

H₂L4 (1.00 g, 2.11 mmol) and NaH (0.203 g, 8.46 mmol) were added to a Schlenk tube and cooled to -78 °C. THF (60 mL) was added, resulting in an off-white suspension, which was warmed to 22 °C and stirred under N₂ for 16 h. A purple suspension of CrCl₃(THF)₃ in THF cooled at -78 °C was transferred via cannula to the resulting ligand/NaH mixture, warmed to 22 °C and stirred under N₂ for 24 h. The resulting brown mixture was filtered via cannula into another Schlenk flask then volatiles were removed under reduced pressure to produce a reddish-brown solid. The residue was dissolved in toluene then filtered over a Celite bed, filtrate collected and volatiles removed under

reduced pressure resulting in a reddish-brown solid; yield 0.869 g (67.4%) MALDI-TOF MS positive mode, anthracene: m/z (%) = 520.1 (56) $[\text{CrL4}]^+$; 555.1 (45) $[\text{CrClL4}]^+$; MALDI-TOF MS negative mode, anthracene: m/z (%) = 555.2 (100) $[\text{CrClL4}]^-$; 590.1 (24) $[\text{CrCl}_2\text{L4}]^-$.

4.4.6 Representative ring-opening polymerization of cyclohexene oxide

4.1 (0.0138 g, 0.0202 mmol) and cyclohexene oxide (2.00 g, 20.2 mmol) were mixed in a vial at 22 °C in a glove box under N_2 . The resulting green solution was stirred magnetically at 22 °C until hindered by increased viscosity (1 h). This green viscous material was exposed to air to stop the reaction and an aliquot for ^1H NMR spectroscopy was taken immediately for determination of conversion. The polymer was dissolved in dichloromethane and precipitated using cold 5% (v/v with 1 M HCl) acidified methanol. The resulting white solid was dried in a vacuum oven at 60 °C overnight. For reactions with in situ infrared monitoring, the catalyst was placed in a vial containing a stir bar and modified rubber septum through which the DiComp probe (all in a glove box) was fitted. The apparatus was taken out of the glove box and the probe was connected to the spectrometer. Dry CHO was then injected via syringe then stirred until viscous while monitored via infrared spectroscopy.

4.4.7 X-ray diffraction analysis procedure for 4.1

Crystallographic and structure refinement data are given in Appendix C, Table C-6. Crystallographic data was collected and solved by Jennifer N. Murphy from the Department of Chemistry at Memorial University of Newfoundland, St. John's,

Newfoundland, A1B 3X7, Canada. Single crystals of $\text{C}_{36}\text{H}_{57}\text{Cl}_4\text{CrN}_2\text{O}_2$ were crystallized from dichloromethane and HMDSO were dichroic, exhibiting green and pink colors. The crystal was kept at 200 K during data collection. Using Olex2,⁵⁷ the structure was solved with the ShelXT⁵⁸ structure solution program using Intrinsic Phasing and refined with the ShelXL⁵⁸ refinement package using Least Squares minimisation.

4.4 References

1. C. M. Kozak, K. Ambrose and T. S. Anderson, *Coord. Chem. Rev.*, 2018, **376**, 565-587.
2. M. R. Kember, A. Buchard and C. K. Williams, *Chem. Commun.*, 2011, **47**, 141-163.
3. D. J. Darensbourg, *Chem. Rev.*, 2007, **107**, 2388-2410.
4. A.-L. Brocas, C. Mantzaridis, D. Tunc and S. Carlotti, *Prog. Polym. Sci.*, 2013, **38**, 845-873.
5. J. Herzberger, K. Niederer, H. Pohlitz, J. Seiwert, M. Worm, F. R. Wurm and H. Frey, *Chem. Rev.*, 2016, **116**, 2170-2243.
6. M. J. Sanford, L. Peña Carrodegua, N. J. Van Zee, A. W. Kleij and G. W. Coates, *Macromolecules*, 2016, **49**, 6394-6400.
7. M. I. Childers, J. M. Longo, N. J. Van Zee, A. M. LaPointe and G. W. Coates, *Chem. Rev.*, 2014, **114**, 8129-8152.
8. T. Dudev and C. Lim, *J. Am. Chem. Soc.*, 1998, **120**, 4450-4458.
9. C. C. Price, *Acc. Chem. Res.*, 1974, **7**, 294-301.
10. C. G. Rodriguez, R. C. Ferrier, A. Helenic and N. A. Lynd, *Macromolecules*, 2017, **50**, 3121-3130.
11. Y. Sarazin and J.-F. Carpentier, *Chem. Rev.*, 2015, **115**, 3564-3614.
12. H. Plommer, I. Reim and F. M. Kerton, *Dalton Trans.*, 2015, **44**, 12098-12102.
13. T. Aida, K. Wada and S. Inoue, *Macromolecules*, 1987, **20**, 237-241.

14. W. Li, H. Ouyang, L. Chen, D. Yuan, Y. Zhang and Y. Yao, *Inorg. Chem.*, 2016, **55**, 6520-6524.
15. S. Dagorne, M. Bouyahyi, J. Vergnaud and J.-F. Carpentier, *Organometallics*, 2010, **29**, 1865-1868.
16. N. Nakata, Y. Saito and A. Ishii, *Organometallics*, 2014, **33**, 1840-1844.
17. N. Merle, K. W. Törnroos, V. R. Jensen and E. Le Roux, *J. Organomet. Chem.*, 2011, **696**, 1691-1697.
18. T. Aida and S. Inoue, *Macromolecules*, 1981, **14**, 1166-1169.
19. S. Asano, T. Aida and S. Inoue, *J. Chem. Soc., Chem. Commun.*, 1985, 1148-1149.
20. M. Mandal, U. Monkowius and D. Chakraborty, *New J. Chem.*, 2016, **40**, 9824-9839.
21. P. C. B. Widger, S. M. Ahmed and G. W. Coates, *Macromolecules*, 2011, **44**, 5666-5670.
22. E. Schön, X. Zhang, Z. Zhou, M. H. Chisholm and P. Chen, *Inorg. Chem.*, 2004, **43**, 7278-7280.
23. P. Chen, M. H. Chisholm, J. C. Gallucci, X. Zhang and Z. Zhou, *Inorg. Chem.*, 2005, **44**, 2588-2595.
24. C. Chatterjee and M. H. Chisholm, *Inorg. Chem.*, 2012, **51**, 12041-12052.
25. R. K. Dean, L. N. Dawe and C. M. Kozak, *Inorg. Chem.*, 2012, **51**, 9095-9103.
26. R. K. Dean, K. Devaine-Pressing, L. N. Dawe and C. M. Kozak, *Dalton Trans.*, 2013, **42**, 9233-9244.

27. K. Devaine-Pressing, L. N. Dawe and C. M. Kozak, *Polym. Chem.*, 2015, **6**, 6305-6315.
28. H. Chen, L. N. Dawe and C. M. Kozak, *Catal. Sci. Technol.*, 2014, **4**, 1547-1555.
29. S. Elmas, M. A. Subhani, M. Harrer, W. Leitner, J. Sundermeyer and T. E. Muller, *Catal. Sci. Technol.*, 2014, **4**, 1652-1657.
30. K. Ni, V. Paniez-Grave and C. M. Kozak, *Organometallics*, 2018, **37**, 2507-2518.
31. M. Adolph, T. A. Zevaco, O. Walter, E. Dinjus and M. Döring, *Polyhedron*, 2012, **48**, 92-98.
32. M. Adolph, T. A. Zevaco, C. Altesleben, O. Walter and E. Dinjus, *Dalton Trans.*, 2014, **43**, 3285-3296.
33. M. Adolph, T. A. Zevaco, C. Altesleben, S. Staudt, O. Walter and E. Dinjus, *New J. Chem.*, 2015, **39**, 9858-9865.
34. R. K. Dean, S. L. Granville, L. N. Dawe, A. Decken, K. M. Hattenhauer and C. M. Kozak, *Dalton Trans.*, 2010, **39**, 548-559.
35. A. E. M. Abdel-Hady, *Monatsh. Chem.*, 2015, **146**, 7-13.
36. D. S. Wankhede, S. Hussain, N. Jadhav, P. B. Wagh, M. D. Chaudhari, A. G. Murke and O. Shankarrao, *Der Chemica Sinica*, 2013, **5**, 79-85.
37. D. J. Darensbourg, M. Ulusoy, O. Karroonnirum, R. R. Poland, J. H. Reibenspies and B. Çetinkaya, *Macromolecules*, 2009, **42**, 6992-6998.
38. D. J. Darensbourg, R. R. Poland and A. L. Strickland, *J. Polym. Sci., Part A: Polym. Chem.*, 2012, **50**, 127-133.
39. D. J. Darensbourg and A. I. Moncada, *Inorg. Chem.*, 2008, **47**, 10000-10008.

40. Y. W. Choi, S. H. Kim, D. N. Lee, C. Kim and Y. Kim, *Acta Crystallogr. Sect. E*, 2006, **62**, m2715-m2716.
41. A. Debnath, F. Hussain and D. T. Masram, *Bioinorg. Chem. Appl.*, 2014, **2014**, 457478-457478.
42. B. Gao, W. Gao, Q. Wu, X. Luo, J. Zhang, Q. Su and Y. Mu, *Organometallics*, 2011, **30**, 5480-5486.
43. D. J. Darensbourg, R. M. Mackiewicz, J. L. Rodgers and A. L. Phelps, *Inorg. Chem.*, 2004, **43**, 1831-1833.
44. S. Wang, P. Day, J. D. Wallis, P. N. Horton and M. B. Hursthouse, *Polyhedron*, 2006, **25**, 2583-2592.
45. T. A. Zevaco, J. K. Sypien, A. Janssen, O. Walter and E. Dinjus, *J. Organomet. Chem.*, 2007, **692**, 1963-1973.
46. G. Martínez, S. Pedrosa, V. Tabernero, M. E. G. Mosquera and T. Cuenca, *Organometallics*, 2008, **27**, 2300-2305.
47. K. Soga, K. Uenishi and S. Ikeda, *J. Polym. Sci., Part A: Polym. Chem.*, 1979, **17**, 415-423.
48. M. I. Childers, A. K. Vitek, L. S. Morris, P. C. B. Widger, S. M. Ahmed, P. M. Zimmerman and G. W. Coates, *J. Am. Chem. Soc.*, 2017, **139**, 11048-11054.
49. M.-A. Munoz-Hernandez, M. L. McKee, T. S. Keizer, B. C. Yearwood and D. A. Atwood, *J. Chem. Soc., Dalton Trans.*, 2002, DOI: 10.1039/B106003C, 410-414.
50. O. W. Webster, *Science*, 1991, **251**, 887-893.
51. S. Carlotti, A. Labbé, V. Rejsek, S. Doutaz, M. Gervais and A. Deffieux, *Macromolecules*, 2008, **41**, 7058-7062.

52. L. S. Morris, M. I. Childers and G. W. Coates, *Angew. Chem. Int. Ed.*, 2018, **57**, 5731-5734.
53. A. D. Jenkins, P. Kratochvíl, R. F. T. Stepto and U. W. Suter, *Pure Appl. Chem.*, 1996, **68**, 2287.
54. Principles of Ring-Opening Polymerization,
<https://polymerdatabase.com/polymer%20chemistry/Ring%20Opening%20Polymerization.html>, (accessed October 17th, 2018).
55. J. Y. Jeon, J. H. Park, D. S. Park, S. Y. Park, C. S. Lee, M. J. Go, J. Lee and B. Y. Lee, *Inorg. Chem. Commun.*, 2014, **44**, 148-150.
56. D. Alhashmialameer, J. Collins, K. Hattenhauer and F. M. Kerton, *Catal. Sci. Technol.*, 2016, **6**, 5364-5373.
57. L. O. Edoaka, C. U. Okoro and I. D. Ugwu, *Asian J. Chem.*, 2015, **27**, 3463-3467.
58. O. V. Dolomanov, L. J. Bourhis, R. J. Gildea, J. A. K. Howard and H. Puschmann, *J. Appl. Crystallogr.*, 2009, **42**, 339-341.
59. G. Sheldrick, *Acta Crystallogr. Sect. A*, 2015, **71**, 3-8.

Chapter 5: Synthesis and Characterization of a Cr(III) Amino-bis(phenolate) Complex as a Catalyst for Copolymerization of Cyclohexene Oxide and CO₂: Modification of Compound 4.1.

5.1 Introduction

Epoxides are 3-membered cyclic ethers with considerable ring strain¹ and therefore highly reactive, thus making them ideal candidates to be transformed into useful materials such as via reaction with CO₂.² Chromium coordination complexes have been shown to be catalysts for CO₂/epoxide copolymerization,³⁻¹² CO₂/epoxide cycloaddition¹³⁻¹⁶ and ring-opening homo-polymerization^{17,18} to produce polycarbonates, cyclic carbonates, and polyethers, respectively. One can overcome limitations to catalyst selectivity via tuning of complex properties such as sterics, electronics and geometry, which is commonly done by varying ligand substituents.^{11,19} It can be deduced that the majority of Cr-containing catalyst systems reported are selective toward CO₂/epoxide copolymerization whereas cyclic carbonate-producing systems are less common.

Throughout the early development of Cr-salen complexes as catalysts for CO₂/epoxide coupling, Darensbourg and co-workers reported the influence of various ligand substituents on CHO/CO₂ copolymerization activity by altering sterics and electronics.²⁰ It was observed that electron-donating substituents on the salen ligand promoted higher activity in terms of TOF. More specifically, a combination of electron-donating substituents in the phenolate donors such as *tert*-butyl and methoxy groups in the *ortho* and *para* sites respectively (**Figure 5.1, i**), produced 82 TO h⁻¹ with CO₂ incorporation of >99%, whereas hydrogen and methoxy as *ortho* and *para* sites

respectively (**ii**), showed the lowest activity. Substituents on the ethylene backbone also influence catalytic activity where cyclohexylene (**iv**) generally promoted the highest activity whereas ethylene (**iii**) showed the lowest. By introducing a methyl substituent into one of the ethylene carbons (**v**) in the ligand backbone (thus affording a chiral complex) Lu and co-workers afforded selectivity toward polypropylene carbonate production using a CrNO_3 -salen complex and its salan analog.²¹ Activity of up to 86 TO h^{-1} with >99% polymer selectivity and molecular weights of 15.6 kg mol^{-1} were observed. The Kozak group reported a Cr-containing catalyst system of similar characteristics containing amino-bis(phenolate) ligands with phenolate donors having *tert*-butyl substituents in the *ortho* and *para* sites (**viii**), with activity toward PPC synthesis from PO/ CO_2 coupling.²² PPC was produced at up to 96% selectivity and molecular weights of up to 21.1 kg mol^{-1} for reactions at 25°C .

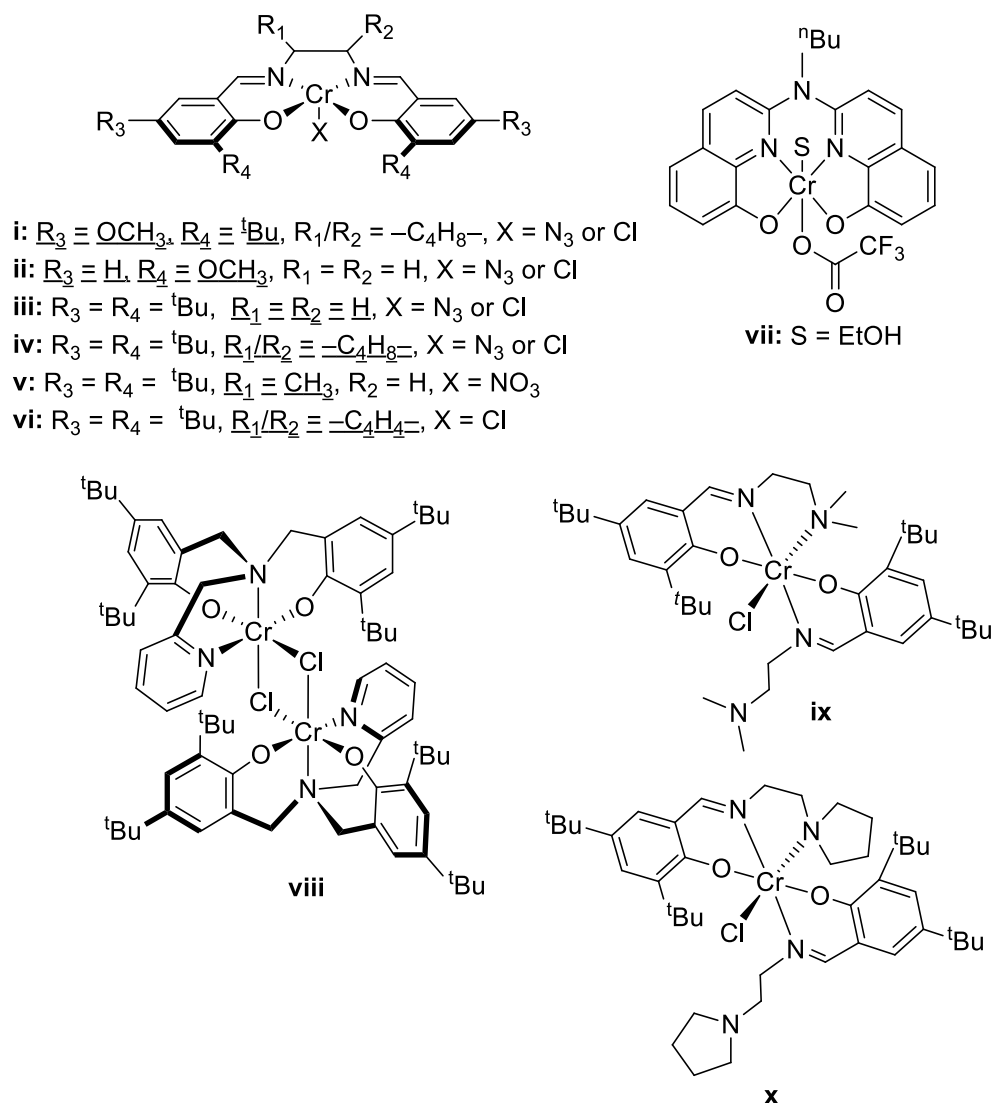


Figure 5.1: Various Cr(III) complexes used as catalyst for reactions of CO_2 with epoxides.

When a phenylene backbone is introduced into the salen ligand (vi), cyclic propylene carbonate is afforded from PO/ CO_2 coupling even at low temperature.^{16,23} North and co-workers reported catalytic activity of a Cr-salen complex containing *tert*-butyl-substituted phenolate (*ortho* and *para* positions) donors and a phenylene backbone with selectivity

strictly toward cyclic carbonates at ambient temperature and pressure. High conversions of up to 100% were observed during epoxide screening.²³ Demonstration of a structure-activity/selectivity relationship was reported by Masdeu-Butl  using a series of Cr-containing [NN'O] Schiff base complexes.²⁴ Although conversions were low, a clear difference in selectivity (polycarbonate vs cyclic carbonate) was observed when donors on the [NN'O] Schiff base ligand were varied between pyrrolidine and NMe₂ amino (**x** vs **ix**).

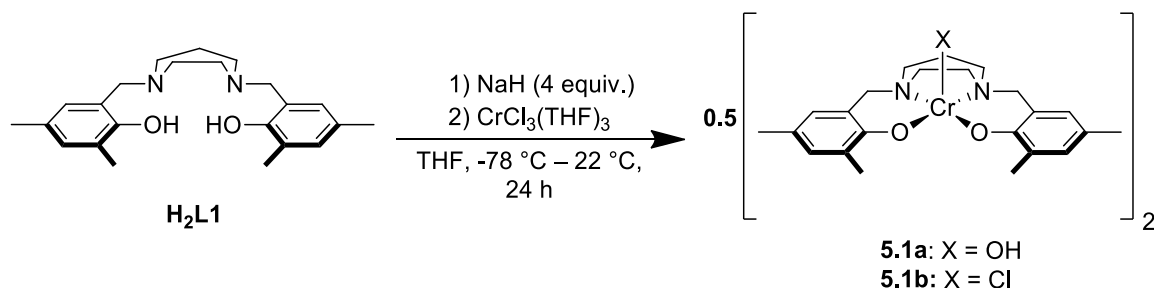
Mechanistic aspects of epoxide/CO₂ copolymerization using salen/salan-type complexes have been studied.^{21,25-27} Some pivotal steps generally shown in these mechanisms are epoxide ring-opening and CO₂-insertion where the metal center becomes coordinatively saturated. These steps require ideal sterics around the metal center to take place, therefore affording selectivity toward polycarbonate, cyclic carbonate or homopolymer production. Increased catalytic activity has been shown with a decrease in steric bulk at the metal coordination sphere.²⁸ M ller, Sundermeyer and co-workers reported a unique bhqba-Cr(III)-OAc^F catalyst, **vii** (where bhqba = bis(hydroxyquinoline), which can undergo a rearrangement of its coordination geometry at the metal center to promote intramolecular epoxide ring-opening/insertion and CO₂-insertion, in the form of an inner-sphere mechanism (see Chapter 1, **Scheme 1.10**).²⁹ When PO is used, direct synthesis of propylene carbonate was observed therefore it was proposed that this chemoselectivity is based on different inner-sphere mechanisms with PO vs CHO.

This chapter presents a discussion of Cr(III) amino-bis(phenolate) complex, **5.1** (related to salan-type complexes), which was synthesized and characterized by MALDI-TOF MS, elemental analysis and X-ray diffraction analysis. Compound **5.1** is a modification of **4.1** whereby *ortho*- and *para*- *tert*-butyl substituents were replaced with methyl groups. Unlike **4.1**, **5.1** was selective toward polycarbonate synthesis from CO₂/CHO. Polymer end-group analysis by MALDI-TOF MS is also presented.

5.2 Results and discussion

5.2.1 Cr(III) complex modification and characterization

Cr(III) amino-bis(phenolate) complex **5.1** was prepared via reaction of the sodium salt of ligand **L1** with CrCl₃(THF)₃ (**Scheme 5.1**). In the Kozak group, this method has been successfully used for preparation of Cr(III) amino-bis(phenolate) complexes.^{10,22,30}



Scheme 5.1: Synthetic route for preparation of Cr(III) amino-bis(phenolate) complex **5.1**. **5.1a** formation discussed in text.

Cr complex **5.1** was characterized by MALDI-TOF mass spectrometry, elemental analysis and X-ray diffraction analysis. The MALDI-TOF mass spectrum of **5.1** in positive reflectron mode showed peaks at m/z 418.0 and 453.0 corresponding to [CrL1]⁺ and [CrClL1]⁺, respectively (see Appendix B, Figure B-23). However, the higher mass

region of the mass spectrum showed dimeric Cr complex fragments. Peaks at m/z 836.2, 853.2 and 871.1 corresponding to $[\text{Cr}_2\text{L1}_2]^+$, $[\text{Cr}_2\text{L1}_2\text{OH}]^+$ and $[\text{Cr}_2\text{L1}_2(\text{OH})_2 + \text{H}]^+$ respectively, were observed. The isotopic patterns of the experimental and theoretical distributions are in good agreement with each other for $[\text{Cr}_2\text{L1}_2]^+$, but, for $[\text{Cr}_2\text{L1}_2\text{OH}]^+$ and $[\text{Cr}_2\text{L1}_2(\text{OH})_2 + \text{H}]^+$ however, there is a slight disagreement in the isotopic patterns, which suggests the presence of two overlapping species for each peak (**Figure 5.2**). That is, at m/z 871.1 for example, the two overlapping species may be $[\text{Cr}_2\text{L1}_2(\text{OH})_2 + \text{H}]^+$ corresponding to m/z 871.3 and $[\text{Cr}_2\text{L1}_2(\text{OH})_2]^+$ corresponding to m/z 870.3. A similar occurrence is likely present at the peak with m/z 853.2. The formation of **5.1a** may likely occur during analysis as the samples are very air sensitive and must be transported outside of the inert atmosphere glove box.

Proposed structures of these dimeric Cr(III) complex fragments are also shown (**Figure 5.2**). Dimeric Cr(III) complex fragments of amino-bis(phenolate) complexes have been previously observed using MALDI-TOF mass spectrometry.^{12,31} In negative reflectron mode, peaks at m/z 453.1 and 488.1 corresponding to $[\text{CrClL1}]^-$ and $[\text{CrCl}_2\text{L2}]^-$ respectively, were observed (see Appendix B, Figure B-24). The experimental isotopic distribution patterns are also in good agreement with the theoretical patterns.

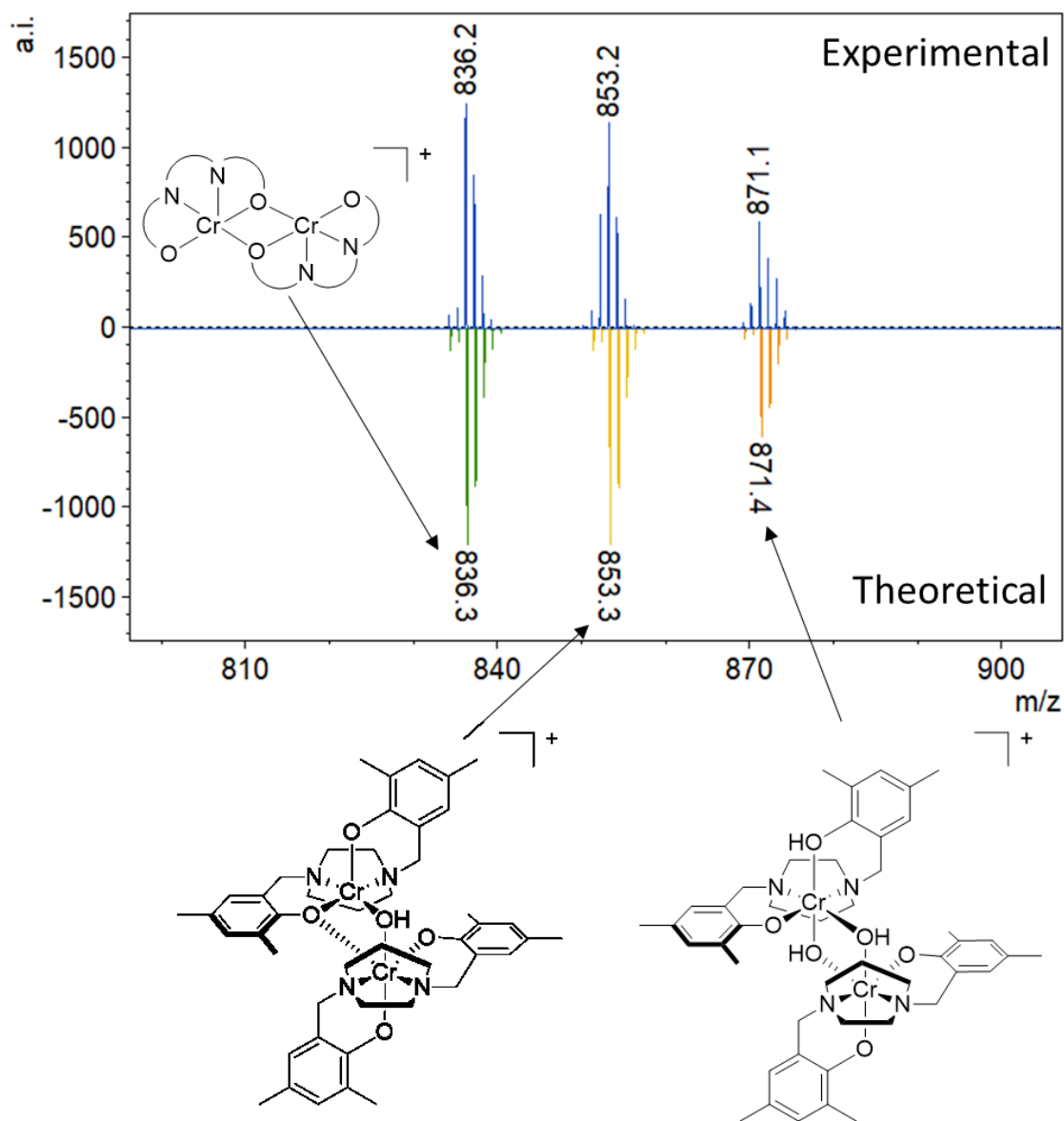


Figure 5.2: MALDI-TOF mass spectrum of **5.1** collected in positive reflectron mode, showing higher mass region and proposed Cr(III) complex fragments.

The occurrence of chloride and hydroxide ancillary ligands in the mass spectrum was consistent with the structural characterization of the two compounds obtained from recrystallization. Single crystals were obtained at 22 °C from a solution of **5.1**/DMAP in

acetonitrile, originally intended for ESI-MS studies of **5.1**-DMAP adducts, in a nitrogen-filled glove box. Analysis of these crystals by X-ray diffraction showed the presence of a μ -hydroxo-bridged dimer, **5.1a**, which is possibly due to the presence of adventitious moisture. The molecular structure of **5.1a** with selected bond lengths and angles is shown in **Figure 5.3**; additional structural data are reported in Appendix C. Similar μ -hydroxo-bridged dimeric Cr(III) amino-bis(phenolate) complexes have previously been reported.^{5,22,32} The complex exhibits distorted octahedral geometries at the Cr(III) centers and contains an inversion center at the Cr₂O₂ rhomboid by inspection. The [O₂N₂] tetradentate ligand occupies four coordination sites and the other two coordination sites are occupied by the bridging hydroxide ligands, where an overall *cis*- β -octahedral coordination pattern is afforded. The distorted octahedral geometry is evidenced by several bond angles deviating from 90° as exemplified by O(3) – Cr(1) – O(1*) and N(2) – Cr(1) – N(1) with values of 92.44(9)° and 74.94(10)° respectively. The Cr(1*) – O(1) – Cr(1) bond angle is 102.83(10)° and is similar to what is reported for a related hydroxo-bridged dimer.³² The Cr–OH bond distances were observed to be 2.003(2) and 1.988(2) Å and are in good agreement with related hydroxo-bridged Cr(III) dimers.^{22,32}

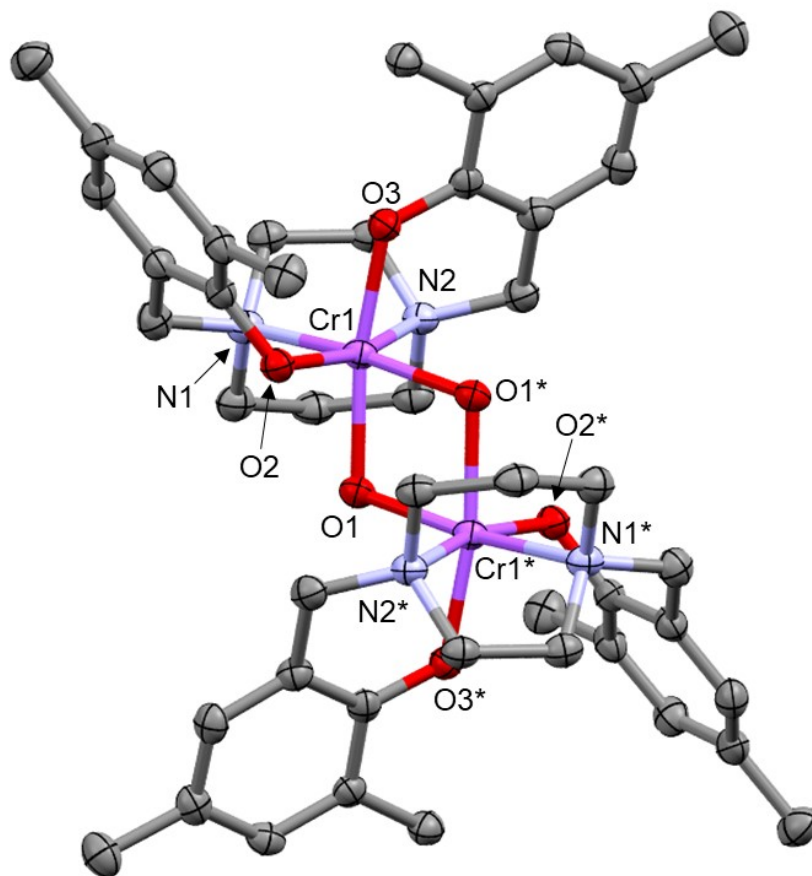


Figure 5.3: Partially labelled molecular structure of μ -hydroxo-bridged **5.1a**. Thermal ellipsoids are drawn at 50% probability with hydrogens and co-crystallized acetonitrile molecule omitted for clarity. Selected bond distances (Å) and angles (deg): Cr(1) – O(1), 2.003(2); Cr(1) – O(1*), 1.988(2); Cr(1) – O(2), 1.933(2); Cr(1) – O(3), 1.920(2); Cr(1) – N(1), 2.125(3); Cr(1) – N(2), 2.120(3) Cr(1)···Cr(1*), 3.119; O(1*) – Cr(1) – O(1), 77.17(10); O(1) – Cr(1) – N(1), 95.03(9); O(1*) – Cr(1) – N(1), 170.23(9); O(1*) – Cr(1) – N(2), 99.99(9); O(1) – Cr(1) – N(2), 97.52(9); O(2) – Cr(1) – O(1*), 94.57(9); O(2) – Cr(1) – O(1), 90.41(9); O(2) – Cr(1) – N(1), 91.33(9); O(2) – Cr(1) – N(2), 164.64(9); O(3) – Cr(1) – O(1), 169.49(9); O(3) – Cr(1) – O(1*), 92.44(9); O(3) – Cr(1) – O(2), 92.02(9); O(3) – Cr(1) – N(1), 95.13(9); O(3) – Cr(1) – N(2), 82.57(9); N(2) – Cr(1) – N(1), 74.94(10); Cr(1*) – O(1) – Cr(1), 102.83(10). Symmetry operation used to generate equivalent atoms: 1.5 - x, 1.5 - y, 1.5 - z

Single crystals were also obtained from a solution of **5.1** dissolved in dichloromethane at 22 °C also in a glove box. X-ray diffraction analysis showed the presence of a chloride-bridged dimer, **5.1b**. The molecular structure and selected bond lengths and angles are shown in **Figure 5.4** with additional structural data reported in Appendix C. This molecular structure exhibits similar geometry and ligand arrangement as the μ -hydroxo-bridged dimer **5.1a**. Several bond angles such as Cl(1*) – Cr(1) – Cl(1) and N(2) – Cr(1) – N(1) with angles values of 83.15(4)° and 75.50(12)° respectively, show a distorted octahedral geometry. The Cr–Cl bond distances were observed to be 2.3805(12) and 2.4244(12) Å and are similar to those of related chlorido-bridged Cr(III) dimers³⁰ but are longer than the Cr–OH bonds in the hydroxo-bridged dimer due to the larger atomic radius of chlorine compared to oxygen.

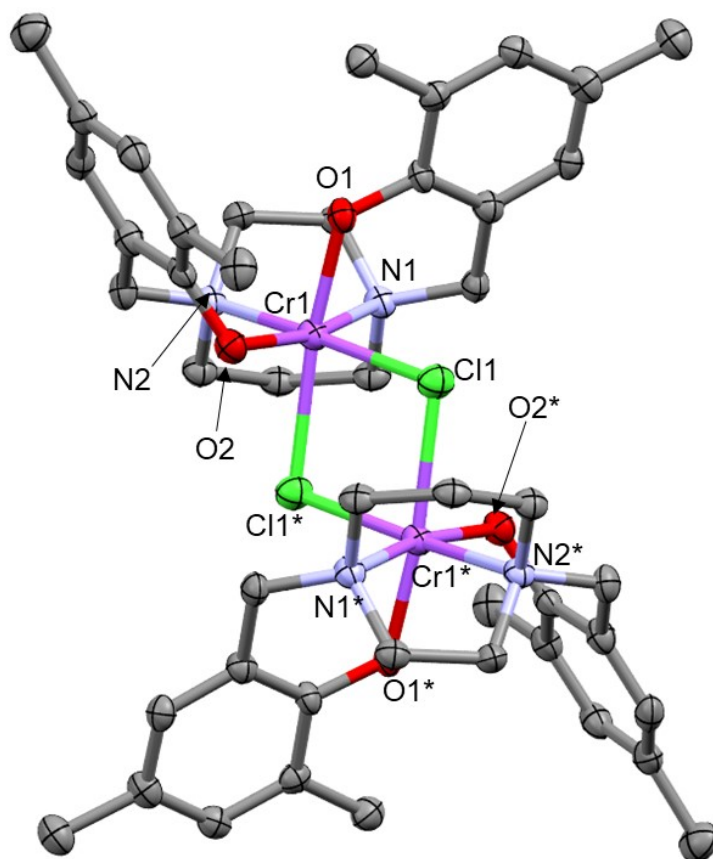


Figure 5.4: Partially labelled molecular structure of chloride-bridged **5.1b**. Thermal ellipsoids are drawn at 50% probability with hydrogens and co-crystallized dichloromethane molecule omitted for clarity. Selected bond distances (Å) and angles (deg): Cr(1) – Cl(1), 2.3805(12); Cr(1) – Cl(1*), 2.4244(12); Cr(1) – O(1), 1.903(3); Cr(1) – O(2), 1.923(3); Cr(1) – N(1), 2.131(3); Cr(1) – N(2), 2.106(3); Cl(1*) – Cr(1) – Cl(1), 83.15(4); O(1) – Cr(1) – Cl(1), 88.54(8); O(1) – Cr(1) – Cl(1*), 171.68(9); O(1) – Cr(1) – O(2), 93.08(11); O(1) – Cr(1) – N(1), 82.65(11); O(1) – Cr(1) – N(2), 95.33(12); O(2) – Cr(1) – Cl(1*), 87.15(9); O(2) – Cr(1) – Cl(1), 92.89(9); O(2) – Cr(1) – N(1), 166.48(12); O(2) – Cr(1) – N(2), 92.22(12); N(1) – Cr(1) – Cl(1*), 98.93(9); N(1) – Cr(1) – Cl(1), 99.78(9); N(2) – Cr(1) – Cl(1*), 92.97(9); N(2) – Cr(1) – Cl(1), 173.41(9); N(2) – Cr(1) – N(1), 75.50(12); Cr(1) – Cl(1) – Cr(1*), 96.85(4). Symmetry operation used to generate equivalent atoms: 1.5 - x, 0.5 - y, 1.5 - z.

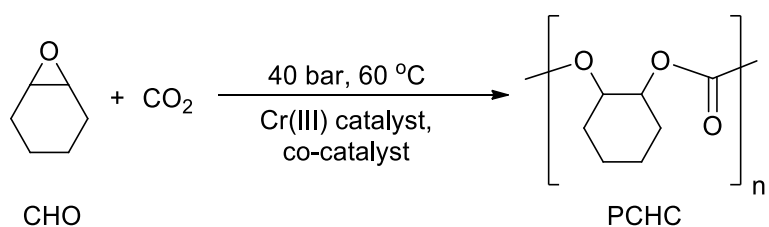
The purity of complex **5.1** could not be unequivocally determined using combustion analysis. The observed C, H, and N percentages can be rationalized by incorporating co-

crystallized solvent in pure **5.1a** or by incorporating a mixture of **5.1a** and **5.1b**. The experimental percentage of C 62.66%, H 7.10% and N 6.41% can be closely matched if 0.4 equiv. of **5.1b** is included in **5.1a**, giving C 62.67%, H 7.02% and N 6.36%. Thus, the product is obtained as a mixture of the two derivatives.

The presence of **5.1a** was unexpected considering that in the past, related syntheses of Cr(III) complexes using $\text{CrCl}_3(\text{THF})_3$ produced $[\text{CrClL}_n]$ complexes (where L_n = tetradentate amino-bis(phenolate) ligand). This outcome suggests the occurrence of hydrolysis by moisture or the presence of a hydrate in the coordination sphere of the Cr precursor. That is, the production of $\text{CrCl}_3(\text{THF})_2\text{H}_2\text{O}$ is possible when prepared via dehydration of $\text{CrCl}_3 \cdot 6\text{H}_2\text{O}$ using Me_3SiCl (trimethylsilyl chloride).³³

5.2.2 Copolymerization of CHO and CO₂ using 5.1

Compound **5.1** (quite likely a mixture of **5.1a** and **5.1b**) was investigated for catalytic activity toward CHO ring-opening polymerization (ROP) and CHO/CO₂ copolymerization. There was no observed activity toward ROP of CHO using compound **5.1** but in the presence of CO₂ however, copolymerization of CHO and CO₂ was observed when co-catalyzed by PPNN₃, PPNCI or DMAP at 60 °C, 40 bar CO₂ pressure and 0.2 mol% catalyst loading, to produce poly(cyclohexene carbonate) (PCHC), **Scheme 5.2**.



Scheme 5.2: Copolymerization of CO_2 and CHO producing PCHC.

Reactions were also monitored using in situ FTIR spectroscopy which recorded the formation of polycyclohexene carbonate and a simultaneous decrease in CO_2 (**Figure 5.5**). The profile at 1749 cm^{-1} shows an increase in peak height with time, which eventually plateaus, resulting from a saturated IR sensor. The resultant PCHC formed a clear green glass-like solid and samples taken immediately after reaction were characterized by ^1H NMR spectroscopy to determine CHO conversion. This showed broad multiplets at 4.61 and 4.65 ppm confirming the presence of PCHC methine protons with no detection of ether linkages (>99% CO_2 incorporation) or cyclic carbonate (see Appendix A, Figure A-17).³⁴ For further polycarbonate analysis (gel-permeation chromatography), purification was performed by dissolving the solid in dichloromethane followed by precipitation using cold 5% v/v acidified methanol (using 1 M HCl), which is a commonly used technique.^{35,36} Characterization of produced PCHC by ^{13}C NMR spectroscopy showed signals at 153.8 and 153.3 ppm corresponding to syndiotactic and isotactic diads respectively, which is consistent with atactic polycarbonate. (see Appendix A, Figure A-18)^{34,37}

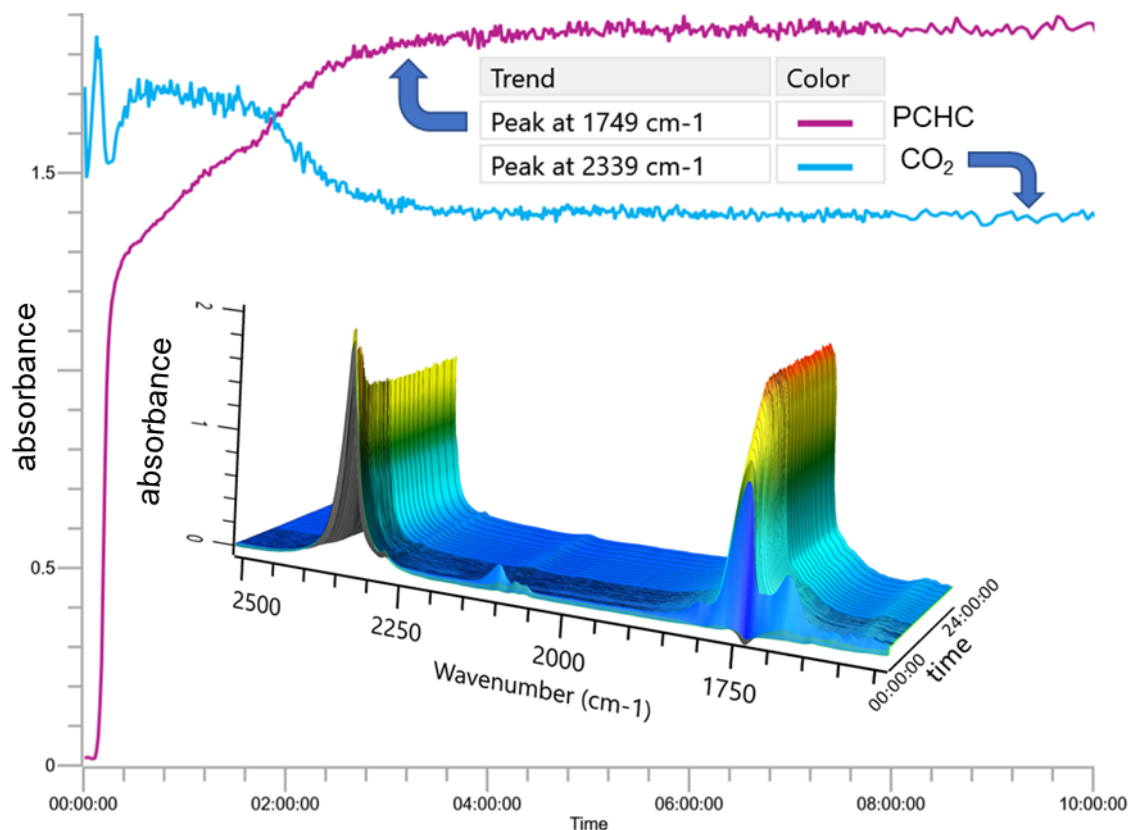


Figure 5.5: Profiles for in situ monitored FTIR absorbances 1749 cm⁻¹ (PCHC) and 2339 cm⁻¹ (CO₂) with overlaid three-dimensional stack plot.

The use of PPNCI (bis(triphenylphosphine)iminium chloride) as a co-catalyst at 0.2 mol% catalyst loading afforded 90% conversion of CHO into PCHC after 24 h (**Table 5.1**, entry 1). The isolated yield was lower than conversion which is likely due to low molecular weight polymer being soluble in the methanolic filtrate. There was no detection of cyclic carbonate (cyclohexene carbonate, CHC) upon analysis of the crude reaction mixture by ¹H NMR spectroscopy immediately after quenching the reaction. Moreover, as mentioned earlier, ether linkages were not observed, which indicates excellent CO₂ incorporation during the propagation stage of polymerization. Employing DMAP and

PPNN₃ as co-catalysts had no effect on CHO conversion but molecular weight however, was approximately doubled with DMAP and PPNN₃, and narrower dispersities were obtained which suggest a more controlled polymerization process (entries 1, 2 and 3).

To further investigate the effect of co-catalyst, reaction profiles from in situ FTIR monitoring at 1749 cm⁻¹ were plotted showing the initial stages of the reaction. Based on the appearance of the slope of each profile, PPNN₃ promotes the fastest initial rate among the three co-catalysts for the copolymerization of CHO and CO₂ using **5.1** (**Figure 5.6**). This finding is consistent with related chromium amino-bis(phenolate) complexes for CO₂/epoxide copolymerization reactions.^{12,20} Furthermore, ESI-TOF mass spectrometry was used to determine the nature of **5.1** in the presence of various ratios of PPNN₃ (**Figure 5.7**). In negative reflectron mode, complex fragment **F1** was not observed at any investigated ratio of **5.1**:PPNN₃. Complex fragment **F3** showed an increase in relative intensity (r. int) with an increase in molar ratio of PPNN₃ to **5.1**. This shows the ability for N₃⁻ to displace Cl⁻ (or OH⁻) from the Cr metal center. When a **5.1**:PPNN₃ ratio of 1:2 was employed for CHO/CO₂ copolymerization the FTIR reaction profile showed multiple initial propagation stages. The first stage was fast and lasted for ~12 min whereas the second lasted for ~2 h. This suggests delayed initiation resulting from the presence of complex **F3** which requires additional time to form the active catalyst. A similar observation has been made using a Cr(III) amino-bis(phenolate) complex where multiple propagation stages were observed, but with 1 equiv. of co-catalyst, for CO₂/CHO copolymerization.¹⁰ The first stage occurred over 4 h whereas the second stage lasted for 150 min. Kozak and co-workers also reported another Cr(III) amino-bis-(phenolate)

complex which produced a slow propagation rate at higher co-catalyst loading (2 equiv. of PPNCI).³⁸ This effect was attributed to the formation of an “ate” complex which required additional time for dissociation of a chloride ligand to produce a vacant site for CHO coordination. It is interesting to note that in positive reflectron mode, only a peak at m/z 538.4 corresponding to $[\text{PPN}]^+$ was observed, for all three ratios of **5.1**:PPNN₃.

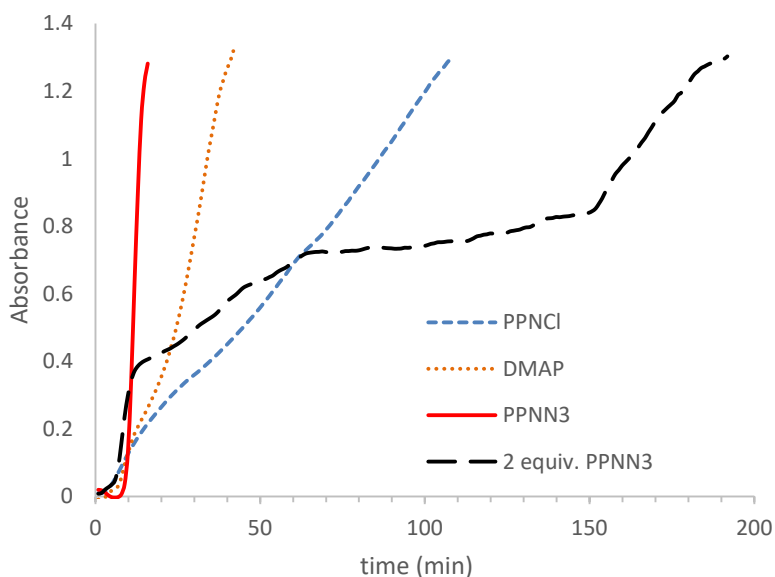


Figure 5.6: Profiles of absorbance vs time at the initial stages of CHO/CO₂ copolymerization using **5.1** co-catalyzed by PPNN₃ (solid red), DMAP (dotted green), PPNCI (dashed blue) and 2 equiv. of PPNN₃ (long-dashed black).

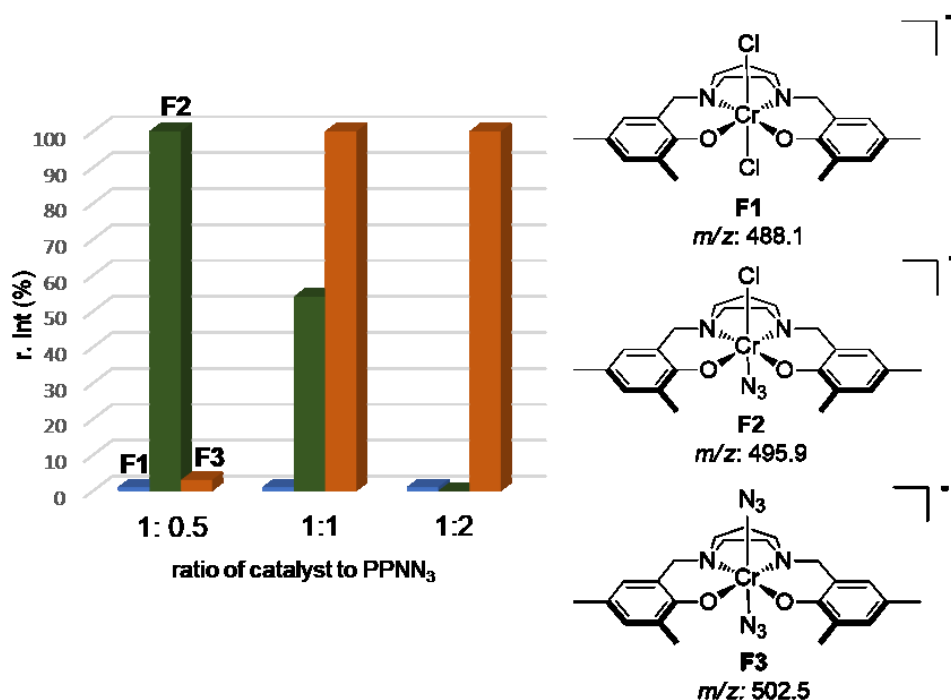


Figure 5.7: Observed fragments of **5.1**/PPNN₃ using ESI-TOF MS in negative reflectron mode at various ratios.

Single crystals suitable for X-ray diffraction analysis were obtained from a 1:1 ratio of **5.1**/PPNN₃ dissolved in dichloromethane in an N₂-filled glove box at 22 °C, and showed the presence of a chromium azido-aquo adduct, **5.2**, formulated as [Cr(OH₂)N₃L1], where the molecular structure is shown in **Figure 5.8**. Unfortunately, the structural data acquired for **5.2** using X-ray diffraction analysis was poor due to weak diffractions; therefore, bond lengths and angles are not discussed in detail but the structure is suitable for the purpose of showing atom connectivity and geometry within the metal coordination sphere (**Figure 5.8**). It is worth noting that bond distances for Cr–OH₂³⁹ and Cr–N₃^{40–42} are in good agreement with similar Cr structures which have been previously reported. The [ONNO] ligand occupies four coordination sites and chelates in

a *trans*-meridional fashion, and the azide and aquo ligands are in a *trans*-axial fashion, thus affording an overall distorted octahedral geometry around the Cr(III) center.

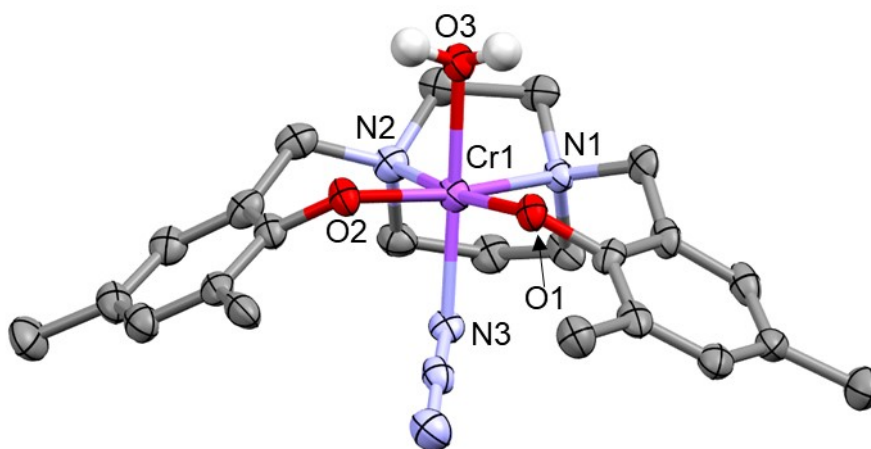


Figure 5.8: Partially labelled molecular structure of **5.2**. Thermal ellipsoids are drawn at 50% probability with hydrogens (except for aquo ligand) and co-crystallized dichloromethane omitted for clarity.

When propylene oxide (PO) was employed for reaction with CO₂ at 60 °C and 40 bar CO₂ pressure, the only observed product was cyclic propylene carbonate with a conversion of >99% (**Table 5.1**, entry 4). A 1 h copolymerization reaction produced 24% conversion of CHO and a low polymer molecular weight of 4.3 kg mol⁻¹ (entry 5) whereas a higher catalyst loading produced 49% conversion while maintaining a similar molecular weight (entries 5 vs 6). The effect of catalyst loading was investigated and when a 0.1 mol% loading was used (entry 7), conversion slightly decreased but molecular weight increased as expected. There was a further decrease in conversion when 0.05 mol% loading was used, however, a further increase in molecular weight was not

observed (entries 7 vs 8). These findings suggest that conversion is dependent on catalyst loading whereas polymer molecular weight is not.

Table 5.1: Copolymerization of CO₂ and CHO using **5.1**.^a

entry	co-catalyst	cat:co-cat: CHO	conversion (%) ^b	isolated yield (%)	TON	M_n (g/mol)	\bar{D} (M_w/M_n)
1	PPNCl	1:1:500	90	82	450	11500	1.31
2	DMAP	1:1:500	87	69	435	22160	1.06
3	PPNN ₃	1:1:500	90	75	450	20710	1.09
4 ^c	PPNCl	1:1:500 ^b	>99	-	495	-	-
5 ^d	PPNN ₃	1:1:500	24	24	120	4269	1.03
6 ^d	PPNN ₃	1:1:250	49	29	123	4251	1.03
7	PPNN ₃	1:1:1000	79	78	790	33990	1.13
8	PPNN ₃	1:1:2000	44	41	880	19980	1.12

^aReactions were performed in neat CHO at 60 °C using shown catalyst loading and 40 bar CO₂ pressure for 24 h unless otherwise stated. ^bDetermined by ¹H NMR; % Conversion = integration of polycarbonate peak (8.45 at 4.83 – 4.49 ppm) divided by the sum of polycarbonate (8.45 at 4.83 – 4.89 ppm) and monomer (1.00 at 3.13 ppm). ^cPropylene oxide used here instead of cyclohexene oxide. ^dReaction was performed for 1 h.

5.2.3 Polycarbonate end-group analysis

Produced PCHC was characterized by MALDI-TOF mass spectrometry for end-group analysis which provides insight into the polymerization initiation mechanism. The mass spectrum obtained for polycarbonate produced from **Table 5.1**, entry 1 appeared to be complicated with no ordered distribution of masses for polymer fragments. Some identified peaks showed sodium ion containing polymer fragments having masses

corresponding to $[35.4 (\text{Cl}) + n(142.1) (\text{repeating cyclohexene carbonate unit}) + 99.1 (\text{C}_6\text{H}_{10}\text{OH})]$. This is expected and suggests that chloride initiation occurs and eventually, termination occurs via protonolysis of the metal-alkoxide bond in methanol during polymer purification. For **Table 5.1**, entry 2 (co-catalyzed by DMAP), the mass spectrum shows a monomodal distribution of masses separated by m/z 142.1 at the higher mass region of the spectrum (see Appendix B, Figure B-25). A magnification of this mass spectrum is shown in **Figure 5.9**. This fragment corresponds to polymers having DMAP and hydroxide end-groups, which may result from initiation by DMAP and protonolysis of the metal-alkoxide bond in methanol.

When **5.1** was co-catalyzed by PPNN_3 for CHO/ CO_2 copolymerization (**Table 5.1**, entry 3), the MALDI-TOF mass spectrum showed an overall monomodal distribution with other low intensity series of fragments demonstrating multiple modalities (see Appendix B, Figure B-26). Multiple low intensity fragments suggest the occurrence of various initiation and termination mechanisms, and chain transfer during the polymerization process.⁴³ A magnification of the mass spectrum (**Figure 5.10**, purple triangle) shows the major fragment corresponding to protonated polymer chains having chloride and azide end groups, resulting from separate azide and chloride-initiated polymer chain combined due to chain transfer mechanisms. One of the minor fragments (red square) however, corresponds to sodium-containing polymer chain with hydroxide and chloride end groups (**Figure 5.10**). This suggests the occurrence of chloride initiation and protonolysis of the metal-alkoxide bond in methanol.

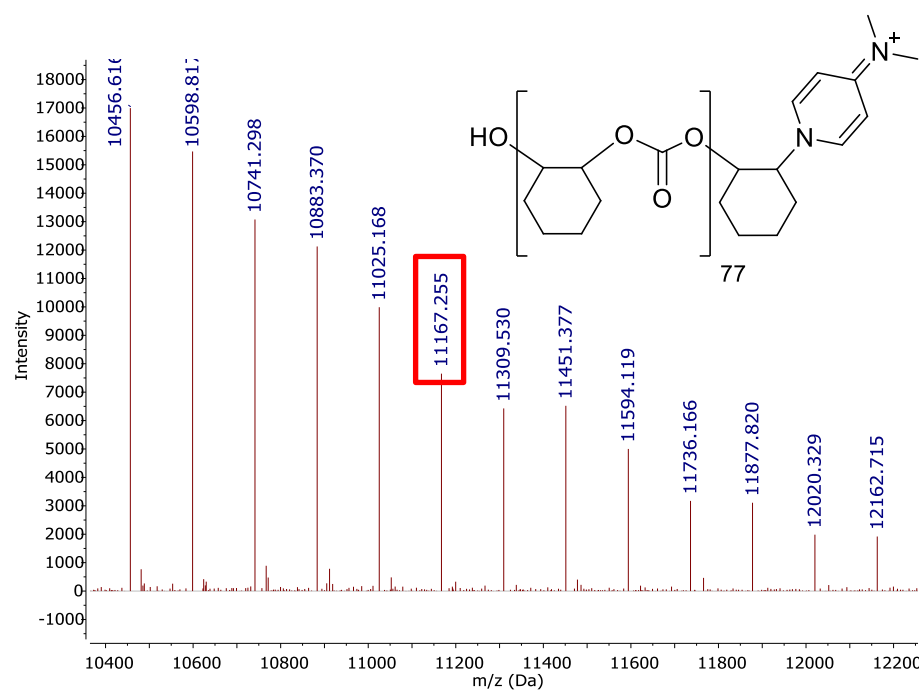


Figure 5.9: Magnified MALDI-TOF mass spectrum (higher mass region, m/z 10350 – 12250) of PCHC obtained from Table 5.1, entry 2. Proposed polymer structure shown.

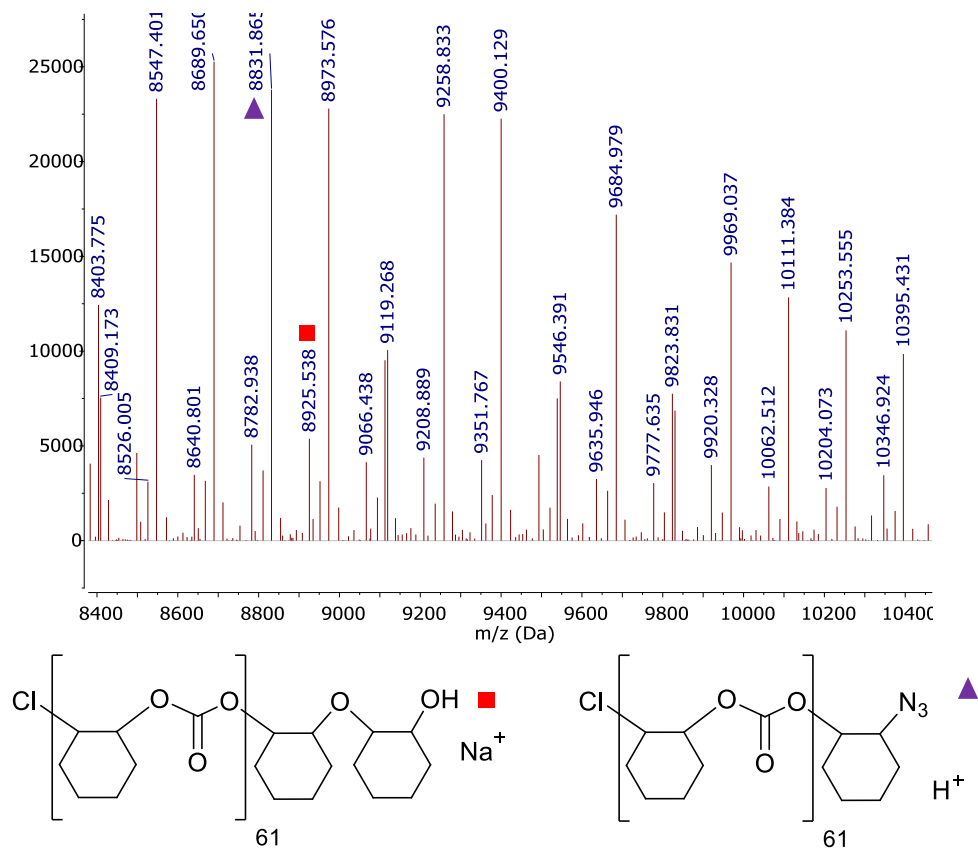


Figure 5.10: Magnified MALDI-TOF mass spectrum (higher mass region, m/z 8040 – 10250) of PCHC obtained from Table 5.1, entry 3. Proposed polymer structures shown.

Reaction order in catalyst concentration can indicate more information about the copolymerization mechanism. For a mononuclear catalyst, a reaction order of 1 indicates a polymerization process occurring in a monometallic fashion, whereas an order of 2 can be expected for a bimetallic mechanism.^{10,44} Kinetics experiments for copolymerization of CHO/CO₂ using **5.1**/PPNN₃ at various catalyst loadings were performed using in situ FTIR monitoring. The initial linear portion of the reaction profiles showing growth of absorbance of the polycarbonate carbonyl C=O band at 1750 cm⁻¹, were normalized and are shown in **Figure 5.11** for comparison of rates. As expected, increased catalyst loading

resulted in increased initial rates, r_{obs} . A plot of $\ln(r_{\text{obs}})$ exhibits a linear relationship giving a reaction order of 0.86 ± 0.058 ($R^2 = 0.9909$) with respect to catalyst concentration (**Figure 5.12**). A reaction order of 0.86, if approximated to 1, for this binary **5.1**/PPNN₃ catalyst system may indicate a monometallic CHO/CO₂ polymerization mechanism. Rieger and co-workers observed a reaction order of 1.69 for a mononuclear Cr(III)-salen complex in PO/CO₂ copolymerization. This value shows contribution of a bimetallic process while having a monometallic rate-determining steps.⁴⁴ In another study, by Kozak and co-workers, a Cr(III) amino-bis(phenolate) complex showed a reaction order of 0.96, which indicates a monometallic mechanism in CHO/CO₂ copolymerization.³¹ A binary Co(III)-salen catalyst system reported by Lu and co-workers was concluded to have a complex CO₂/epoxide copolymerization system as it showed a reaction order of 1.61 in catalyst concentration.⁴⁵

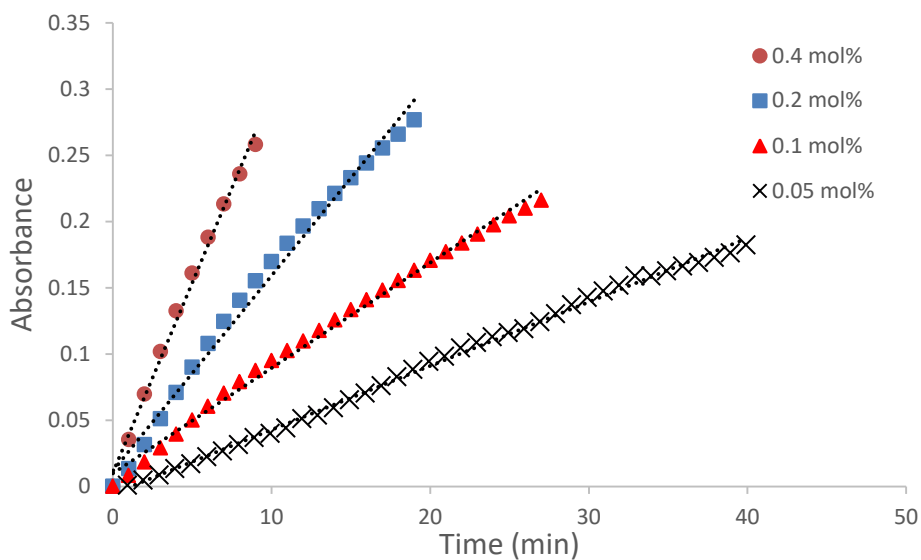


Figure 5.11: Normalized absorbance vs time plots for linear portion of reaction profile showing growth of absorbance of the polycarbonate carbonyl C=O band at 1750 cm^{-1} , for copolymerization of CHO/CO₂ using **5.1**/PPNN₃. Best fit linear regression lines produced relative rates (r_{obs}) of 0.00504 (0.05 mol%, X), 0.00795 (0.1 mol%, \blacktriangle), 0.0147 (0.2 mol%, \blacksquare) and 0.0299 (0.4 mol%, \bullet)

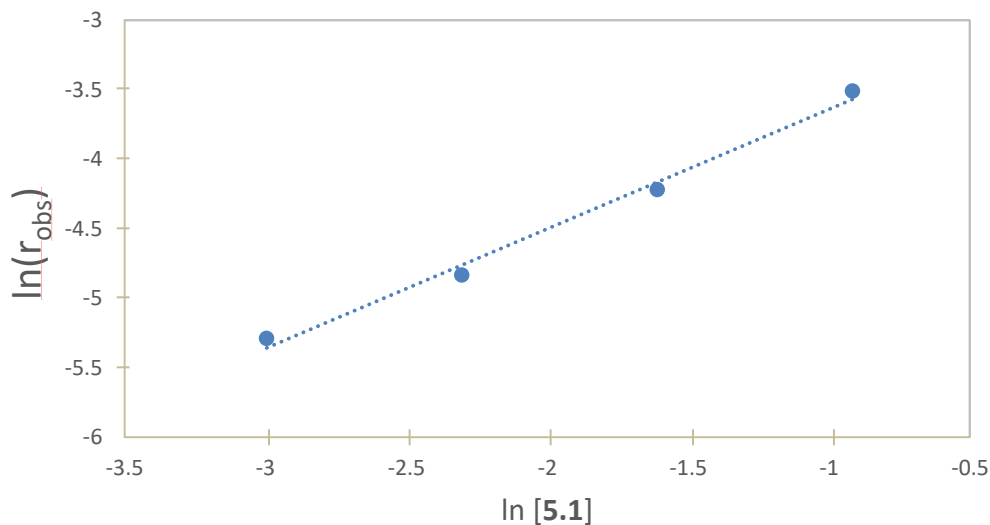


Figure 5.12: Plot of $\ln(r_{\text{obs}})$ against $\ln[5.1]$ for copolymerization of CHO/CO₂. Equation of linear regression: $y = 0.859x + 2.789$, $R^2 = 0.9909$.

5.3 Conclusions

Modification of compound **4.1** by substitution of *tert*-butyl phenolate substituents for methyl groups afforded the production of a mixture of products, **5.1a** and **5.1b**. Catalytic activity showed a switch in selectivity from homopolymerization of CHO to copolymerization with CO₂, with excellent CO₂ incorporation and polycarbonate selectivity. Co-catalyst effects were observed where PPNN₃ exhibited the highest initial reaction rate when monitored by in situ FTIR spectroscopy. Polymer end-group analysis using MALDI-TOF mass spectrometry, suggests initiation by external nucleophiles of the co-catalyst as well as chloride displaced from the metal center. Reaction order with respect to catalyst concentration was 0.86, which indicates a copolymerization mechanism with monometallic character.

5.4 Experimental

5.4.1 General experimental considerations

CHO and PO were dried using CaH₂ and purified by distillation under N₂ before use. Inert atmosphere syntheses were conducted under N₂ using Schlenk techniques or using an N₂-filled MBraun Labmaster DP glove box. Dry dichloromethane was acquired from an MBraun Solvent Purification System. Anhydrous tetrahydrofuran (THF) was acquired via distillation from sodium/benzophenone ketyl under nitrogen. CrCl₃(THF)₃ was prepared according to a commonly recommended procedure³³ and in other instances via reaction of CrCl₃·6H₂O with trimethylsilyl chloride. NMR spectra were recorded using Bruker AVANCE III 300 MHz and Bruker AVANCE 500 MHz spectrometers with chemical shifts in ppm relative to residual solvent signal or TMS. NMR solvents were

purchased from Cambridge Isotope Laboratories and used without further purification. Mass spectrometry was performed using an Applied Biosystems 4800 MALDI TOF/TOF Analyzer equipped with a reflectron, delayed ion extraction and high-performance nitrogen laser (200 Hz operating at 355 nm) Mass spectrometry was also performed using a Bruker ultrafleXtremeTM MALDI TOF/TOF Analyzer with a Bruker smartbeam-IITM laser (up to 2 kHz, operating at 355 nm) for linear and reflectron mode. Anthracene was used as a matrix for analysis of **5.1** and dihydrobenzoic acid (DHBA) was used as a matrix for polymer analysis. Anthracene and complex were dissolved in dichloromethane at a ratio of 2:1 and overall concentration of 6 mg·mL⁻¹. DHBA and polymer were combined at a ratio of 4:1 in THF at an overall concentration of 12 mg·mL⁻¹. Aliquots of 0.5 – 1 µL of these samples were spotted and solvent allowed to evaporate. MALDI-TOF MS data was processed and images prepared using mMass software (www.mmass.org). Mass spectrometry was also performed using an Agilent 1260 Infinity HPLC coupled with an Agilent 6230 TOF LC/MS. Samples were prepared by dissolving the metal complex in an ESI-compatible solvent at a concentration of 1 mg/mL in an N₂-containing glove box.

Elemental analysis was performed on a Perkin Elmer 2400 CHN analyzer at the Department of Ocean Sciences, Memorial University, Newfoundland, Canada. The X-ray structures of **5.1a**, **5.1b** and **5.2** were acquired using a Rigaku AFC8-Saturn 70 single crystal X-ray diffractometer equipped with an Oxford Cryosystems 800 Series Cryostream Cooler containing an AD51 Dry Air Unit and a SHINE optic. Copolymerization reactions with in situ monitoring were performed using a 100 mL Parr

4560 reactor equipped with a Mettler Toledo SiComp ATR Sentinel sensor connected to a ReactIR 15 base unit through a silver-halide Fiber-to-Sentinel conduit. Profiles for absorbance height at 1750 cm^{-1} (polycyclohexene carbonate) and it is important to note that IR absorbance increases linearly with the concentration of polycarbonate.^{12,46} Gel permeation chromatography (GPC) for polymer molecular weight and dispersity determination was performed using an Agilent 1260 Infinity HPLC equipped with two Phenogel 10^3 \AA , $300 \times 4.60\text{ mm}$ columns with THF as an eluent at a flow rate of 0.30 mLmin^{-1} . The HPLC was coupled to triple detectors manufactured by Wyatt technologies (along with Astra 6 software package); Multi-angle Light Scattering (MALS), ViscoStar II viscometer and Optilab T-rEX refractometer. The proligands **H₂L1** were prepared using a previously described procedure and dried in anhydrous THF using MgSO_4 under N_2 .⁴⁶

5.4.2 Synthesis of **5.1**

H₂L1 (1.00 g, 2.71 mmol) and NaH (0.260 g, 10.8 mmol) were added to a Schlenk tube and cooled to $-78\text{ }^\circ\text{C}$. THF (50 mL) was added, resulting in an off-white suspension, warmed to $22\text{ }^\circ\text{C}$ and stirred under N_2 for 24 h. The mixture was transferred via filter cannula to a Schlenk flask containing a purple suspension of $\text{CrCl}_3(\text{THF})_3$ (1.02 g, 2.71 mmol) in THF cooled to $-78\text{ }^\circ\text{C}$ then warmed to $22\text{ }^\circ\text{C}$ and stirred under N_2 for 24 h. Volatiles from the resulting green solution were removed under reduced pressure to produce a dark green solid. This solid was dissolved in a mixture of dichloromethane and THF then the resulting dark green mixture was filtered through a Celite bed and the filtrate collected. Volatiles were removed under reduced pressure and dried *in vacuo* to a

yield 1.01 g (86%, assuming **5.1a** as product) of a reddish-brown solid. Crystals suitable for X-ray diffraction were obtained via slow evaporation of a **5.1**/DMAP in acetonitrile at 22 °C in a N₂-containing glove box. MALDI-TOF MS positive mode, anthracene: *m/z* (%) = 418.0 (72) [Cr**L1**]⁺ ; 453.0 (100) [CrCl**L1**]⁺ ; 836.2 (30) {[Cr**L1**]₂}⁺; 853.2 {OH[Cr**L1**]₂}⁺; 871.1 (14) {[Cr(μ-OH)-**L1**]₂}⁺. MALDI-TOF MS negative mode, anthracene: *m/z* (%) = 453.0 (100) [CrCl**L1**]⁻; 488.1 (98) [CrCl₂**L1**]⁻. *Anal.* Calc. for C₄₆H₆₂Cr₂N₄O₆·0.4(C₄₆H₆₀ClCr₂N₄O₄): C, 62.67; H, 7.02; N, 6.36. Found: C, 62.66; H, 7.10; N, 6.41.

5.4.3 Representative procedure for CHO/CO₂ copolymerization

In an N₂-filled glove box, bis(triphenylphosphine)iminium chloride, PPNCl, (54.9 mg, 0.957 mmol) and **5.1** (0.0400 g, 0.957 mmol) were dissolved in dichloromethane (5 mL) in a vial, resulting in a green solution, which was stirred for 15 minutes. Dichloromethane was then removed under reduced pressure followed by the addition of cyclohexene oxide (4.70 g, 47.9 mmol). The resulting green solution was taken out of the glove box and injected via syringe into a pre-dried (under vacuum at 80 °C overnight) pressure reactor and pressurized to 40 bar CO₂ pressure (99.998% pure) then stirred at 60 °C for 24 h. Upon cooling to room temperature, the reactor was vented into the fume hood and opened. A clear green solid evenly distributed at the bottom of the vessel was obtained, and a sample was taken for characterization and quantification by ¹H NMR. The polymer was dissolved in dichloromethane and precipitated using cold 5% acidified methanol (using 1 M HCl, v/v), where the resulting white solid was collected and dried in a vacuum oven overnight at 60 °C.

5.4.4 X-ray diffraction analysis procedure for 5.1a

Crystallographic and structure refinement data are given in Appendix C, Table C-6. Crystallographic data was collected by Timothy S. Anderson and solved by Jennifer N. Murphy from the Department of Chemistry at Memorial University of Newfoundland, St. John's, Newfoundland, A1B 3X7, Canada. Single crystals of $C_{48}H_{65}Cr_2N_5O_6$ were crystallized from acetonitrile and were green. The crystal was kept at 100 K during data collection. Using Olex2,⁴⁷ the structure was solved with the ShelXT⁴⁸ structure solution program using Intrinsic Phasing and refined with the ShelXL⁴⁹ refinement package using Least Squares minimisation.

5.4.5 X-ray diffraction analysis procedure for 5.1b

Crystallographic and structure refinement data are given in Appendix C, Table C-6. Crystallographic data was collected and solved by Jennifer N. Murphy from the Department of Chemistry at Memorial University of Newfoundland, St. John's, Newfoundland, A1B 3X7, Canada. Single crystals of $C_{47}H_{62}Cl_4Cr_2N_4O_4$ were crystallized from dichloromethane and were green. The crystal was kept at 100 K during data collection. Using Olex2,⁴⁷ the structure was solved with the ShelXT⁴⁸ structure solution program using Intrinsic Phasing and refined with the ShelXL⁴⁹ refinement package using Least Squares minimisation.

5.5 References

1. T. Dudev and C. Lim, *J. Am. Chem. Soc.*, 1998, **120**, 4450-4458.
2. S. J. Poland and D. J. Darensbourg, *Green Chem.*, 2017, **19**, 4990-5011.
3. J. Wang, X. Shan, S. Shan, H. Su, S. Wu and Q. Jia, *Catal. Commun.*, 2015, **59**, 116-121.
4. D. J. Darensbourg, M. Ulusoy, O. Karroonnirum, R. R. Poland, J. H. Reibenspies and B. Çetinkaya, *Macromolecules*, 2009, **42**, 6992-6998.
5. D. J. Darensbourg, R. R. Poland and A. L. Strickland, *J. Polym. Sci., Part A: Polym. Chem.*, 2012, **50**, 127-133.
6. D. J. Darensbourg and W.-C. Chung, *Macromolecules*, 2014, **47**, 4943-4948.
7. D. J. Darensbourg, W.-C. Chung, C. J. Arp, F.-T. Tsai and S. J. Kyran, *Macromolecules*, 2014, **47**, 7347-7353.
8. K. Xu, J.-G. Chen, W. Kuan, Z.-W. Liu, J.-Q. Jiang and Z.-T. Liu, *J. Macromol. Sci., Pure Appl. Chem.*, 2014, **51**, 589-597.
9. B. Han, L. Zhang, S. J. Kyran, B. Liu, Z. Duan and D. J. Darensbourg, *J. Polym. Sci., Part A: Polym. Chem.*, 2016, **54**, 1938-1944.
10. K. Devaine-Pressing, L. N. Dawe and C. M. Kozak, *Polym. Chem.*, 2015, **6**, 6305-6315.
11. G. Si, L. Zhang, B. Han, H. Zhang, X. Li and B. Liu, *RSC Adv.*, 2016, **6**, 22821-22826.
12. K. Ni and C. M. Kozak, *Inorg. Chem.*, 2018, **57**, 3097-3106.

13. L. Cuesta-Aluja, M. Djoufak, A. Aghmiz, R. Rivas, L. Christ and A. M. Masdeu-Bultó, *J. Mol. Catal. A: Chem.*, 2014, **381**, 161-170.
14. J. Liang, Y.-Q. Xie, X.-S. Wang, Q. Wang, T.-T. Liu, Y.-B. Huang and R. Cao, *Chem. Commun.*, 2018, **54**, 342-345.
15. M. Adolph, T. A. Zevaco, C. Altesleben, O. Walter and E. Dinjus, *Dalton Trans.*, 2014, **43**, 3285-3296.
16. R. L. Paddock and S. T. Nguyen, *J. Am. Chem. Soc.*, 2001, **123**, 11498-11499.
17. L. S. Morris, M. I. Childers and G. W. Coates, *Angew. Chem. Int. Ed.*, 2018, **57**, 5731-5734.
18. P. Chen, M. H. Chisholm, J. C. Gallucci, X. Zhang and Z. Zhou, *Inorg. Chem.*, 2005, **44**, 2588-2595.
19. Y. Wang and D. J. Darensbourg, *Coord. Chem. Rev.*, 2018, **372**, 85-100.
20. D. J. Darensbourg, R. M. Mackiewicz, J. L. Rodgers, C. C. Fang, D. R. Billodeaux and J. H. Reibenspies, *Inorg. Chem.*, 2004, **43**, 6024-6034.
21. D.-Y. Rao, B. Li, R. Zhang, H. Wang and X.-B. Lu, *Inorg. Chem.*, 2009, **48**, 2830-2836.
22. R. K. Dean, K. Devaine-Pressing, L. N. Dawe and C. M. Kozak, *Dalton Trans.*, 2013, **42**, 9233-9244.
23. J. A. Castro-Osma, K. J. Lamb and M. North, *ACS Catal.*, 2016, **6**, 5012-5025.
24. S. Iksi, A. Aghmiz, R. Rivas, M. D. González, L. Cuesta-Aluja, J. Castilla, A. Orejón, F. El Guemmout and A. M. Masdeu-Bultó, *J. Mol. Catal. A: Chem.*, 2014, **383-384**, 143-152.

25. D. Adhikari, S. T. Nguyen and M.-H. Baik, *Chem. Commun.*, 2014, **50**, 2676-2678.
26. D. J. Darensbourg and J. C. Yarbrough, *J. Am. Chem. Soc.*, 2002, **124**, 6335-6342.
27. K. Devaine-Pressing and C. M. Kozak, *ChemSusChem*, 2017, **10**, 1266-1273.
28. D. J. Darensbourg, *Chem. Rev.*, 2007, **107**, 2388-2410.
29. S. Elmas, M. A. Subhani, M. Harrer, W. Leitner, J. Sundermeyer and T. E. Müller, *Catal. Sci. Technol.*, 2014, **4**, 1652-1657.
30. R. K. Dean, L. N. Dawe and C. M. Kozak, *Inorg. Chem.*, 2012, **51**, 9095-9103.
31. C. M. Kozak, A. M. Woods, C. S. Bottaro, K. Devaine-Pressing and K. Ni, *Faraday Discuss.*, 2015, **183**, 31-46.
32. D. J. Darensbourg, E. B. Frantz and J. R. Andreatta, *Inorg. Chim. Acta*, 2007, **360**, 523-528.
33. J. Y. Jeon, J. H. Park, D. S. Park, S. Y. Park, C. S. Lee, M. J. Go, J. Lee and B. Y. Lee, *Inorg. Chem. Commun.*, 2014, **44**, 148-150.
34. A. Buchard, M. Kember, K. Sandeman and C. K. Williams, *Chem. Commun.*, 2011, **47**, 212-214.
35. M. R. Kember, A. J. P. White and C. K. Williams, *Macromolecules*, 2010, **43**, 2291-2298.
36. M. Taherimehr, S. M. Al-Amsyar, C. J. Whiteoak, A. W. Kleij and P. P. Pescarmona, *Green Chem.*, 2013, **15**, 3083-3090.
37. K. Nozaki, K. Nakano and T. Hiyama, *J. Am. Chem. Soc.*, 1999, **121**, 11008-11009.
38. K. Ni, V. Paniez-Grave and C. M. Kozak, *Organometallics*, 2018, **37**, 2507-2518.

39. Z.-H. Ni, H.-Z. Kou, L.-F. Zhang, C. Ge, R.-J. Wang and A.-L. Cui, *J. Chem. Crystallogr.*, 2006, **36**, 465-472.
40. D. J. Darensbourg and A. I. Moncada, *Inorg. Chem.*, 2008, **47**, 10000-10008.
41. B. Shaabani, A. A. Khandar, N. Ramazani, M. Fleck, H. Mobaiyen and L. Cunha-Silva, *J. Coord. Chem.*, 2017, **70**, 696-708.
42. D. J. Darensbourg and R. M. Mackiewicz, *J. Am. Chem. Soc.*, 2005, **127**, 14026-14038.
43. M. R. Kember, F. Jutz, A. Buchard, A. J. P. White and C. K. Williams, *Chem. Sci.*, 2012, **3**, 1245-1255.
44. S. Klaus, S. I. Vagin, M. W. Lehenmeier, P. Deglmann, A. K. Brym and B. Rieger, *Macromolecules*, 2011, **44**, 9508-9516.
45. J. Liu, W.-M. Ren, Y. Liu and X.-B. Lu, *Macromolecules*, 2013, **46**, 1343-1349.
46. M. W. Lehenmeier, S. Kissling, P. T. Altenbuchner, C. Bruckmeier, P. Deglmann, A.-K. Brym and B. Rieger, *Angew. Chem. Int. Ed.*, 2013, **52**, 9821-9826.
47. D. Alhashmialameer, J. Collins, K. Hattenhauer and F. M. Kerton, *Catal. Sci. Technol.*, 2016, **6**, 5364-5373.
48. O. V. Dolomanov, L. J. Bourhis, R. J. Gildea, J. A. K. Howard and H. Puschmann, *J. Appl. Crystallogr.*, 2009, **42**, 339-341.
49. G. Sheldrick, *Acta Crystallogr. Sect. A*, 2015, **71**, 3-8.
50. G. Sheldrick, *Acta Crystallogr. Sect. C*, 2015, **71**, 3-8.

Chapter 6: Attempted Experiments, Future Directions and Conclusions

6.1 Introduction

This chapter contains results obtained that were proved inconclusive at this stage and were therefore not included in the main results of Chapters 3 – 5 when presented. Chapter 3 of this thesis described polycarbonate synthesis from CHO/CO₂ copolymerization, using a Co amino-bis(phenolate) complex for the first time in the Kozak group. Compound **3.1** was selective toward cyclohexene carbonate production when co-catalyzed by TBAB (tetrabutylammonium bromide) with increased selectivity at higher temperature while simultaneously diminishing polycarbonate selectivity. The cyclohexene carbonate produced was isolated and characterized using ¹H and ¹³C NMR spectroscopy which was shown to be the *cis*-isomer.¹ Some researchers have shown that poly(cyclohexene carbonate) can be synthesized by ring-opening polymerization of cyclohexene carbonate (CHC).^{2,3} Experiments were conducted to investigate ROP of CHC using **3.1** and these results are presented below.

Chapter 4 involved a Cr(III) amino-bis(phenolate) complex which exhibited activity toward ROP of CHO to produce PCHO, where different reaction parameters were investigated. Efforts were made to afford CO₂/epoxide copolymerization to polycarbonate and coupling to cyclic carbonate. The complex exhibited different color changes in different environments such as coordinating *vs* non-coordinating species; therefore, UV-visible spectroscopy was used to further understand the nature of the complex under these

conditions. Only preliminary results were acquired for the investigation **4.1** in the presence of THF. Compound **4.1** was highly active towards PCHO formation for reactions involving CHO and low conversion toward PCHO in the presence of CO₂, therefore **4.1** was modified by changing the phenolate substituents in the *ortho* and *para* positions from *tert*-butyl to methyl, which afforded complexes **5.1a** and **5.1b**. These new complexes were active toward CO₂/CHO copolymerization with excellent CO₂ incorporation and polymer selectivity. Using propylene oxide resulted in only cyclic carbonate being produced. However, preliminary PO/CHO/CO₂ terpolymerization results showed potential for incorporation of PO into polycarbonate formation when **5.1**/PPNN₃ is used. Herein, the findings of these studies are discussed.

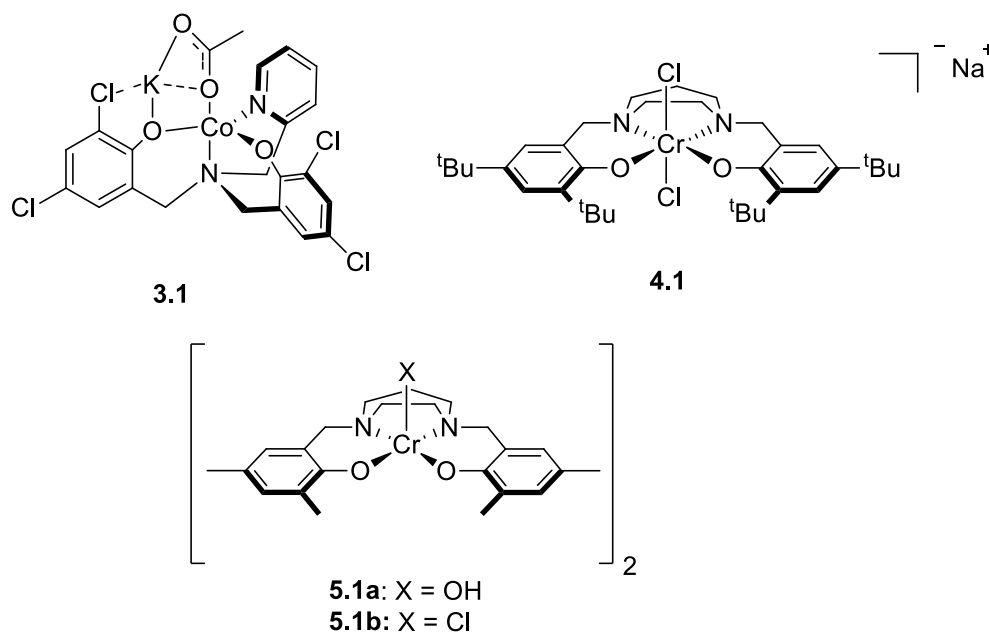


Figure 6.1: Co and Cr amino-bis(phenolate) complexes discussed in this chapter.

6.2 Discussion

6.2.1 Ring-opening polymerization of cyclohexene carbonate using **3.1**

The copolymerization of CHO/CO₂ using cobalt complex **3.1** was monitored using in situ FTIR spectroscopy as mentioned in Chapter 3. FTIR profiles for CHO/CO₂ copolymerization reactions by **3.1**/TBAB or **3.1**/PPNCl both showed an initial production of CHC followed by polymer formation (Chapter 3, **Figure 3.2** and **Figure 6.2**) where **3.1**/PPNCl showed a decrease in CHC upon formation of PCHC (**Figure 6.2**). Due to this observation, the afforded CHC was isolated and purified using distillation under reduced pressure. Characterization of the purified CHC by ¹H and ¹³C NMR spectroscopy showed the *cis*-isomer (see Appendix A, Figures A-14 and A-15). To investigate the potential for a CHC ring-opening polymerization mechanism, mixtures of CHC, **3.1** and a co-catalyst (PPNCl or TBAB) were dissolved in toluene and stirred under identical conditions for copolymerization reactions reported in Chapter 3. In situ FTIR monitoring showed no evidence of polycarbonate formation. Further reactions involving the use of benzyl alcohol as a co-initiator² both with and without CO₂ were also employed but no polycarbonate was detected. Guillaume and co-workers showed the synthesis of PCHC from *trans*-CHC and computational studies performed showed that the calculated ΔG for ring-opening of *trans*-CHC using methanol was -15 kJ mol^{-1} whereas *cis*-CHC was 10.9 kJ mol^{-1} both at 127 K, suggesting that it is more difficult to ring-open the *cis*-isomer. Moreover, they did not observe any PCHC formation when *cis*-CHC was used, which is the same as here.

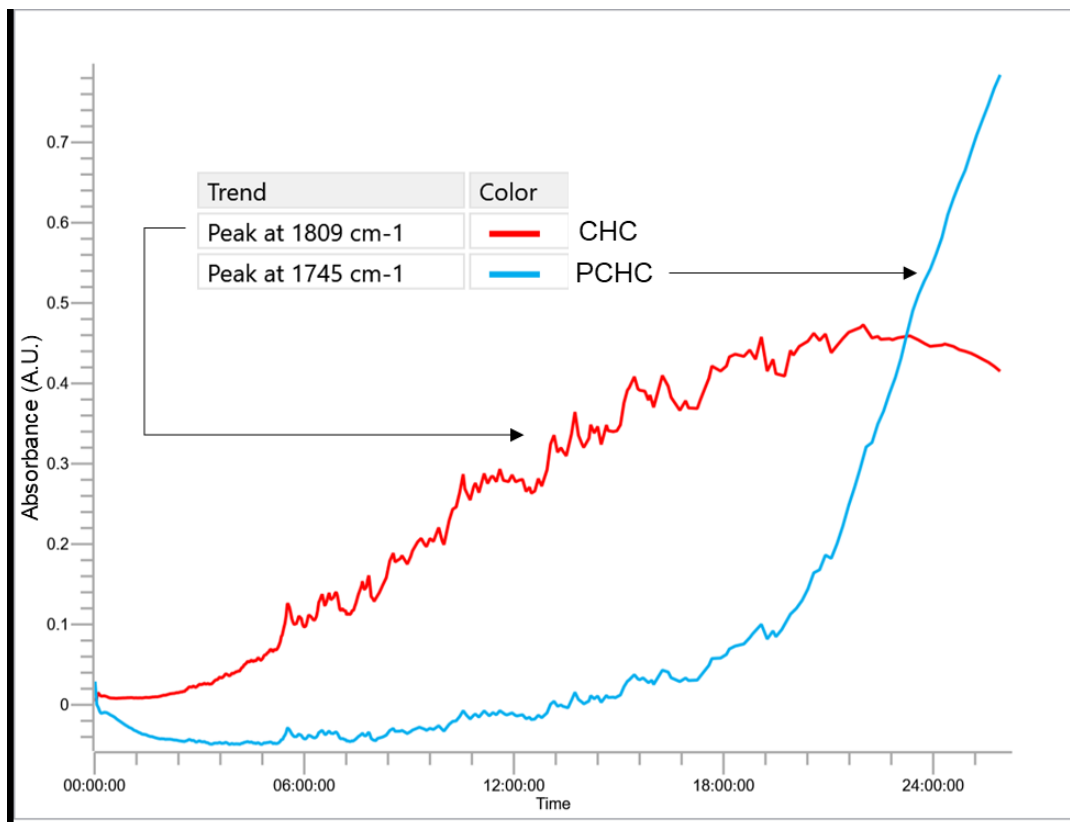


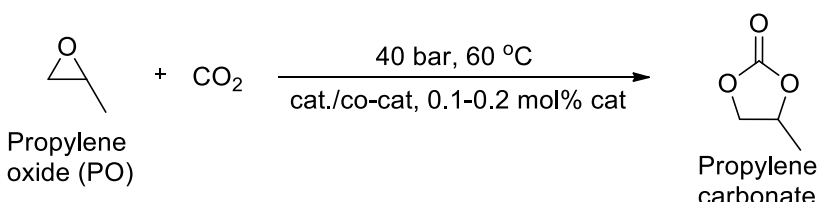
Figure 6.2: Profiles for in situ monitored FTIR absorbances at 1745 cm^{-1} (PCHC) and 1809 cm^{-1} (CHC) for CHO/ CO_2 copolymerization over 24 h using **3.1**/PPNCl.

6.2.2 CO_2 /epoxide coupling and attempted copolymerization, and UV/vis studies using **4.1**

Cr(III) complex **4.1** (**Figure 6.1**) was highly active toward ring-opening polymerization of CHO to produce PCHO but no activity for ROP of PO. In the presence of CO_2 however, **4.1** was active toward cyclic carbonate formation from PO/ CO_2 coupling when co-catalyzed by PPNCl or TBAB, and preliminary results are summarized in **Table 6.1**. Varying the co-catalyst between PPNCl and TBAB appeared to have a minimal effect on conversion (**Table 6.1**, entry 1 vs entry 2). Decreasing temperature

from 60 °C to 40 °C, however, showed approximately 25% decrease in conversion (entry 1 vs entry 3). At a lower catalyst loading however, an increase in temperature resulted in a decrease in conversion (entry 4 vs entry 5). The effect of CO₂ pressure was observed in entries 4, 6 and 7 with lower pressure giving lower conversion, which suggests that 40 bar CO₂ may be the optimal pressure at 0.1 mol% catalyst loading.

Table 6.1: Cycloaddition of propylene oxide and CO₂ using **4.1**.^a



Propylene oxide (PO) + CO₂ $\xrightarrow[\text{cat./co-cat, 0.1-0.2 mol\% cat}]{40 \text{ bar, } 60 \text{ }^{\circ}\text{C}}$ Propylene carbonate

Entry	[Cat]:[CHO]	Temperature (°C)	Conversion ^b (%)	TON
1	1:500	60	>99	495
2 ^c	1:500	60	95	475
3	1:500	40	75	375
4	1:1000	60	82	820
5	1:1000	80	72	720
6 ^d	1:1000	60	78	780
7 ^e	1:1000	60	64	640

^aReaction conditions: 40 bar CO₂ pressure, 60 °C, PPNCI co-catalyst and 22 h.

^bConversion determined by ¹H NMR. ^cTBAB used as a co-catalyst here. ^dReaction performed at 20 bar CO₂ pressure. ^eReaction performed at 10 bar CO₂ pressure.

To promote copolymerization of CO₂ and CHO using **4.1**, some experiments were performed with efforts of inhibiting homopolymerization. In the absence of co-catalyst **4.1** was added to the reactor which allowed brief exposure to air, then evacuated, followed by injection of CHO and pressurization with CO₂. FTIR monitoring showed no reaction occurred. Repeating this method with the reactor taken into a nitrogen-filled glove box, showed a 14% conversion to PCHO. Similar results showing low conversion were also observed when performed with co-catalysts such as DMAP and PPNCI.

Modification of **4.1** to produce **5.1a** and **5.1b** suggests that its inability to catalyze polycarbonate formation may have been a case of steric hinderance where the methyl group promoted some steric relief at the Cr center.

Due to observed color changes of Cr complexes in the presence of coordinating species, previous work in the Kozak group has used UV-vis spectroscopy to monitor the binding of various species such as N_3^- , Cl^- and CHO to the Cr metal center.⁴ Increasing the PPnCl:catalyst ratio led to a decrease in intensity of a peak at 616 nm corresponding to a dimeric Cr complex, and growth of a new peak at 537 nm corresponding to a monomeric ionic complex. For **4.1**, however, a similar procedure using various ratios of THF:catalyst in dichloromethane, showed no significant evolution or disappearance of peaks in the visible region of the spectrum although there was a visible color change especially at the ratio of 1:400 (**Figure 6.3**). This suggests that the color change in this THF/ CH_2Cl_2 solvent combination is not significant enough to result in a clear isosbestic point. Additional experiments using a more nucleophilic species such as N_3^- , using PPNN₃, may be more effective.

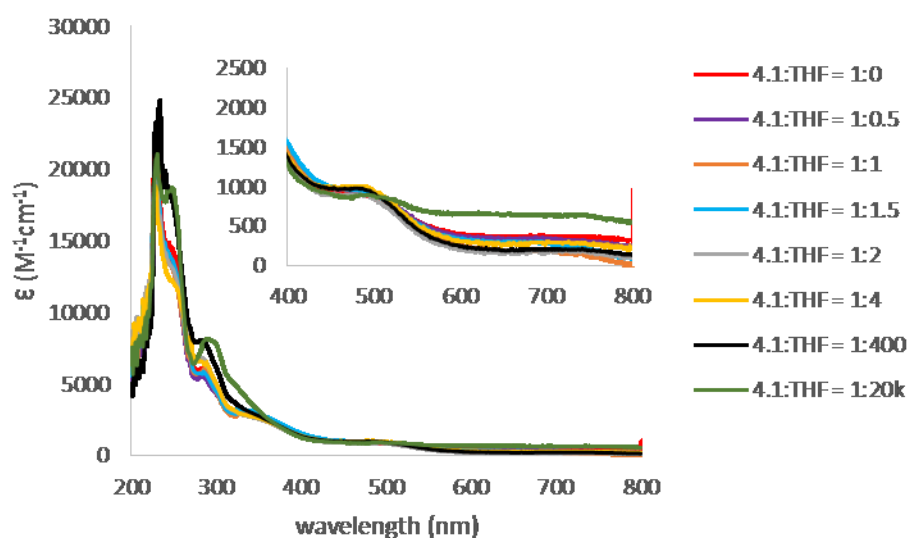


Figure 6.3: UV-vis spectra of **4.1** in dichloromethane with various ratios of THF added.

6.2.3 Terpolymerization of epoxides using **5.1**

Terpolymerization of PO/CHO/CO₂ and VCHO/CHO/CO₂ has been previously shown using Cr-salan complexes.^{5,6} Compound **5.1** was employed for attempted terpolymerization of CHO/CO₂ with PO, ECH (epichlorohydrin) and glycidol when co-catalyzed by PPNN₃ using a similar procedure outlined in Chapter 5 for CHO/CO₂ copolymerization, and preliminary results are summarized in **Table 6.2**. Polycarbonate formation was monitored using in situ FTIR spectroscopy for absorbances created by C=O functionality on the polycarbonate backbone. Different polymeric monomer units could not be identified due to similarity in C=O absorbances (around 1750 cm⁻¹). Therefore, ¹H NMR spectroscopy was used to determine the ratios of polycarbonate formed (m:n, **Table 6.2**) from different epoxides, by comparing methine signals. When terpolymerization of CHO/PO/CO₂ was explored, increasing the ratio of PO:CHO

showed a trend towards increased PO incorporation (**Table 6.2**, entries 2, 3 and 4) into the polycarbonate, thus affording the highest PPC:PCHC ratio of 1:6 (**Table 6.2**, entry 3). The glass transition temperature (T_g) of pure PCHC and PPC produced by CO₂/epoxide copolymerization are 118 °C and 42 °C respectively.⁷ It is worth noting that variations are possible especially at different molecular weights. Nevertheless, there was a decrease in T_g following a simultaneous increase in PO incorporation (entries 2, 3 and 4). This suggests the presence of polymer chains containing cyclohexene carbonate and propylene carbonate units as it is expected for the T_g of the terpolymer to lie somewhere between that of the respective pure copolymers (i.e. PPC and PCHC).⁵ When DMAP was used as a co-catalyst for CHO/PO/CO₂ terpolymerization, the PCHC:PPC ratio was approximately the same (entry 4 vs 5) but a decrease in molecular weight and an increase in \bar{D} were observed. This suggests the occurrence of a less controlled process. CHO/ECH/CO₂ terpolymerization also showed a decrease in T_g which suggests the presence of polymer chains having cyclohexene carbonate and chloropropylene carbonate, as the T_g of pure atactic poly(chloropropylene carbonate) is 31 °C.⁸ Interestingly, when CHO/glycidol/CO₂ terpolymerization (entry 7) was explored, no conversion of either monomer was observed. This indicates an inhibition of the catalyst system occurring in the presence of glycidol likely due to irreversible binding of glycidol to the Cr(III) metal center thus affording an inactive species. Characterization of CHO/PO/CO₂ terpolymers by MALDI-TOF MS produced a very complicated mass spectrum showing a vast number of peaks without the appearance of a clear Gaussian distribution which suggests that the terpolymerization process may be random. Further inspection of peaks however, showed m/z differences of both 102.1 and 142.1, corresponding to propylene carbonate and

cyclohexene carbonate monomers respectively. It is worth noting that these results strongly indicate but do not confirm the presence single polymer chains containing both cyclohexene carbonate and propylene carbonate units therefore, another NMR characterization technique such as Diffusion-Ordered Spectroscopy (DOSY) can be used.

Table 6.2: Terpolymerization of CO₂/CHO/epoxides using **5.1**.^a

Entry	Ratio (CHO:PO)	Isolated yield (%)	^b Ratio of m:n	<i>M_n</i> (g/mol)	<i>D</i>	<i>T_g</i> / <i>M.p.</i> (°C)
1	1:0	84	-	20710	1.09	97.7/ 110.6
2	9:1	67	1:35	18150	1.1	99.7/107.8
3	7:3	50	1:13	9771	1.04	89.6/ 80.0
4	4:6	38	1:6	8911	1.09	71.9/ 80.6
5 ^c	4:6	34	1:5.5	1980	1.30	78.3/ 88.6
6 ^d	4:6	18	1:21	2285	1.08	63.2/ 54.9
7 ^e	4:6	0	NA	NA	NA	NA

^aReaction conditions: 0.2 mol% catalyst loading, 60 °C, 40 bar CO₂ and 24 h unless otherwise stated. ^bDetermined by ¹H NMR. ^cDMAP used as a co-catalyst. ^dEpichlorohydrin and CHO used here. ^eGlycidol and CHO used here.

6.3 Experimental

General experimental conditions were previously discussed in Chapter 5.

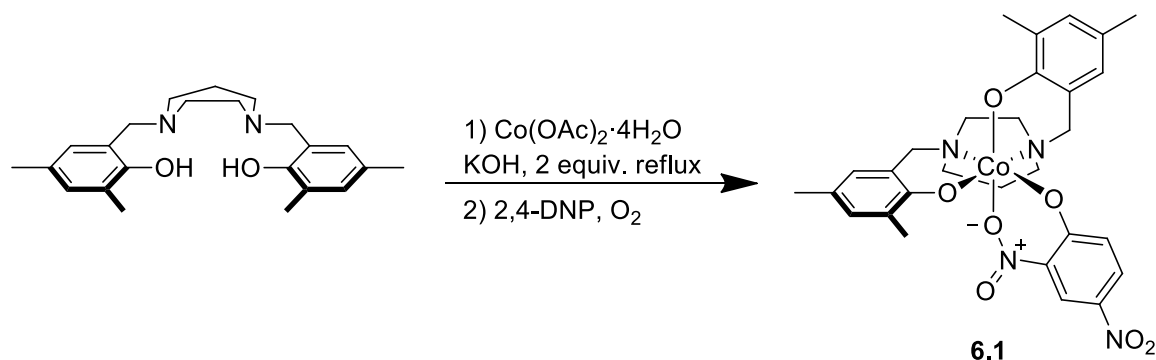
6.3.1 Attempted ring-opening polymerization of CHC

Cyclohexene carbonate (1.00 g, 7.03 mmol), TBAB (11.3 mg, 0.0349 mmol), benzyl alcohol (0.0379 g, 0.0349 mmol) and **3.1** (18.0 mg, 0.0349 mmol) were dissolved in toluene (3.51 mL) then injected via syringe into a pre-dried pressure reactor and

pressurized to 40 bar CO₂ then stirred at 80 °C for 24 h. Upon cooling to room temperature, the reactor was vented into a fume hood and opened. A dark purple solution remained, and an aliquot was taken for characterization and quantification by ¹H NMR.

6.4 Ideas for future directions

Given the success using **5.1** for CHO/CO₂ copolymerization, a potential future direction for the cobalt project could involve the synthesis of Co complexes using the new amino-bis(phenolate) ligand, **H₂L1** from Chapter 5 (6,6'-((1,4-diazepane-1,4-diyl)bis-(methylene))bis(2,4-dimethylphenol)). The first step involves simultaneous deprotonation of the proligand and metalation using Co(OAc)₂·4H₂O which will be isolated and characterized then subsequent oxidation and addition of a 2,4-dinitrophenolate ligand (**Scheme 6.1**) Once successfully characterized, investigations into catalyst activity for CO₂/epoxide coupling should follow.



Scheme 6.1: Synthetic route to new Co(III) amino-bis(phenolate) complex.

A possible lucrative route to polyester synthesis is via metal-catalyzed alternating ring-opening copolymerization of epoxides and cyclic diacid anhydrides.⁹⁻¹² Variants

is a literary review on Co and Cr-containing catalyst systems for CO₂/epoxide coupling to produce cyclic carbonates and polycarbonates, highlighting any advantages of the catalyst systems along with any interesting mechanistic considerations. In the absence of CO₂ some catalysts can homopolymerize epoxides to produce polyethers therefore, a brief survey on metal and metal-free catalyst systems capable of epoxide homopolymerization, including mechanistic aspects was also discussed.

Some investigations in the literature have shown that ancillary ligands play an important role in catalyst activity and selectivity during catalyst development. For example, some catalysts are only selective toward the production of cyclic carbonate production which are useful materials with a wide variety of applications such as polar aprotic solvents with low volatility and precursor compounds for polymer synthesis. Chapter 2 involved the modification of previously reported Co(II)-containing amino-bis(phenolate) complexes in the Kozak group, via oxidation to Co(III) and addition of various ancillary ligands such as [2,4-DNP]⁻, OAc, ⁻O₂CCF₃, Cl⁻, OSO₂CF₃ and 4-NP. Due to a lack of unequivocal characterization, some complexes were deemed inconclusive hence not employed as catalysts. However, Co complexes with sufficient characterization were employed as catalysts for CO₂/epoxide coupling reactions where selectivity toward cyclic carbonates was observed. Temperature, co-catalyst and ligand phenolate substituent (*t*-butyl vs Cl) effects were observed and therefore, the most active catalyst system was **2.8a**/TBAB. Functional group tolerance was also demonstrated as various epoxides were screened for cyclic carbonate production.

Chapter 3 demonstrated a shift in catalyst selectivity by increasing Lewis acidity at the Co(II) metal center via introducing electron-withdrawing chlorine *ortho* and *para*-phenolate substituents. Compound **3.1** was produced, and this afforded selectivity towards polycarbonate synthesis from CHO/CO₂ with moderate conversions, selectivity and high CO₂ incorporation. Of importance is that compound **3.1** also afforded the production of the unusual *cis* isomer of cyclohexene carbonate at elevated temperatures. Structural characterization of **3.1** showed the presence of Co·KOAc adducts in the solid state. The acetate ions served as minor initiators during the polymerization reaction as shown by end group analysis using MALDI-TOF MS. This represented one of two reports involving Co-based catalyst systems containing these types of tripodal amino-bis(phenolate) ligands for copolymerization of CHO and CO₂. Although these results represented the first observation of CHO/CO₂ copolymerization using a Co amino-bis(phenolate) complex in the Kozak group, moving on to a different project was necessary.

Chapter 4 described synthesis and characterization of new Cr(III) amino-bis(phenolate) complexes, **4.1** – **4.4**, bearing a homopiperazine (**4.1** and **4.2**) and piperazine (**4.3** and **4.4**) backbones, and *ortho-para tert*-butyl and methoxy functional groups on the phenolate donors. Characterization methods such as MALDI-TOF MS, elemental analysis and X-ray diffraction analysis were employed to elucidate the complex structures. The Cr(III) complexes showed high activity toward ring-opening polymerization of cyclohexene oxide resulting in high molecular weight poly(cyclohexene oxide) without the use of a co-catalyst. Various reaction parameters

such as catalyst loading, temperature and solvent effects were investigated. These Cr(III) amino-bis(phenolate) complexes were proposed to exist as “ate” complexes with *cis*-axial chloride ligands which serve as nucleophiles for epoxide ring-opening to initiate the ROP process. X-ray diffraction analysis showed an interesting molecular structure where one of the phenolate donors is protonated thus affording an overall neutral species which was likely due to the presence of adventitious water during crystallization. Kinetic studies of **4.1** revealed an activation barrier for PCHO formation to be 68.6 kJ/mol. Further analysis of data indicated a polymerization process similar to that of condensation-polymerization, more specifically, chain-growth polymerization.

To afford selectivity toward CHO/CO₂ copolymerization **4.1** was modified by changing the phenolate *ortho*- and *para*-phenolate functional groups to methyl groups thus producing **5.1**. Characterization by MALDI-TOF MS, elemental analysis and X-ray diffraction analysis strongly suggested the presence of both μ -hydroxo-bridged and chloride-bridged dimeric Cr(III) amino-bis(phenolate) species of **5.1**. Catalytic activity showed a switch in selectivity from homopolymerization of CHO to copolymerization with CO₂, with excellent CO₂ incorporation and polycarbonate selectivity. This suggested that steric bulk created by *tert*-butyl groups (compound **4.1**) may have inhibited copolymerization from occurring. Co-catalyst effects were observed where PPNN₃ exhibited the highest initial reaction rate when monitored by in situ FTIR spectroscopy and that more than a 1:1 ratio of **5.1**:PPNN₃ slowed down the initial rate of copolymerization. Polymer end-group analysis using MALDI-TOF mass spectrometry,

suggests initiation by external nucleophiles of the co-catalyst as well as nucleophilic ligands displaced from the metal center, such as chloride.

A summary of attempted experiments performed was presented in Chapter 6. In situ FTIR monitoring may have indicated that **3.1**/co-catalyst forms cyclic carbonate, which is subsequently ring-opening to form polycarbonate. Experiments to investigate this phenomenon, by starting with cyclohexene carbonate/**3.1** showed no activity of ring-opening polymerization. Compound **4.1** exhibits a color change in a coordinating vs non-coordinating (THF vs CH₂Cl₂) environment therefore UV-vis was employed to monitor this behaviour. Unfortunately, UV-vis data clearly indicating the formation of a new species (i.e. **4.1**·THF) were not obtained due to overlapping bands of the different species. Further attempted experiments involved the use of **5.1** for terpolymerization of epoxides with CO₂. Preliminary results indicated the production of CHO/PO/CO₂ and CHO/ECH/CO₂ terpolymers using NMR and DSC data (*T_g* and melting point). A CHO/glycidol/CO₂ terpolymerization attempt however, showed no polymerization activity which suggested catalyst inactivity caused by glycidol.

To summarize, this thesis showed the synthesis and characterization of a series of cobalt(II)/(III) complexes which were able to couple and copolymerize carbon dioxide with epoxides. Results from X-ray diffraction analysis and polymer end group analysis by MALDI-TOF MS for one of the cobalt catalysts, showed the source of acetate which served as minor initiators during the polymerization process. Using a slightly different ligand, chromium(III) complex **4.1** was synthesized, which was able to homopolymerize CHO. With a slight modification, **5.1** was afforded which was able to copolymerize CHO

and CO₂ to produce poly(cyclohexene carbonate) with high CO₂ incorporation and selectivity.

6.6 References

1. A. Buchard, M. Kember, K. Sandeman and C. K Williams, *Chem. Commun.*, 2011, **47**, 212-214.
2. W. Guerin, A. K. Diallo, E. Kirilov, M. Helou, M. Slawinski, J.-M. Brusson, J.-F. Carpentier and S. M. Guillaume, *Macromolecules*, 2014, **47**, 4230-4235.
3. A. K. Diallo, W. Guerin, M. Slawinski, J.-M. Brusson, J.-F. Carpentier and S. M. Guillaume, *Macromolecules*, 2015, **48**, 3247-3256.
4. K. Ni, V. Paniez-Grave and C. M. Kozak, *Organometallics*, 2018, **37**, 2507-2518.
5. D. J. Darensbourg, M. Ulusoy, O. Karroonnirum, R. R. Poland, J. H. Reibenspies and B. Çetinkaya, *Macromolecules*, 2009, **42**, 6992-6998.
6. D. J. Darensbourg, R. R. Poland and A. L. Strickland, *J. Polym. Sci., Part A: Polym. Chem.*, 2012, **50**, 127-133.
7. M. R. Kember, A. Buchard and C. K. Williams, *Chem. Commun.*, 2011, **47**, 141-163.
8. G.-P. Wu, P.-X. Xu, X.-B. Lu, Y.-P. Zu, S.-H. Wei, W.-M. Ren and D. J. Darensbourg, *Macromolecules*, 2013, **46**, 2128-2133.
9. M. Hatazawa, R. Takahashi, J. Deng, H. Houjou and K. Nozaki, *Macromolecules*, 2017, **50**, 7895-7900.
10. C.-H. Chang, C.-Y. Tsai, W.-J. Lin, Y.-C. Su, H.-J. Chuang, W.-L. Liu, C.-T. Chen, C.-K. Chen and B.-T. Ko, *Polymer*, 2018, **141**, 1-11.

11. C. Martín, A. Pizzolante, E. C. Escudero-Adán and A. W. Kleij, *Eur. J. Inorg. Chem.*, **2018**, 1921-1927.
12. M. J. Sanford, L. Peña Carrodegua, N. J. Van Zee, A. W. Kleij and G. W. Coates, *Macromolecules*, 2016, **49**, 6394-6400.

Appendix A: ^1H and ^{13}C NMR Spectra

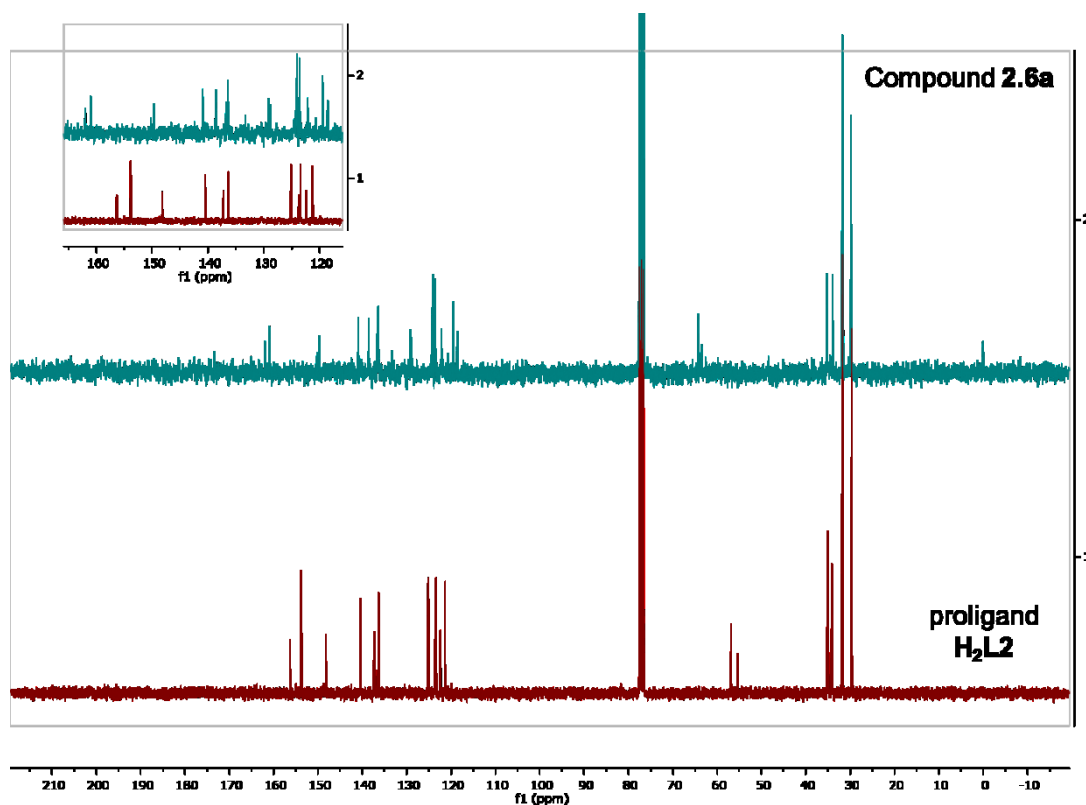


Figure A - 1: Stacked ^{13}C NMR spectra of **2.6a** and prolignand **$\text{H}_2\text{L2}$** in CDCl_3

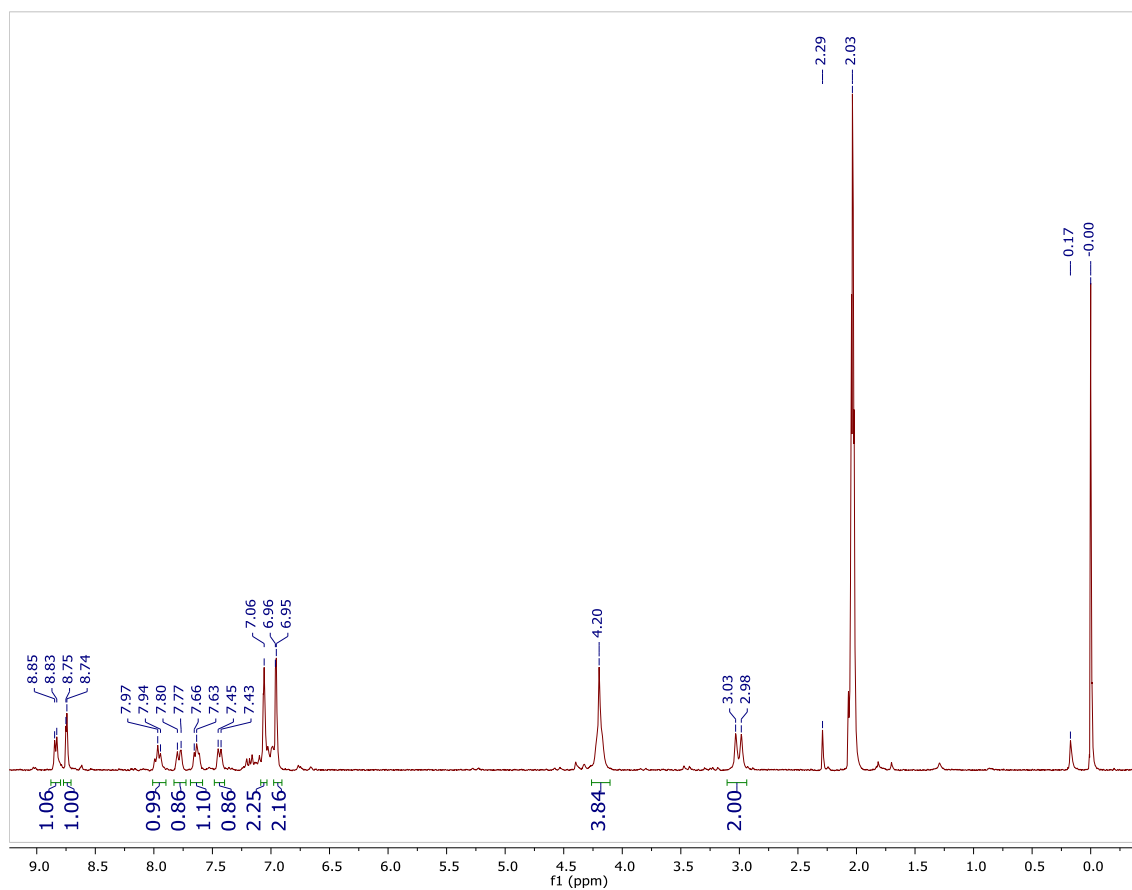


Figure A - 2: Representative ^1H NMR spectrum of **2.8a** in $\text{Acetone-}d_6$.

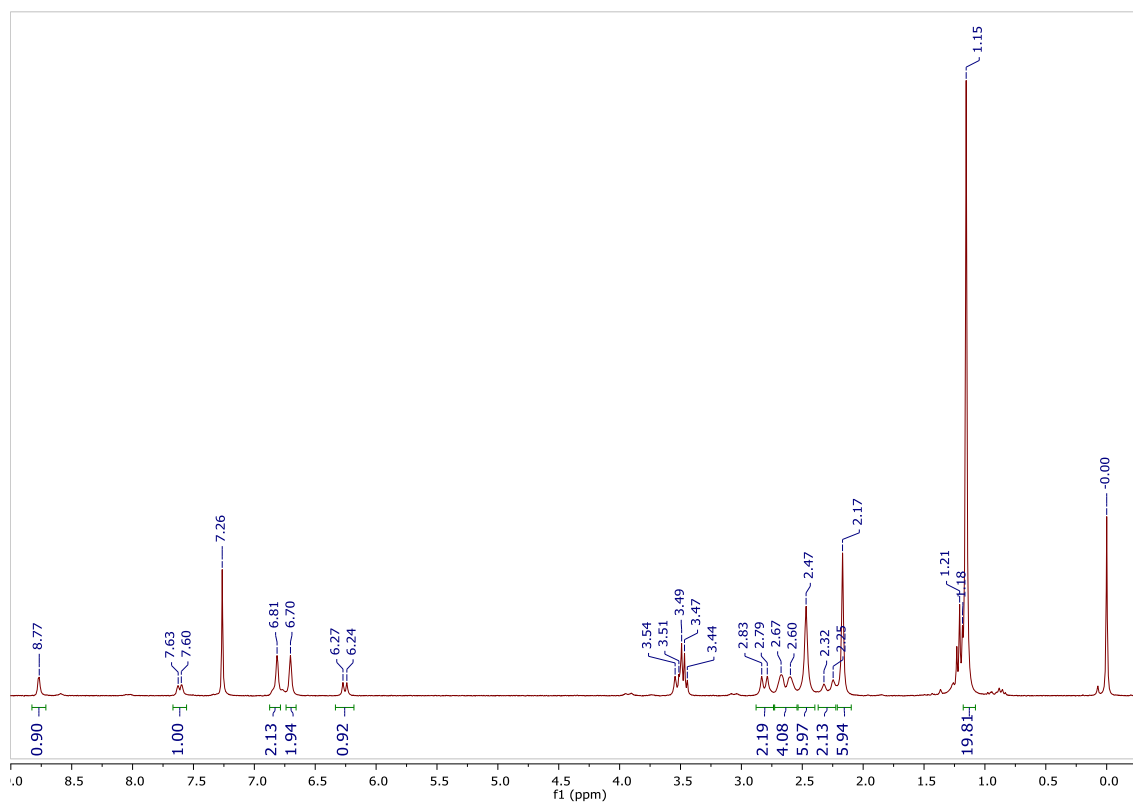


Figure A - 3: Representative ^1H NMR spectrum of **2.9a** in CDCl_3 .

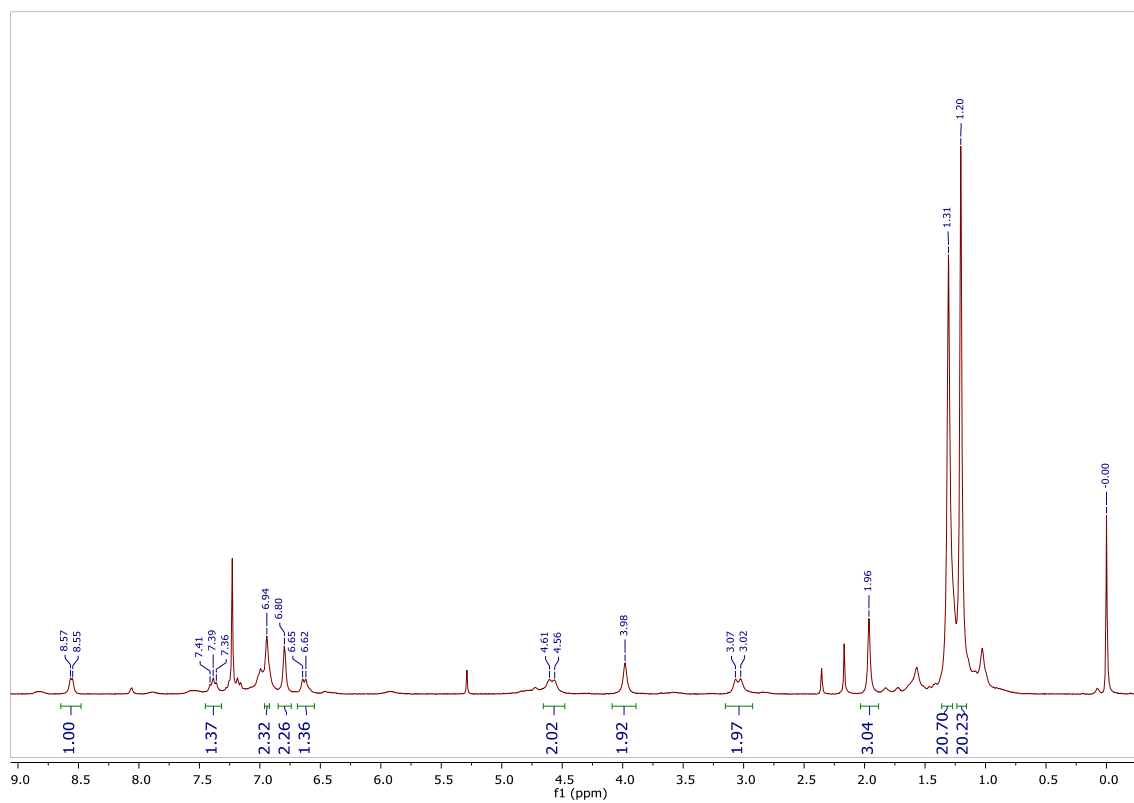


Figure A - 4: Representative ^1H NMR spectrum of **2.6b** in CDCl_3 .

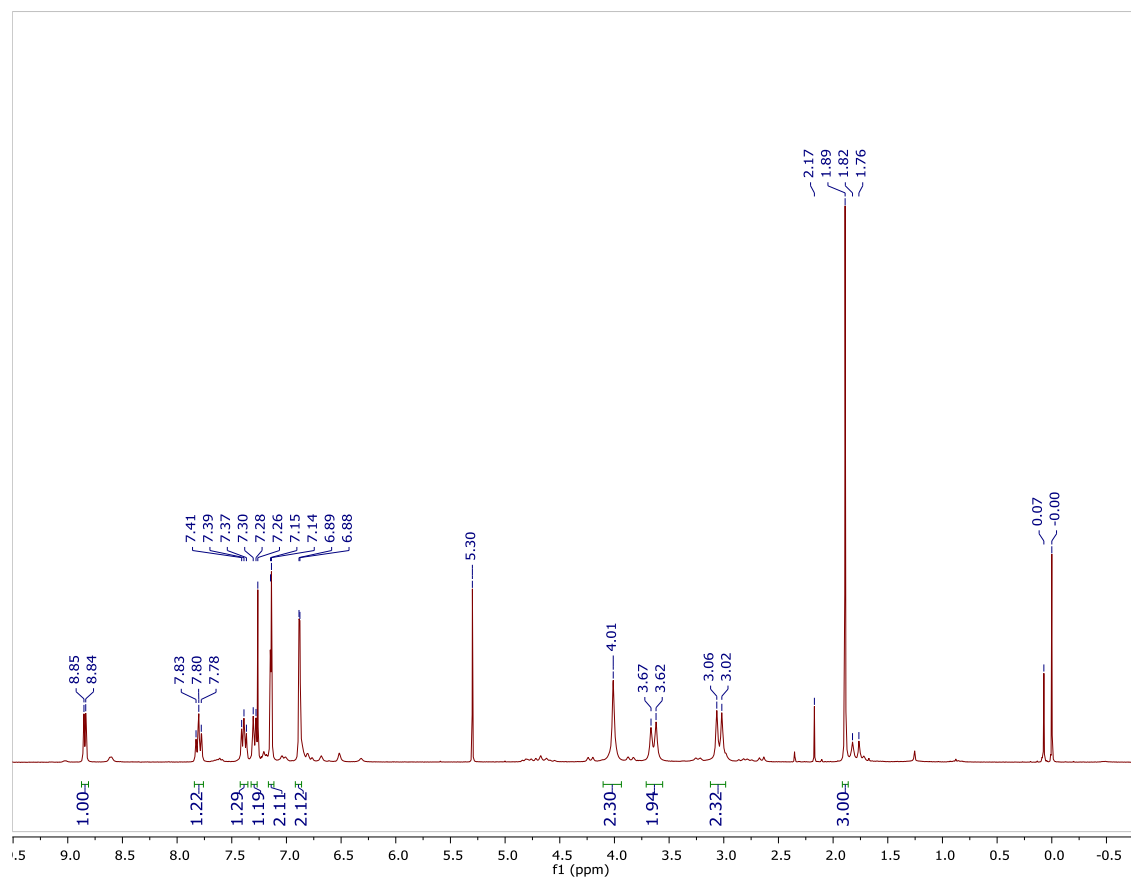


Figure A - 5: Representative ¹H NMR spectrum of **2.8b** in CDCl₃.

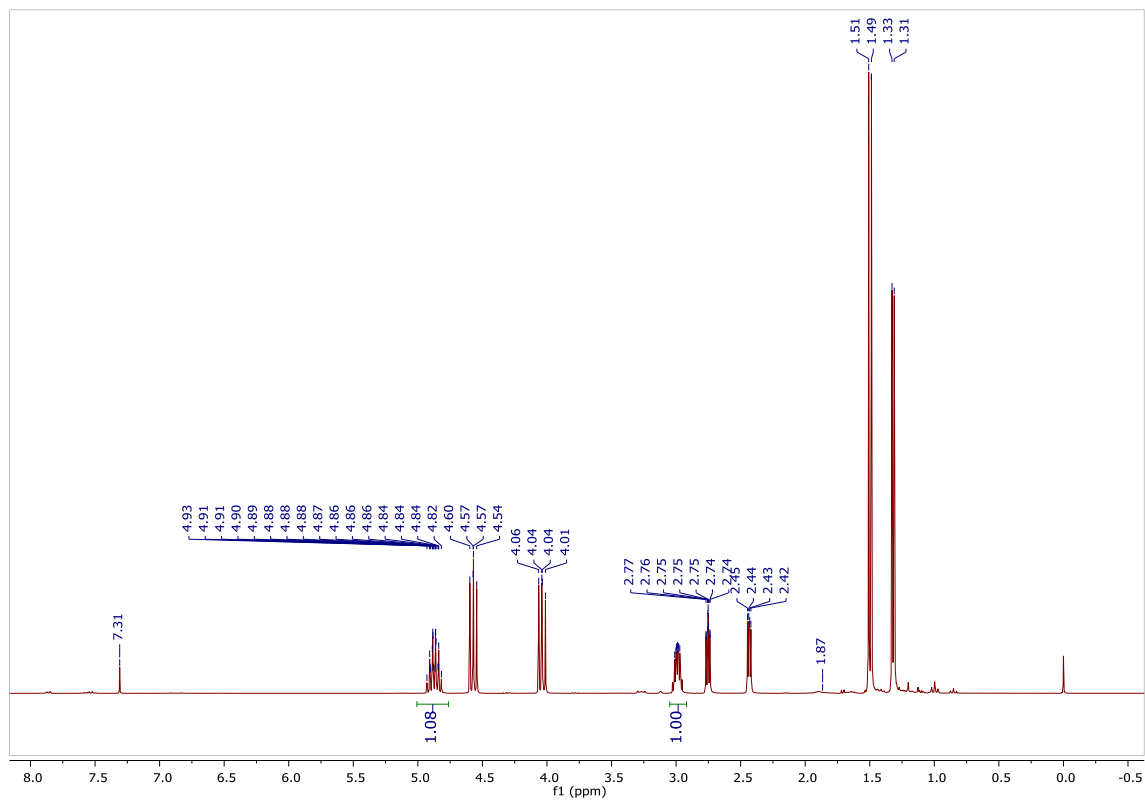


Figure A - 6: Representative ^1H NMR spectrum in CDCl_3 of aliquot taken immediately after reaction (Table 2.1, entry 5). % Conversion = integration of cyclic carbonate methine multiplet (1.08 at 4.88 ppm) divided by the sum of cyclic carbonate methine multiplet (1.08 at 2.99 ppm) and monomer (1.00 at 2.99 ppm).

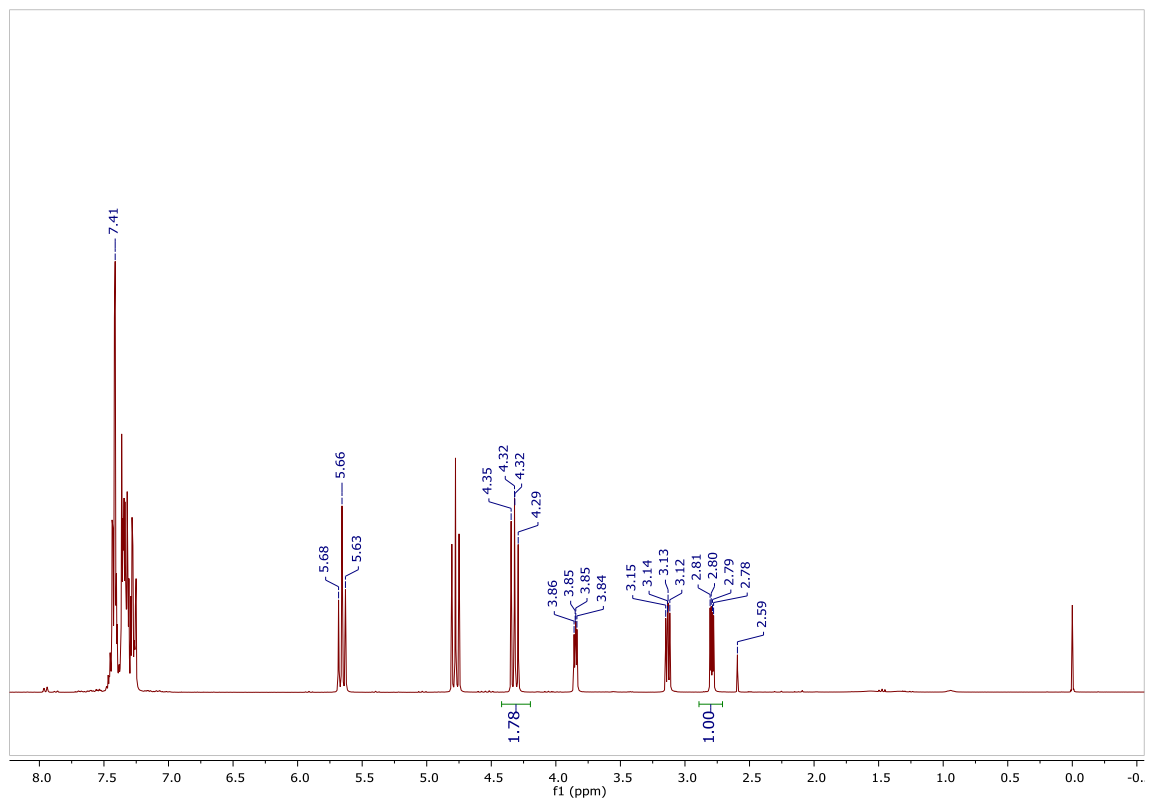


Figure A - 7: Representative ^1H NMR spectrum in CDCl_3 of aliquot taken immediately after reaction (Table 2.1, entry 10).

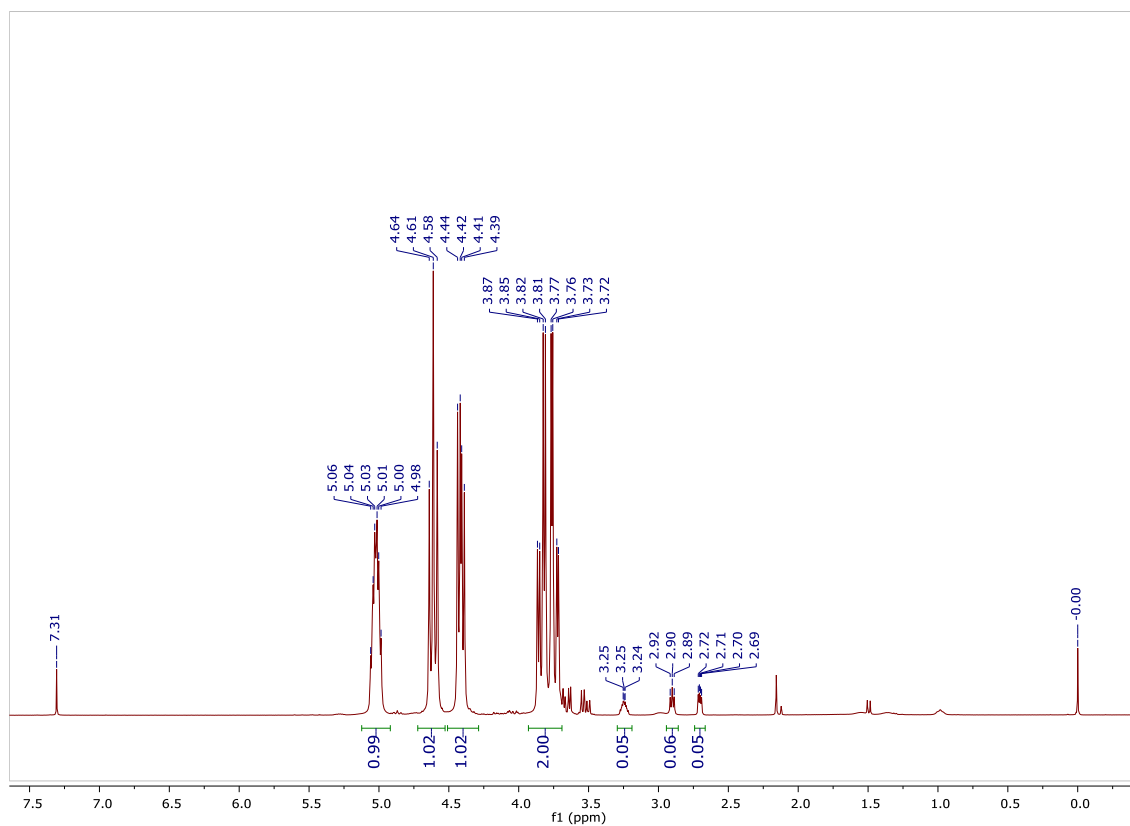


Figure A - 8: Representative ¹H NMR spectrum in CDCl₃ of aliquot taken immediately after reaction (Table 2.1, entry 11).

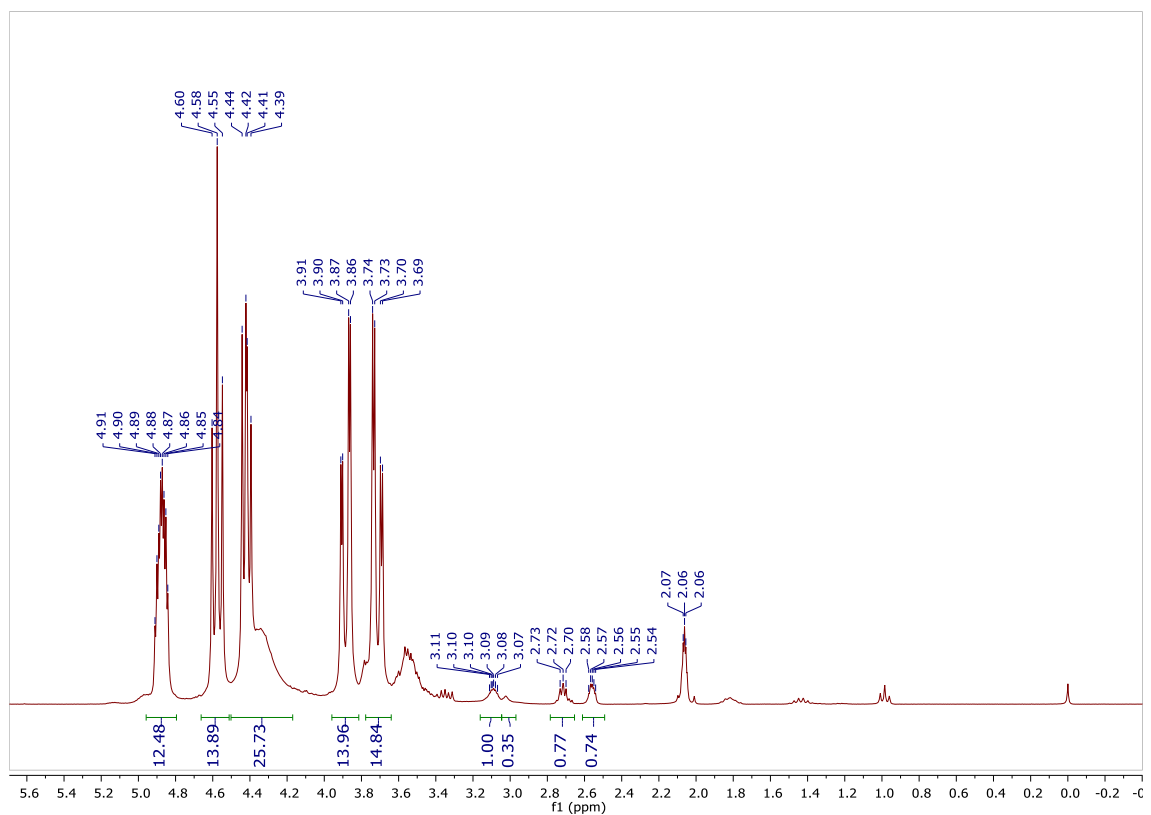


Figure A - 9: Representative ^1H NMR spectrum in CDCl_3 of aliquot taken immediately after reaction (Table 2.1, entry 12).

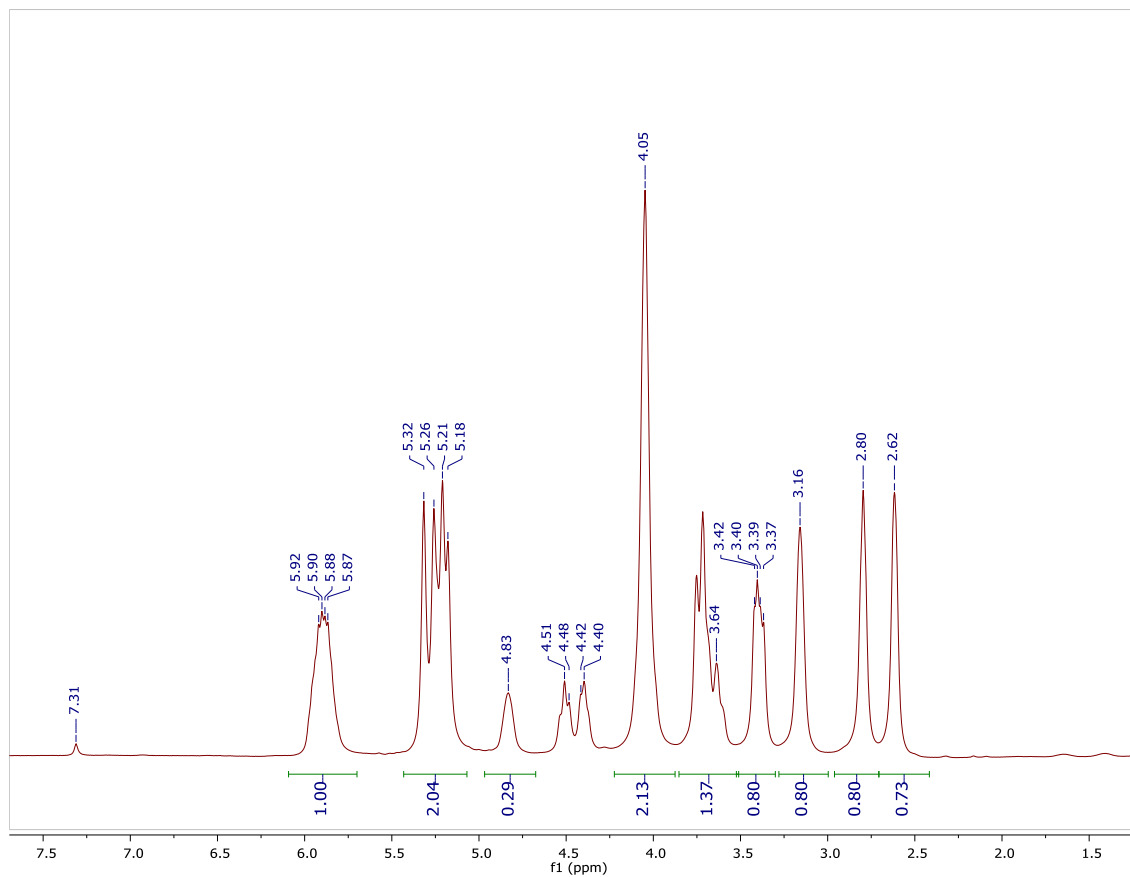


Figure A - 10: Representative ^1H NMR spectrum in CDCl_3 of aliquot taken immediately after reaction (Table 2.1, entry 13).

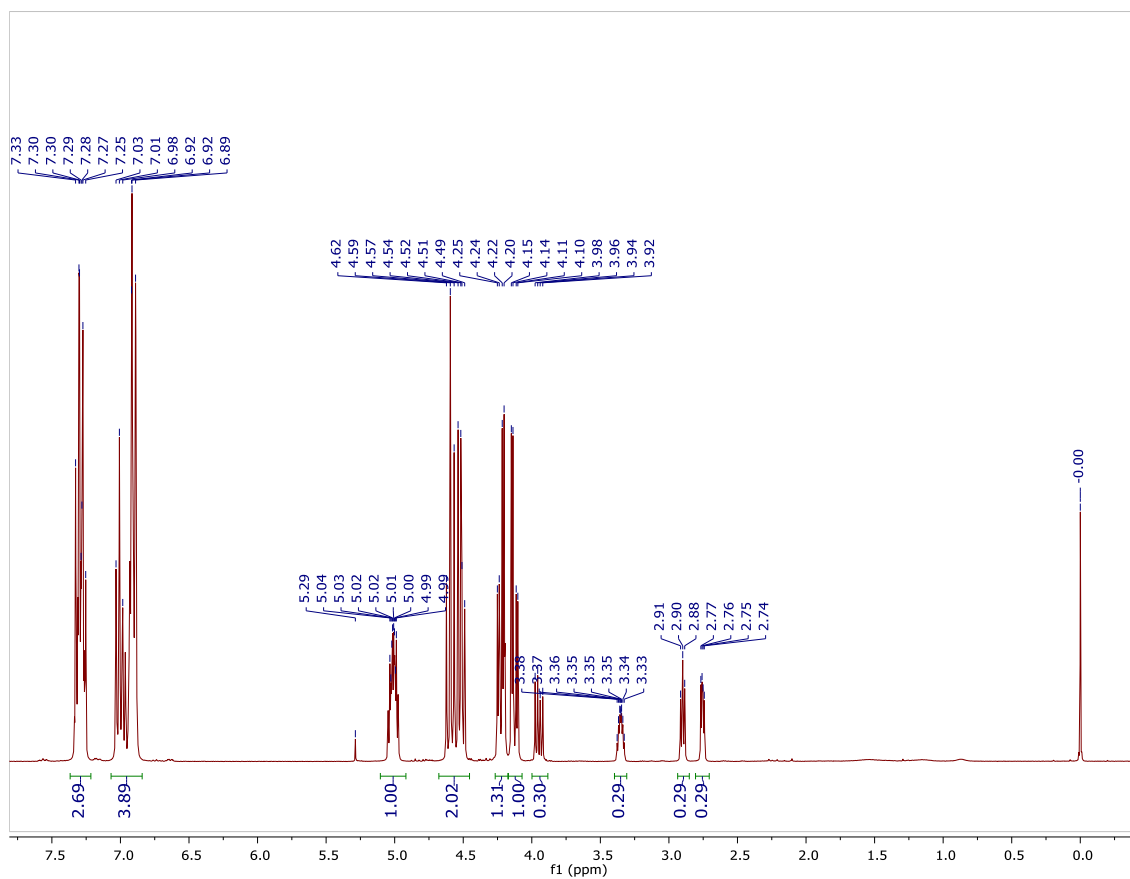


Figure A - 11: Representative ¹H NMR spectrum in CDCl₃ of aliquot taken immediately after reaction (Table 2.1, entry 14).

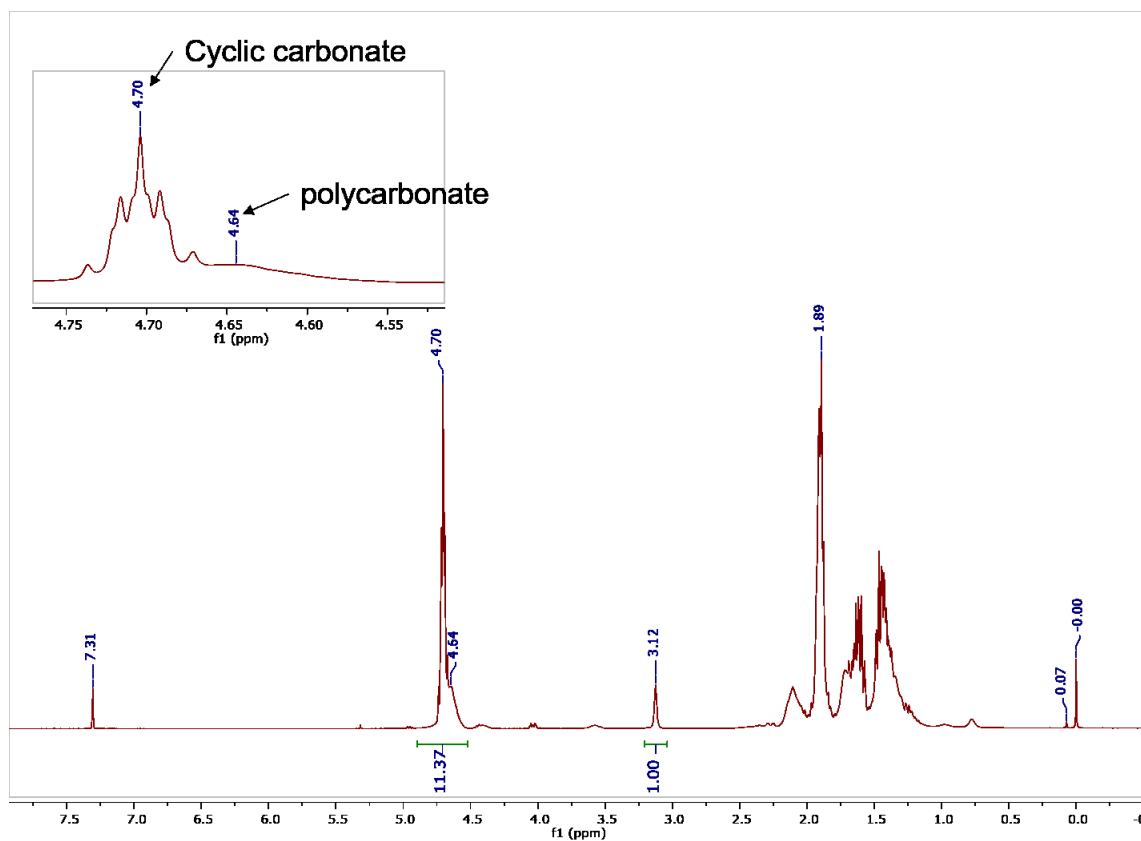


Figure A - 12: Representative ^1H NMR spectrum of aliquot taken immediately after reaction (Table 3.1, entry 7) in CDCl_3 . % Conversion = integration of polymer/cyclic carbonate peaks (11.37 at 4.89 – 4.52 ppm) divided by the sum of cyclic carbonate/polymers (11.37 at 4.89 – 4.52 ppm) and monomer (1.00 at 3.12 ppm).

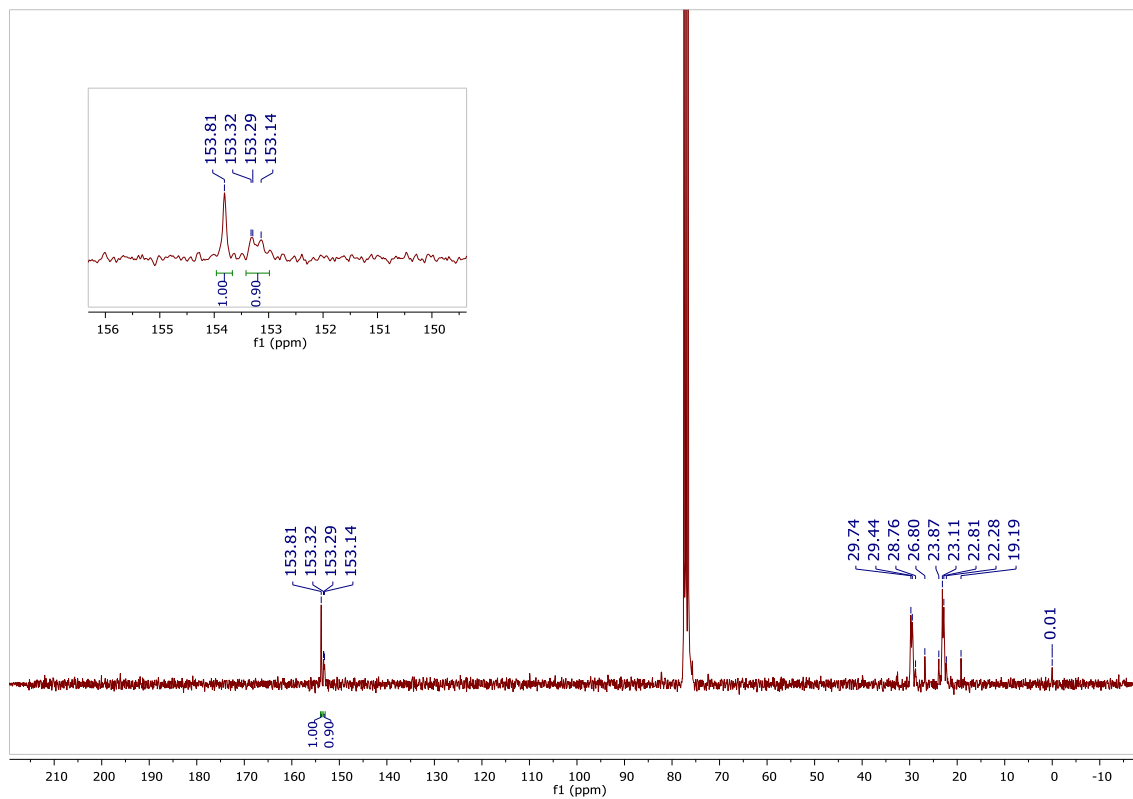


Figure A - 13: Representative ^{13}C NMR spectrum of aliquot taken immediately after reaction (Table 3.1, entry 1) in CDCl_3 . Syndiotactic and isotactic diads observed at 153.2 and 153.8 ppm respectively. Integration ratios of 1:1 suggests atactic polymer.

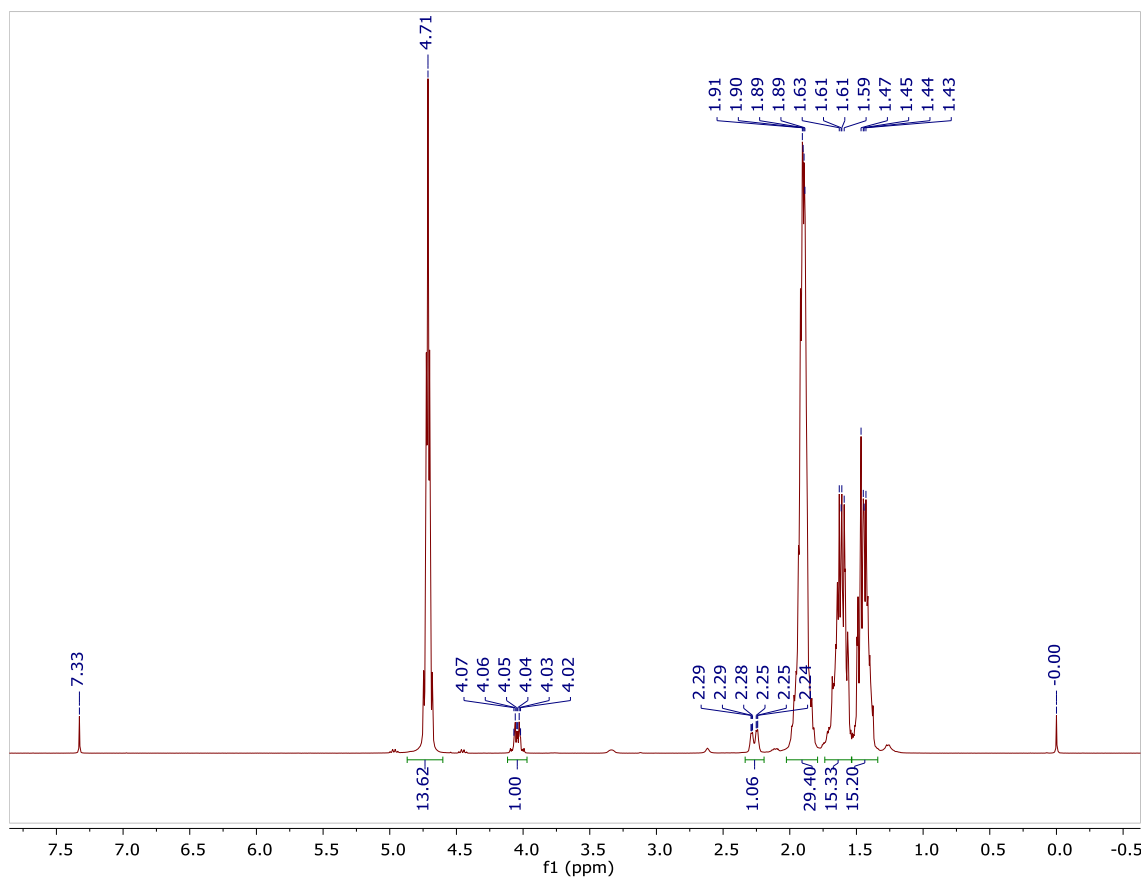


Figure A - 14: Representative ^1H NMR spectrum of isolated cyclohexene carbonate in CDCl_3 . Peak at 4.71 ppm represents methine protons from *cis* isomer whereas multiplet at 4.02-4.07 ppm represents that of *trans* isomer.

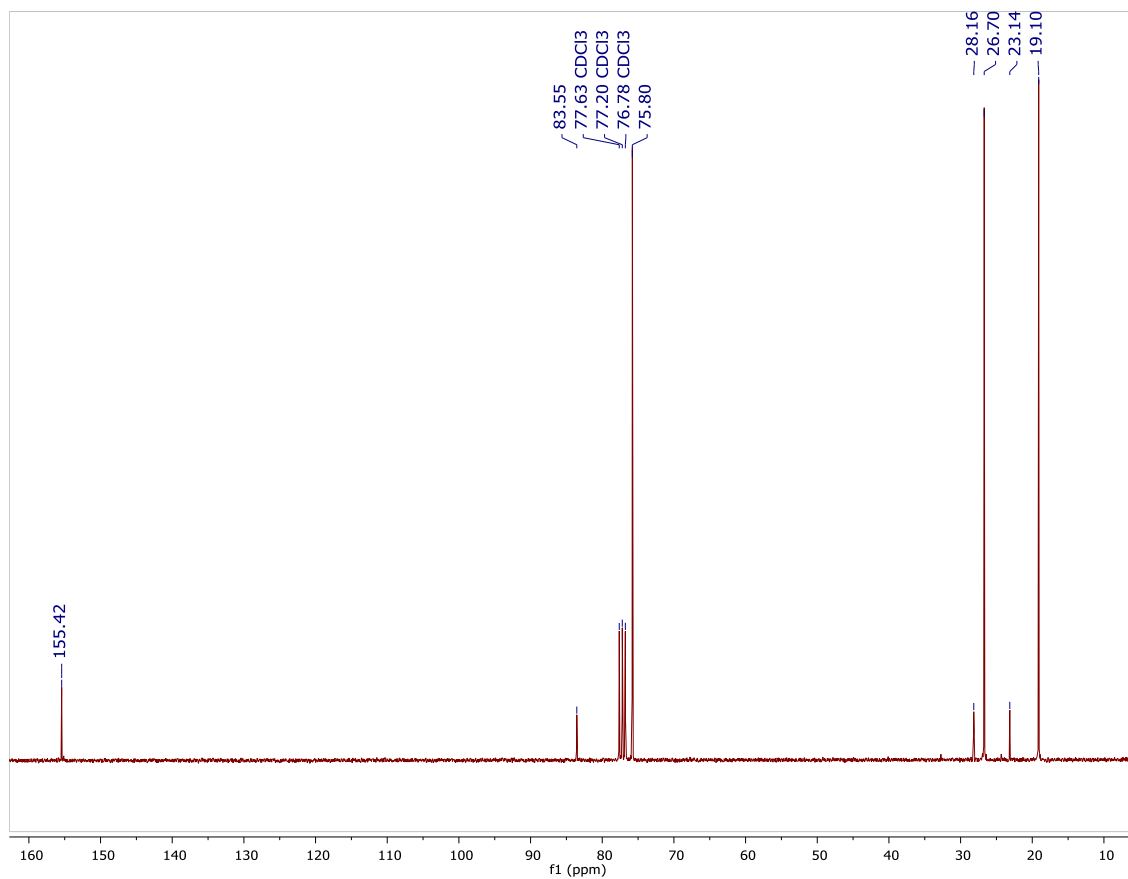


Figure A - 15: Representative ^{13}C NMR spectrum of isolated cyclohexene carbonate in CDCl_3 . Peaks at 23.14, 28.16 and 83.55 ppm correspond to carbons from *trans*-CHC and the more intense counterparts (19.10, 26.70 and 75.8 ppm) correspond to *cis*-CHC. Signal at 155.4 ppm corresponds to the carbonyl carbon from both isomers.

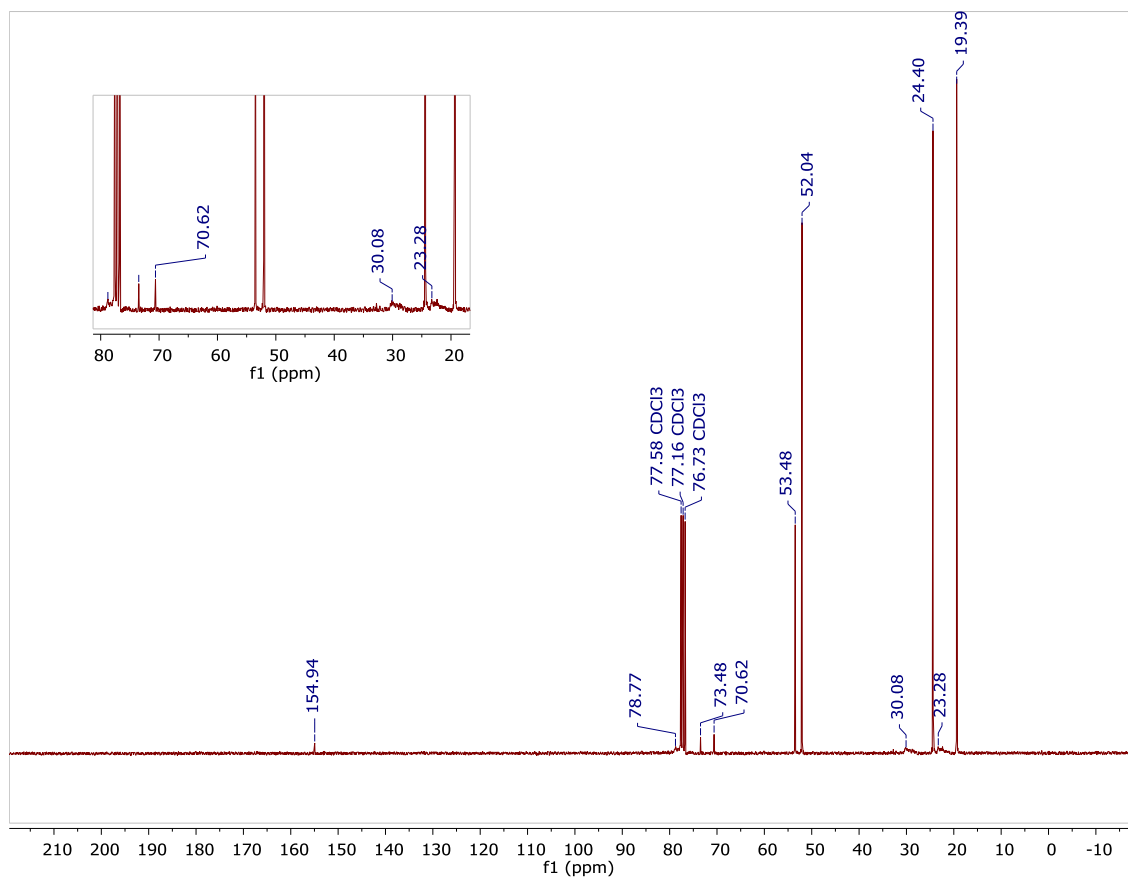


Figure A - 16: Representative crude ^{13}C NMR spectrum of PCHO in CDCl_3 from Table 4.1, entry 12 with enlarged area showing characteristic polymer signal (23.28, 30.08, 70.62, 73.48 and 78.77 ppm).

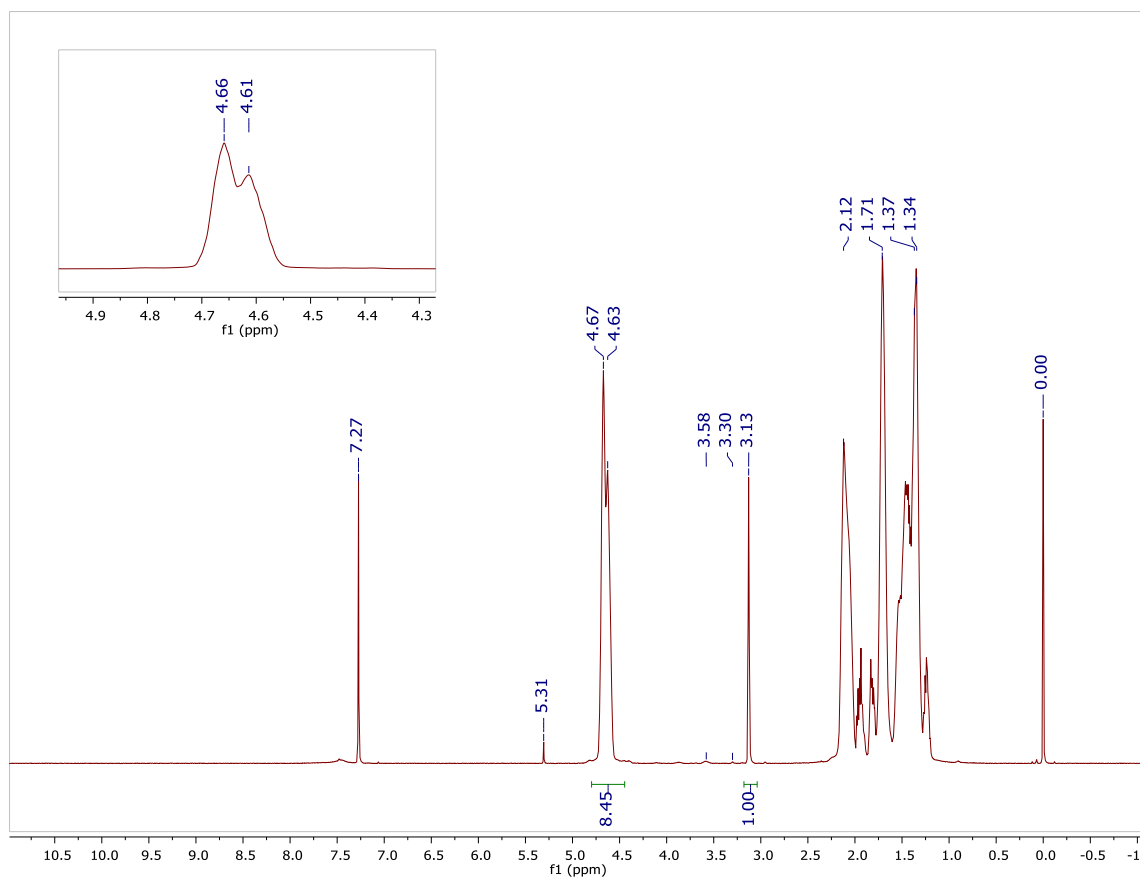


Figure A - 17: Representative crude ^1H NMR spectrum of PCHC in CDCl_3 from Table 5.1, entry 1 with enlarged area showing characteristic polymer signal (4.66 and 4.61 ppm).

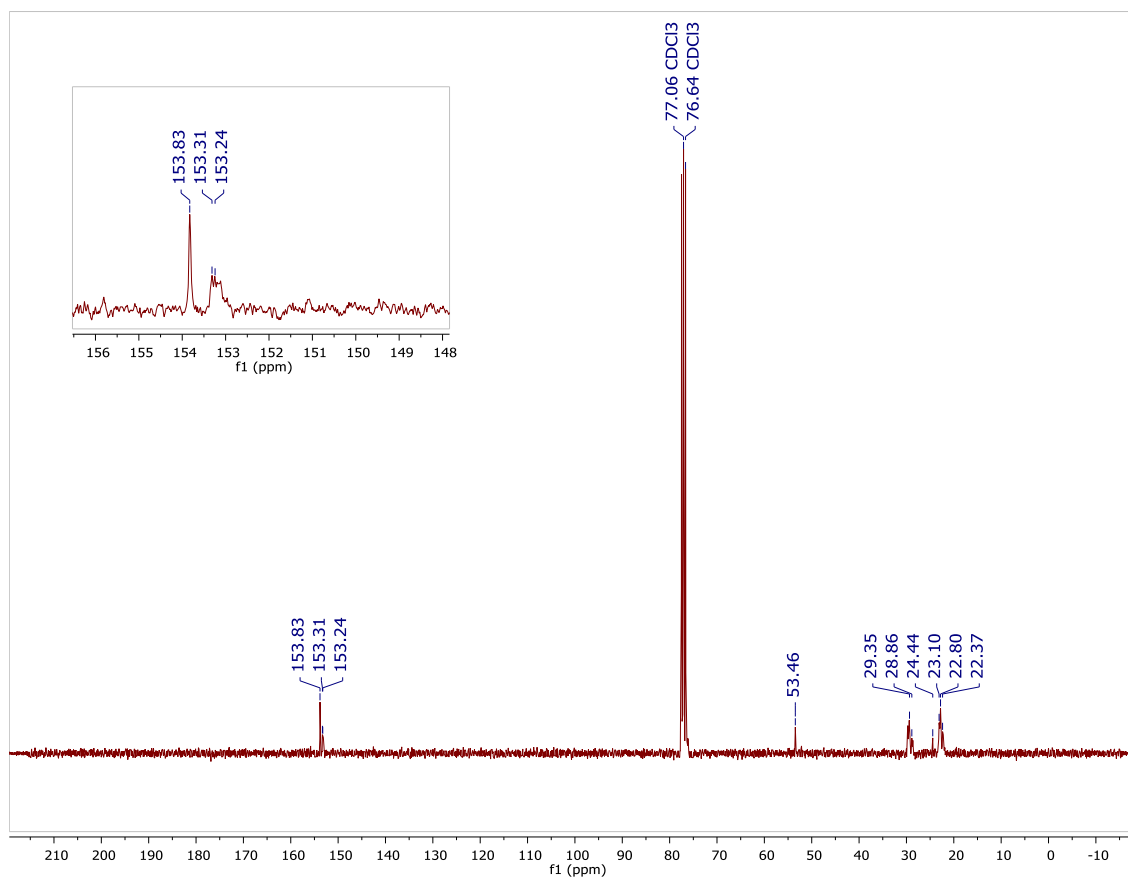


Figure A - 18: Representative crude ^{13}C NMR spectrum of PCHC in CDCl_3 from Table 5.1, entry 1 with enlarged area showing characteristic polymer syndiotactic and isotactic diads (153.8 and 153.3 ppm respectively).

Appendix B: MALDI-TOF Mass Spectra of Complexes and Polymers

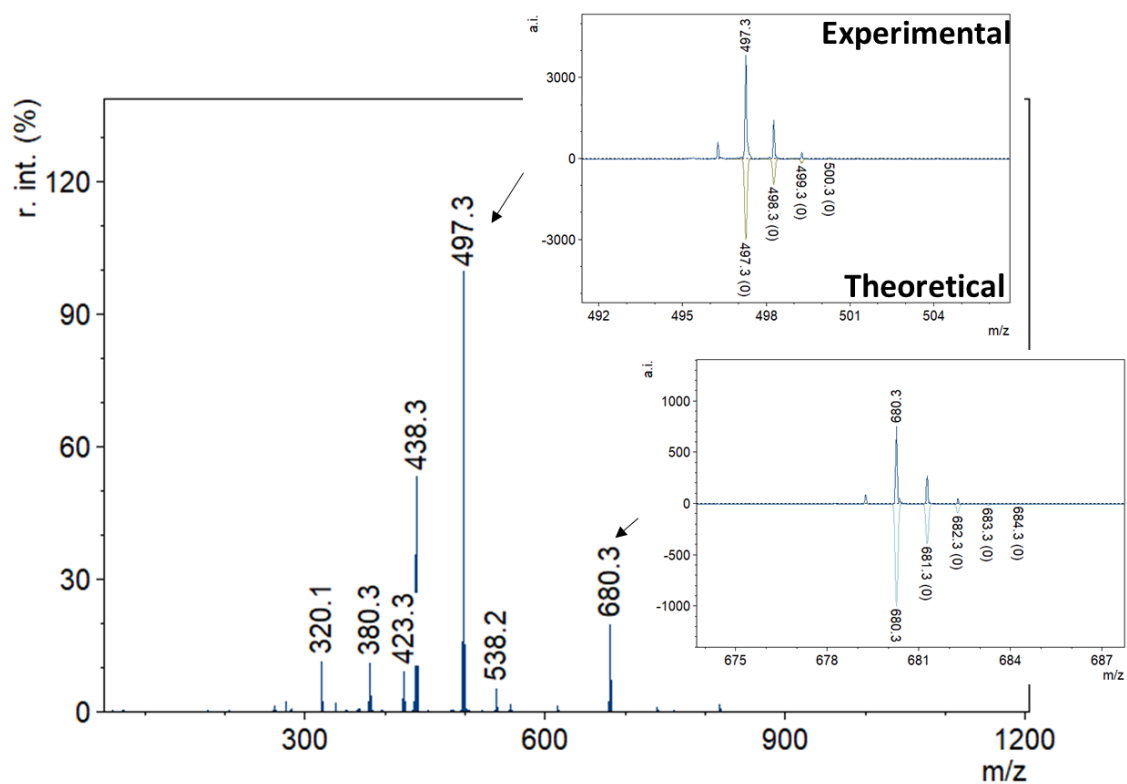


Figure B - 1: MALDI-TOF mass spectrum of **2.9a**.

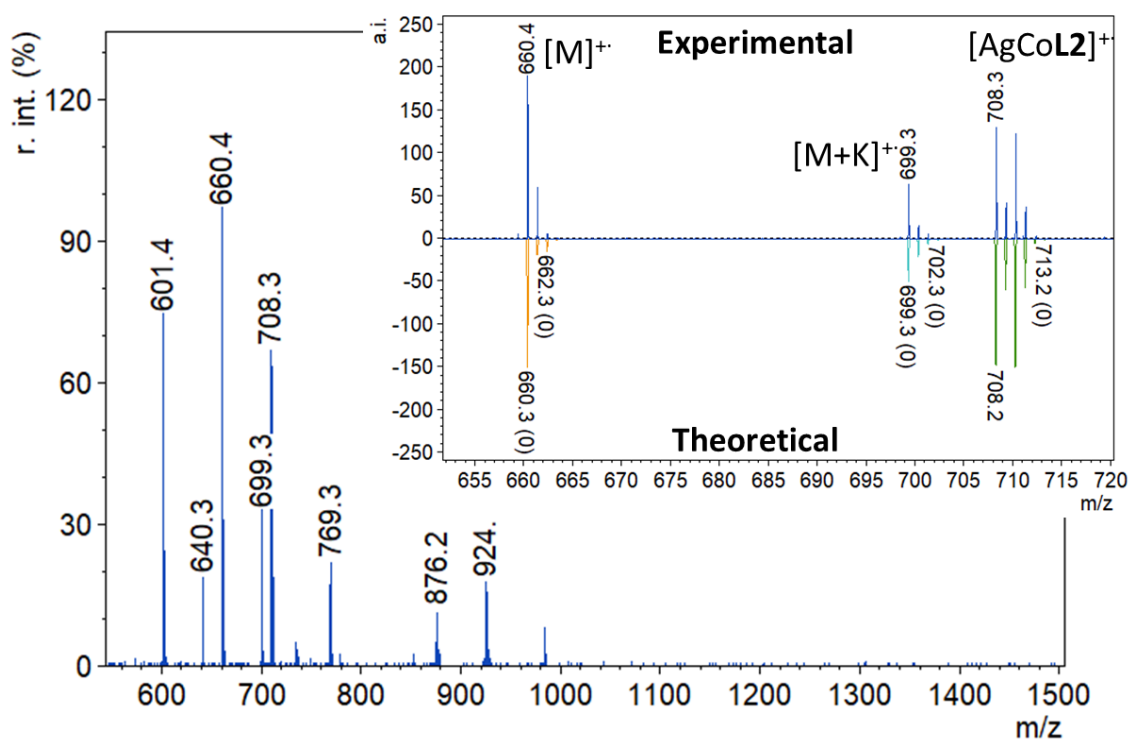


Figure B - 2: MALDI-TOF mass spectrum of **2.6b**.

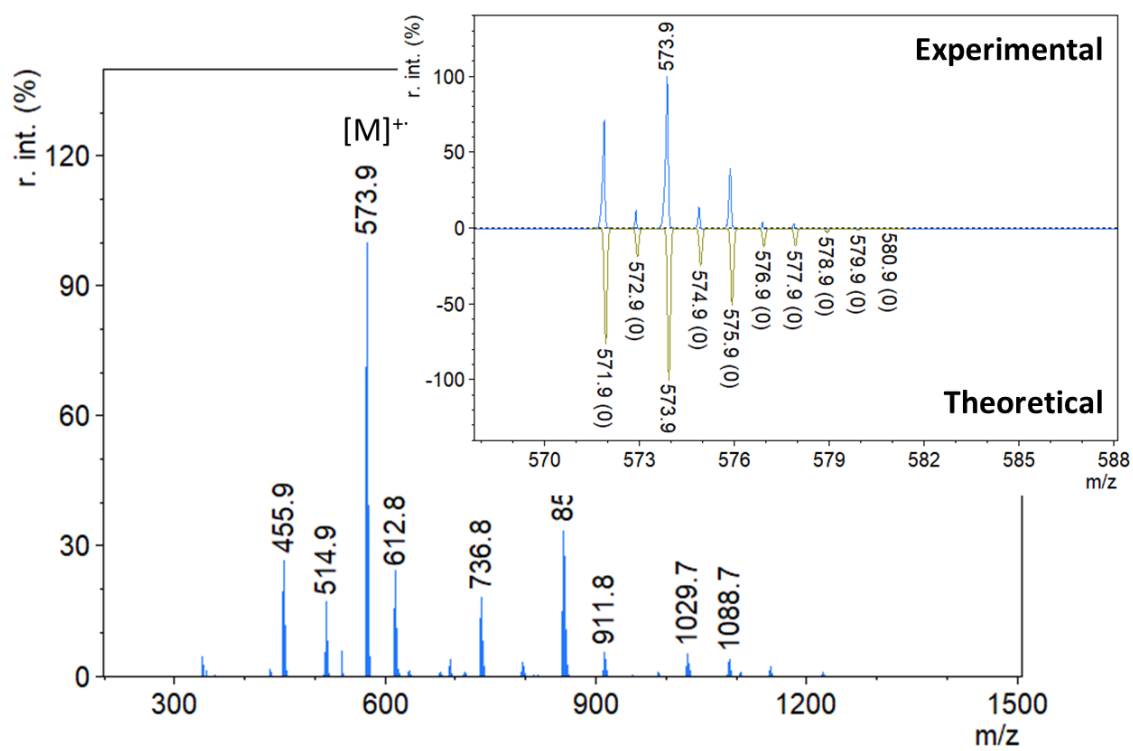


Figure B - 3: MALDI-TOF mass spectrum of **2.8b**.

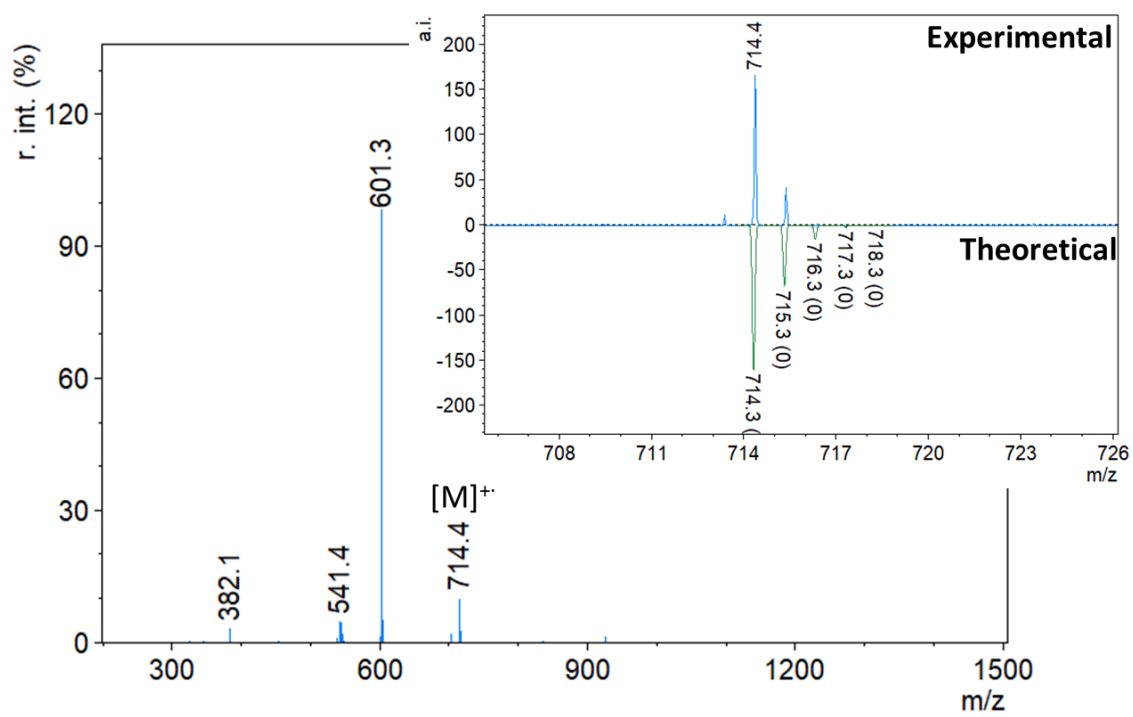


Figure B - 4: MALDI-TOF mass spectrum of **2.6c**.

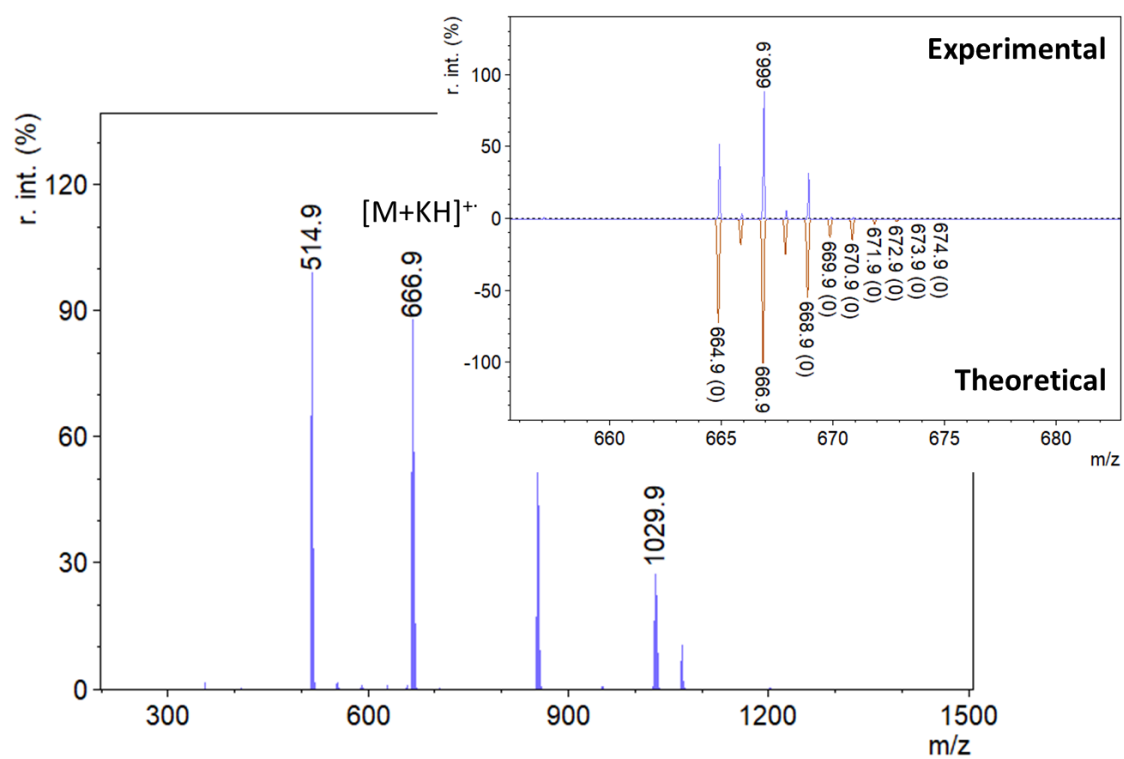


Figure B - 5: MALDI-TOF mass spectrum of **2.8c**.

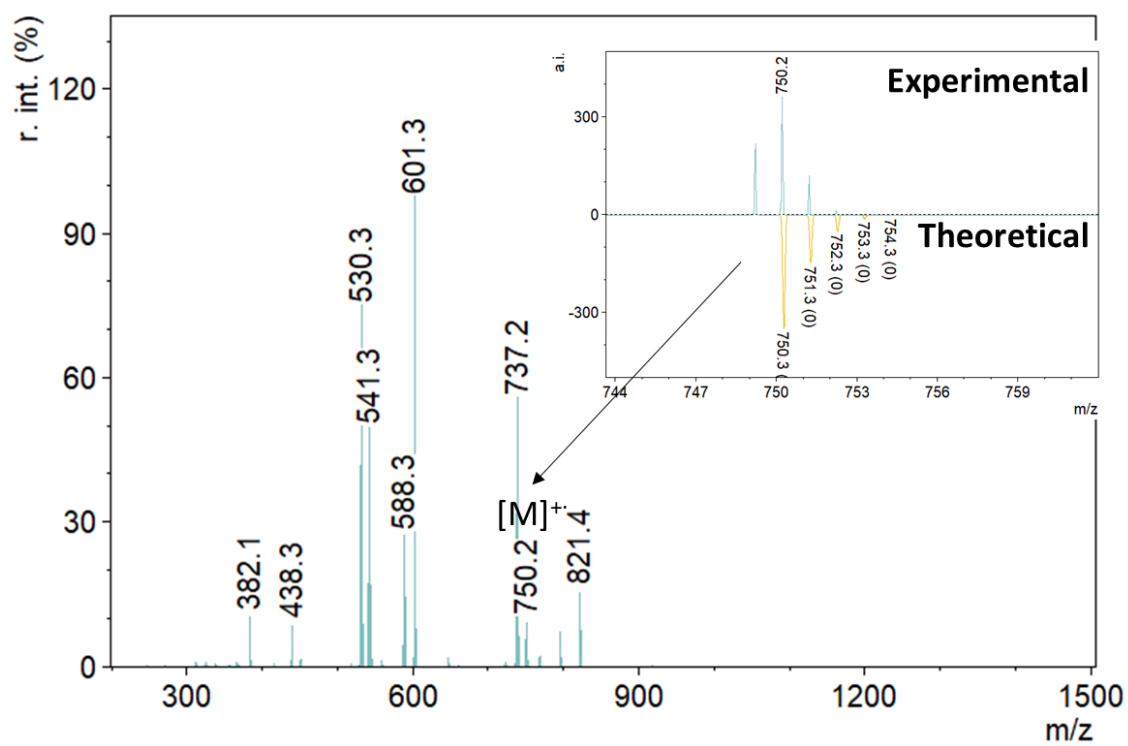


Figure B - 6: MALDI-TOF mass spectrum of **2.6d**.

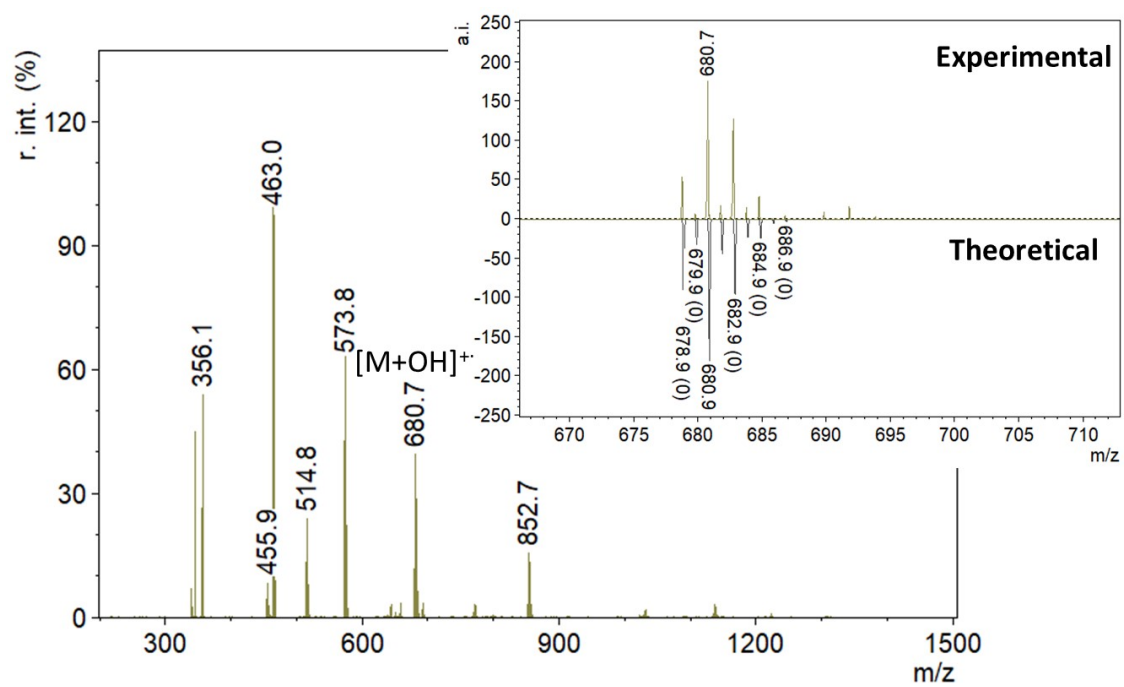


Figure B - 7: MALDI-TOF mass spectrum of **2.8d**.

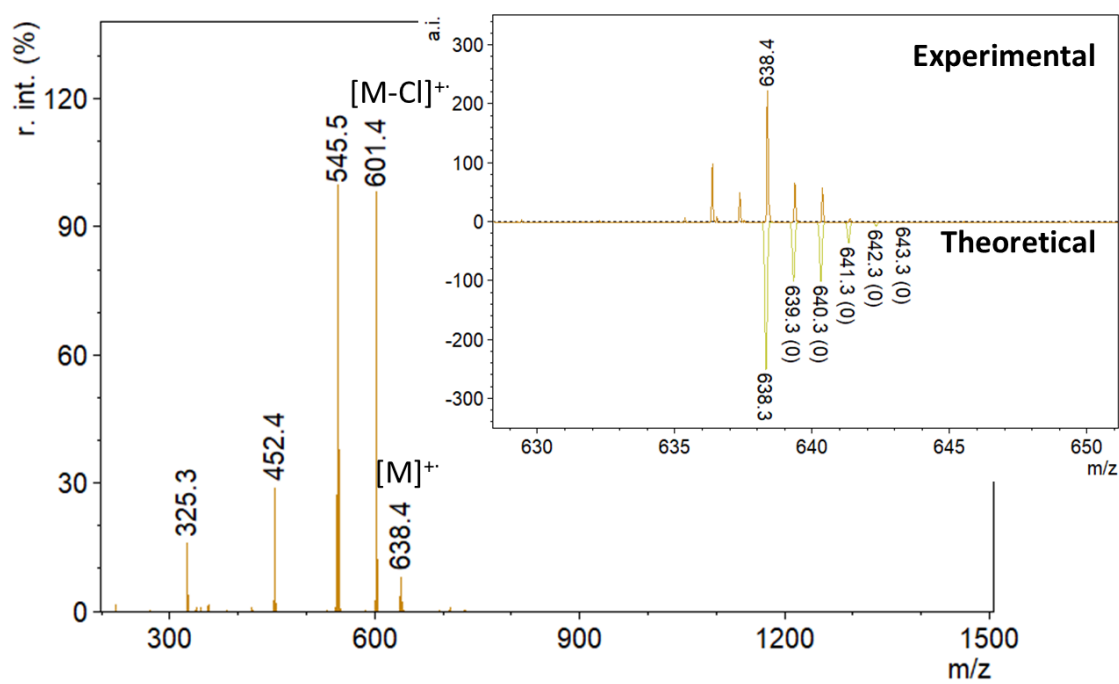


Figure B - 8: MALDI-TOF mass spectrum of **2.6e**.

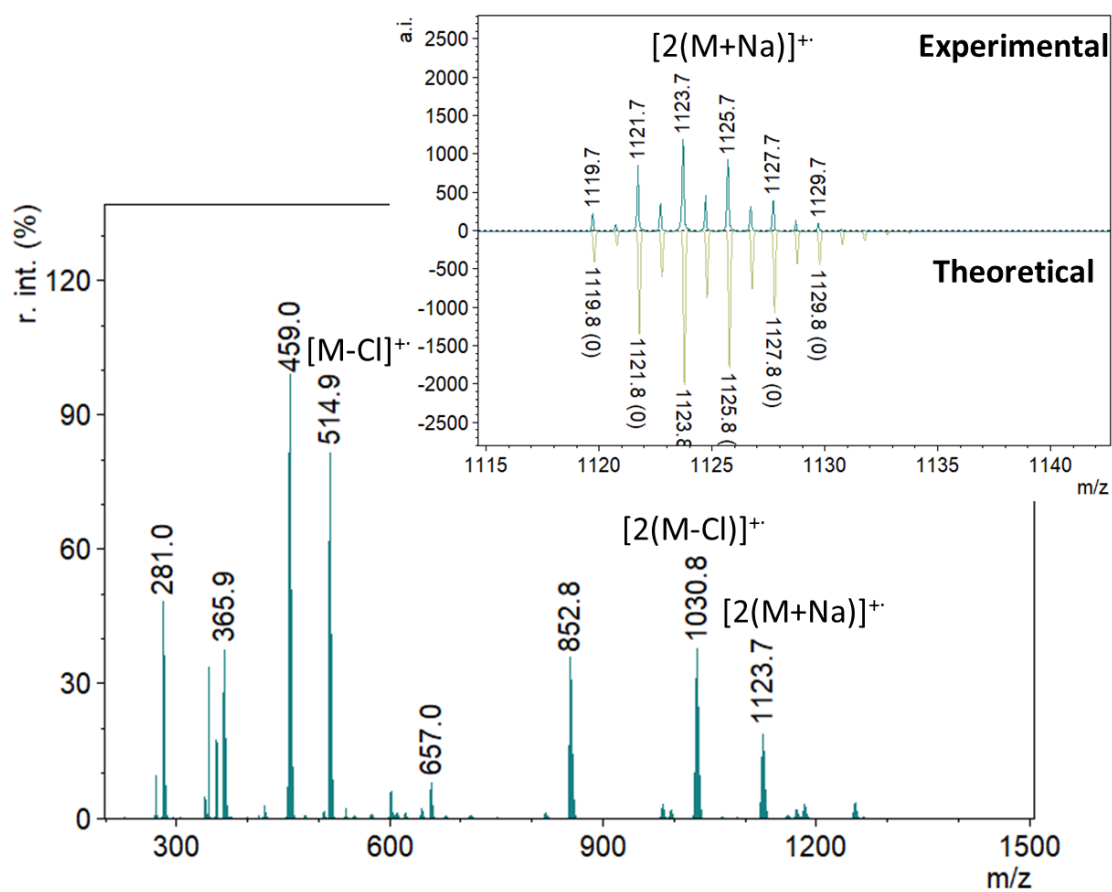


Figure B - 9: MALDI-TOF mass spectrum of 2.8e.

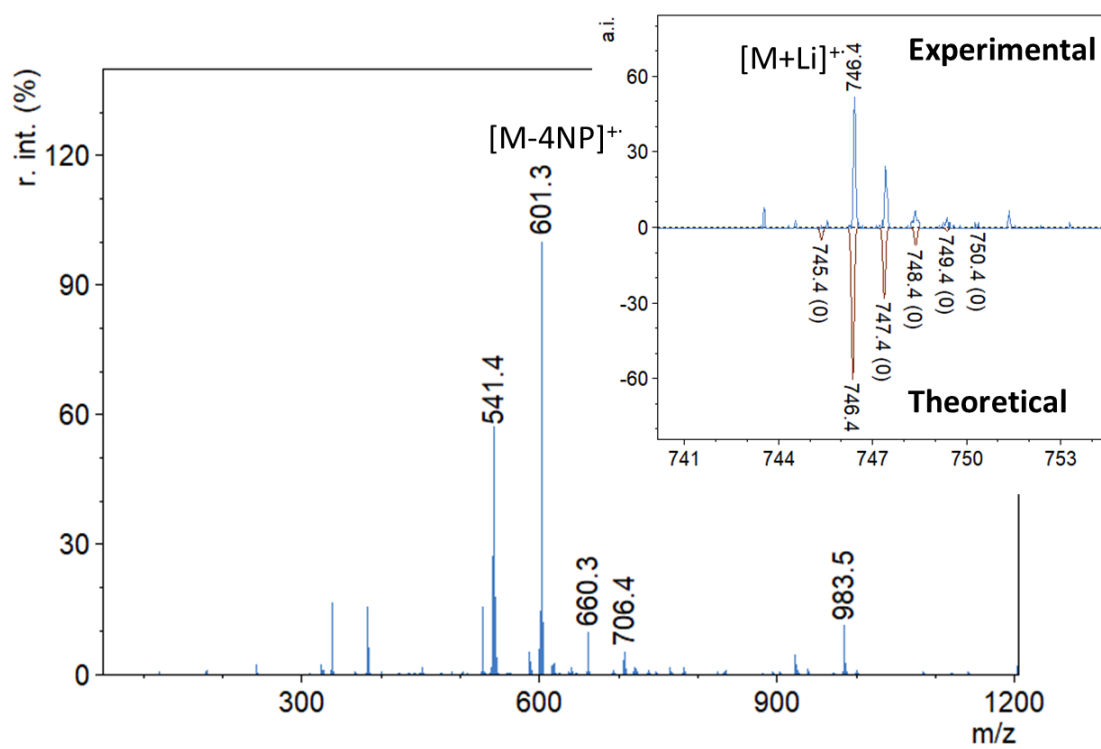


Figure B - 10: MALDI-TOF mass spectrum of **2.6f**.

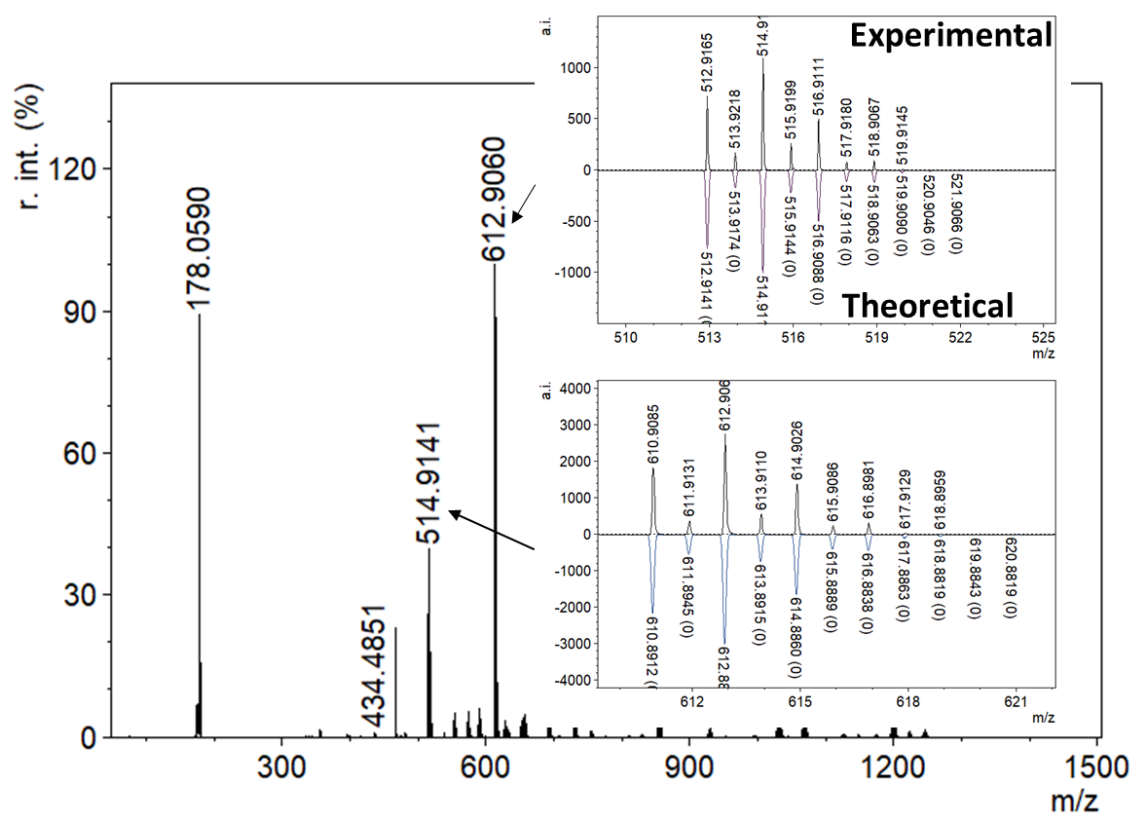


Figure B - 11: MALDI-TOF mass spectrum of **3.1** and comparison to calculated isotopic pattern.

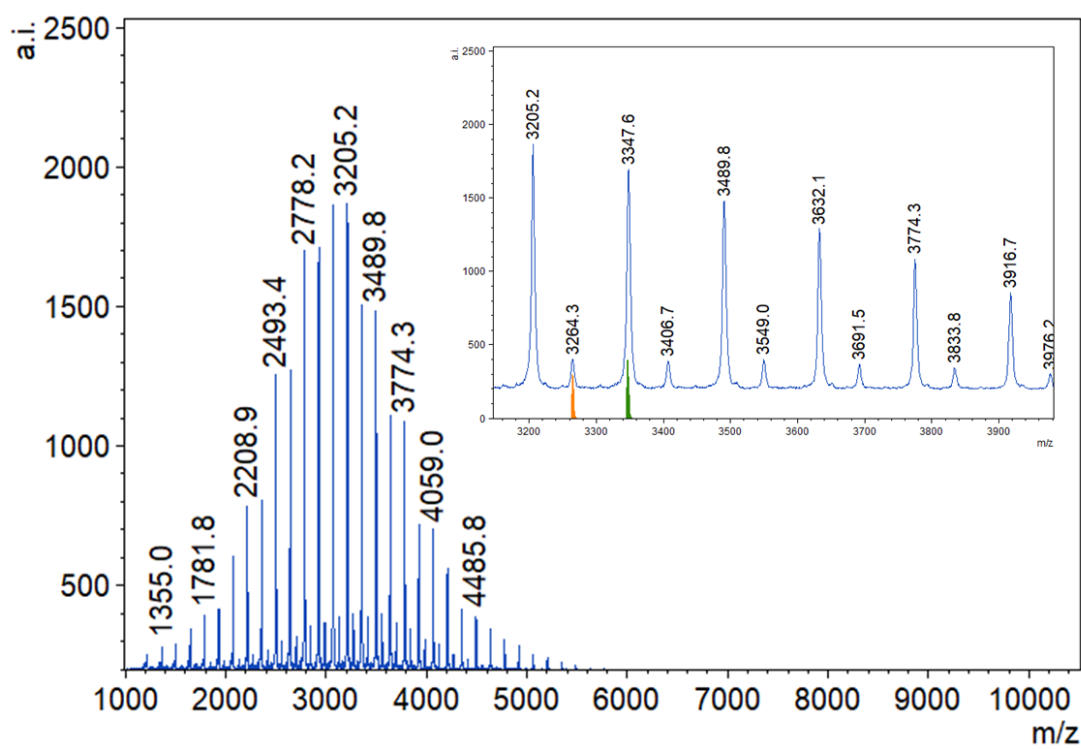


Figure B - 12: MALDI-TOF mass spectrum of polycarbonate obtained from Table 1, entry 1.

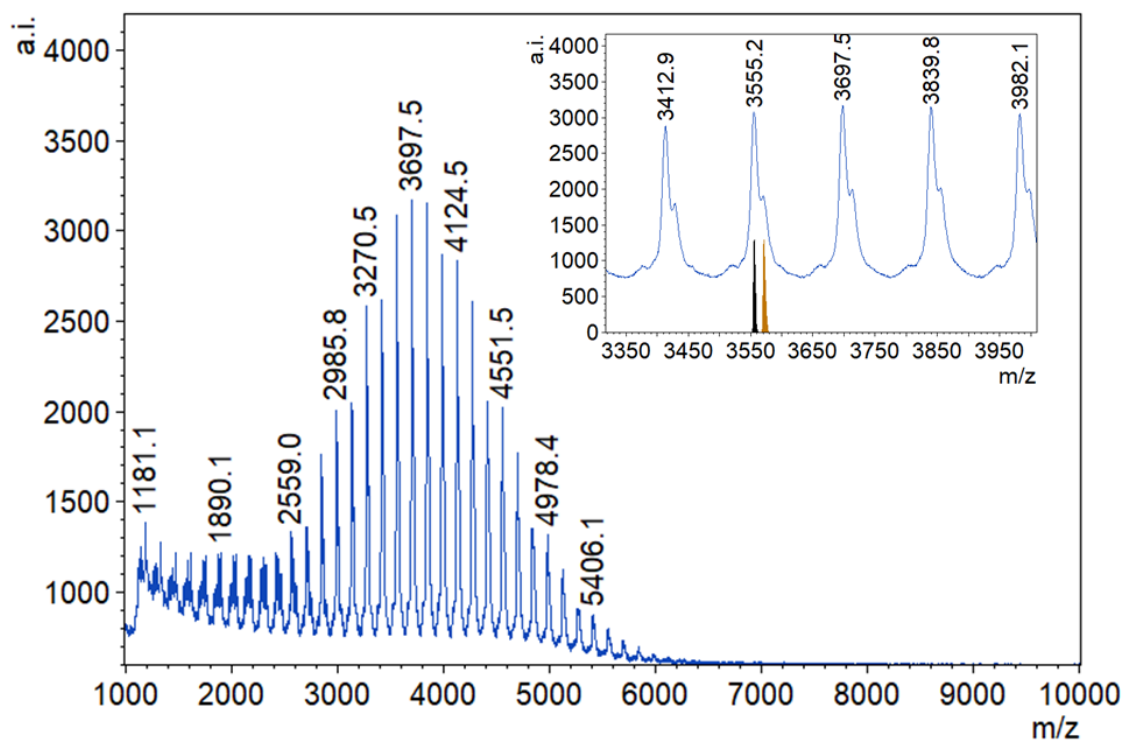


Figure B - 13: MALDI-TOF mass spectrum of polycarbonate obtained from Table 1, entry 9.

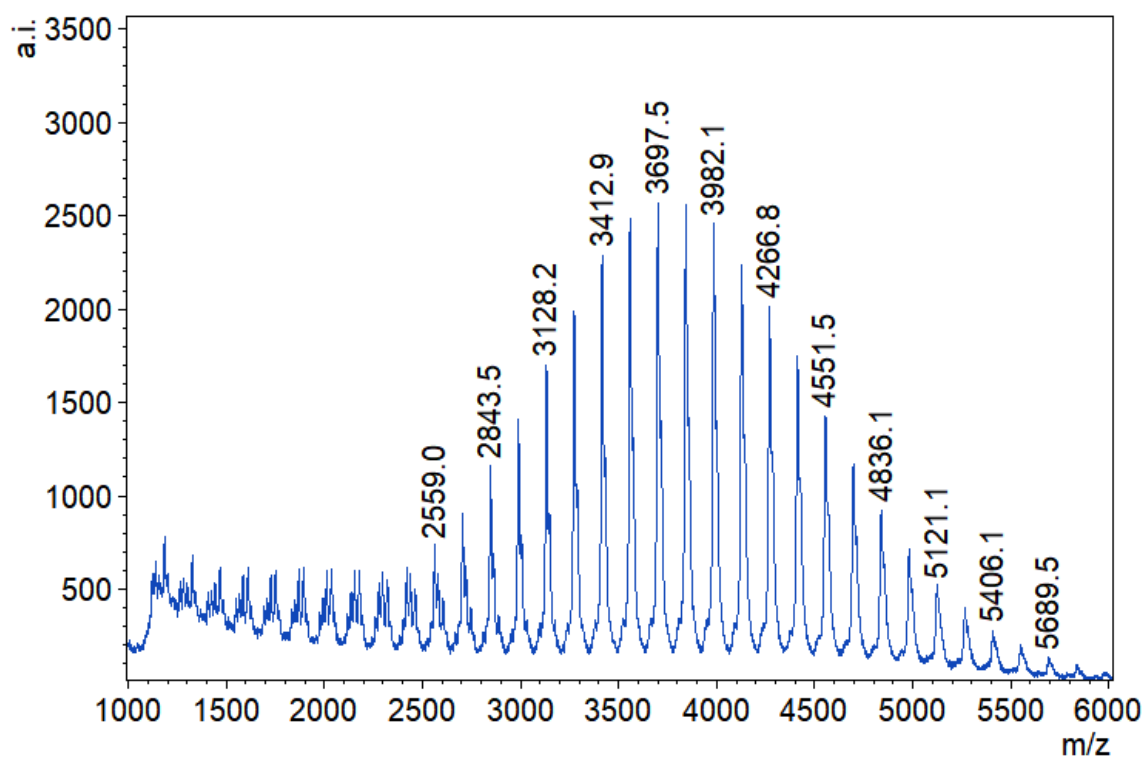


Figure B - 14: Expanded MALDI-TOF mass spectrum of polycarbonate obtained from Table 1, entry 9.

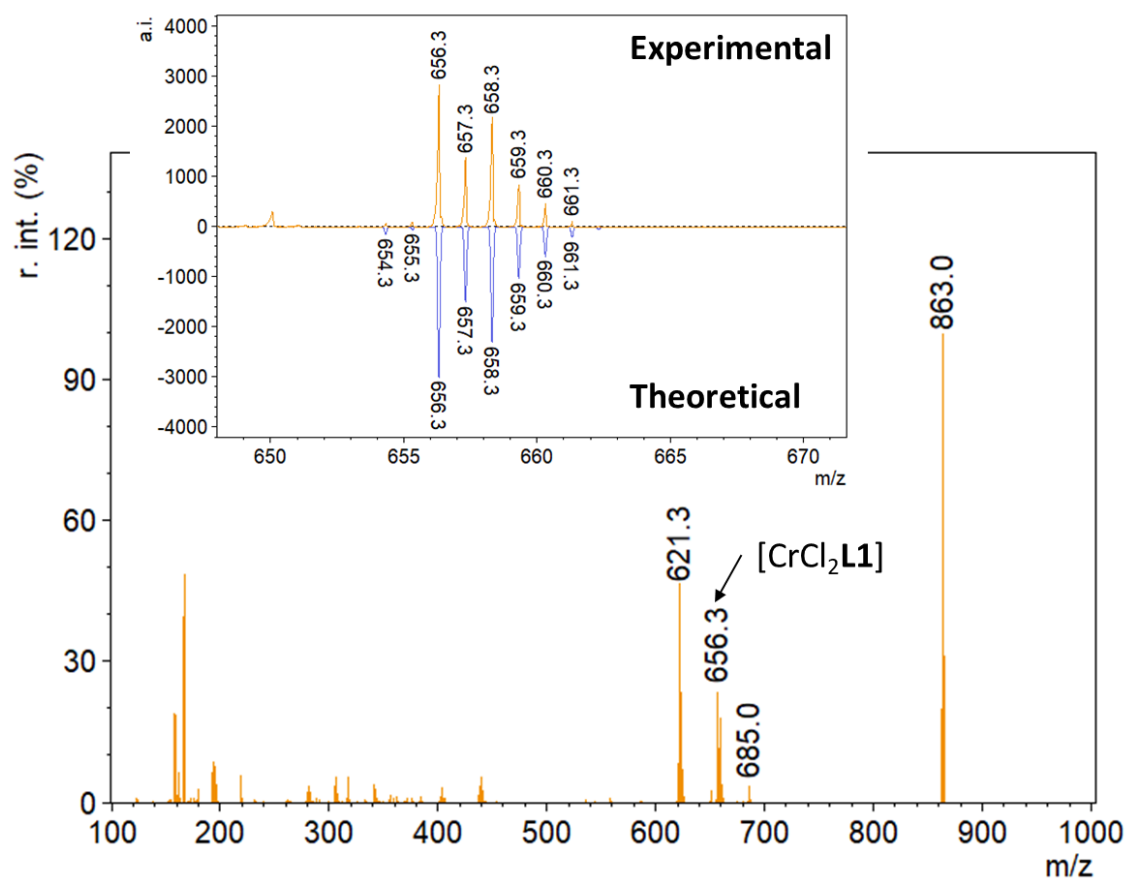


Figure B - 15: MALDI-TOF mass spectrum of **4.1** in negative reflectron mode.

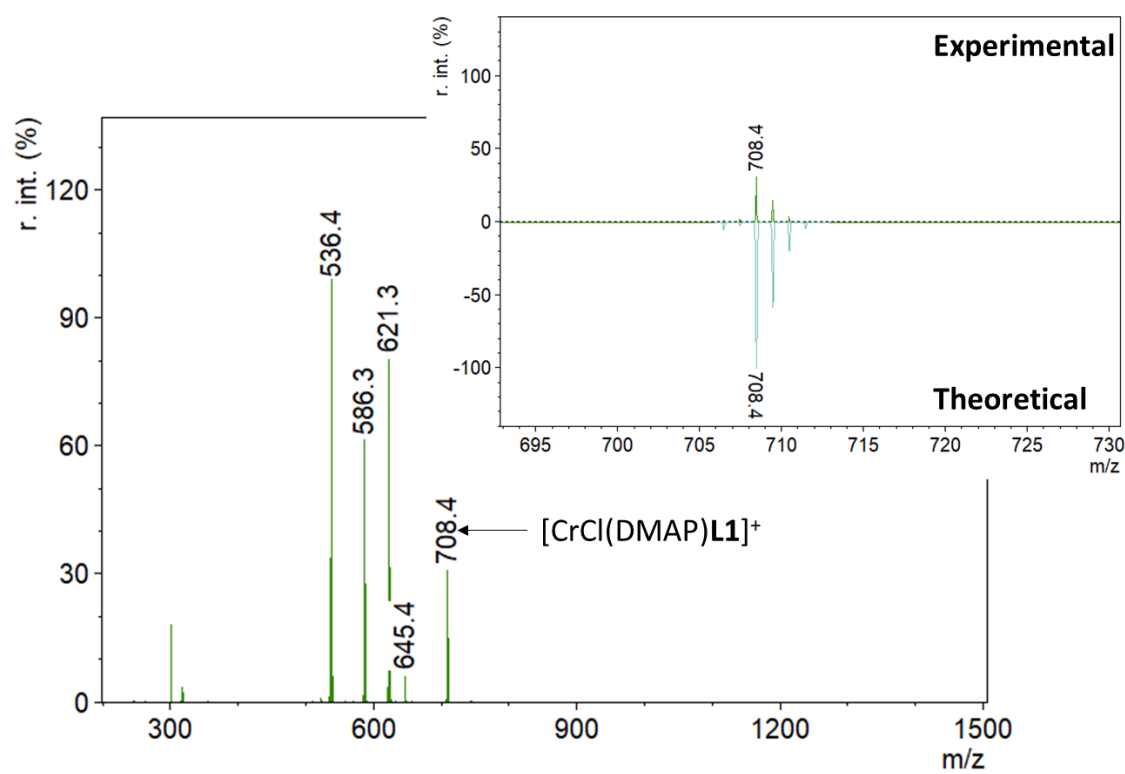


Figure B - 16: MALDI-TOF mass spectrum of **4.1**/DMAP in positive reflectron mode. Ratio of Cr to DMAP is 1:4.

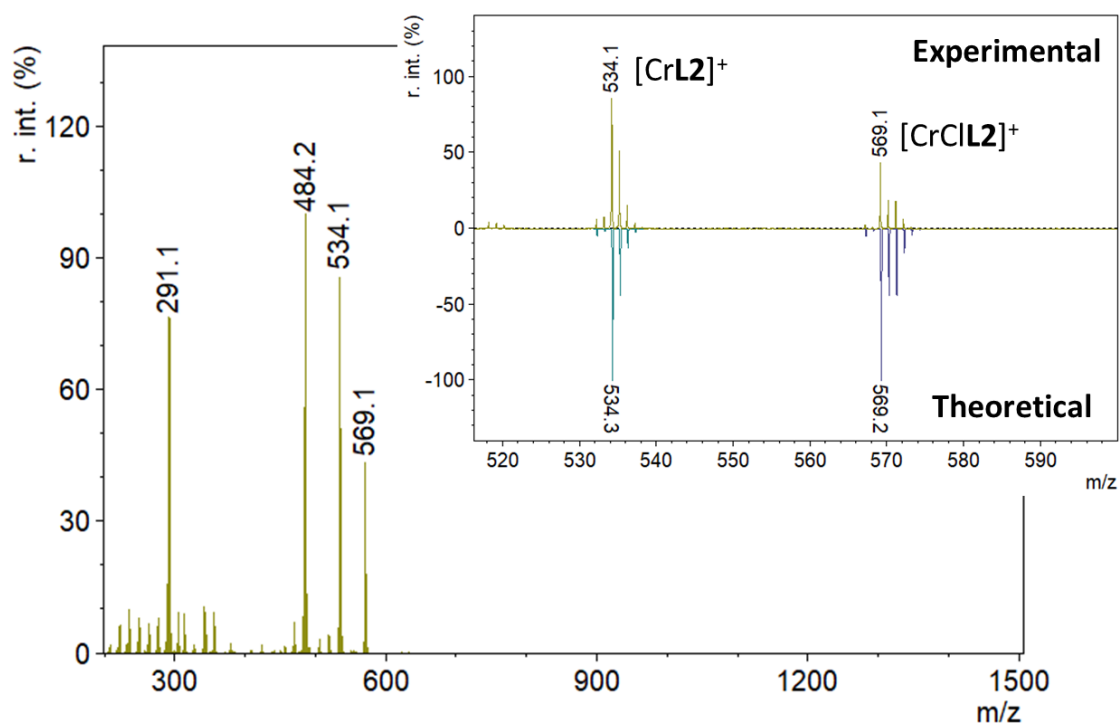


Figure B - 17: MALDI-TOF mass spectrum of **4.2** in positive reflectron mode.

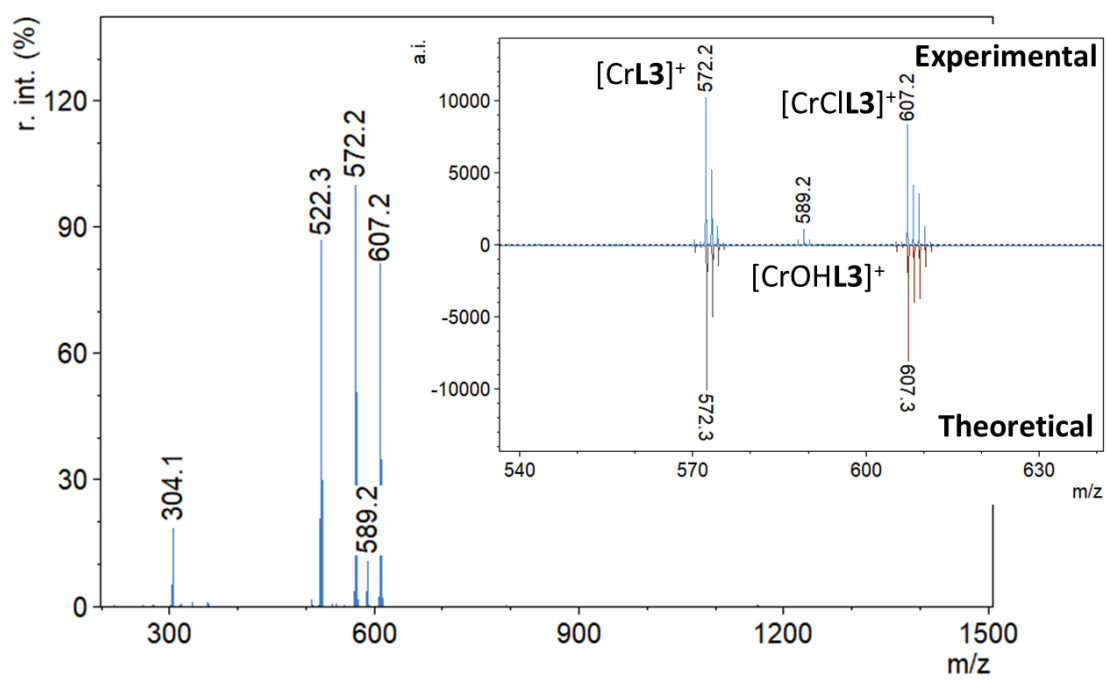


Figure B - 19: MALDI-TOF mass spectrum of **4.3** in positive reflectron mode.

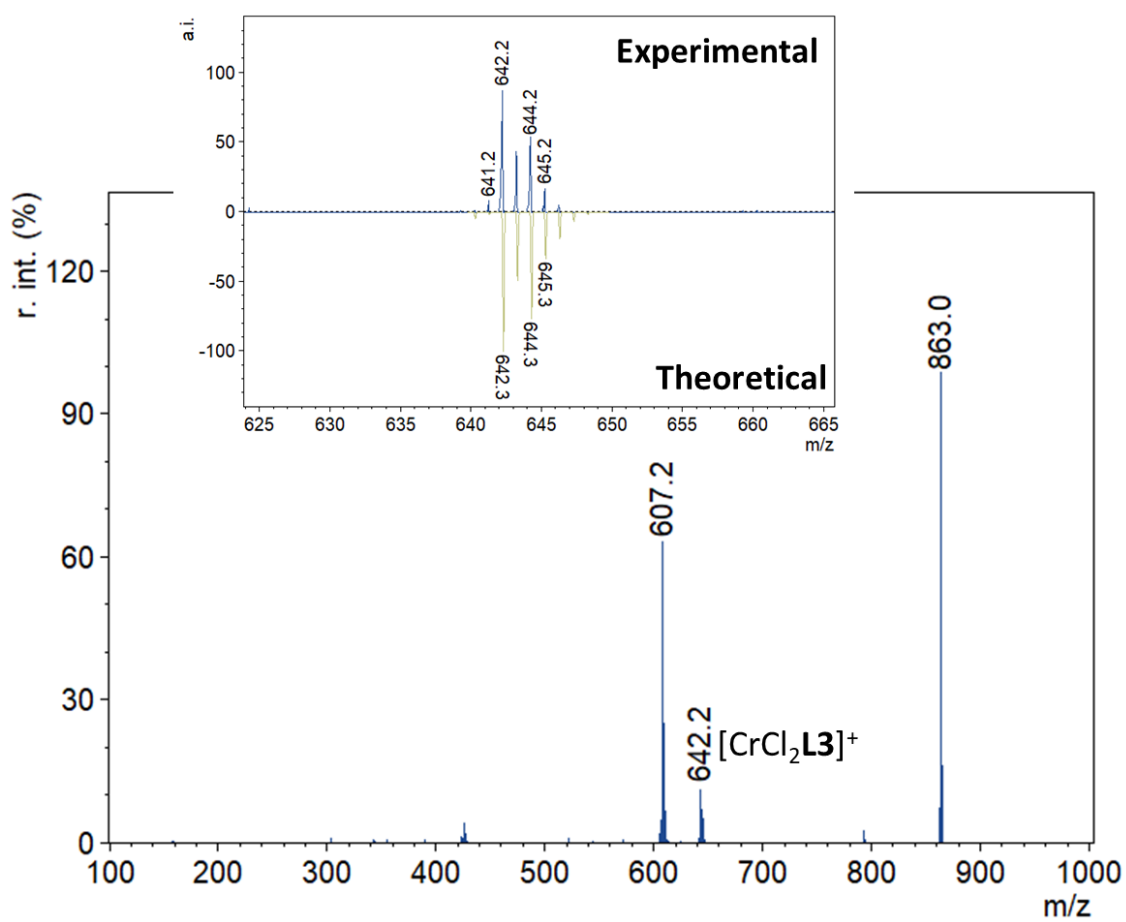


Figure B - 20: MALDI-TOF mass spectrum of **4.3** in negative reflectron mode

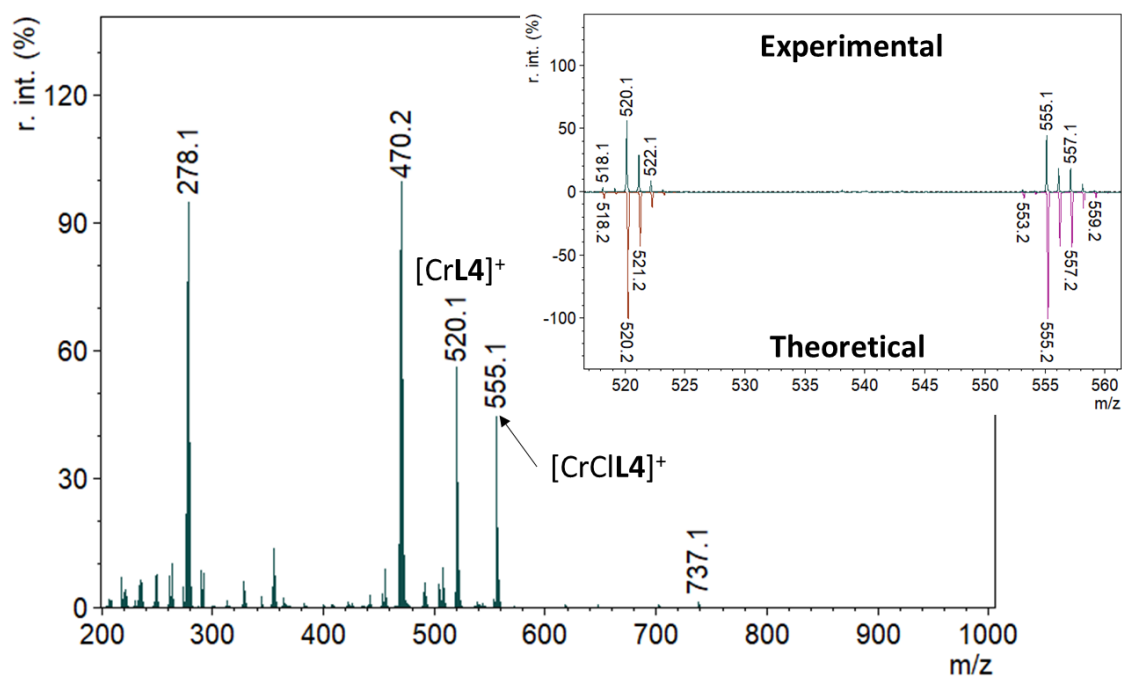


Figure B - 21: MALDI-TOF mass spectrum of **4.4** in positive reflectron mode.

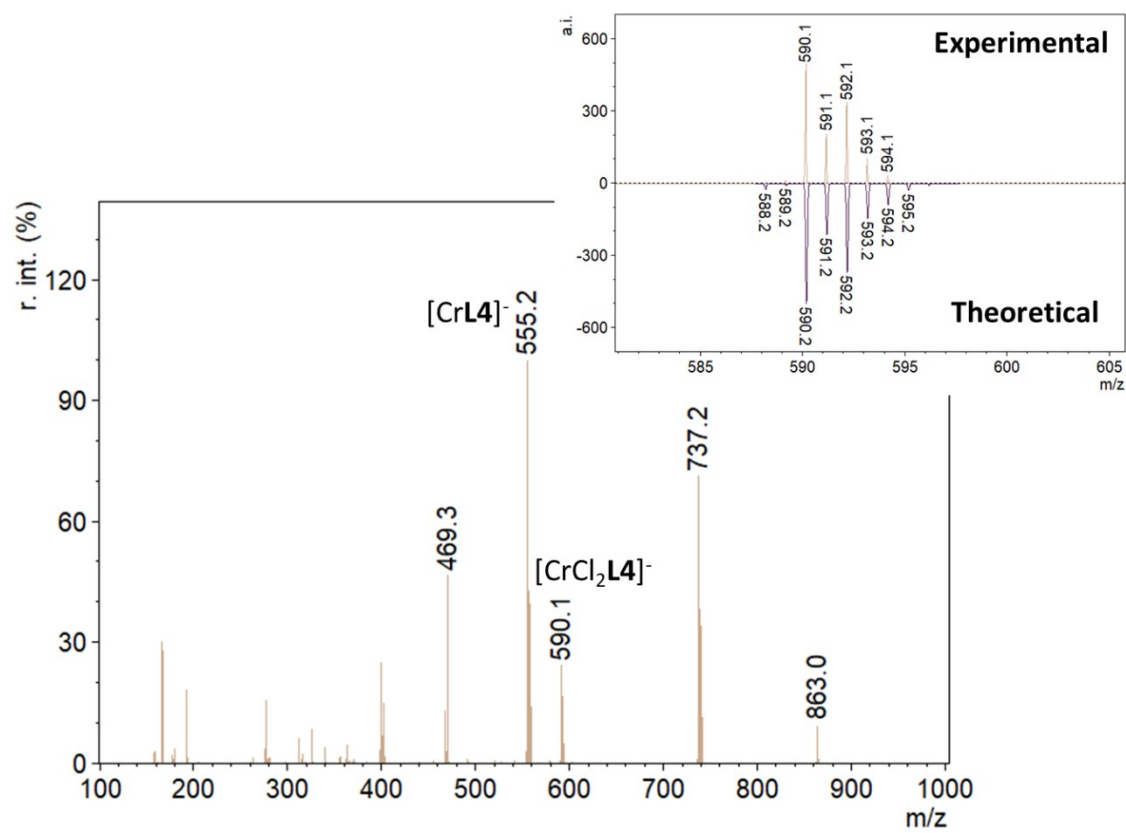


Figure B - 22: MALDI-TOF mass spectrum of **4.4** in negative reflectron mode.

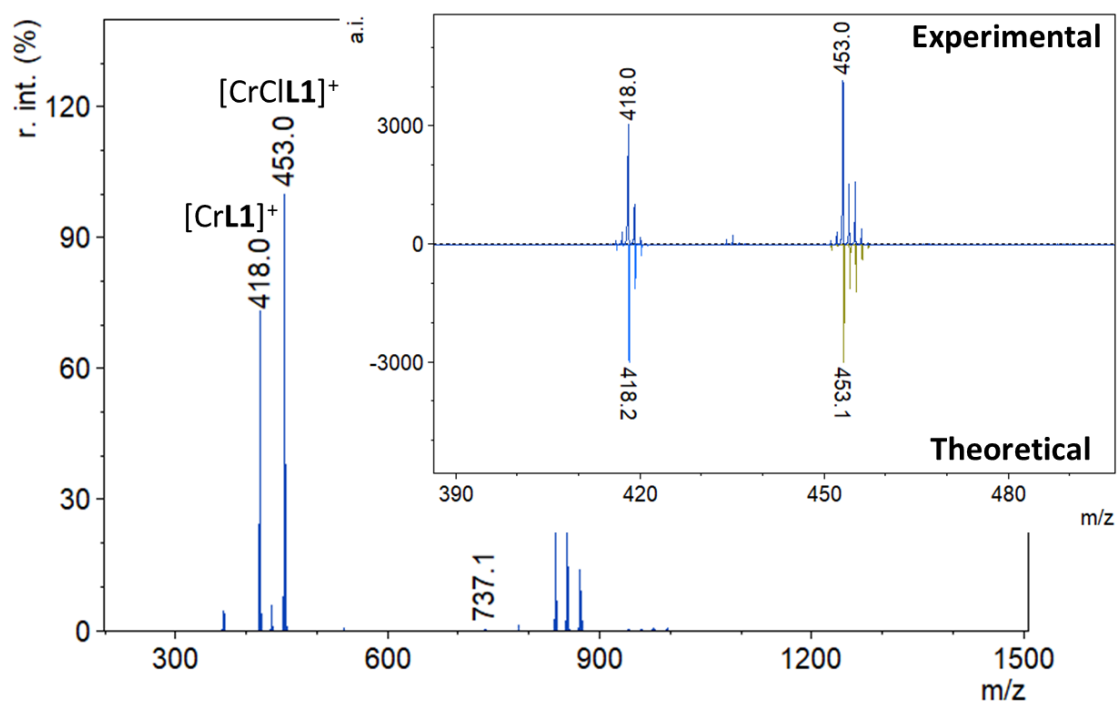


Figure B - 23: MALDI-TOF mass spectrum of **5.1** in positive reflectron mode showing complex monomeric fragments.

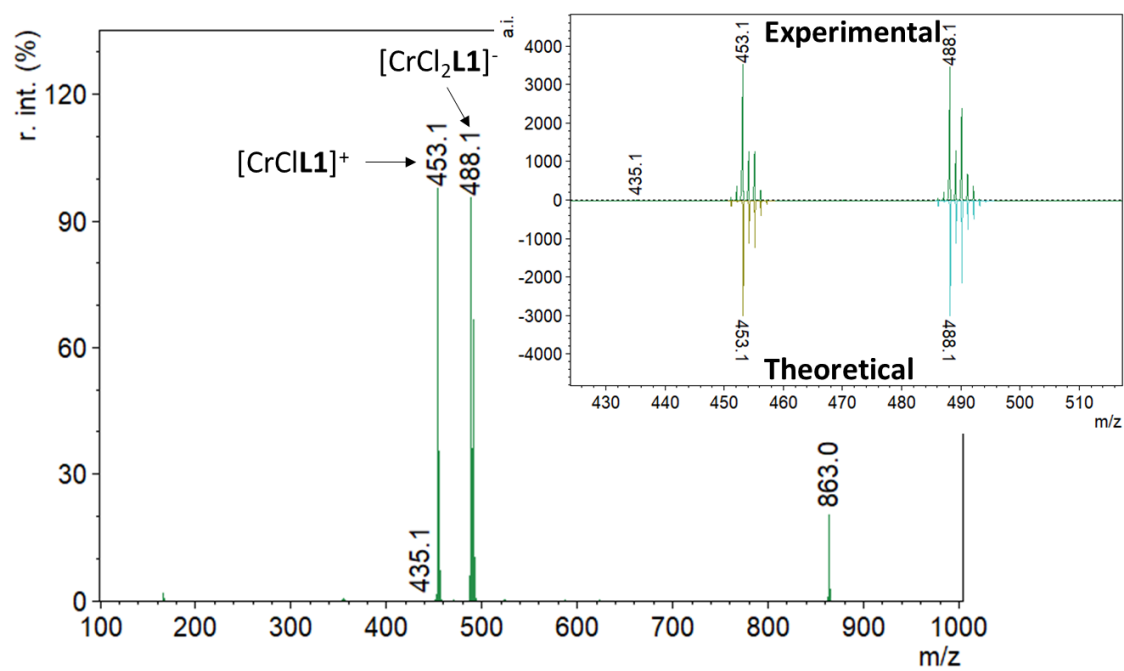


Figure B - 24: MALDI-TOF mass spectrum of **5.1** in negative reflectron mode.

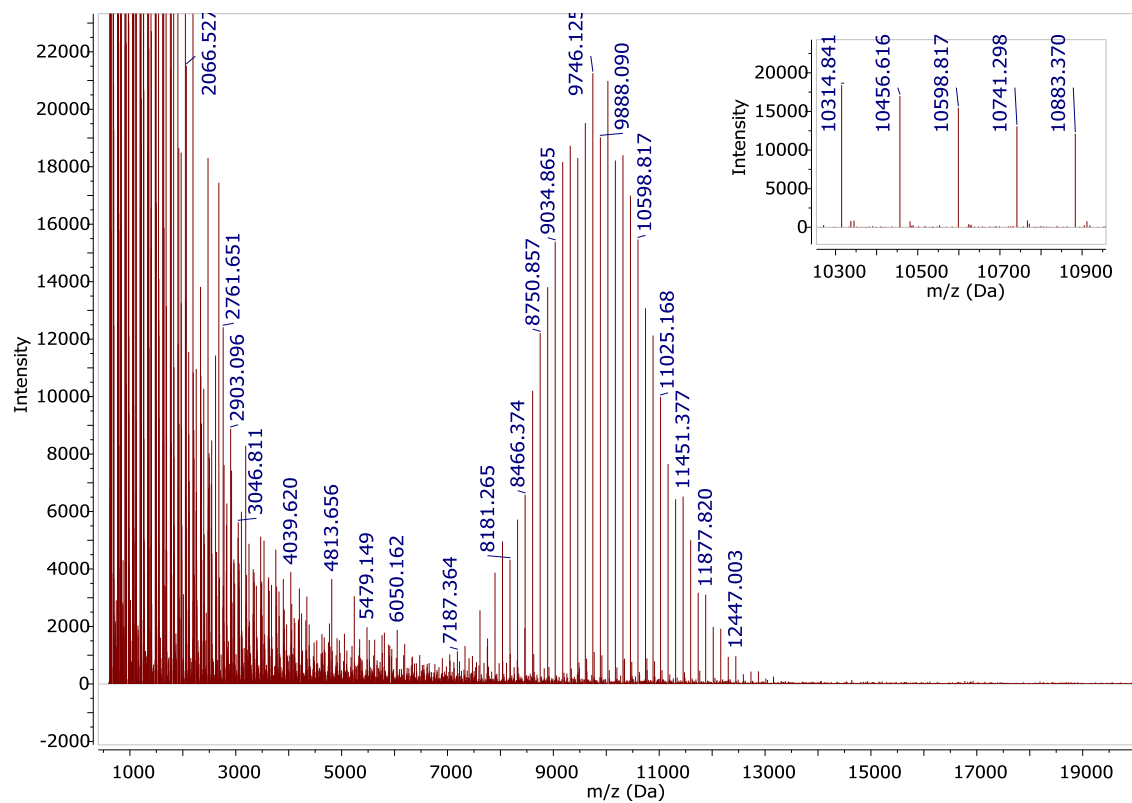


Figure B - 25: MALDI-TOF mass spectrum of polycarbonate obtained from Table 5.1, entry 2.

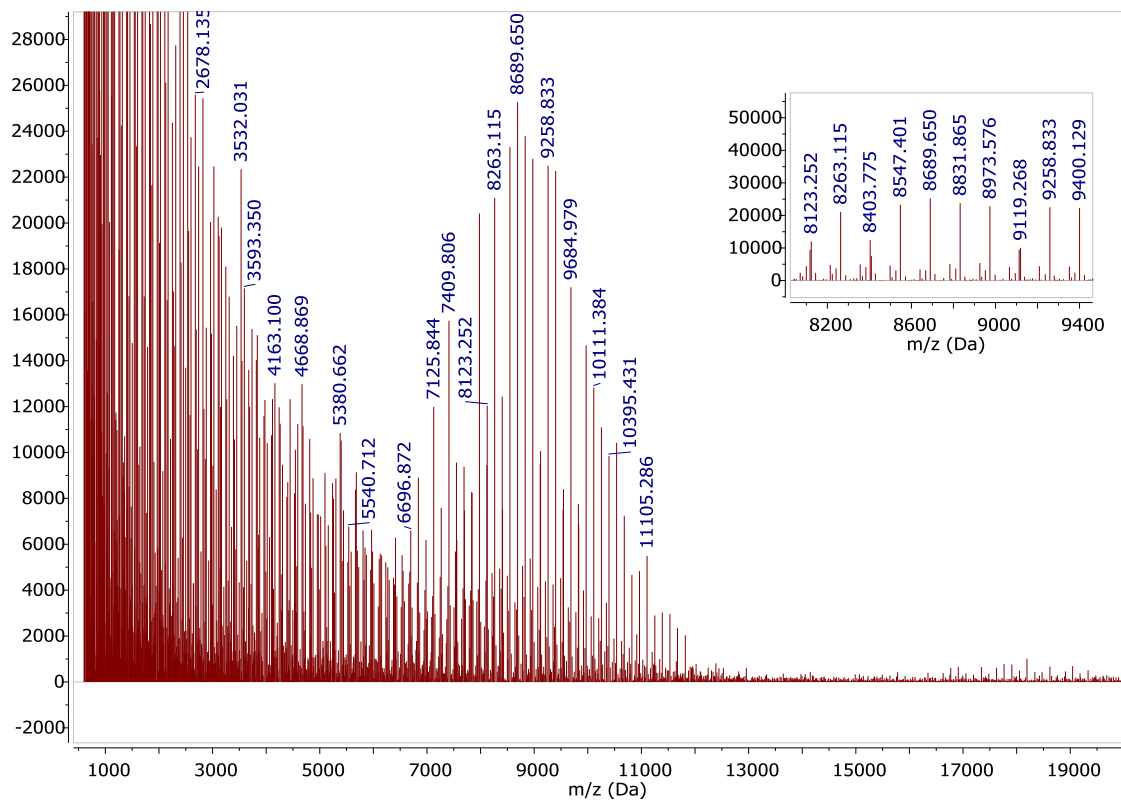


Figure B - 26: MALDI-TOF mass spectrum of polycarbonate obtained from Table 5.1 entry 3.

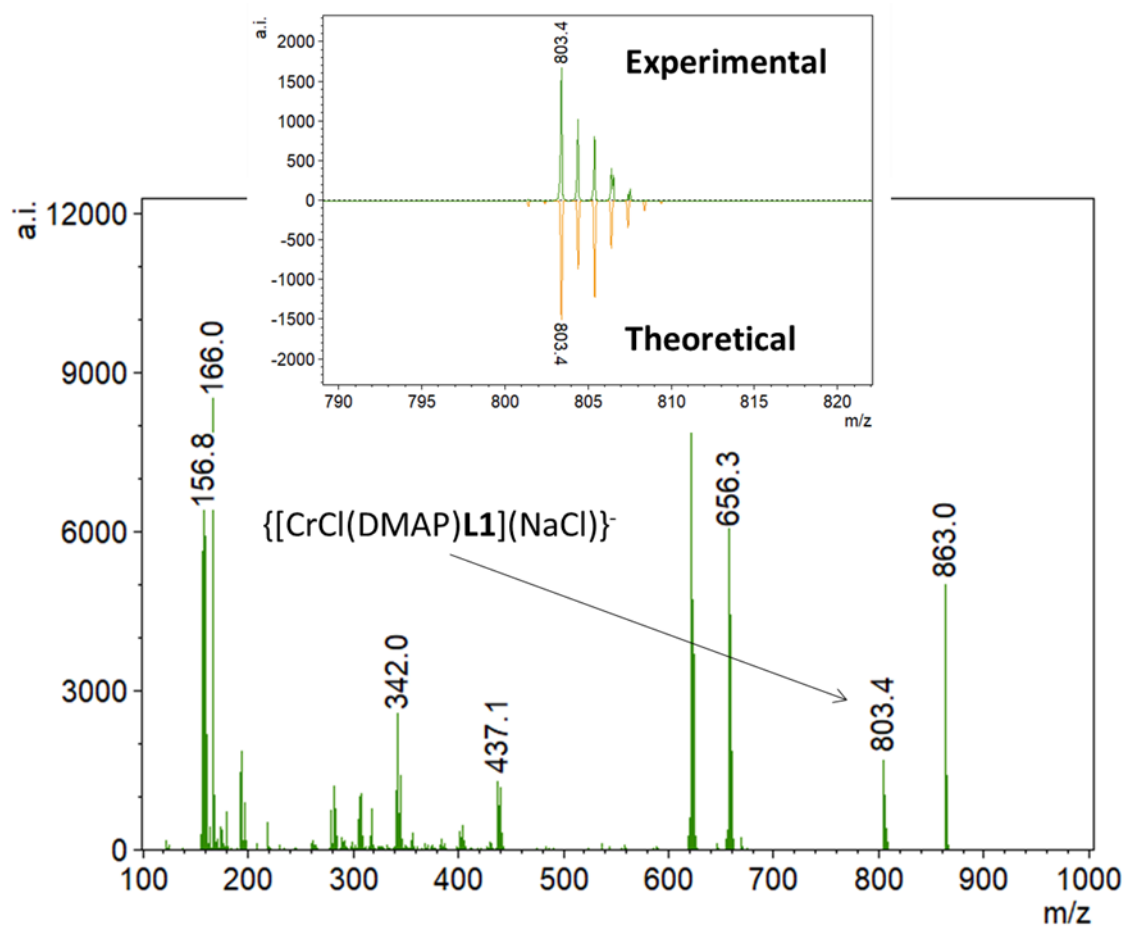


Figure B - 27: MALDI-TOF mass spectrum of **4.1**/DMAP in negative reflectron mode. Ratio of Cr to DMAP is 1:4.

Appendix C: Crystallographic and Structure Refinement Data

Table C - 1: Crystal data and structure refinement of Compound **2.9a**.

Compound	2.9a	3.1
Empirical formula	C ₃₅ H ₄₇ Cl ₂ CoN ₄ O ₇	C ₆₆ H ₅₃ Cl ₁₂ Co ₃ K ₃ N ₆ O ₁₃
Formula weight	765.59	1857.63
Temperature/K	158	125(2)
Crystal system	triclinic	tetragonal
Space group	P-1	P4 ₁ 2 ₁ 2
a/Å	11.7395(16)	21.863(3)
b/Å	13.1332(17)	21.863(3)
c/Å	13.2990(18)	58.231(8)
α/°	77.736(6)	90
β/°	75.262(5)	90
γ/°	78.565(6)	90
Volume/Å³	1915.0(4)	27833(9)
Z	2	8
ρ_{calc}/cm³	1.328	0.887
μ/mm⁻¹	0.637	0.708
F(000)	804.0	7496.0
Crystal size/mm³	0.2 × 0.2 × 0.2	0.345 × 0.287 × 0.212
Radiation	MoKα (λ = 0.71075)	MoKα (λ = 0.71073)
2θ range for data collection/°	6.244 to 52.744	2.33 to 39.112
Index ranges	-15 ≤ h ≤ 13, -16 ≤ k ≤ 16, -17 ≤ l ≤ 16	-20 ≤ h ≤ 16, -20 ≤ k ≤ 18, -54 ≤ l ≤ 52
Reflections collected	19278	90364
Independent reflections	7787 [R _{int} = 0.0407, R _{sigma} = 0.0531]	10617 [R _{int} = 0.0872, R _{sigma} = 0.0945]
Data/restraints/parameters	7787/18/479	10617/2671/929
Goodness-of-fit on F²	1.150	1.032
Final R indexes [I ≥ 2σ (I)]	R ₁ = 0.0738, wR ₂ = 0.2069	R ₁ = 0.0695, wR ₂ = 0.1689
Final R indexes [all data]	R ₁ = 0.0943, wR ₂ = 0.2454	R ₁ = 0.1250, wR ₂ = 0.1974
Largest diff. peak/hole / e Å⁻³	2.59/-1.22	0.28/-0.27

Table C - 2: Bond lengths from structural data of **2.9a**.

Selected bond Lengths		
Atom	Atom	Length/Å
Co1	O5	1.877(2)
Co1	O1	1.903(2)
Co1	O3	1.926(2)
Co1	O2	1.931(2)
Co1	N1	1.950(3)
Co1	N2	2.029(3)

Table C - 3: Bond angles from structural data of **2.9a**.

Selected Bond Angles			
Atom	Atom	Atom	Angle/°
O5	Co1	O1	88.97(10)
O5	Co1	O3	93.21(9)
O5	Co1	O2	89.89(9)
O5	Co1	N1	91.42(10)
O5	Co1	N2	179.60(9)
O1	Co1	O3	86.36(9)
O1	Co1	O2	174.83(9)
O1	Co1	N1	92.06(10)
O1	Co1	N2	90.87(10)
O3	Co1	O2	88.67(9)
O3	Co1	N1	175.08(9)
O3	Co1	N2	87.14(10)
O2	Co1	N1	93.01(10)
O2	Co1	N2	90.30(10)
N1	Co1	N2	88.23(11)

Table C - 4: Selected bond lengths for **3.1**.

Selected Bond Lengths		
Atom	Atom	Length/Å
Co1	O2	1.886(13)
Co1	O1	1.959(13)
Co1	N2	2.045(15)
Co1	O3	2.051(13)
Co1	N1	2.207(16)
Co1	K3	3.590(5)

Co1	K1	3.808(5)
Co2	O5	1.934(13)
Co2	O6	1.973(12)
Co2	N4	2.069(17)
Co2	O7	2.098(12)
Co2	N3	2.180(16)
Co2	K2	3.589(5)
Co2	K1	3.808(5)
Co3	O9	2.033(13)
Co3	N6	2.086(17)
Co3	O10	2.097(13)
Co3	O11	2.114(12)
Co3	N5	2.210(17)
Co3	O8	2.220(12)
Co3	K2	3.544(5)
Co3	K3 ¹	3.748(5)

Table C - 5: Selected bond angles for **3.1**.

Selected Bond Angles			
Atom	Atom	Atom	Angle/°
O2	Co1	O1	112.8(5)
O2	Co1	N2	122.9(6)
O1	Co1	N2	123.1(6)
O2	Co1	O3	90.9(5)
O1	Co1	O3	89.6(5)
N2	Co1	O3	99.6(6)
O2	Co1	N1	89.1(6)
O1	Co1	N1	90.9(6)
N2	Co1	N1	80.0(6)
O3	Co1	N1	179.5(6)
O2	Co1	K3	78.2(4)
O1	Co1	K3	49.8(4)
N2	Co1	K3	149.1(5)
O3	Co1	K3	54.4(4)
N1	Co1	K3	126.1(4)
O2	Co1	K1	47.0(4)
O1	Co1	K1	117.4(4)
N2	Co1	K1	108.5(4)
O3	Co1	K1	46.5(4)
N1	Co1	K1	133.3(5)
K3	Co1	K1	67.64(10)

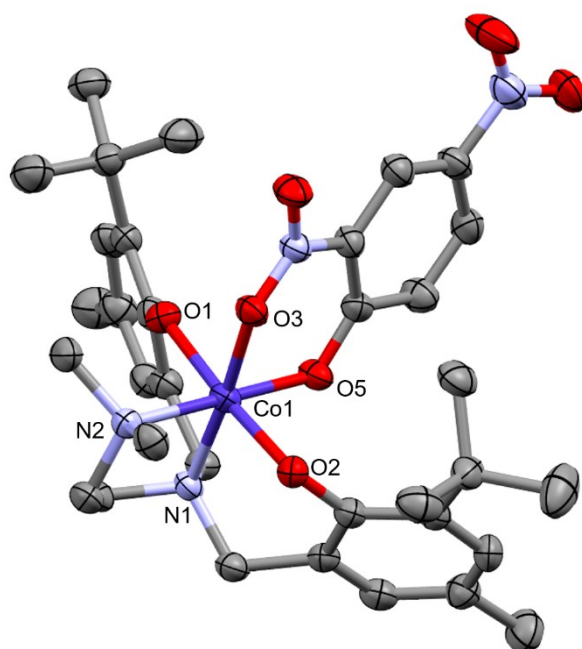


Figure C - 1: Partially labelled molecular structure of compound **2.9a**. Thermal ellipsoids are drawn at 50% probability with hydrogens and co-crystallized dichloromethane molecule omitted for clarity.

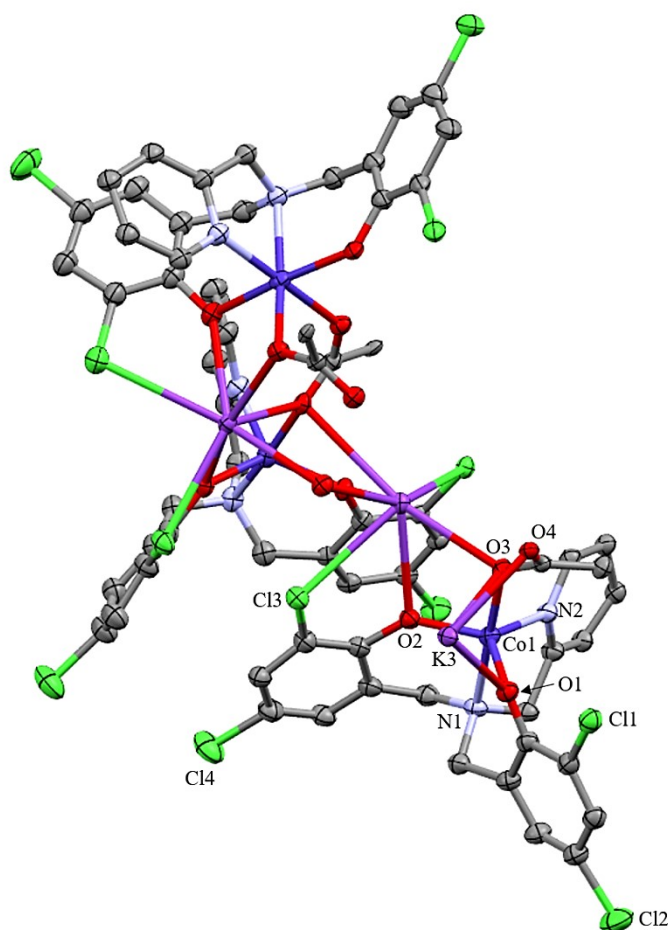


Figure C - 2: Partially labelled molecular structure of compound **3.1**. Thermal ellipsoids are drawn at 10% probability. Structure of the asymmetric unit shown, and hydrogens omitted for clarity.

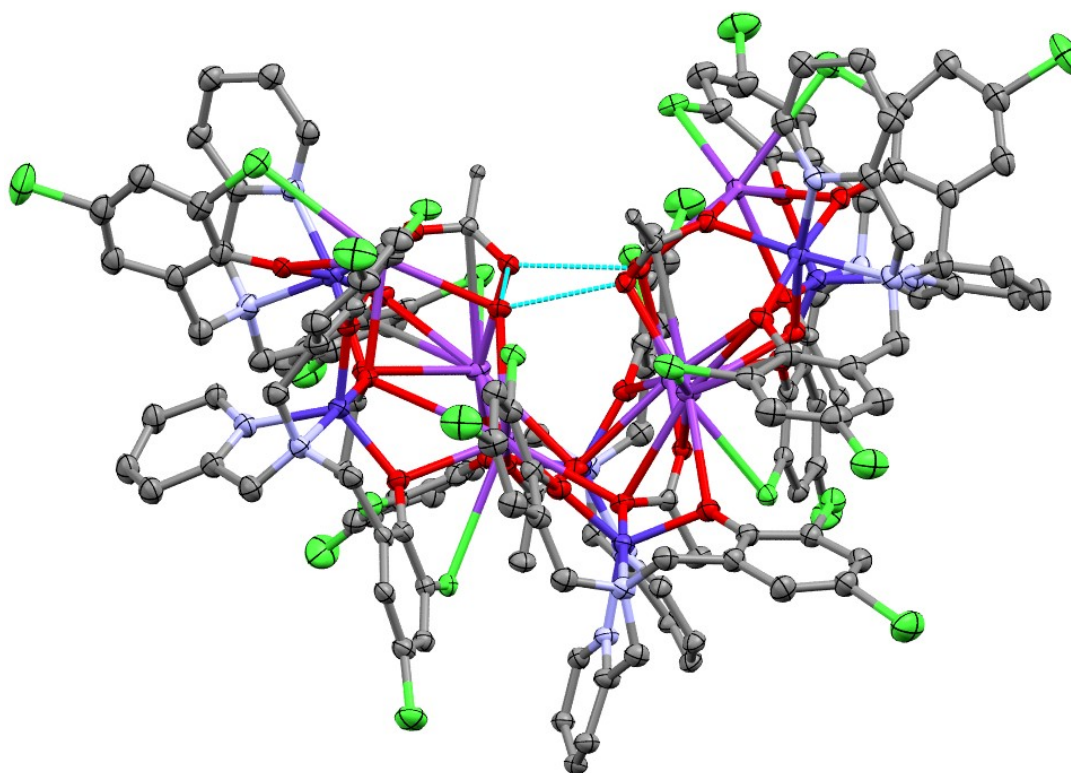


Figure C - 3: Hexacobalt cluster of **3.1** showing inner cavity formed by hydrogen bonding.

Table C - 6: Crystal data and structure refinement of Cr(III) amino-bis(phenolate) complexes.

Compound	4.1	5.1a	5.1b
Empirical formula	C ₃₆ H ₅₇ Cl ₄ CrN ₂ O ₂	C ₄₈ H ₆₅ Cr ₂ N ₅ O ₆	C ₄₇ H ₆₂ Cl ₄ Cr ₂ N ₄ O ₄
Formula weight	743.63	912.05	992.80
Temperature/K	200	100	100
Crystal system	monoclinic	monoclinic	monoclinic
Space group	P ₂ 1/n	I2/a	I2/a
a/Å	18.5813(4)	24.6373(7)	26.0093(7)
b/Å	10.9133(2)	8.4395(2)	8.2812(2)
c/Å	20.9170(4)	21.4764(6)	21.1095(6)
α/°	90	90	90
β/°	105.725(2)	95.014(3)	94.158(3)

$\gamma/^\circ$	90	90	90
Volume/ \AA^3	4082.87(14)	4448.4(2)	4534.8(2)
Z	4	4	4
$\rho_{\text{calc}}/\text{g/cm}^3$	1.210	1.362	1.454
μ/mm^{-1}	0.573	0.544	0.764
F(000)	1580.0	1936.0	2080.0
Crystal size/ mm^3	$0.4 \times 0.25 \times 0.2$	$0.1 \times 0.1 \times 0.01$	$0.2 \times 0.15 \times 0.1$
Radiation	MoK α (λ = 0.71073)	MoK α (λ = 0.71073)	MoK α (λ = 0.71073)
2 Θ range for data collection/ $^\circ$	4.552 to 51.364	4.828 to 51.352	4.804 to 51.364
Index ranges	$-22 \leq h \leq 22, -13 \leq k \leq 13, -25 \leq l \leq 25$	$-30 \leq h \leq 30, -10 \leq k \leq 10, -26 \leq l \leq 26$	$-31 \leq h \leq 31, -10 \leq k \leq 10, -25 \leq l \leq 25$
Reflections collected	52554	28725	29027
Independent reflections	7755 [R _{int} = 0.0585, R _{sigma} = 0.0319]	4233 [R _{int} = 0.1047, R _{sigma} = 0.0535]	4299 [R _{int} = 0.0972, R _{sigma} = 0.0589]
Data/restraints/parameters	7755/85/435	4233/10/295	4299/3/280
Goodness-of-fit on F ²	1.076	1.096	1.051
Final R indexes [$I \geq 2\sigma(I)$]	R ₁ = 0.0573, wR ₂ = 0.1500	R ₁ = 0.0660, wR ₂ = 0.1533	R ₁ = 0.0671, wR ₂ = 0.1512
Final R indexes [all data]	R ₁ = 0.0672, wR ₂ = 0.1618	R ₁ = 0.0783, wR ₂ = 0.1634	R ₁ = 0.0876, wR ₂ = 0.1659
Largest diff. peak/hole / e \AA^{-3}	0.74/-0.42	0.83/-0.53	0.71/-0.77

Table C - 7: Bond lengths from structural data of **4.1''**.

Atom	Atom	Length/ \AA	Atom	Atom	Length/ \AA
Cr1	Cl1	2.3870(7)	C8	C9A	1.515(15)
Cr1	Cl2	2.3208(7)	C12	C13	1.536(4)
Cr1	O1	1.8979(18)	C12	C14	1.536(4)
Cr1	O2	2.0946(17)	C12	C15	1.529(4)
Cr1	N1	2.067(2)	C16	C17	1.503(4)
Cr1	N2	2.150(2)	C17	C18	1.390(4)
O1	C7	1.342(3)	C17	C22	1.389(4)
O2	C18	1.419(3)	C18	C19	1.389(4)
N1	C1	1.490(3)	C19	C20	1.396(4)
N1	C31	1.502(3)	C19	C23	1.538(4)
N1	C35	1.501(3)	C20	C21	1.384(4)
N2	C16	1.494(3)	C21	C22	1.389(4)

N2	C32	1.504(3)	C21	C27	1.533(4)
N2	C33	1.502(3)	C23	C24	1.531(4)
C1	C2	1.504(4)	C23	C25	1.540(4)
C2	C3	1.395(4)	C23	C26	1.534(4)
C2	C7	1.414(4)	C27	C28	1.512(6)
C3	C4	1.382(4)	C27	C29	1.518(6)
C4	C5	1.399(4)	C27	C30	1.549(7)
C4	C8	1.532(4)	C27	C28A	1.528(14)
C5	C6	1.397(4)	C27	C29A	1.479(14)
C6	C7	1.411(4)	C27	C30A	1.526(14)
C6	C12	1.537(4)	C31	C32	1.541(4)
C8	C9	1.524(5)	C33	C34	1.530(4)
C8	C10	1.508(5)	C34	C35	1.516(4)
C8	C11	1.528(5)	C14	C36	1.716(6)
C8	C10A	1.534(16)	C15	C36	1.712(6)
C8	C11A	1.518(15)			

Table C - 8: Bond angles from structural data of **4.1''**.

Atom	Atom	Atom	Angle/°	Atom	Atom	Atom	Angle/°
Cl2	Cr1	Cl1	168.59(3)	C11A	C8	C4	113(3)
O1	Cr1	Cl1	86.79(5)	C11A	C8	C10A	107(2)
O1	Cr1	Cl2	87.78(6)	C9A	C8	C4	112(3)
O1	Cr1	O2	99.55(7)	C9A	C8	C10A	108(2)
O1	Cr1	N1	95.98(8)	C9A	C8	C11A	110(2)
O1	Cr1	N2	171.16(8)	C13	C12	C6	112.6(2)
O2	Cr1	Cl1	83.60(5)	C14	C12	C6	110.6(2)
O2	Cr1	Cl2	87.41(5)	C14	C12	C13	106.9(3)
O2	Cr1	N2	88.85(8)	C15	C12	C6	110.1(2)
N1	Cr1	Cl1	100.25(6)	C15	C12	C13	107.0(3)
N1	Cr1	Cl2	90.29(6)	C15	C12	C14	109.5(3)
N1	Cr1	O2	164.20(8)	N2	C16	C17	116.7(2)
N1	Cr1	N2	75.79(8)	C18	C17	C16	120.7(2)
N2	Cr1	Cl1	91.47(6)	C22	C17	C16	120.4(3)
N2	Cr1	Cl2	95.38(6)	C22	C17	C18	118.8(3)
C7	O1	Cr1	125.36(16)	C17	C18	O2	116.8(2)
C18	O2	Cr1	116.53(14)	C19	C18	O2	120.1(2)
C1	N1	Cr1	109.01(16)	C19	C18	C17	123.0(2)
C1	N1	C31	108.9(2)	C18	C19	C20	115.4(3)

C1	N1	C35	110.6(2)	C18	C19	C23	123.5(2)
C31	N1	Cr1	107.25(16)	C20	C19	C23	121.1(2)
C35	N1	Cr1	112.43(16)	C21	C20	C19	124.1(3)
C35	N1	C31	108.6(2)	C20	C21	C22	117.8(3)
C16	N2	Cr1	113.48(15)	C20	C21	C27	120.2(3)
C16	N2	C32	111.9(2)	C22	C21	C27	122.0(3)
C16	N2	C33	105.7(2)	C21	C22	C17	120.8(3)
C32	N2	Cr1	104.42(15)	C19	C23	C25	111.0(2)
C33	N2	Cr1	113.64(16)	C24	C23	C19	110.1(2)
C33	N2	C32	107.7(2)	C24	C23	C25	109.8(3)
N1	C1	C2	115.0(2)	C24	C23	C26	107.9(3)
C3	C2	C1	119.4(2)	C26	C23	C19	111.5(2)
C3	C2	C7	119.9(3)	C26	C23	C25	106.5(2)
C7	C2	C1	120.4(2)	C21	C27	C30	108.4(4)
C4	C3	C2	122.2(3)	C28	C27	C21	113.6(3)
C3	C4	C5	116.6(3)	C28	C27	C29	109.3(4)
C3	C4	C8	121.3(3)	C28	C27	C30	107.6(4)
C5	C4	C8	122.0(3)	C29	C27	C21	110.2(3)
C6	C5	C4	124.2(3)	C29	C27	C30	107.6(5)
C5	C6	C7	117.5(2)	C28A	C27	C21	100.8(12)
C5	C6	C12	120.8(2)	C29A	C27	C21	115.3(12)
C7	C6	C12	121.7(2)	C29A	C27	C28A	111.8(15)
O1	C7	C2	119.7(2)	C29A	C27	C30A	113.4(16)
O1	C7	C6	120.7(2)	C30A	C27	C21	106.5(13)
C6	C7	C2	119.5(2)	C30A	C27	C28A	108.1(16)
C4	C8	C10A	107(3)	N1	C31	C32	111.2(2)
C9	C8	C4	110.9(3)	N2	C32	C31	109.6(2)
C9	C8	C11	107.5(4)	N2	C33	C34	113.8(2)
C10	C8	C4	112.1(3)	C35	C34	C33	118.2(2)
C10	C8	C9	108.1(4)	N1	C35	C34	112.3(2)
C10	C8	C11	109.8(4)	Cl5	C36	Cl4	116.4(3)
C11	C8	C4	108.3(3)				

Table C - 9: Bond lengths from structural data of **5.1a**.

Atom	Atom	Length/Å	Atom	Atom	Length/Å
Cr1	O1	2.003(2)	C3	C4	1.394(5)
Cr1	O1*	1.988(2)	C4	C5	1.385(5)
Cr1	O2	1.933(2)	C4	C9	1.511(5)

Cr1	O3	1.920(2)	C5	C6	1.382(4)
Cr1	N1	2.125(3)	C6	C7	1.418(4)
Cr1	N2	2.120(3)	C6	C8	1.498(5)
O2	C7	1.338(4)	C10	C11	1.520(4)
O3	C12	1.335(4)	C11	C12	1.415(4)
N1	C1	1.492(4)	C11	C16	1.396(4)
N1	C19	1.479(4)	C12	C13	1.414(4)
N1	C23	1.498(4)	C13	C14	1.390(4)
N2	C10	1.486(4)	C13	C17	1.506(4)
N2	C20	1.496(4)	C14	C15	1.398(4)
N2	C21	1.487(4)	C15	C16	1.386(5)
N3	C25	1.1623	C15	C18	1.506(4)
C25	C26	1.4533	C19	C20	1.536(4)
C1	C2	1.508(4)	C21	C22	1.520(4)
C2	C3	1.395(4)	C22	C23	1.529(5)
C2	C7	1.403(4)			

Table C - 10: Bond angles from structural data of **5.1a**.

Atom	Atom	Atom	Angle/°	Atom	Atom	Atom	Angle/°
O1 ¹	Cr1	O1	77.17(10)	C3	C2	C7	120.0(3)
O1	Cr1	N1	95.03(9)	C7	C2	C1	118.4(3)
O1 ¹	Cr1	N1	170.23(9)	C4	C3	C2	121.6(3)
O1 ¹	Cr1	N2	99.99(9)	C3	C4	C9	121.8(3)
O1	Cr1	N2	97.52(9)	C5	C4	C3	117.2(3)
O2	Cr1	O1 ¹	94.57(9)	C5	C4	C9	121.0(3)
O2	Cr1	O1	90.41(9)	C6	C5	C4	123.7(3)
O2	Cr1	N1	91.33(9)	C5	C6	C7	118.4(3)
O2	Cr1	N2	164.64(9)	C5	C6	C8	122.3(3)
O3	Cr1	O1	169.49(9)	C7	C6	C8	119.2(3)
O3	Cr1	O1 ¹	92.44(9)	O2	C7	C2	120.4(3)
O3	Cr1	O2	92.02(9)	O2	C7	C6	120.5(3)
O3	Cr1	N1	95.13(9)	C2	C7	C6	119.1(3)
O3	Cr1	N2	82.57(9)	N2	C10	C11	113.0(2)
N2	Cr1	N1	74.94(10)	C12	C11	C10	123.2(3)
Cr1 ¹	O1	Cr1	102.83(10)	C16	C11	C10	117.4(3)
C7	O2	Cr1	114.82(18)	C16	C11	C12	119.2(3)
C12	O3	Cr1	125.21(18)	O3	C12	C11	124.0(3)
C1	N1	Cr1	112.61(18)	O3	C12	C13	117.6(3)

C1	N1	C23	107.3(2)	C13	C12	C11	118.4(3)
C19	N1	Cr1	105.53(18)	C12	C13	C17	118.3(3)
C19	N1	C1	110.4(2)	C14	C13	C12	120.0(3)
C19	N1	C23	110.3(2)	C14	C13	C17	121.7(3)
C23	N1	Cr1	110.71(18)	C13	C14	C15	122.3(3)
C10	N2	Cr1	109.24(18)	C14	C15	C18	121.9(3)
C10	N2	C20	110.2(2)	C16	C15	C14	117.0(3)
C10	N2	C21	109.4(2)	C16	C15	C18	121.1(3)
C20	N2	Cr1	107.78(17)	C15	C16	C11	123.0(3)
C21	N2	Cr1	110.79(18)	N1	C19	C20	110.3(2)
C21	N2	C20	109.5(2)	N2	C20	C19	110.6(2)
N3	C25	C26	180.0	N2	C21	C22	111.4(2)
N1	C1	C2	114.3(3)	C21	C22	C23	117.0(3)
C3	C2	C1	121.5(3)	N1	C23	C22	115.0(3)

Table C - 11: Bond lengths from structural data of **5.1b**.

Atom	Atom	Length/Å	Atom	Atom	Length/Å
Cr1	Cl1	2.3805(12)	C4	C5	1.393(6)
Cr1	Cl1 ¹	2.4244(12)	C4	C8	1.502(6)
Cr1	O1	1.903(3)	C5	C6	1.395(6)
Cr1	O2	1.923(3)	C6	C7	1.397(6)
Cr1	N1	2.131(3)	C6	C9	1.509(6)
Cr1	N2	2.106(3)	C10	C11	1.522(5)
O1	C16	1.343(4)	C11	C12	1.396(5)
O2	C3	1.345(5)	C11	C16	1.406(5)
N1	C10	1.482(5)	C12	C13	1.381(6)
N1	C19	1.504(5)	C13	C14	1.406(5)
N1	C23	1.495(5)	C13	C17	1.502(6)
N2	C1	1.498(5)	C14	C15	1.383(5)
N2	C20	1.489(5)	C15	C16	1.420(5)
N2	C21	1.504(5)	C15	C18	1.497(5)
C1	C2	1.506(5)	C19	C20	1.537(5)
C2	C3	1.402(6)	C21	C22	1.529(5)
C2	C7	1.389(6)	C22	C23	1.533(6)
C3	C4	1.413(6)	Cl2	C24	1.750(4)

Table C - 12: Bond angles from structural data of **5.1b**.

Atom	Atom	Atom	Angle/°	Atom	Atom	Atom	Angle/°
Cl1	Cr1	Cl1 ¹	83.15(4)	C7	C2	C3	119.9(4)
O1	Cr1	Cl1	88.54(8)	O2	C3	C2	120.3(3)
O1	Cr1	Cl1 ¹	171.68(9)	O2	C3	C4	119.6(4)
O1	Cr1	O2	93.08(11)	C2	C3	C4	120.1(4)
O1	Cr1	N1	82.65(11)	C3	C4	C8	119.9(4)
O1	Cr1	N2	95.33(12)	C5	C4	C3	117.8(4)
O2	Cr1	Cl1 ¹	87.15(9)	C5	C4	C8	122.2(4)
O2	Cr1	Cl1	92.89(9)	C4	C5	C6	123.1(4)
O2	Cr1	N1	166.48(12)	C5	C6	C7	117.6(4)
O2	Cr1	N2	92.22(12)	C5	C6	C9	120.4(4)
N1	Cr1	Cl1 ¹	98.93(9)	C7	C6	C9	121.9(4)
N1	Cr1	Cl1	99.78(9)	C2	C7	C6	121.4(4)
N2	Cr1	Cl1 ¹	92.97(9)	N1	C10	C11	112.6(3)
N2	Cr1	Cl1	173.41(9)	C12	C11	C10	117.8(3)
N2	Cr1	N1	75.50(12)	C12	C11	C16	119.3(3)
Cr1	Cl1	Cr1 ¹	96.85(4)	C16	C11	C10	122.7(3)
C16	O1	Cr1	126.4(2)	C13	C12	C11	122.8(4)
C3	O2	Cr1	113.1(2)	C12	C13	C14	117.1(4)
C10	N1	Cr1	108.9(2)	C12	C13	C17	120.7(4)
C10	N1	C19	110.7(3)	C14	C13	C17	122.2(4)
C10	N1	C23	110.0(3)	C15	C14	C13	122.3(4)
C19	N1	Cr1	107.5(2)	C14	C15	C16	119.5(4)
C23	N1	Cr1	110.8(2)	C14	C15	C18	121.7(4)
C23	N1	C19	109.0(3)	C16	C15	C18	118.9(3)
C1	N2	Cr1	111.5(2)	O1	C16	C11	124.2(3)
C1	N2	C21	108.2(3)	O1	C16	C15	116.8(3)
C20	N2	Cr1	105.3(2)	C11	C16	C15	118.9(3)
C20	N2	C1	110.4(3)	N1	C19	C20	110.5(3)
C20	N2	C21	109.5(3)	N2	C20	C19	110.4(3)
C21	N2	Cr1	112.0(2)	N2	C21	C22	115.9(3)
N2	C1	C2	114.1(3)	C21	C22	C23	118.0(3)
C3	C2	C1	117.6(4)	N1	C23	C22	111.7(3)
C7	C2	C1	122.4(4)	Cl2 ²	C24	Cl2	111.1(4)

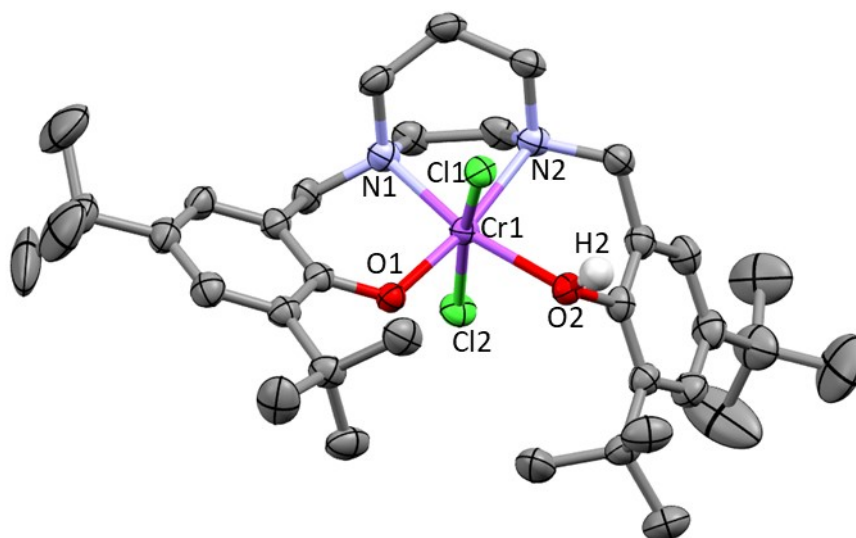


Figure C - 4: Partially labelled molecular structure of compound **4.1''**. Thermal ellipsoids are drawn at 50% probability with hydrogens (except H(2)) and co-crystallized solvent molecule omitted for clarity.

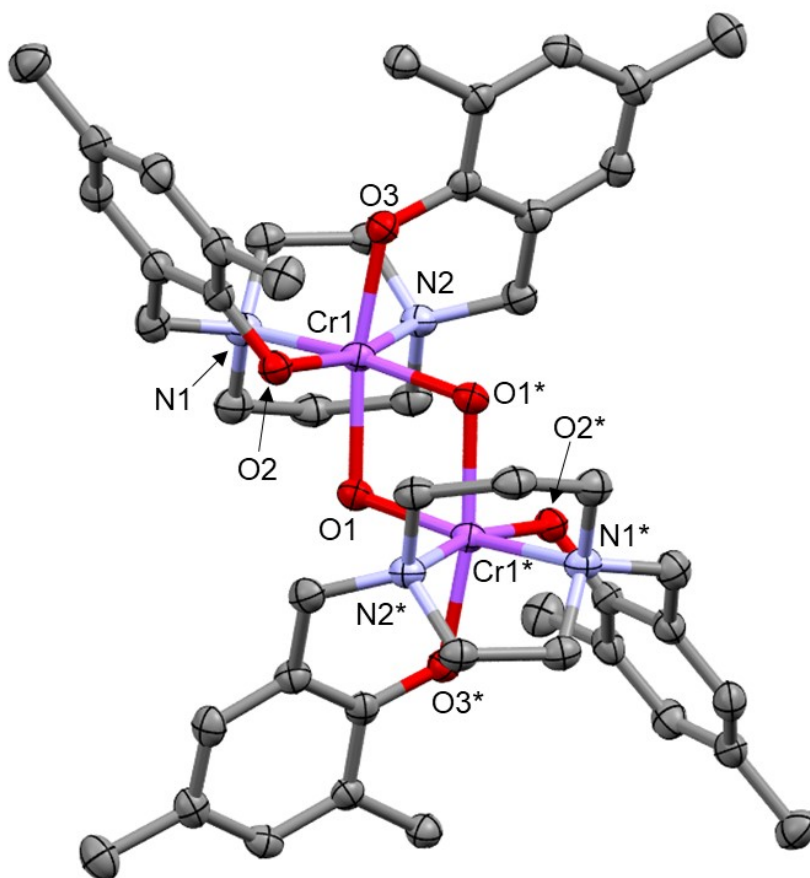


Figure C - 5: Partially labelled molecular structure of **5.1a**. Thermal ellipsoids are drawn at 50% probability with hydrogens and co-crystallized acetonitrile molecule omitted for clarity.

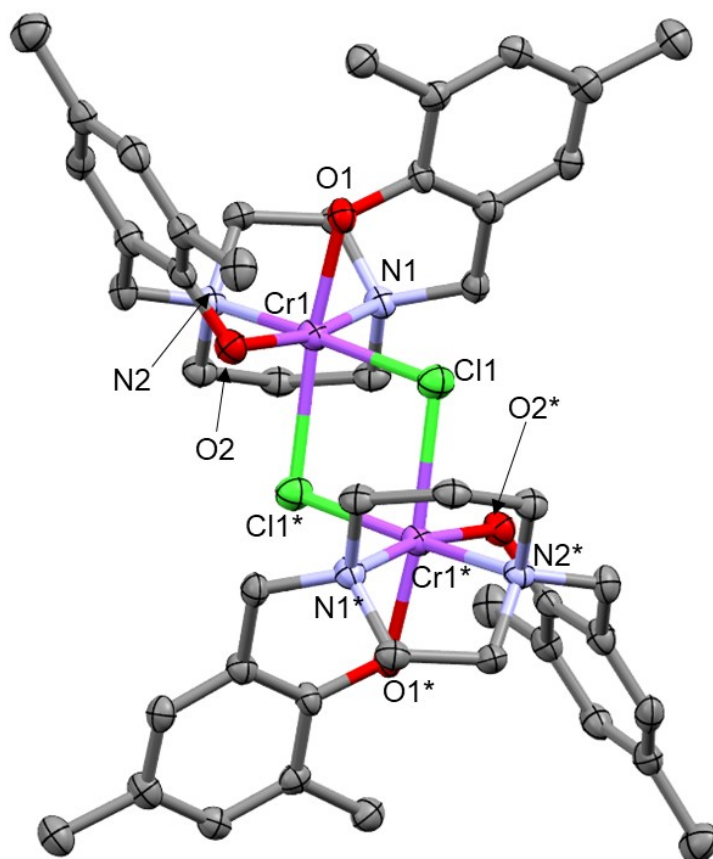


Figure C - 6: Partially labelled molecular structure of **5.1b**. Thermal ellipsoids are drawn at 50% probability with hydrogens and co-crystallized dichloromethane molecule omitted for clarity.

Table C - 13: Crystal data and structure refinement data for **5.2**.

Compound	5.2
Empirical formula	C ₂₅ H ₃₆ Cl ₄ CrN ₅ O ₃
Formula weight	648.39
Temperature/K	100
Crystal system	triclinic
Space group	P-1
a/Å	11.6364(11)
b/Å	12.1029(14)
c/Å	12.7523(9)
α/°	117.065(9)

$\beta/^\circ$	110.298(8)
$\gamma/^\circ$	91.107(9)
Volume/ \AA^3	1465.8(3)
Z	2
$\rho_{\text{calc}}/\text{g/cm}^3$	1.469
μ/mm^{-1}	0.791
F(000)	674.0
Crystal size/ mm^3	$0.1 \times 0.1 \times 0.1$
Radiation	MoK α ($\lambda = 0.71073$)
2 Θ range for data collection/ $^\circ$	4.238 to 51.358
Index ranges	$-14 \leq h \leq 14, -14 \leq k \leq 14, -15 \leq l \leq 15$
Reflections collected	11612
Independent reflections	11612 [$R_{\text{int}} = 0.4856, R_{\text{sigma}} = 0.1609$]
Data/restraints/parameters	11612/26/376
Goodness-of-fit on F^2	0.892
Final R indexes [$I \geq 2\sigma(I)$]	$R_1 = 0.0877, wR_2 = 0.2204$
Final R indexes [all data]	$R_1 = 0.1611, wR_2 = 0.2376$
Largest diff. peak/hole / $e \text{ \AA}^{-3}$	1.66/-0.74

Table C - 14: Bond lengths from structural dat of **5.2**.

Atom	Atom	Length/ \AA	Atom	Atom	Length/ \AA
Cr1	O1	1.944 (5)	C10	C11	1.473 (9)
Cr1	O2	1.946 (4)	C11	C12	1.400 (9)
Cr1	O3	2.036 (4)	C11	C16	1.408 (9)
Cr1	N1	2.085 (5)	C12	C13	1.412 (9)
Cr1	N2	2.104 (6)	C13	C14	1.390 (10)
Cr1	N3	2.007 (6)	C13	C18	1.457 (10)
O1	C7	1.346 (7)	C14	C15	1.378 (10)
O2	C12	1.342 (8)	C15	C16	1.379 (10)
N1	C1	1.485 (8)	C15	C17	1.513 (10)
N1	C20	1.506 (8)	C19	C20	1.521 (9)
N1	C21	1.477 (8)	C21	C22	1.520 (9)
N2	C10	1.500 (8)	C22	C23	1.518 (9)
N2	C19	1.506 (8)	C13	C25	1.779 (13)
N2	C23	1.477 (8)	C13	C15	2.216 (13)
N3	N4	1.158 (7)	C14	C25	1.744 (16)
N4	N5	1.177 (8)	C14	C16	2.339 (9)
C1	C2	1.475 (9)	C14	C15	0.967 (12)

C2	C3	1.389 (9)	Cl4	C26	1.62 (3)
C2	C7	1.400 (9)	C25	Cl5	1.536 (18)
C3	C4	1.361 (10)	C25	C26	0.71 (2)
C4	C5	1.392 (10)	Cl1	C24	1.760 (8)
C4	C8	1.516 (9)	Cl2	C24	1.704 (9)
C5	C6	1.367 (9)	Cl6	C26	1.67 (3)
C6	C7	1.404 (9)	Cl5	C26	1.70 (3)
C6	C9	1.509 (9)			

Table C - 15: Bond angles from structural data of **5.2**.

Atom Atom Atom			Angle/°	Atom Atom Atom			Angle/°
O1	Cr1	O2	95.94 (18)	C12	C11	C10	120.0 (7)
O1	Cr1	O3	87.15 (18)	C12	C11	C16	118.8 (6)
O1	Cr1	N1	93.8 (2)	C16	C11	C10	121.0 (6)
O1	Cr1	N2	169.6 (2)	O2	C12	C11	119.9 (6)
O1	Cr1	N3	90.3 (2)	O2	C12	C13	119.9 (6)
O2	Cr1	O3	86.15 (18)	C11	C12	C13	120.2 (7)
O2	Cr1	N1	169.0 (2)	C12	C13	C18	119.8 (6)
O2	Cr1	N2	93.8 (2)	C14	C13	C12	117.7 (7)
O2	Cr1	N3	90.8 (2)	C14	C13	C18	122.5 (6)
O3	Cr1	N1	89.20 (19)	C15	C14	C13	123.6 (7)
O3	Cr1	N2	89.9 (2)	C14	C15	C16	117.8 (7)
N1	Cr1	N2	76.2 (2)	C14	C15	C17	119.7 (7)
N3	Cr1	O3	175.8 (2)	C16	C15	C17	122.5 (7)
N3	Cr1	N1	94.3 (2)	C15	C16	C11	121.8 (7)
N3	Cr1	N2	93.2 (2)	N2	C19	C20	110.9 (5)
C7	O1	Cr1	121.6 (4)	N1	C20	C19	110.4 (5)
C12	O2	Cr1	120.7 (4)	N1	C21	C22	112.9 (5)
C1	N1	Cr1	110.7 (4)	C23	C22	C21	117.3 (6)
C1	N1	C20	109.2 (5)	N2	C23	C22	113.2 (6)
C20	N1	Cr1	106.2 (4)	C25	Cl3	Cl5	43.5 (5)
C21	N1	Cr1	112.3 (4)	C25	Cl4	Cl6	69.3 (5)
C21	N1	C1	109.6 (5)	Cl5	Cl4	C25	61.4 (8)
C21	N1	C20	108.9 (5)	Cl5	Cl4	Cl6	115.7 (8)
C10	N2	Cr1	109.8 (4)	Cl5	Cl4	C26	77.5 (13)
C10	N2	C19	110.2 (5)	C26	Cl4	C25	24.0 (9)
C19	N2	Cr1	105.7 (4)	C26	Cl4	Cl6	45.7 (10)
C23	N2	Cr1	111.3 (4)	Cl4	C25	Cl3	110.1 (9)

C23	N2	C10	110.9 (5)	Cl5	C25	Cl3	83.6 (8)
C23	N2	C19	108.8 (5)	Cl5	C25	Cl4	33.5 (5)
N4	N3	Cr1	122.0 (5)	C26	C25	Cl3	169 (4)
N3	N4	N5	175.2 (7)	C26	C25	Cl4	68 (3)
C2	C1	N1	114.2 (6)	C26	C25	Cl5	90 (3)
C3	C2	C1	121.4 (6)	Cl2	C24	Cl1	113.2 (5)
C3	C2	C7	118.2 (7)	C26	Cl6	Cl4	43.8 (11)
C7	C2	C1	119.9 (6)	Cl4	Cl5	Cl3	125.5 (10)
C4	C3	C2	123.4 (7)	Cl4	Cl5	C25	85.1 (9)
C3	C4	C5	117.3 (7)	Cl4	Cl5	C26	68.7 (13)
C3	C4	C8	121.1 (7)	C25	Cl5	Cl3	52.9 (6)
C5	C4	C8	121.5 (7)	C25	Cl5	C26	24.7 (9)
C6	C5	C4	122.1 (7)	C26	Cl5	Cl3	77.4 (10)
C5	C6	C7	119.6 (7)	Cl4	C26	Cl6	90.5 (16)
C5	C6	C9	120.7 (7)	Cl4	C26	Cl5	33.8 (7)
C7	C6	C9	119.7 (6)	C25	C26	Cl4	88 (4)
O1	C7	C2	120.0 (6)	C25	C26	Cl6	168 (5)
O1	C7	C6	120.6 (6)	C25	C26	Cl5	65 (3)
C2	C7	C6	119.4 (6)	Cl6	C26	Cl5	118.2 (19)
C11	C10	N2	114.9 (6)				

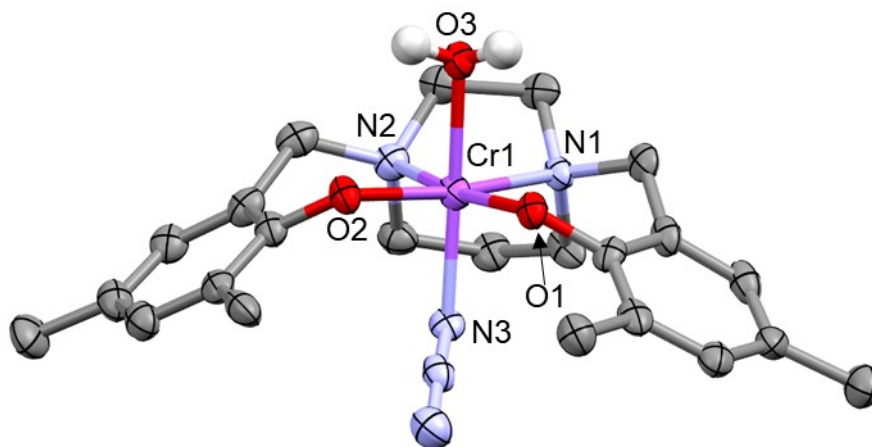


Figure C - 7: Partially labelled molecular structure of **5.2**. Thermal ellipsoids are drawn at 50% probability with hydrogens (except aquo ligand) and co-crystallized dichloromethane molecules omitted for clarity.

Appendix D: DSC of polymers

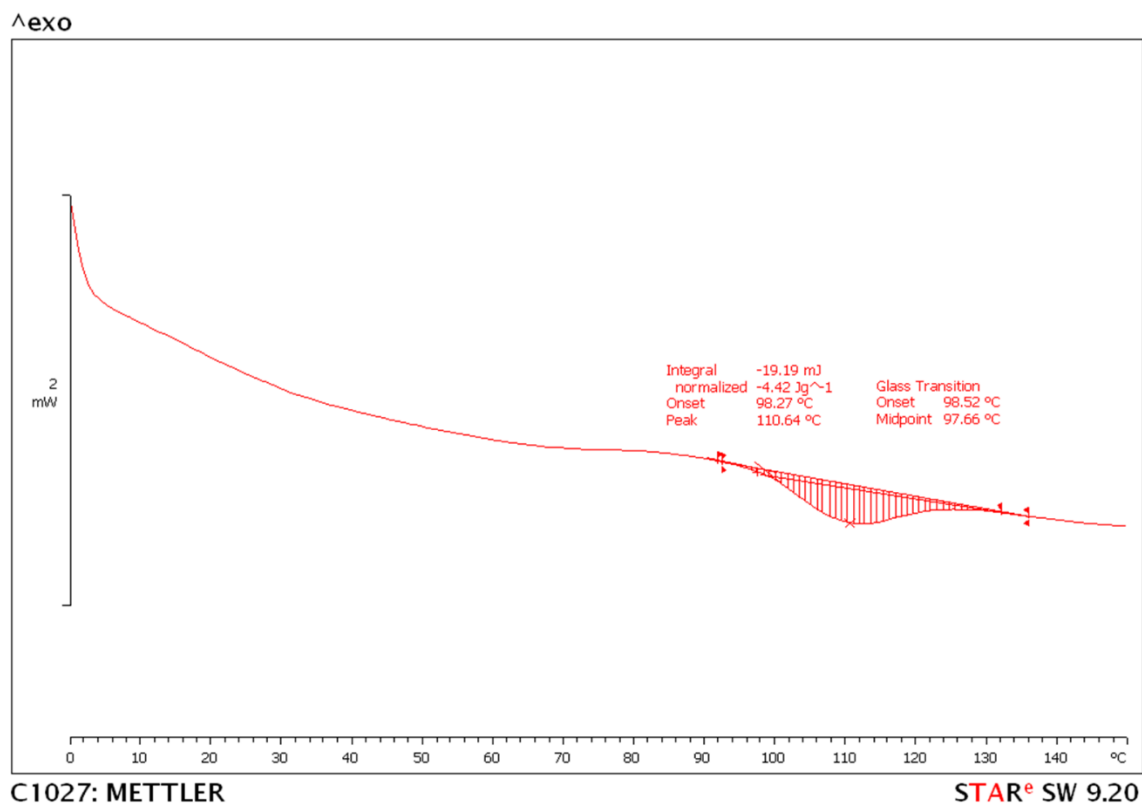


Figure D - 1: Representative DSC second heating curve of polymer produced by 5.1/PPNN₃ for copolymerization of CHO/CO₂.

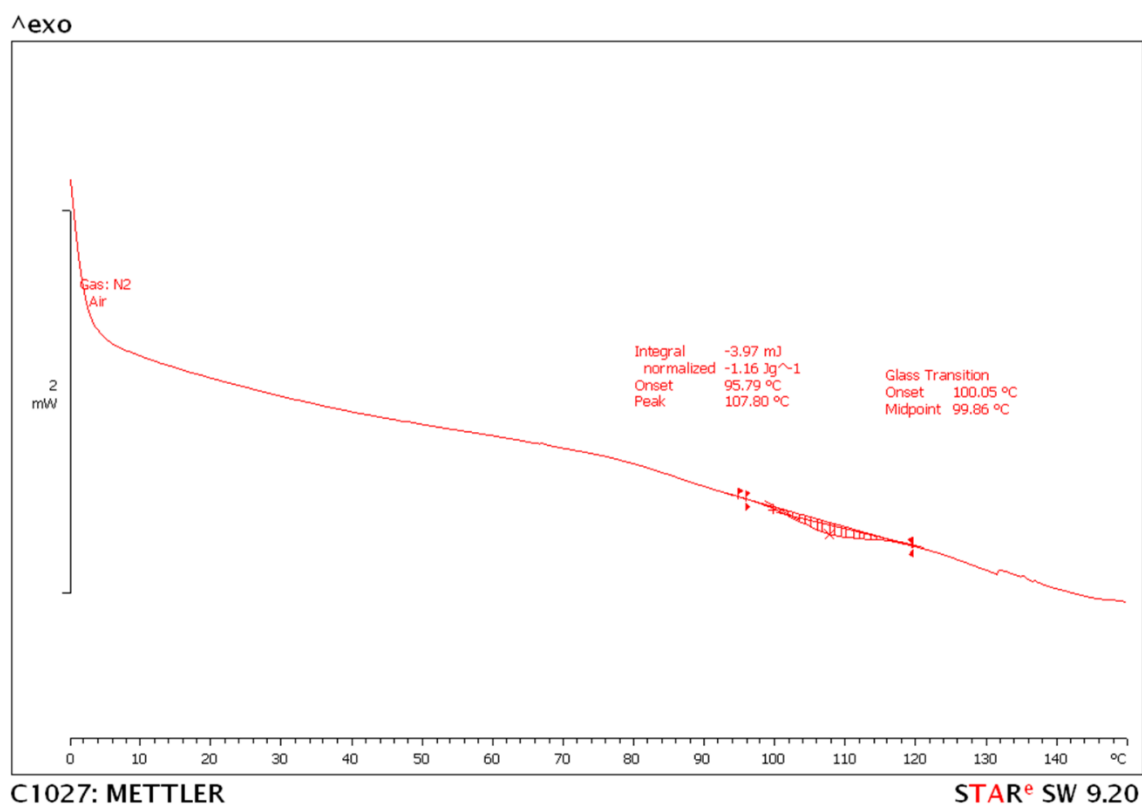


Figure D - 2: Representative DSC second heating curve of polymer produced by 5.1/PPNN₃ for terpolymerization of CHO/PO/CO₂ (Table 6.2, entry 2).

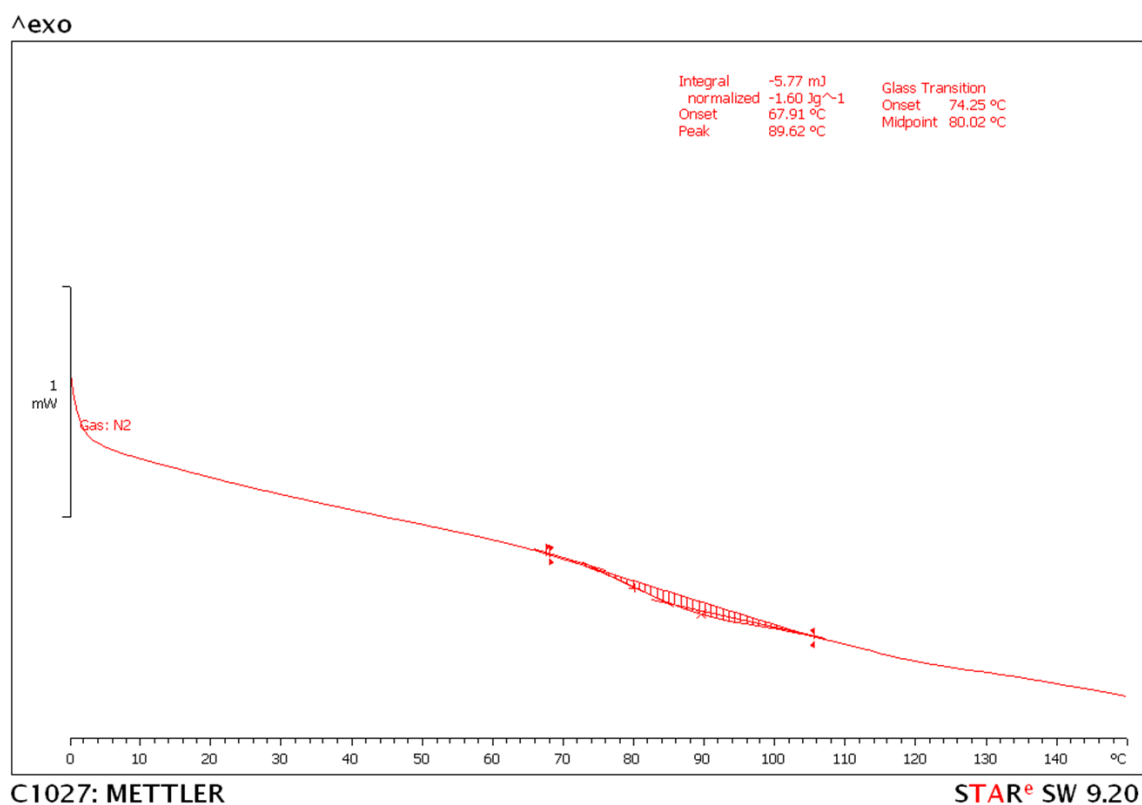


Figure D - 3: Representative DSC second heating curve of polymer produced by 5.1/PPNN₃ for terpolymerization of CHO/PO/CO₂ (Table 6.2, entry 3).

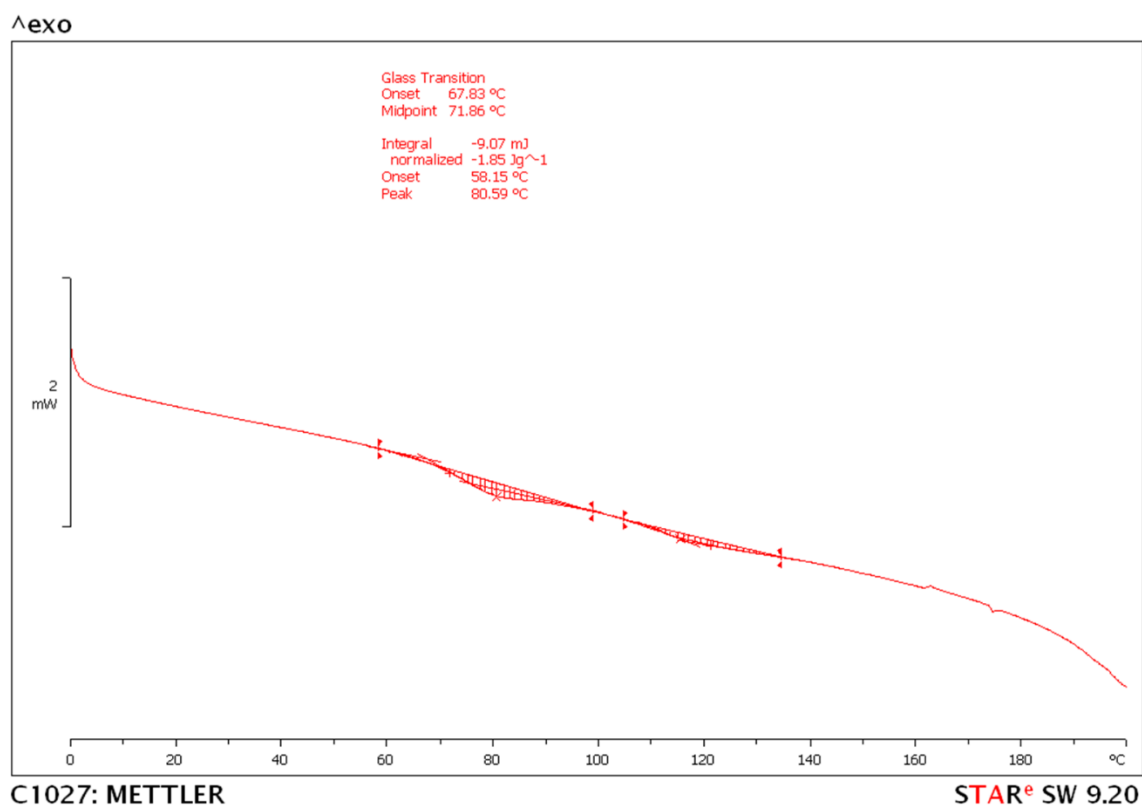


Figure D - 4: Representative DSC second heating curve of polymer produced by 5.1/PPNN₃ for terpolymerization of CHO/PO/CO₂ (Table 6.2, entry 4).

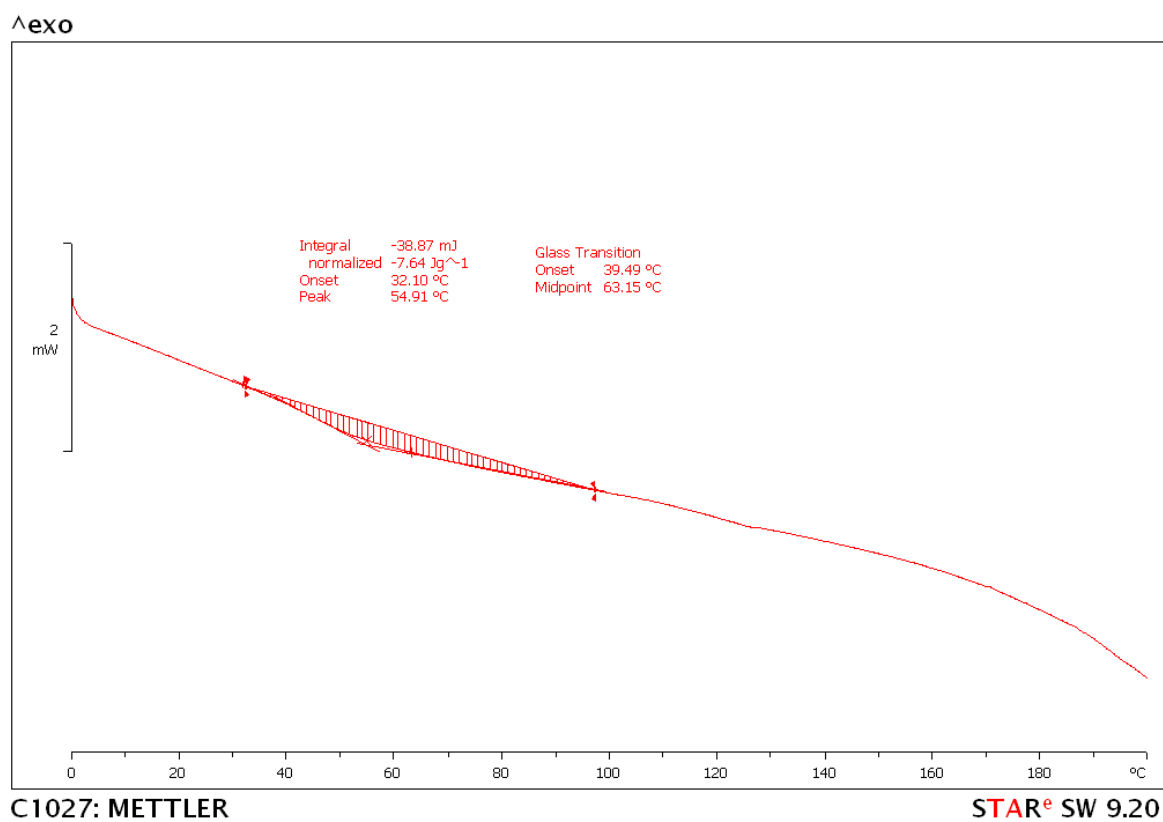


Figure D - 5: Representative DSC second heating curve of polymer produced by 5.1/PPNN₃ for terpolymerization of CHO/ECH/CO₂ (Table 6.2, entry 6).